Sustainable Methods for the Chemical Synthesis of Amides and Amide-Containing Aromatic Compounds

Lyndsay Anne Ledingham

PhD

University of York

Chemistry

August 2016

Abstract

Described in this thesis is work based on silica and palladium catalysis which focusses on the formation of amide-containing compounds. Efforts were made towards expanding the substrate scope of direct amide bond formation reactions catalysed by an activated K60 silica catalyst. Two of the resulting amides were then investigated as substrates in single and oxidative C–H functionalisation reactions to form phenanthridin-6(5H)-ones.

An investigation into the reaction conditions used in the K60 silica-catalysed amide bond formation reactions was carried out, highlighting the need to measure background reactions in this type of chemistry. Preliminary investigations into the expansion of the substrate scope of the silica-catalysed reaction revealed that there were limitations, particularly with bulky and polar substrates. A route to the anti-TB drug, isoniazid, was successfully developed using the K60 silica-catalysed methodology.

Two palladium catalysts, previously developed in the Fairlamb group, were successfully tested in the oxidative C–H functionalisation reaction of N-phenylbenzamide. One of these catalysts, Pd(tfs)$_2$(MeCN)$_2$ was characterised by X-ray diffraction and found to exist in a cis-configuration. Efforts to develop a one-pot synthesis of phenanthridin-6(5H)-one from benzoic acid and aniline were met with difficulties which could not be overcome.

The Pd-catalysed C–H functionalisation reaction of 2-bromo-N-phenylbenzamide afforded the unexpected product, 5-phenylphenanthridin-6(5H)-one, formed from 2 molecules of starting amide. Investigations into the mechanism of this transformation were undertaken, with a broad route deduced, and several palladium species from the catalytic cycle detected by mass spectrometry. The reaction was highly selective towards the phenanthridinone product, but there were eight other compounds detected in the crude reaction mixture, for which structures and mechanisms have been proposed.

Contents

List of Figures

List of Tables

14

List of Schemes

18

Acknowledgements

Firstly, I would like to thank my supervisors, Ian Fairlamb and Duncan Macquarrie, for all their advice, encouragement and support over the past 4 years. They have allowed me the opportunity to work both independently and within a larger team and I have learnt a great deal from both of them.

I have had the pleasure of supervising three undergraduate students, Becky, Alex and Stefan, in the laboratory and I thank them all for their hard work, some of which now forms part of this thesis.

I am very grateful for the excellent technical support at York and thanks must go to Heather Fish and Pedro Aguiar (NMR), Karl Heaton (Mass spectrometry), Adrian Whitwood (X-ray diffraction), Paul Elliott (Green Chemistry) and in particular, Charlotte Elkington who is a super technician and whose organisational skills are an inspiration. Thank you also to YorCat for the training and helpful discussion throughout my PhD and to IMI-(Chem21) for the funding and opportunities to present my research.

I would like to thank the Fairlamb and green chemistry groups for making my time in York so enjoyable and for the parties, bbq's, and outstanding fancy dress. In particular, Tom R (for the grammar lessons), Jess (for everything), Josh (for keeping me sane in the lab and knowing when I needed a drink), Philippa (for the 3am cakes), Alan (for making sure everyone knew about the Chem21 trips), George (for the messages in my cards), Kate (for her NMR expertise), Ben (for being Ben), George C (for thorough proof reading) and Neil (for the constant insults). Special thanks must go to Rachael and Julia who have been the most supportive friends I could have wished for during my PhD. I wouldn't have got here without them both.

This PhD would never have been possible without the unwavering support of my parents, particularly in these last few months. They have always been behind me in everything I have done and I am hugely grateful to them for their advice, encouragement and 'geriantics'.

Author's Declaration

I confirm that all work presented in this thesis is my own except where clearly referenced or acknowledged. The basis of the work in chapter 5 was carried out by Rebecca Campbell and Alex Pagett under my supervision and their contribution has been acknowledged appropriately in the text. The work in this thesis was carried out at the University of York between October 2012 and August 2016.

Chapter 1

Introduction

1.1   Catalysis and the pharmaceutical industry

With the growing regulations seen in the chemical industries,[1] the need for catalytic processes has increased. Companies are keen to avoid the waste that can be produced in stoichiometric processes, as this costs time and money to dispose of. Industry is driven by the need to have efficient, low cost processes; a need that can be satisfied by the development of new catalytic reactions. The efficiency and cost minimisation required in new processes is most prevalent in the fine chemical and pharmaceutical industries due to the complexity of the compounds they produce and, therefore, the number of steps needed to produce them. For many years these industries have collaborated with academia to advance the field of catalysis.[1] Chem21 is a project designed to encourage collaboration between academia and the pharmaceutical industry with the aim of developing sustainable catalytic processes which can replace the most problematic reactions used in industry.

Catalysis is one of the twelve principles of green chemistry and catalytic processes can be seen to cover more than one principle. With catalysis comes less waste, lower energy usage, an increased yield and higher selectivity.[1] In 2008, Barnard suggested that the focus of catalysis research should be on readily available substrates, simple ligand preparation and lower catalyst loadings.[2] These three areas are key to developing sustainable, efficient processes for industrial use.

Two reactions commonly used in the chemical industries are amide bond forming reactions and Pd-catalysed cross-coupling reactions. It follows that one of the focusses of catalytic research should be the development of catalytic processes for these reactions that are atom economical, efficient and cost effective.

1.2 Direct amide bond forming reactions

Within the compounds produced by the pharmaceutical industry amide bonds are a very common occurrence, with up to 25% of drugs containing the amide bond motif including Atorvastatin **1** and Flutamide **5** (Figure 1).[3] An analysis of reactions performed in the medicinal chemistry industry found that 12% were acylation reactions and 66% of those were an amide bond forming reaction.[4]
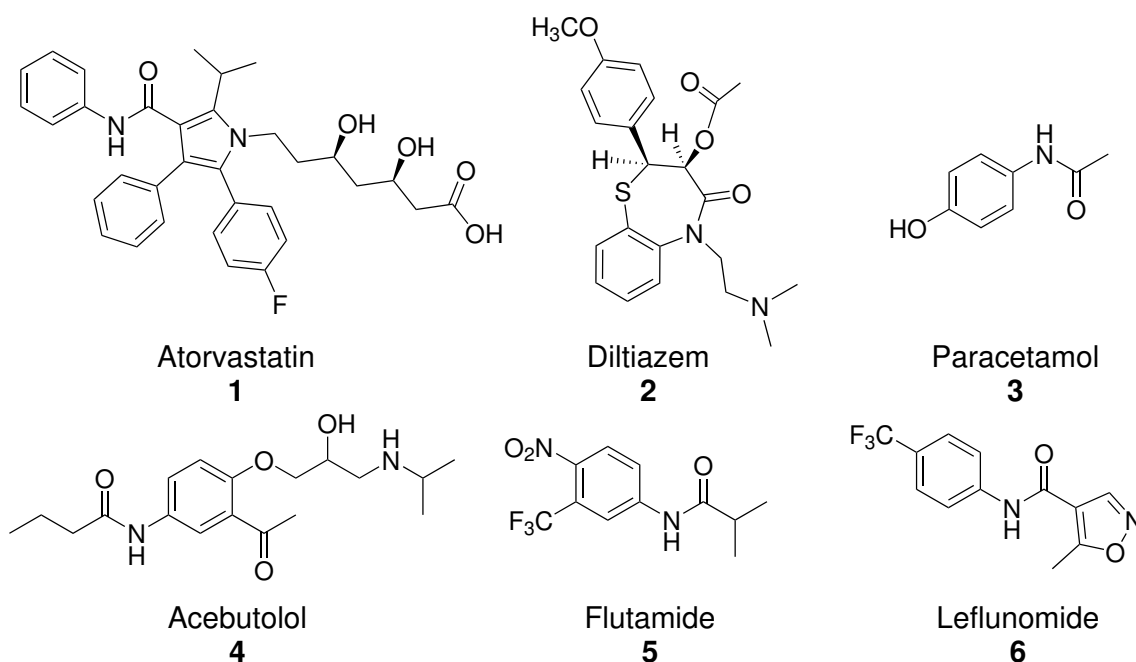
Figure 1: Examples of pharmaceutical compounds containing amides.

In nature, synthesis of an amide bond is done efficiently and selectively using enzymes. Within a cell the enzyme activates the amino acid to the amino ester which then goes into a process using hundreds of other biological molecules, producing a peptide at the end.[3]

Amide bond synthesis is a well developed area within synthetic organic chemistry with many routes existing. Unfortunately, many of these routes are highly inefficient and wasteful and the area was highlighted by Carey's review in 2006 as a reaction in urgent need of development.[4] New methods are constantly emerging from research groups throughout the world. Some of these methods involve direct amide bond formation from carboxylic acids and amines, while others use aldehydes or aryl halides as starting materials.[2] Described herein are some of the most common methods for direct amide bond formation including

those currently favoured by pharmaceutical companies.

1.2.1 Carboxylic acid activation *via* acid chlorides and carboxylic anhydrides

Acid chlorides were one of the first activation routes to be discovered for amide bond formation. Published by Schotten in 1884[5] and then by Baumann in 1886,[6,7] the Schotten-Baumann synthesis of amides involves the use of stoichiometric activating agents, such as oxalyl chloride **7** and thionyl chloride, to activate the carboxylic acid to the acid chloride before reaction with the amine, releasing hydrochloric acid along with the desired amide (Scheme 1). Reacting the acyl chloride with an amine to produce the desired amide is usually very easy and will give high yields, as seen in the amide synthesis shown in Scheme 1 which is part of the synthesis of a series of aurora kinase inhibitors used for the treatment of cancer.[8]
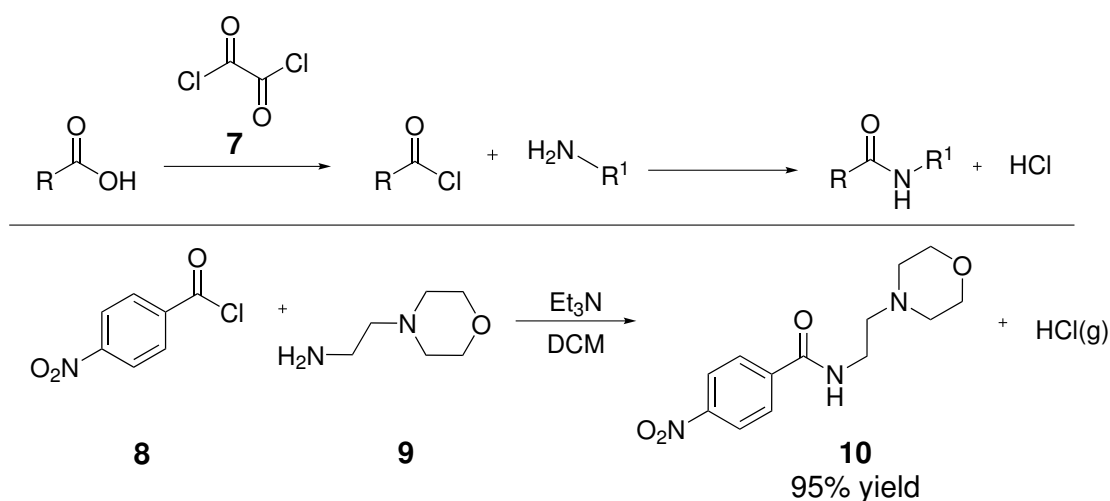
Scheme 1: Reaction of an acid with oxalyl chloride giving an acid chloride which goes on to react with an amine. Amide bond formation step of a series of aurora kinase inhibitors from 4-nitrobenzoylchloride **8**.[8]

The by-product of the reaction is HCl which can cause problems, i.e. with acid sensitive substrates and products. While this is the only waste produced from the amide bond formation, the acid chloride formation must be taken into account with the waste from the activating agent making a significant contribution, for example, thionyl chloride releases

sulphur dioxide, a toxic gas with many environmental concerns and oxalyl chloride releases carbon monoxide. Common to both of these is the release of hydrochloric acid. In addition to the waste, the activating agents used in acid chloride synthesis can be toxic, corrosive and generally unpleasant to handle.

Anhydrides are used in amide synthesis in a manner similar to acid chlorides. The intermediates can be either homo-anhydrides or mixed anhydrides. Homo-anhydrides are simple to make, through dehydration with dicyclohexylcarbodiimide (DCC), diisopropylcarbodiimide (DIC) *etc.*, however purification can be a problem as separating the urea by-product can be difficult.
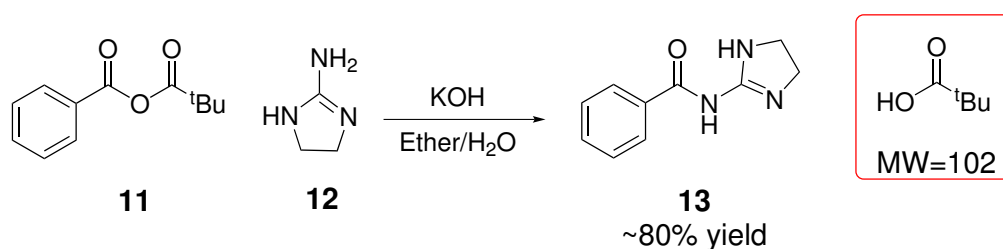
Scheme 2: Mixed anhydrides can be reacted with amines to give an amide and an acid by-product such as pivalic acid.[9]

Use of the homo-anhydride is straight-forward but this synthesis uses two equivalents of acid per amine and the second equivalent is left over as waste. Mixed anhydrides can provide a valuable alternative particularly when using an expensive acid. In these cases, the selectivity can be enhanced by the use of, for example, pivalic anhydrides where one half of the anhydride is bulky and does not react as shown in Scheme 2.[9] Waste is still a huge problem from this reaction as, again, one half of the anhydride is unused.

1.2.2 Reactions involving coupling reagents

Coupling reagents are very commonly used in the pharmaceutical industry. Included in this field are HATU **14**, TBTU **15**, T3P, DCC **16** and DIC **17** however there is an enormous range in the literature.[10] DCC is generally inexpensive, gives high yields and its urea by-product is insoluble in most organic solvents and, generally, can be easily removed (Figure 2). This can, however, be a drawback if the product is insoluble leading to problems separating the

by-product, dicyclohexylurea **18**. DCC also has some health concerns as it is a sensitizer and so is quite often avoided unless there is no alternative. DIC is a viable alternative, with fewer health concerns however as with DCC and many other carbodiimide coupling reagents, the bulky by-product is a problem from a waste perspective.
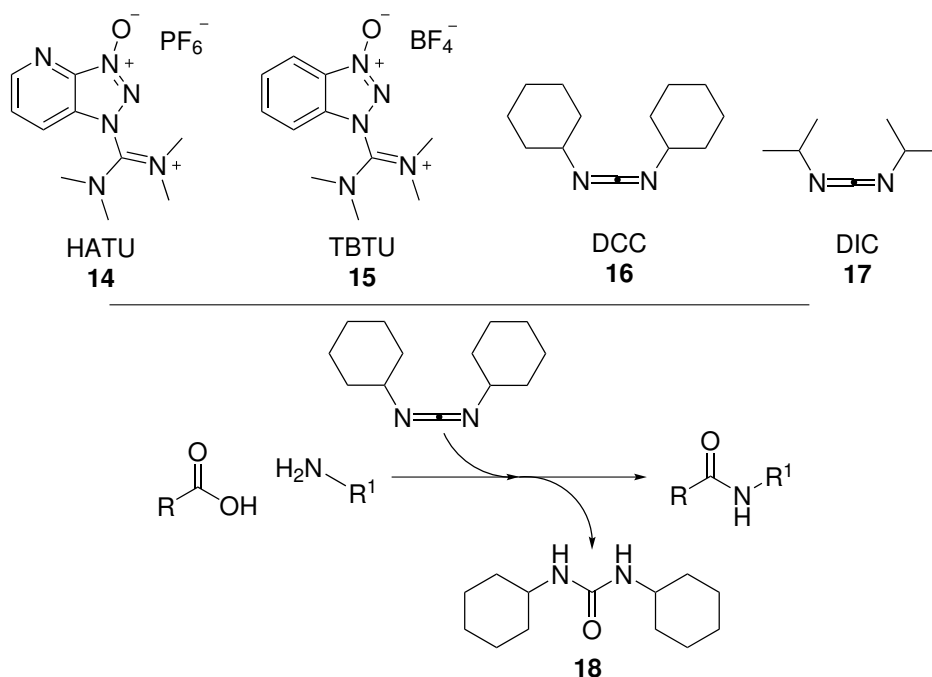
Figure 2: Examples of coupling reagents used in amide bond forming reactions. Use of carbodiimides as coupling reagents in condensation reactions produce urea by-products.

Benzotriazole compounds, such as HATU **14** and TBTU **15** (shown in Figure 2), are also well known amide coupling reagents. These are used as additives with carbodiimides to reduce epimerisation in reactions but are also used independently as reagents for amide bond forming reactions. A huge range of benzotriazole compounds has been developed for use as coupling reagents but care must be taken with these as the compounds can be explosive.[10]

A paper published by Pfizer in 2011 detailed a robust amide bond formation by the use of T3P and pyridine which was effective for substrates, such as compound **20**, that are prone to epimerisation (Scheme 3).[11] The main byproduct from the reaction is water soluble and easily separated, however in terms of mass efficiency, compound **19** is particularly heavy and so lowers the mass efficiency significantly. T3P is now used as the reagent of choice for many amide couplings, in both academia and industry.
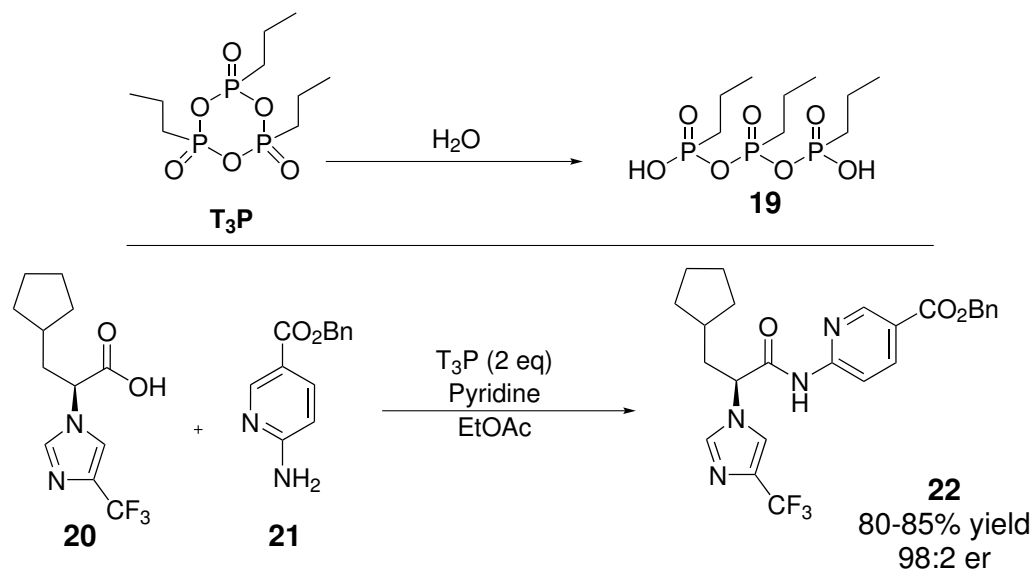
Scheme 3: T3P and its use as a coupling agent in the synthesis of an intermediate used in the production of a glucokinase inhibitor.

1.2.3   Catalysts to form amides

Enzymes as catalysts

Biocatalysis is a relatively new field, exploiting the use of enzymes in synthetic chemistry. Several enzymes have been reported for their use in amide bond synthesis, the most prevalent of which are lipases. Lipases are popular due to their stability, substrate specificity and amide tolerance (*i.e.* they do not hydrolyse the product).[12]
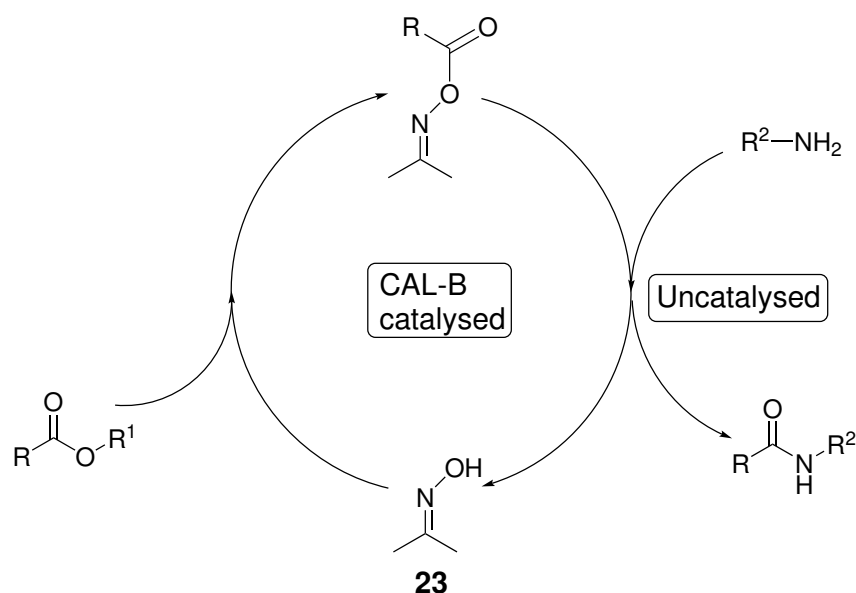
Scheme 4: Amide bond formation catalysed by *Candida Antarctica Lipase B.*

Scheme 4 shows an amide formation catalysed by *Candida Antarctica Lipase B* (CAL-B) using acetoneoxime **23** to activate the acyl donor.[13] Unfortunately, enzymes are often substrate specific meaning the active site can limit the size of substrate that can be accepted by the enzyme. This problem can sometimes be avoided by using the enzyme to activate the acid or ester, then conducting an uncatalysed aminolysis outside the active site as illustrated in Scheme 4. The reported scope of the reaction using CAL-B is relatively narrow.[13] The best results were found using anilines as the amine and so the scope was investigated using only aniline derivatives and no change in the ester. *Pseudomonas stutzeri lipase* has also been reported as an efficient catalyst.[12] This enzyme is more effective when using secondary amine nucleophiles, such as amine **25**, and its scope has been extended to difficult esters, *e.g.* methyl 3-phenylpropionate **24** (Scheme 5).
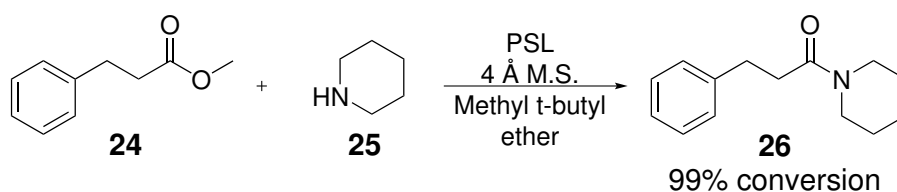
Scheme 5: Amide bond formation between an ester and amine catalysed by *Pseudomonas stutzeri lipase*.

Both of these enzymes are relatively new in the amide bond formation field and are therefore still being explored. The results so far show that there is scope for enzymes to become important in the field. Indeed, these are already highlighted by GSK as their preferred way of forming amides. Searching in the literature, little was found on the preparation of the enzymes so it is not possible at the moment to speculate on their green credentials. Amidases and proteases, usually known for cleaving amide bonds, have also been found to be effective catalysts for amide bond formation simply by changing the reaction conditions, pushing the equilibrium the other way.[3]

Organo-boronic Acids as catalysts

In 1996, Yamamoto *et al.* first reported the use of boronic acid catalyst **27** for the condensation reaction between simple acids and amines.[14] This was followed up in 2005 by a new range of catalysts, *N*-alkyl-4-boronopyridinium salts **28**, which are more stable and can be attached to polystyrene resins giving a heterogeneous catalyst that can be easily recycled.[15] In 2006, Yamamoto reported catalyst **29** with an easy *in situ* synthesis involving boric acid and tetrachlorocatechol.[16] This catalyst was found to be efficient at catalysing reactions using bulky carboxylic acids giving yields of up to 99%.
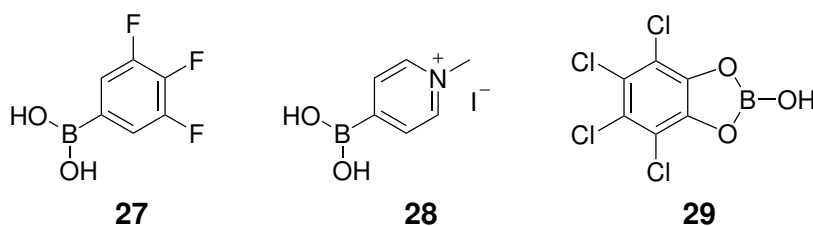
Figure 3: Three examples of organo-boronic acid based catalysts developed by Yamamoto for amide bond synthesis.

Since then, many more catalysts have been reported covering a wide substrate range and different reaction conditions.[17,18] Most of the catalysts reported require water removal from the reaction either by azeotropic reflux or the use of molecular sieves. Sheppard *et al.* reported in 2010 an efficient borate ester reagent and improved the reaction, in 2013, with reactions that do not require water to be removed from the reaction and have mild conditions with a straightforward purification, *via* solid phase resins (Scheme 6).[19] The reagent is easily

formed from boric anhydride and 2,2,2-trifluoroethanol and is reported to give yields of up to 99%, with a range of substrates.
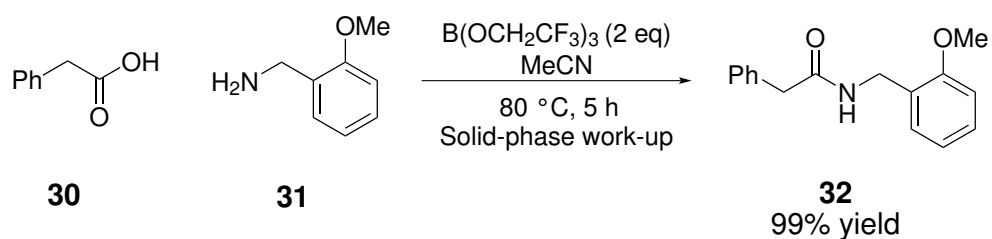
Scheme 6: Use of a tri-fluoroethyoxyborate catalyst to couple phenylacetic acid and 2-methoxybenzylamine.

The mechanism suggested for the boron-catalysed amidations proceeds through an activated ester intermediate and this is supported by computational calculations using DFT methods. Marcelli reports the lowest-energy pathway, which includes activation of the acid **33** followed by hemiaminal **37** formation, before the water is eliminated and the amide **39** released (Scheme 7).[20]
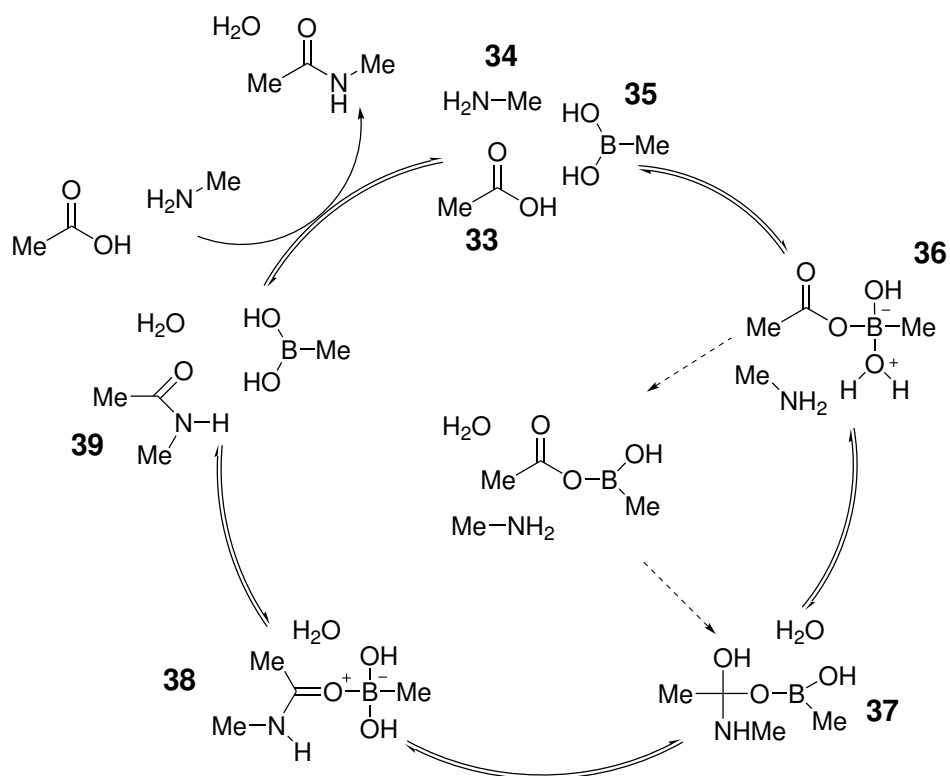
Scheme 7: Mechanism of action for the boronic acid-catalysed amide bond formation based on DFT calculations.

Organo-boronic acids are efficient catalysts for amide bond formation and, in terms of literature, have proven very popular; however when the green metrics are examined, the E factor associated with their production and use is high: $\sim$400.[21] E factor, or environmental factor, was created by Prof. Roger Sheldon and is defined in the equation below.[22,23] It is a metric that is easy to use and can be adapted to fit different processes.

$$E\,factor = \frac{waste\,(kg)}{product\,(kg)} \qquad\qquad \text{Eq. (1)}$$

From a sustainable industrial chemistry point of view, organo-boronic acids are unlikely to be used in large scale synthesis. Having to deal with large amounts of waste is unfavourable.

Metals as catalysts for amide bond formation

Several metal-catalysed processes have been reported in the literature for amide bond formation, two of which are detailed here. In 2012, Adolfsson *et al.* reported a zirconium chloride-catalysed coupling of unactivated acids and amines.[24] In addition to working with a wide substrate range including indomethacin **41** (Scheme 8), this reaction is excellent for enantiomerically-pure starting materials, with no racemisation occurring.
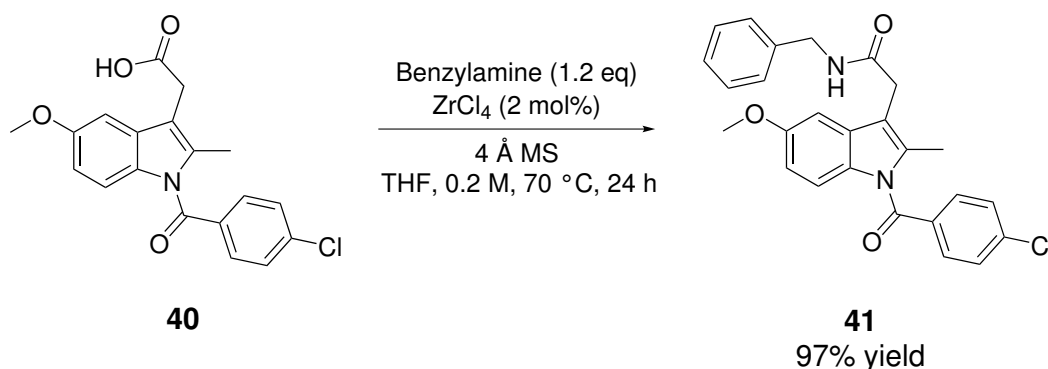
Scheme 8: Synthesis of indomethacin **41** using $ZrCl_4$ as a catalyst.

More recently, Beller reported an oxidative reaction between benzyl alcohols and amines using a zinc catalyst.[25] The reactions require no solvent and can be carried out in air on a wide range of substrates. Most reactions produced amides in moderate to good yields, with only a few problem substrates, such as thiophen-2-ylmethanol (yields <30%).
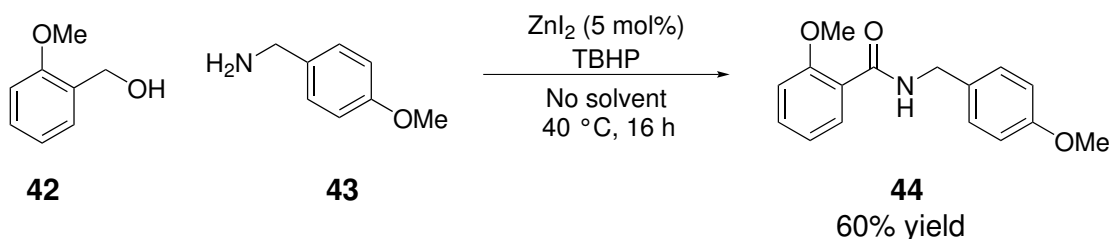
Scheme 9: Use of ZnI$_2$ to oxidatively couple a benzyl alcohol and amine.

Heterogeneous Catalysts

Heterogeneous catalysts are widely used in industry due to their easy recycling and re-usability. Their potential for use in flow chemistry is one that is particularly interesting from a green chemistry point of view. Many are now reported in the literature as efficient catalysts for amide bond formation.

In 2012, Mukhopadhyay reported an alumina-based catalyst for amide bond formation.[26] The catalyst is made of small round balls of alumina (approx. 2-3 mm diameter) which are calcined at 700 °C before use. Very little is known about the structure of this catalyst, it is obtained from only one supplier. They used a solvent-free reaction mixture at 140 °C with acid, amine and 10 weight percent of alumina ball catalyst, achieving yields of up to 98% (Scheme 10). The catalyst was re-useable but does require solvent to separate it from the reaction mixture. The E-factor of the reaction was excellent, reported as 0.15, indicating that for every kg of product there is only 0.15 kg waste.[26] Taking work-up and purification solvent into account, and assuming 90% recovery of solvent, the E-factor increased to 1.88.
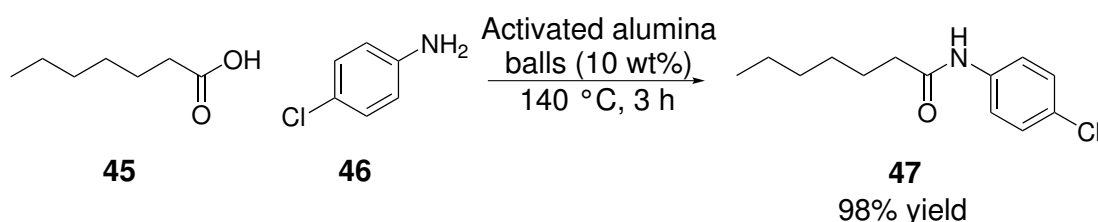
Scheme 10: Reaction between heptanoic acid **45** and 4-chloroaniline **46** catalysed by activated alumina balls.

Silica catalysts for amide bond formation were reported by Clark *et al.* in 2009.[21] The standard reaction used cheap, chromatographic K60 silica, with a 60 Å pore size and 35-

75 μm particle size, activated at 700 °C for four hours to catalyse the condensation of a carboxylic acid and amine (Scheme 11). As with the alumina balls described previously, the catalyst could be recovered easily and was reusable up to four times. This was a versatile catalyst which had a high water tolerance, as demonstrated by Comerford who obtained an identical yield when the toluene was saturated with water as when it was used as received from the supplier.
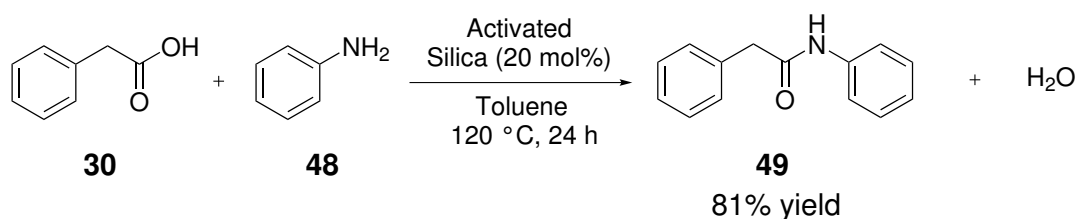
Scheme 11: Reaction between phenylacetic acid **30** and aniline **48** catalysed by activated silica.

1.3 Palladium Catalysis
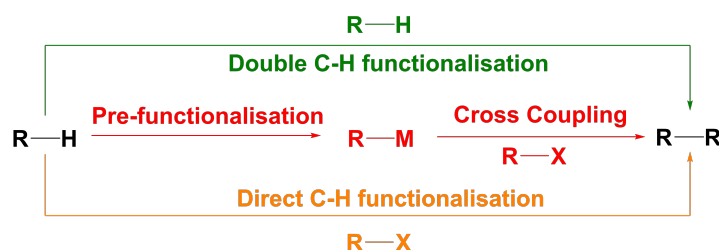
Figure 4: Three methods of cross-coupling to form C–C bonds.

There are a wide variety of reactions used to form new C–C bonds from Friedel-Crafts to Grignard and Michael reactions. The introduction of Pd catalysis, in reactions such as Suzuki, Stille and Sonagashira, provided a totally new, robust method of making C–C bonds and revolutionised the field.[27,28] These traditional Pd-catalysed cross-coupling reactions to form new C–C bonds involve the pre-functionalisation of one of the substrates using metals such as boron, tin and copper before transmetallation to transfer the substrate to the Pd intermediate. The other coupling partner is generally an aryl halide which can oxidatively add to the active Pd catalyst.
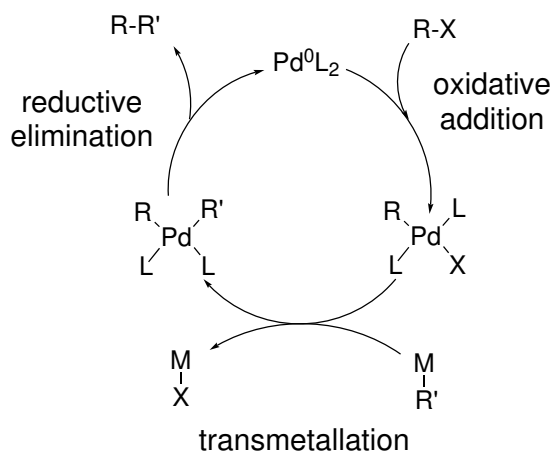
Figure 5: Typical Pd cross-coupling catalytic cycle.

Such reactions are popular in the chemical industries due to the high selectivity involved but from a green perspective, leave much to be desired. The pre-functionalisation of the substrate by a metal, often in a stoichiometric amount, dramatically decreases the atom economy of the reaction. These traditional cross-couplings also involve the use of an alkyl/aryl halide C–X bond rather than a C–H bond and this further decreases the atom economy as the halide is lost in the reaction.

1.3.1 C–H functionalisation

Recent work in Pd catalysis has been directed toward direct C–H functionalisation with alkyl/aryl halide substrates in a wide range of reactions including arylation, alkylation, allylation and amination.[29] This negates the need for a transmetallating agent in the reaction and significantly improves the green credentials of the reaction. These reactions involve a metal catalyst such as Pd, Pt, Cu or Ru; sometimes with a phosphine ligand, and a base, such as K_2CO_3 or AgOAc in a wide variety of solvents.[29,30] C–H functionalisation is becoming more common for use in both natural product synthesis and pharmaceuticals due to the developments being made in the field allowing more versatility in reactions, and because sustainability in the chemical industry is becoming more and more important.[1] For this reason, it has been one of the focusses of the Chem21 project.

The literature on direct arylation *via* C–H functionalisation has amplified in recent years, in part due to the work into new catalyst systems. For example, Scheme 12 shows the direct

arylation of benzothiophene using a simple catalyst system of Pd(OAc)$_2$ at low catalyst loadings.[31] The authors do not comment on the mechanism of this reaction but do hint at the beginning of the paper of the formation of Pd nanoparticles based on the work of de Vries.[31] The reaction requires 1.5 equivalents of base, in this case KOAc proved most successful, meaning that a potassium salt by-product must be disposed of at the end of the reaction.
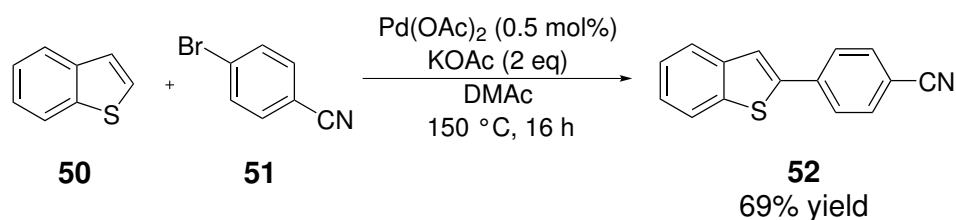
Scheme 12: Direct arylation of benzothiophene.[31]

The natural product synthesis of Celogentin C involved a direct arylation *via* C–H functionalisation (Scheme 13).[32] It required the use of AgOAc in 1.5 equivalents and the complex starting material **53** in two equivalents compared with the substituted indole. The use of silver acetate as a base results in the need to dispose of silver iodide, and possibly residual silver acetate.
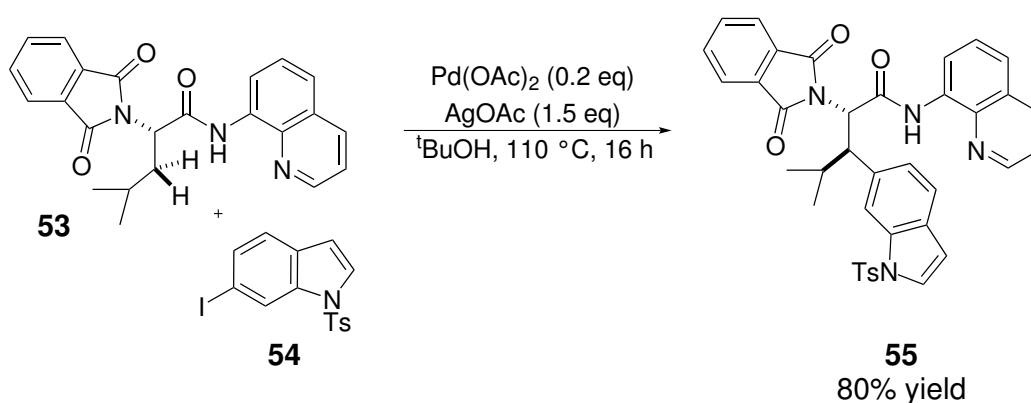
Scheme 13: C–H functionalisation step in the total synthesis of Celogentin C.[32]

One of the main problems with C–H functionalisation chemistry is the potential for multiple reactions. It can be possible for the product to be more reactive than the starting material and therefore can undergo further C–H functionalisation reactions.[30] Selectivity can also be a problem and often a directing group is employed to ensure that the desired C–H bond

is activated. Common directing groups are carboxylic acids and amides which are often *ortho* to the desired C–H activation site and allow co-ordination of the catalyst.[33] The base required in C–H functionalisation reactions means that these reactions are not as green as they at first appear. For these reasons, it is important to take into consideration the reagents and catalysts used in a reaction as well as selectivity, as a good atom economy and yield do not always mean a green reaction.

1.3.2 Oxidative C–H functionalisation

In the same way that C–H functionalisation is more sustainable than traditional Pd-catalysed reactions, oxidative C–H functionalisation can be seen as the greenest of the three. It requires no transmetallating agent and no aryl halide. Simply, two C–H bonds are converted to a C–C bond where the loss from the starting materials to the product is two hydrogen atoms. The ideal oxidative C–H functionalisation would release H_2 gas which could be utilised in another process. The reality is that these reactions are difficult as the C–H bond is a lot stronger and less reactive than the C–X bond and functionalising two of these bonds requires a very active catalyst.

In 2011 Fagnou reported the oxidative C–H functionalisation of *N*-protected indoles, with a high selectivity for arylation at the C3 position.[34] No homocoupling was seen and the yields were generally good (42–84% over 9 examples). It was discovered that with the use of microwave heating, the reaction time and catalyst loading could be significantly decreased with a higher conversion seen.
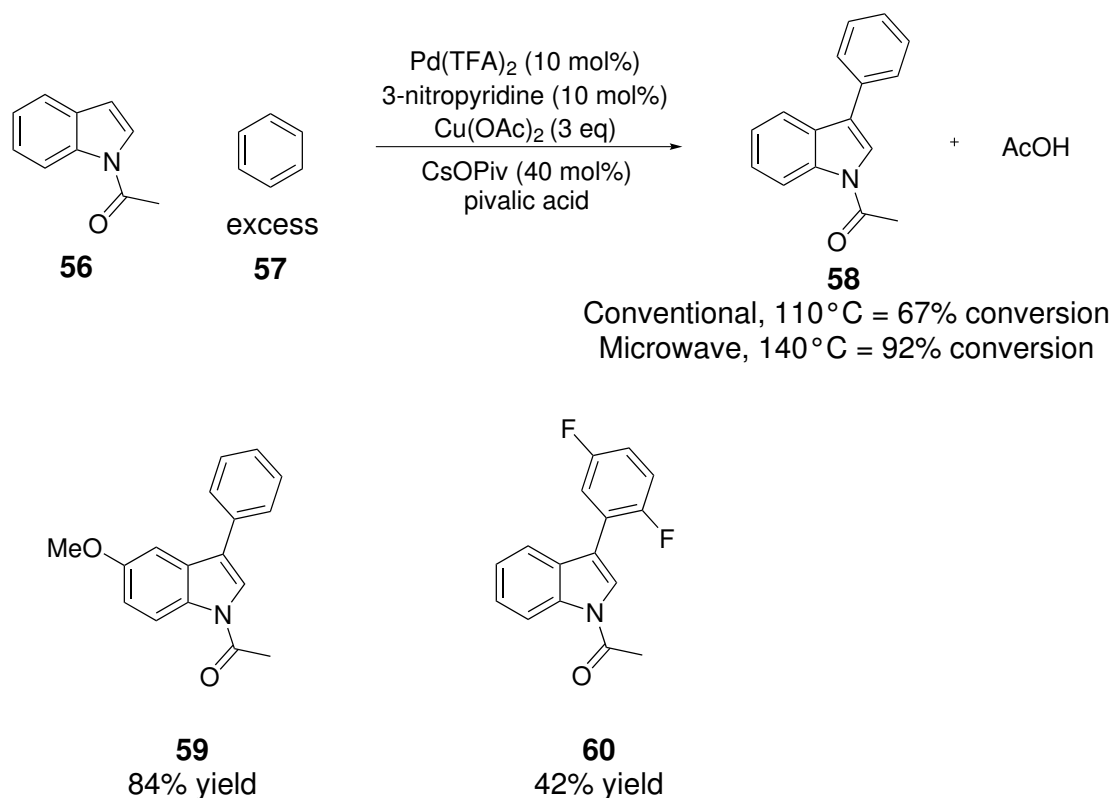
Scheme 14: Oxidative C–H functionalisation used in the arylation of indoles.

Shafiee, in 2013, reported the arylation of coumarins, with a wide scope, including free OH groups.[35] As with many examples of oxidative C–H functionalisation some homocoupling of the pentylbenzene was seen, and the reactions did not proceed to full conversion. The mechanism was expected to begin with an *in-situ* Pd(TFA)$_2$ synthesis, making the catalyst similar to the one reported in Scheme 14.
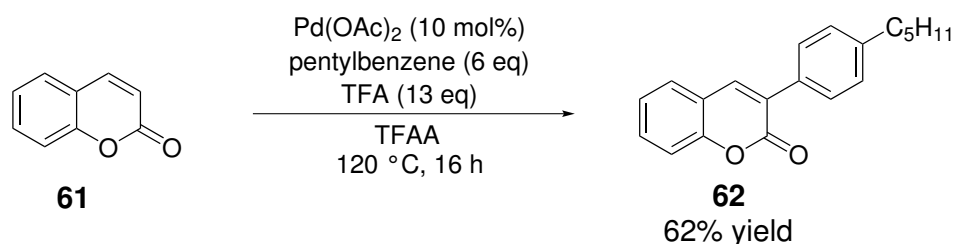
Scheme 15: Arylation of coumarins using oxidative C–H functionalisation.

It is necessary to think critically about oxidative C–H functionalisation reactions from a green perspective. They are without a doubt the most atom economical Pd-catalysed trans-formations available to chemists, however as seen in the examples above, they can involve

higher than stoichiometric amounts of reagents. The reaction in Scheme 15 uses six equivalents of pentylbenzene and 13 equivalents of trifluoroacetic acid while the reaction in Scheme 14 uses three equivalents of copper acetate. These reagents will then create by-products which have to be separated from the desired product and disposed of.

As with single C–H functionalisation, one of the main challenges with oxidative C–H functionalisation is selectivity. There is the potential for multiple C–H activation on both of the substrates and, again, directing groups are employed to overcome this problem. From this perspective, the oxidative C–H functionalisation reaction does not appear so green. However with some work and the force of the green chemistry movement, *vis à vis* Chem21, behind it there is the potential for this type of reaction to transform the pharmaceutical industry.

1.4 Green Metrics

The sustainability of the chemistry in this thesis was measured using a set of green metrics that were chosen by the Chem21 project. Detailed here are the particulars of each metric used.

Yield, selectivity and conversion are the most obvious metrics to consider first. A process in the pharmaceutical industry is of little use if it produces barely any product or several side products. A green process must give a high conversion to the desired product and that product must then be isolated to give the high yield required.

Atom economy (AE) is the next metric to consider. This metric quantifies how much of the starting materials become the product (Eq. 2) and therefore represents how much of the reagents become waste. The aim of a truly green reaction would be to have an atom economy as close to 1 (or 100%) as possible. This helps to minimise waste from the reaction however, it only takes into account the reactants, not reagents, solvents or any work-up and purification.

$$AE = \frac{m.w.\ of\ desired\ product}{m.w.\ of\ starting\ materials} \qquad \text{Eq. (2)}$$

The ACS green chemistry institute pharmaceutical roundtable has collected data from seven

pharmaceutical companies on the process of small molecule drug synthesis.[36] Included on their website is a representation showing the proportions of each section of a pharmaceutical process with regards to mass intensity (Figure 6). Reactants account for only 9% of the total process, and so AE must be used in conjunction with other, wider mass-based metrics.
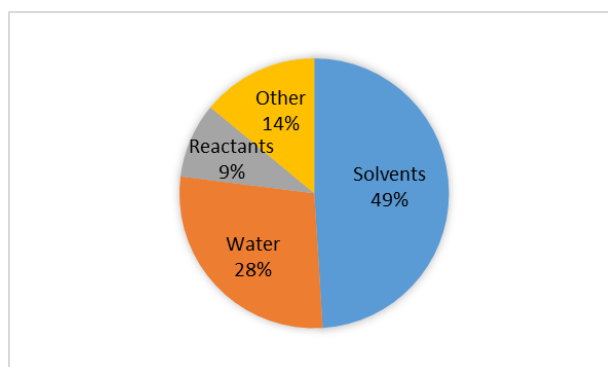
Figure 6: A breakdown of the synthesis of an API.[36]

Reaction mass efficiency (RME) takes into account atom economy, yield and stoichiometry of the reactants. It is defined in equation 3 below and can be seen as a step up from atom economy. As RME takes into account the yield and the stoichiometry, the closer the RME is to the atom economy, the more efficient the reaction is.

$$RME = (\frac{(m.w.\ of\ C)}{(m.w.\ of\ A\ +\ (m.w.\ of\ B\ \times\ molar\ ratio\ B/A))}) \times yield \qquad \text{Eq. (3)}$$

It does not evaluate solvents, work-up or purification, all of which are important factors to consider in any green process. To examine these we must consider mass intensity (MI). MI gives an overall view of the process and can be split into reaction and work-up, which can in turn be separated into chemicals and solvents.[37] It is defined as the mass of materials used to produce a specified mass of product and therefore can include the reactants, reagents, reaction solvents, catalysts and purification chemicals and solvents. What is included depends on which part of the reaction is to be looked at and this can highlight the problematic areas of a reaction. For the purpose of this project, the MI was split into reaction and work-up which were in turn separated into chemicals and solvents.

$$MI = \frac{(total\ mass\ in\ a\ process\ (kg))}{(mass\ of\ product\ (kg))} \qquad \text{Eq. (4)}$$

These mass-based metrics only show quantitative measures of sustainability and do not take into account toxicity of chemicals, energy usage or catalytic processes so a flag system was brought in to allow qualitative analysis of the process. For example, any solvents that were particularly hazardous were flagged red to allow a potential solvent switch to be identified. A yellow flag indicated that a solvent should be replaced if possible and a green flag reported that the solvents were acceptably green. The fourth flag in use was black which indicated that a particular solvent or chemical must be replaced if the reaction is to be developed. This is the case for diethyl ether which has a low flash point and low vapour pressure. This system is in place for health and safety, catalysts, reactor type, elements used, energy usage and work-up type.

As the metrics consider different parts of a process, it is essential that a range of metrics are considered. The metrics described in this section allow both a broad overview and a detailed analysis of a process and while not exhaustive, they do cover a wide range of sustainability indicators.

1.5   Aims and Objectives

1.5.1   Aims

- To develop green methods of amide bond formation focussing on targets relevant to the pharmaceutical industry.

- To examine Pd-catalysed cross-coupling reactions of simple biaryl amides and identify possibilities for making these reactions more sustainable.

- To compare the principal reactions developed in this thesis to their corresponding literature using green metrics analysis.

1.5.2   Objectives

- To identify the optimum reaction conditions of a silica-catalysed amide bond formation reaction and to compare this reaction with a series of different silica-based

catalysts and a new alumina balls catalyst by analytical methods. (Chapter 2)

- To synthesise isoniazid *via* a silica-catalysed amide bond formation reaction and to measure the green metrics of that reaction in comparison with the literature. (Chapter 3)

- To further the scope of the silica-catalysed amide bond formation reaction using a series of complex substrates including heterocyclic, heteroaromatic and bulky compounds. (Chapter 3)

- To examine new Pd catalysts in the oxidative C–H bond functionalisation reaction of *N*-phenylbenzamide and to explore the possibility of a one-pot reaction to form phenanthridin-6(5*H*)-one. (Chapter 4)

- To probe the mechanism of the formation of 5-phenylphenanthridin-6(5*H*)-one and the side-products of the reaction using NMR, MS and substrates with mechanistic handles. (Chapter 5)

Chapter 2

Optimisation and Catalyst Investigation of Amide Bond Forming Reactions

2.1 Introduction

With amide bond formation playing such an important role in the pharmaceutical industry, it is essential that new methods are found and fully investigated so that the industry has plenty of options to choose from. To this end, the first two chapters of this thesis focus on investigating the conditions, mechanism and extended substrate scope of silica- and alumina-catalysed amide bond forming reactions.

The initial work by Comerford *et al.* used a reaction between phenylbutyric acid and aniline to look at a variety of heterogeneous catalysts including calcined Kieselgel 60 (K60) silica.[21] They found that a calcined K60 silica catalyst gave the highest activity, with the optimum temperature for activation at 700 °C. These silica gel catalysts showed a variety of surface areas but there was no correlation with catalyst activity.

Some investigation was done into the mechanism of the catalyst, including infrared (IR) measurements of silicas activated at different temperatures.[38] Diffuse reflectance infra-red fourier transform spectroscopy (DRIFTS) is an IR technique used to study powders and it is particularly useful for studying silica. An IR beam is directed at the surface of the sample which is commonly diluted by a non-absorbant material such as KBr. The rough surface of the bulk material causes diffuse reflections which are then collected by a curved mirror and focused into the detector. Figure 7 shows the three types of silanol which are distinguishable by IR and Table 1 explains each of the bands seen in an IR spectrum of silica.
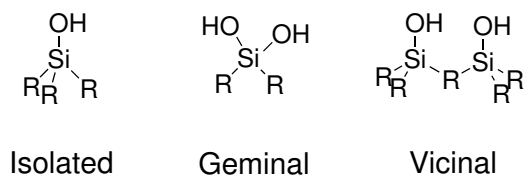
Figure 7: Three types of silanol groups found in silica.
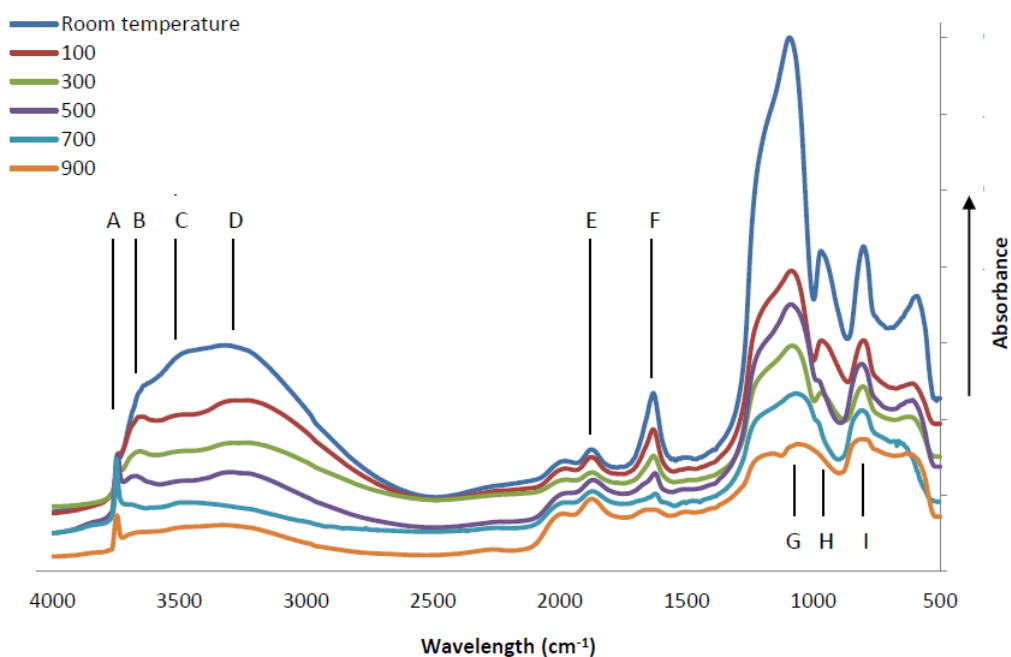
Figure 8: Overlaid DRIFT spectra of K60 silica activated at various temperatures.[38]

Table 1: Assignment of IR bands for K60 silica.[39,40]

	Wavenumber (cm^{-1})	Vibration
A	3747	Isolated silanol
B	3742, 3725	Geminal & vicinal silanol
C	3520	Vicinal silanol
D	3250	Adsorbed water
E	1875	Si-O-Si overtones
F	1629	Physisorbed water
G	1082	Asymmetric Si-O-Si stretch
H	970	Si-O-(H...H$_2$O) bend
I	804	Geminal in plane OH bend

43

Figure 8 shows that the hydrogen bonded silanols, seen at 3720-3730 and 3520 cm^{-1}, disappear upon heating, while the isolated, 'free' silanols, seen at $\sim$3750 cm^{-1}, remain. It is suggested by the authors that the active catalyst sites are the isolated silanols, and they function by either forming an activated ester or anhydride intermediate or *via* hydrogen bonding.[38] The application of a pyridine probe to a K60 silica sample activated at various temperatures and subsequent analysis by IR spectroscopy showed that the surface was either weakly Brønsted acidic, or that the pyridine was hydrogen bonded to the surface. As the activation temperature of the silica increases, the ability of the silica surface to hydrogen bond and its acidity decrease. No IR spectroscopic evidence for any strong Lewis or Brønsted acidity or basicity was found.

The hydrogen bonding ability was investigated further using molecular probes and analysing *via* ultra violet-visible (UV-visible) spectroscopy.[38] Three probes were used in these studies, Reichardt's betaine, 4-nitroaniline and *N,N*-diethyl-4-nitroaniline. The use of Reichardt's betaine and *N,N*-diethyl-4-nitroaniline showed that the surface hydrogen bond donating ability decreased as the activation temperature increased. This was to be expected as the surface is dehydroxylated. Further use of *N,N*-diethyl-4-nitroaniline along with 4-nitroaniline was used to study hydrogen bond accepting ability. Comerford reported that the ability to accept hydrogen bonds decreased up to 300-500 °C but then increased again with a maximum at 700 °C.[38] He proposed that this could be due to the increased dispersal of the silanols or from the structural relaxation of the siloxanes seen above 650 °C. Measurement of the polarisability, the ability of the surface to stabilise charge, showed a similar trend to the hydrogen bond accepting ability with a maximum at 700 °C. It is suggested by Comerford that this could be due to the formation of 'silanol nests' where a charge can be stabilised in three dimensions.[38]

Porosimetry measurements showed very definite trends, with the surface area, total pore volume and overall volume of nitrogen adsorbed decreasing but the pore diameter increasing as the activation temperature was increased.[38] The results from these measurements were unsurprising as the surface of the silica changes considerably during the activation process. The reason proposed for the increase in the pore diameter is the destruction of bottle neck type pores and disappearance of smaller pores. Scanning electron microscopy (SEM) mea-

surements showed no change in the particle size upon activation.[38]

However, these results give only a suggestion as to the mechanism of the silica catalyst and do not confirm any particular theory. At the beginning of this project it was intended that further mechanistic study of the activated K60 silica catalyst and of other silica-based catalysts would give more evidence to support one of the two mechanisms proposed so far; either hydrogen bonding between the acid and silica or formation of a silyl ester or anhydride intermediate.

2.2 Optimisation of the activated K60 silica-catalysed amide formation

The motivation behind this PhD project was to provide green, sustainable synthetic methods for use in the pharmaceutical industry as part of the European-wide consortium, Chem21. With this in mind, the project started with a short study of the reaction conditions used in the silica-catalysed amide forming reaction with the aim of identifying practical reaction conditions giving the highest yield, with minimal waste. The activity of the K60 activated silica catalyst was examined through a series of optimisation experiments using the previously reported reaction between phenylacetic acid **30** and aniline **48** as a benchmark.[21]
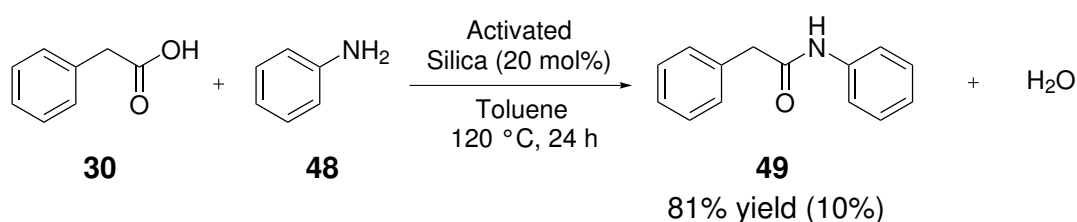
Scheme 16: Reaction between phenylacetic acid and aniline catalysed by activated silica; background reaction shown in parentheses.

As one of the principles of green chemistry involves energy efficiency, an attempt was made to lower the temperature of the reaction below reflux. The set temperature of the heating apparatus was varied from $20\,^{\circ}\text{C}$ to $110\,^{\circ}\text{C}$ in $20\,^{\circ}\text{C}$ intervals with each reaction conducted for 24 hours, and the results are shown in Table 2. As the reaction temperature was lowered,

it is apparent that the conversion decreases significantly with very little conversion seen below 100 °C which suggests a high temperature is essential for this system.

Table 2: Conversion of aniline by GC at a range of temperatures lower than benchmark reaction conditions. The temperature indicates the hotplate set point.

Temperature / °C	Conversion of aniline by GC [a] / %
20	4.0
40	6.0
60	6.6
80	16
100	48
110	67

[a] Conversion calculated using peak areas of aniline and tetradecane as an internal standard

Concentration of the reaction mixture was then varied with the aim of reducing solvent use. The model reaction had been performed at 0.6 mol dm^{-3} with respect to each substrate (12 mmol in 20 cm^3 solvent) and so solvent volume was varied between 30 cm^3 and 0.5 cm^3. Results, shown in Table 3, indicate that as the concentration is increased, the conversion to product increases, plateauing between 12 and 24 mol dm^{-3}. Conducting the reaction with no solvent at 110 °C gave a conversion of 50% indicating that a little solvent is useful, most likely allowing better mixing of the reagents and catalyst.
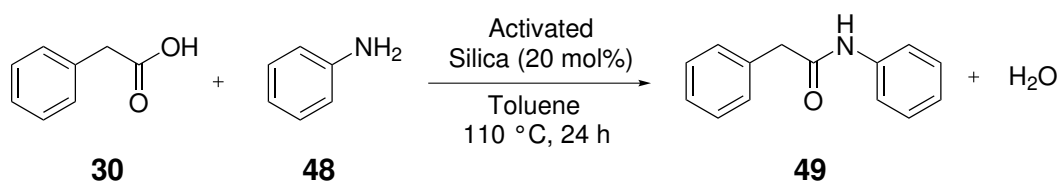
Scheme 17: Reaction between phenylacetic acid and aniline catalysed by activated silica.

Table 3: Dependence of concentration on the conversion of aniline **48** to 2,*N*-diphenylacetamide **49**, measured by GC.

Concentration / mol dm^{-3}	Conversion of aniline by GC [a] / %
0.4	15
0.6	42
0.9	36
1.2	46
2.4	60
4	66
12	73
24	74
neat	50

[a] Conversion calculated using peak areas of aniline and tetradecane as an internal standard

It was thought that, following on from the results of both the temperature and concentration studies, if the reaction temperature could be increased past the boiling point of toluene, as was seen with mesitylene by Comerford, conversion may increase further.[38] A study was undertaken on increasing the temperature of the solvent-free reaction up to 150 °C. Figure 9 shows a clear trend of the conversion of aniline increasing with temperature. The conversions, calculated from GC chromatograms, are thought to be unreliable due to difficulties sampling the reaction mixture. Sampling the mixture using either a glass pipette or needle resulted in the sample solidifying and caused difficulty in dissolution. Warming the glass pipette did not solve this problem. Some components of the mixture could have solidified faster than others resulting in an unrepresentative sample. This is thought to be quite likely given the negative conversions seen. However the results in Figure 9 show an obvious trend and so it was worth investigating further.
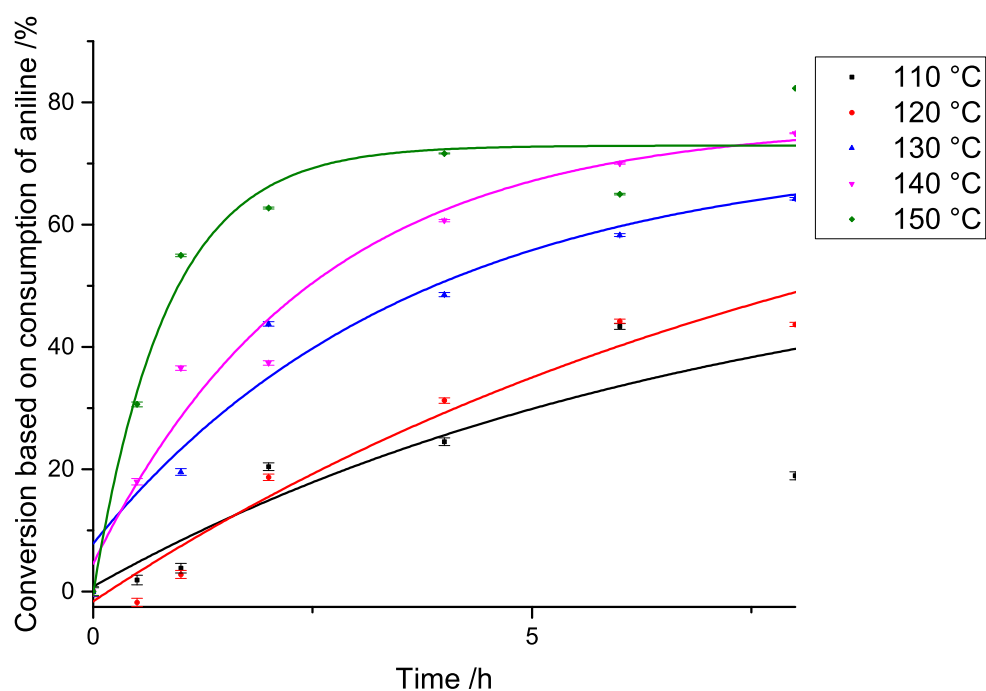
Figure 9: Graph showing the conversion of aniline to *N*-diphenylacetamide at five temperatures across a 24 hour time period. The negative conversion can be attributed to the difficulty sampling the reaction – the sample was not representative.

Due to the challenges encountered when sampling the reaction mixture for analysis by GC, it was decided to quench the reaction mixture with cold ethyl acetate after a specific time period to allow a representative sample to be taken. Solvent-free reactions from 120 °C to 150 °C (in 10 °C increments) were conducted as all the previous reactions, with the reaction quenched after 4 hours. An upwards trend was seen with increasing temperature (Table 4) and the conversions calculated were close to the conversions calculated for the model reaction after 24 hours. A further study at 140 °C showed that the increase in conversion was minimal after 4 hours, with 6 and 8 hours giving 74% and 77% conversion respectively.

Table 4: Conversion of aniline **48** to 2,*N*-diphenylacetamide **49** in solvent-free conditions after 4 hours at 4 temperatures; 120, 130, 140 and 150 °C.

Temperature °C	Conversion of aniline by GC [a] / %
120	57
130	62
140	73
150	77

[a] Conversion calculated using peak areas of aniline and tetradecane as an internal standard

Before any conclusions could be drawn from these results, it was necessary to examine the effect of the optimisation on the background reaction (i.e. in the absence of silica). A reaction was conducted at 140 °C under solvent-free conditions for 3 hours with no catalyst present and GC analysis showed a conversion of 86%. With this information in hand it was decided that the best conditions for the benchmark system were those shown in Scheme 16 where the catalyst is still effective and the use of solvent makes the reaction easier to handle.

A short study was conducted into the use of microwave heating rather than conventional heating in an attempt to significantly shorten the reaction time, thereby saving energy. This was done using the benchmark reaction and did not show much promise.
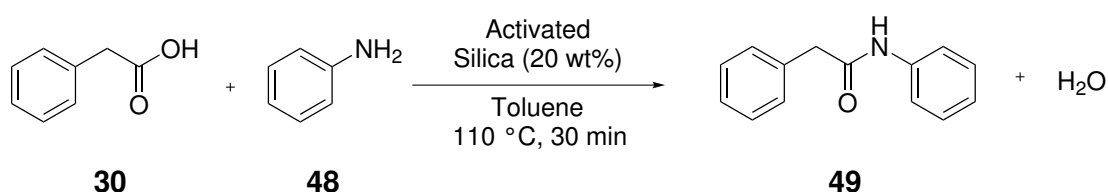
Scheme 18: Reaction between phenylacetic acid **30** and aniline **48** catalysed by activated silica, conducted at 3 mmol under microwave heating.

The standard conditions used in scheme 18 gave no product peak by GC which was attributed to the fact that toluene is not a good solvent for the absorption of microwave energy and the desired temperature was never obtained. It can be conclude from this experiment that the silica catalyst is not good at absorbing the microwaves. Addition of graphite and an increase in the temperature set point of the microwave helped significantly with heating;

150 °C was reached after 15 minutes and 18% conversion was obtained after 30 minutes. As with the optimisation using conventional heating, the reaction was attempted with no solvent. The reaction proceeded without problem but the same result was obtained — a significant background reaction was also seen and hence the catalyst was not necessary.

2.3   Investigation into other types of silica and alumina in amide forming reactions

From an industrial perspective, the cheaper and more available the materials in a process, the better. With this in mind, various types of silica were tested as catalysts using the benchmark reaction. The silica types chosen are used in bulk chemical manufacturing with a wide variety of uses. K60 silica is a high purity grade silica used for column chromatography with a pore size of 60 Å and a high surface area. Hi-sil 233D is an amorphous silica used as a reinforcing filler in rubber. Gasil AB725 is also an amorphous silica and is used in plastic films and as a food additive. Aerosil is a hydrophilic fumed silica, meaning it is produced by pyrolysis of $SiCl_4$ or quartz sand, with a surface area of 200 m^2 g^{-1}. It is used in cosmetics, paints, rubber, adhesives *etc.* Cabosil M-5 is fumed silica with a small particle size and large surface area. It is used in a variety of industries. The assumption was made that as K60 silica was most active after calcination at 700 °C, all other silicas would also be most active (or at least give a good comparison) having been calcined at 700 °C for 4 hours. All catalysts were activated at 700 °C before use and treated in exactly the same way to allow a fair comparison.

Table 5: The conversion of aniline **48** to 2,*N*-diphenylacetamide **49** using a variety of silica-based materials as catalysts.
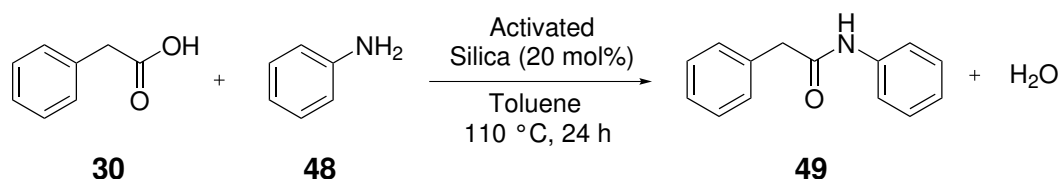
Silica Type	Conversion of aniline by GC / %
K60	78
Gasil AB725	54
Cabosil M-5	42
Hi-sil 233-D	33
Aerosil	26

Table 5 shows the conversion by GC of each system. Given that the background reaction for this system is low, the results were positive, with two of the catalysts giving between 40 and 55% conversion. As is clearly seen in the table however, K60 silica gave the best conversion for this reaction by a significant amount and so this was used for all further experiments in this thesis.

Following the publication of the use of an activated alumina balls catalyst for efficient amide formation,[26] it was decided to look further into the use of this catalyst and compare with standard aluminas and our silica catalyst. The interest in this catalyst came from results obtained previously in the group. Comerford *et al.* reported that zeolite catalysts became more effective as their Si : Al ratio increased so it seemed unusual that an alumina catalyst had such high activity.[21] Two reactions were used in this investigation, our standard benchmark reaction (Scheme 16, page 45) and one of the reactions published by Mukhopadhyay between heptanoic acid **45** and 4-chloroaniline **46** (Scheme 19).[26]
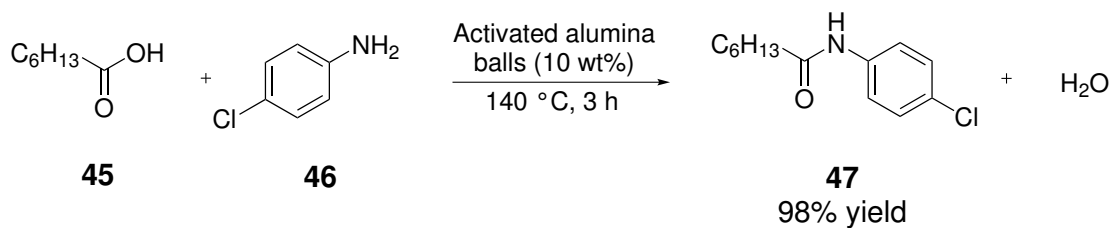
Scheme 19: Reaction between heptanoic acid **45** and 4-chloroaniline **46** catalysed by activated alumina balls.

Firstly, the catalyst was compared to neutral, basic and acidic alumina using the benchmark reaction between phenylacetic acid **30** and aniline **48** (Scheme 20). The alumina balls catalyst was used after activation at 700 °C as described in the literature.[26]
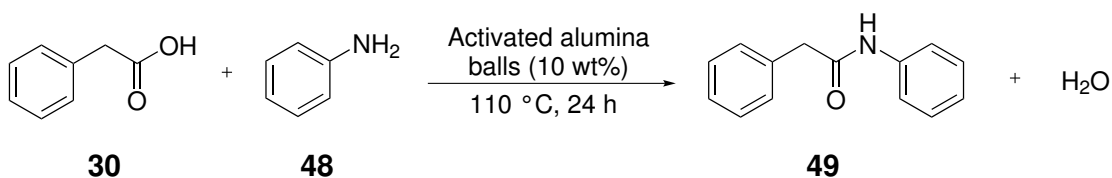
Scheme 20: Reaction between phenylacetic acid **30** and aniline **48** catalysed by activated alumina balls.

Table 6: Conversion of aniline **48** to 2,*N*-diphenylacetamide **49** by a selection of alumina catalysts.

Alumina Catalyst	Conversion of aniline by GC /%
Activated Alumina Balls	16
Neutral Alumina	9
Acidic Alumina	5
Basic Alumina	7

The acidic, neutral and basic alumina all showed very little activity in this reaction with conversions similar to the background reaction between phenylacetic acid **30** and aniline **48** (Table 6). The activated alumina balls catalyst showed only a marginally higher conversion of 16%.

Changing the reaction conditions to reflect that in the literature (140 °C with no solvent) improved the conversion to 55% in 3 hours, suggesting that temperature is important, as seen in section 2.2 with the silica catalyst. These reaction conditions were retained to examine the catalyst before activation which saw a higher conversion of 67%, while crushing the unactivated alumina balls gave a lower conversion of 46%. The lower activity of the crushed alumina balls suggests that the structure of the ball is important for its activity. There is also the possibility that the process of crushing the alumina balls has in some way changed the chemical structure of the alumina.

A different reaction, that between heptanoic acid **45** and 4-chloroaniline **46** was used to compare the activated alumina balls catalyst with the activated silica catalyst. The reaction conditions used were those described in the literature (shown in Scheme 19).[26] The conversions for each reaction are shown in Table 7.

Table 7: Conversion of 4-chloroaniline **46** by GC using a selection of catalysts.

Catalyst	Reaction Time	Conversion /%
Alumina Balls	3 h	31
Alumina Balls	24 h	76
Silica	24 h	76
None	24 h	73

Interestingly, following the reported protocol gave only a 31% conversion to amide product, not the 98% reported. Allowing the reaction to continue to 24 hours gave 76% conversion which was also seen with the activated K60 silica catalyst. The background reaction was reported in the literature as completely non-existent whereas we found that using the reported conditions at 140 °C for 24 hours, there was a significant background reaction and the catalyst was making very little difference.

The reactions were repeated in toluene at reflux with sampling at various time points and analysed by GC. Figure 10 shows the conversion over time, with silica catalyst giving a faster initial reaction rate and a slightly higher overall conversion. The activated alumina balls catalyst gives a curve very similar to the background reaction.
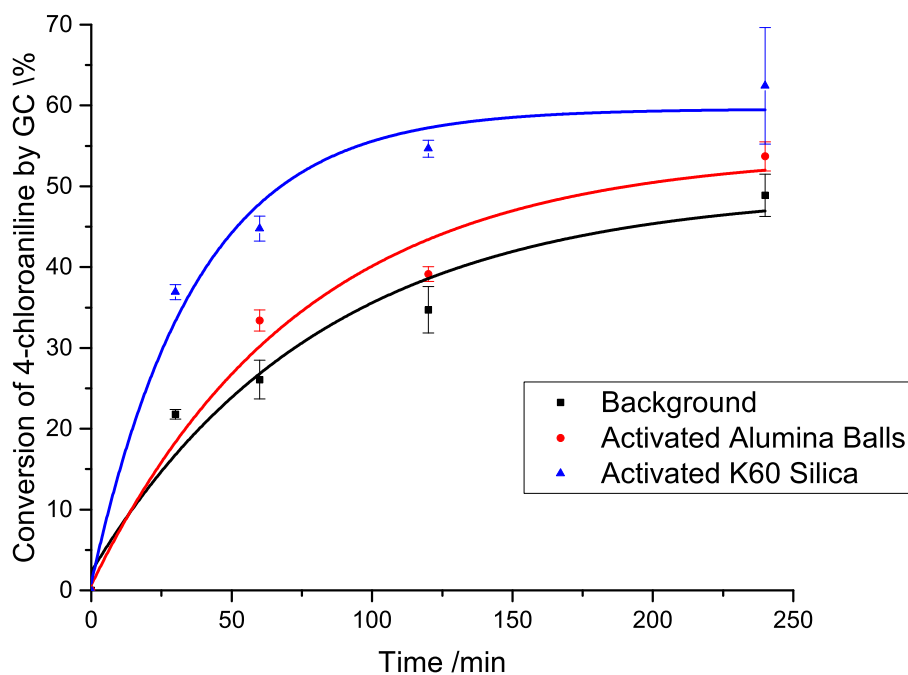
Figure 10: Graph showing the conversion of 4-chloroaniline **46** by activated alumina balls and activated silica across a 4 hour time period.

2.3.1 Analysis of Activated Alumina Balls

With these results in hand, it was interesting to see if IR, porosimetry and ICP-MS measurements could explain the differences in activity between the alumina catalysts.

Infrared analysis of two of the alumina materials, the activated alumina balls after crushing and the neutral alumina showed only a couple of small differences. Three small peaks were seen at 1573, 1460, and 1052 cm^{-1} in the activated alumina balls spectrum that were not present in the neutral alumina spectrum. These peaks could perhaps indicate the presence of other materials within the alumina or other aluminium-based groups which could be performing the catalysis.
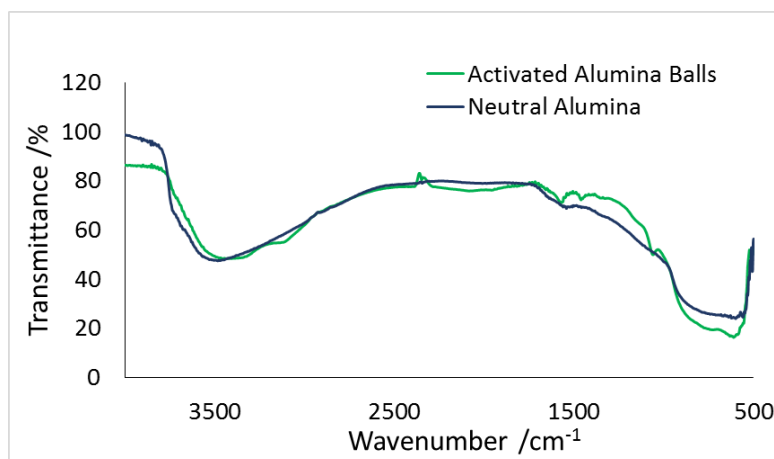
Figure 11: Overlaid DRIFT spectrum of activated balls and neutral alumina.

Similarly to silica, the comparison of surface area and pore volume of the alumina balls gave differing results after calcination. The surface area decreased from 348 m^2 g^{-1} to 150 m^2 g^{-1} suggesting some of the pores may be lost and showing that the surface must change considerably upon activation. Such a significant decrease in surface area could be due to the loss of material during calcination possibly resulting in a smoother surface and hence a smaller area. The total pore volume increased from 0.38 cm^3 g^{-1} to 0.47 cm^3 g^{-1}. This perhaps suggests there is something else in the pores possibly burnt out in the calcination, a theory supported by the ICP-MS results of the crushed alumina balls. Below are the elements making a significant contribution to the bulk material (>300 parts per million (ppm)).

Table 8: Proportions of elements measured in one sample of crushed alumina balls by ICP-MS in ppm and each calculated as a percentage of the total ppm elements.

Metal	ppm	%
Al	278400	97.77
Ca	407.2	0.14
Fe	309.4	0.11
Na	4199.8	1.48
S	563.0	0.20
Si	325.9	0.11

The table shows the elements detected within the sample in significant quantities. It is inter-

esting perhaps to note the presence of iron in the sample as it is well documented that iron-based Lewis acid catalysts are effective catalysts for amide bond forming reactions.[41,42] The high levels of sodium and calcium are also of interest as both sodium methoxide and calcium iodide have been found to be particularly good catalysts for amidation of esters.[43,44] Conversions by the two catalysts, pre and post calcination, are slightly different, the calcined alumina balls giving a slightly lower conversion in the reaction between phenylacetic acid and aniline. It is possible that there is some catalysis by a binder or metal impurity in the alumina balls which is destroyed or chemically altered during the calcination process. Further ICP-MS analysis of the calcined alumina balls and other aluminas may reveal some differences which could explain these results. It is interesting to note that the results published by Mukhopadhyay *et al.* gave the opposite conclusion, that the calcined catalyst was better than the untreated catalyst.[26] One possible explanation for this is that the catalysis is substrate dependent and, as with the silica catalyst, the properties of the pre and post calcination catalysts are suited to different substrates.

The investigation into the alumina balls catalyst shows that while the catalyst is active and efficient in certain cases, some care must be taken into determining the level of the background reaction under the conditions used. The mechanism of this catalyst is unclear and analysis by IR, porosimetry and ICP-MS has not helped uncover any concrete evidence about the mechanism. These techniques have confirmed that the activated alumina balls catalyst is not a simple alumina and have helped to identify some important considerations to keep in mind with these types of heterogeneous catalysts such as the presence of trace metals or contaminants in the pores.

2.4 Mechanistic investigation of silica-catalysed amide formation

The mechanism of the silica-catalysed amide forming reaction was proposed by Comerford (Scheme 21) and involves either hydrogen bonding between the isolated silanol group and the acid or formation of an anhydride followed by nucleophilic attack by the amine.[38] The support for these mechanisms came from the previously discussed IR work, which demon-

strated the hydrogen bonding ability of the silica using pyridine as a probe.
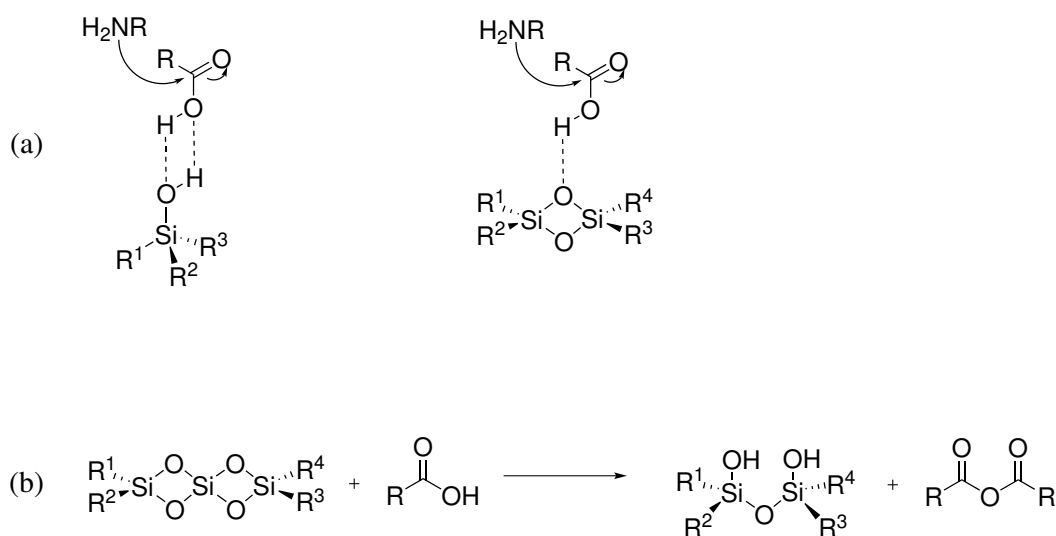
Scheme 21: Two mechanisms for the silica-catalysed amide formation reaction proposed by Comerford; (a) hydrogen bonding to either the silanol or the siloxane oxygen activates the acid for a nucleophilic attack by the amine; (b) the siloxane oxygens catalyse the formation of the more reactive anhydride which can then undergo nucleophilic attack by the amine.[38]

Some characterisation of the silica materials used in section 2.3 was carried out to try to identify the necessary properties for activity as a catalyst. In order to compare the results the catalysts were analysed by porosimetry and DRIFTS. Both of these techniques give information on the surface of the material. Porosimetry measurements can be used to calculate the surface area, pore volume and pore size, while DRIFTS can give information as to the functional groups present on the surface.

2.4.1   DRIFTS analysis of silica catalysts

DRIFTS analysis showed very little difference between the silicas. A sample spectrum of activated Gasil is shown in Figure 12. The most useful piece of information to be taken from the DRIFTS analysis is the sharp isolated silanol peak ($\sim$3747 cm^{-1}) which is present in all silicas. No silica tested showed any geminal or vicinal silanol peaks after activation at 700 °C as evidenced by the loss of peaks below 3746 cm^{-1}. This is to be expected as previous work in the Green Chemistry group showed the disappearance of these peaks upon activation of the silica.[38]
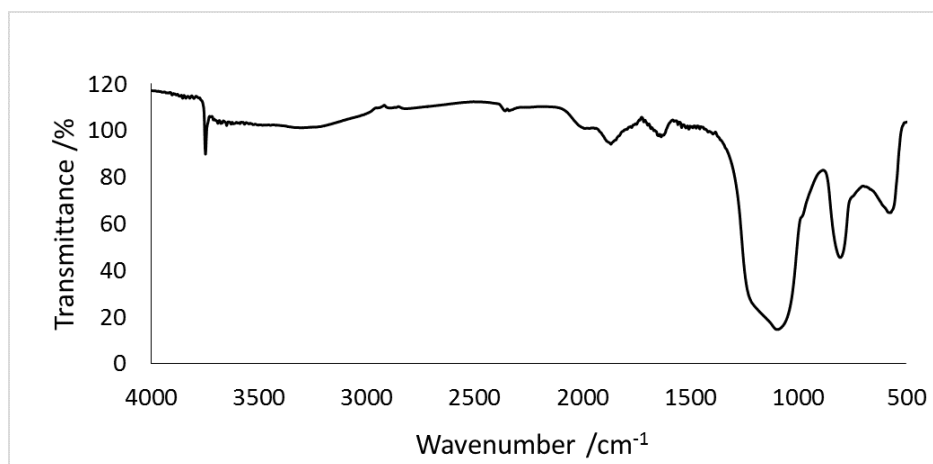
Figure 12: DRIFT spectrum of activated Gasil silica. Selected peaks: Isolated silanol (3747 cm^{-1}), Si-O-Si stretch (1080 cm^{-1}).

Use of Ammonia to Probe the Silica Surface

As DRIFT spectroscopy is useful for studying the bulk properties of a material, acetic acid was loaded onto the silica by heating at reflux in toluene, before removing the solvent and excess acetic acid *in vacuo*. This sample was analysed by DRIFT spectroscopy and was then subjected to a mixture of ammonia gas in nitrogen (approx. 10%). The aim of this experiment was to try to observe the reaction between acetic acid and ammonia on the surface of the silica and to see if IR spectra could give any more mechanistic detail.

Figure 13 shows the spectra obtained from this experiment. The results appear promising at first. The sample loading with acetic acid shows a peak at 1705 cm^{-1} and a broad band at 3187 cm^{-1}. As ammonia was flowed over the sample surface *in situ* both peaks are seen to disappear and a small peak appears at 2211 cm^{-1}. A small peak remains at 1705 cm^{-1} which does not disappear with heating.

58
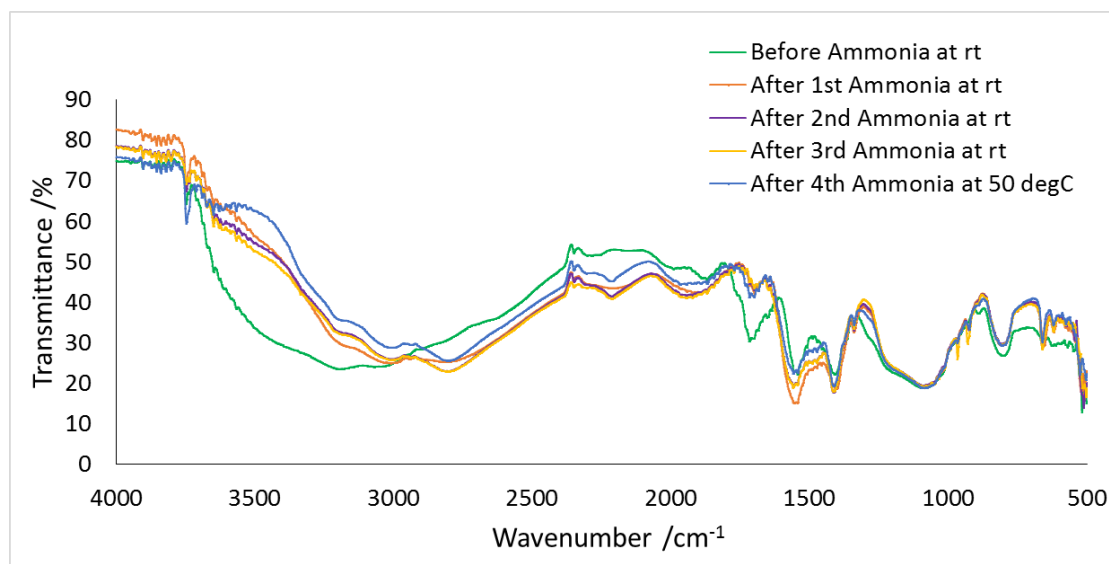
Figure 13: DRIFT spectra of activated silica treated with acetic acid taken before and after the addition of gaseous ammonia in nitrogen to the DRIFTS environmental chamber. Broad band at 3187 cm^{-1} and sharp peak at 1705 cm^{-1} seen to decrease over time.

At first it was thought that these changes in transmittance could be from the acetic acid reacting with the ammonia and being released from the silica surface. In order to support this theory, a control was done with the same batch of acetic acid-treated silica, but this time, it was treated only with nitrogen gas (Figure 14). The same changes were seen in the IR spectra and so it was concluded that the acetic acid is simply evaporating from the surface of the silica, aided by the flow of gas over the sample. The small peak that remains at 1705 cm^{-1} could be surface bound acetic acid but it was not possible to react it with the ammonia even when the temperature was increased to 50 °C.

Due to the volatility of acetic acid, the same experiment was conducted using phenylacetic acid. The initial IR spectra again showed a peak at 1713 cm^{-1} and broad band at 3460 cm^{-1} but also two sharp peaks at 2993 cm^{-1} (presumably the aryl C–H stretches of the acid) and 1386 cm^{-1}. This experiment was conducted as a control, flowing only nitrogen gas over the sample (Figure 15). Very little change was seen at room temperature, however as the sample was heated all of the peaks mentioned above disappeared and the sample closely resembled the spectrum of fresh silica catalyst when activated at 700 °C.
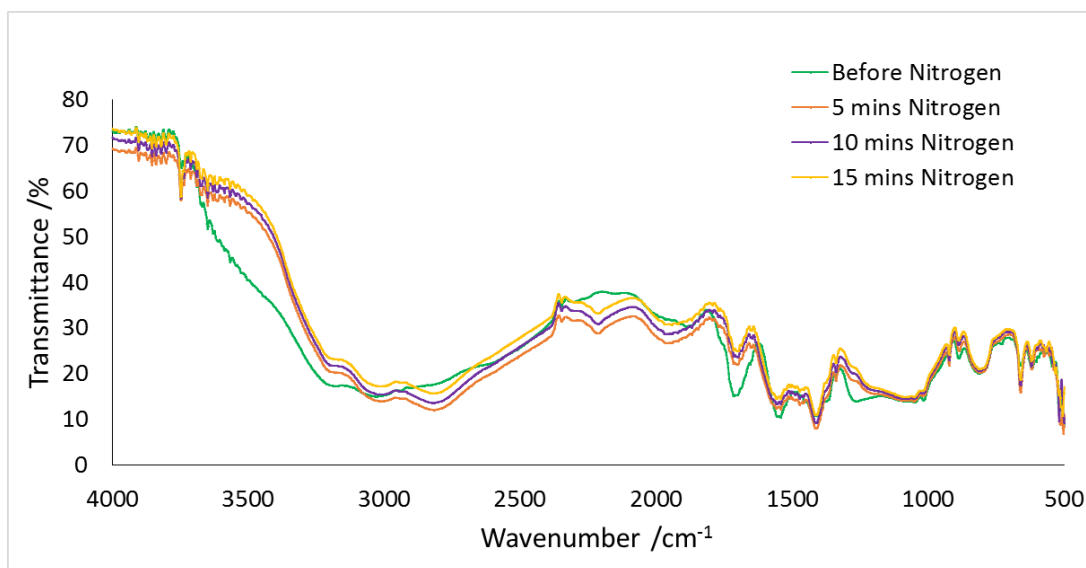
Figure 14: DRIFT spectra of the silica catalyst loaded with acetic acid. The green spectrum shows the silica catalyst loaded with acetic acid before being treated with nitrogen. Spectra were then recorded every 5 minutes with nitrogen flowing over the sample.
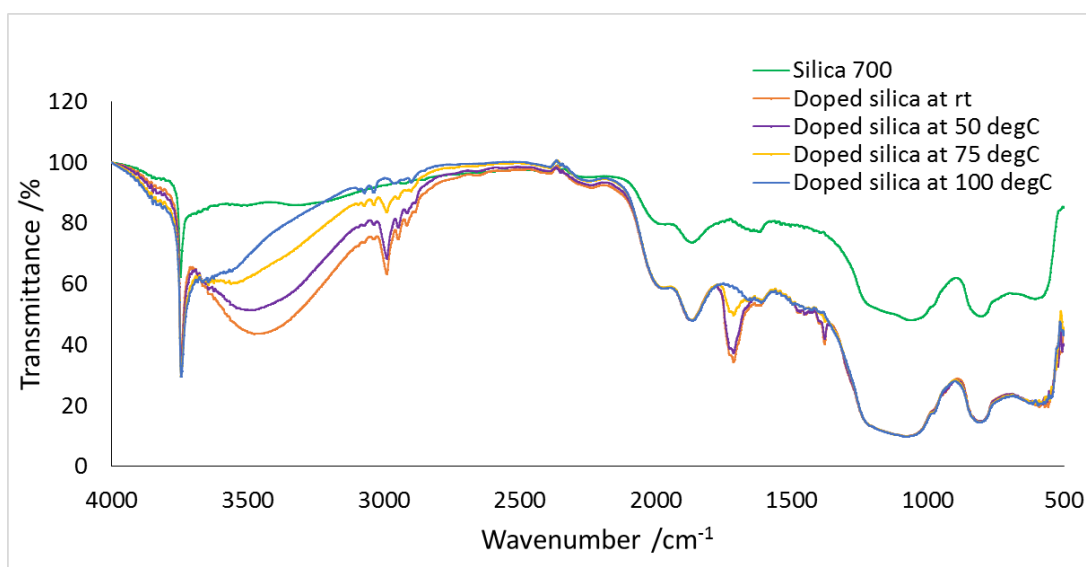
Figure 15: DRIFT spectra of the silica catalyst loading with phenylacetic acid. Spectra were recorded at room temperature, 50 °C, 75 °C and 100 °C with nitrogen flowing over the sample and compared with a spectrum of the fresh activated silica catalyst.

2.4.2 Porosimetry analysis of silica catalysts

Porosimetry analysis of each of the materials revealed significant differences in surface properties. These were the surface area, calculated using the BET theory; the total pore

volume, given as the cumulative volume of pores per gram of material, and the average pore radius. These results were compared with the conversion in the benchmark reaction (Scheme 16, page 45), and there were a few interesting results to be picked out.

Table 9: Relationship between the conversion and BET calculated surface area of silica materials used as catalysts.

Silica Type	Conversion /%	BET Surface Area / m^2 g^{-1}
K60 silica specification	-	500
K60 silica	78	325
Gasil AB725	54	178
Cabosil M-5	42	186
Hi-sil 233-D	33	109
Aerosil	26	167

Firstly in a comparison of the porosimetry results of the calcined K60 silica catalyst with the literature specification of commercial K60 silica, surface area was found to decrease upon calcination from 500 to 325 m^2 g^{-1} (Table 9). The measured total pore volume also decreased slightly from 0.75 to 0.62 cm^3 g^{-1} (Table 10). As the conversion increases when the K60 silica is activated,[21] these results could suggest that a lower surface area and smaller total pore volume give increased activity.

The two highest yielding silicas (K60 and Gasil) had a difference of 24% in the conversion of aniline and the results obtained from the porosimeter may be used to suggest a reason for this difference. The surface area for Gasil was almost half that of K60 while the total pore volume and pore radius were larger. This could suggest a balance between pore size and surface area is needed for efficient catalysis.

Table 10: Desorption total pore volumes and average pore radii for the tested silica materials.

Silica Type	Conversion /%	Desorption Pore Volume /cm^3 g^{-1}	Pore radius (desorption) /Å
K60 silica specification	-	0.75	-
K60 silica	78	0.62	28
Gasil AB725	54	0.84	68
Cabosil M-5	42	0.57	94
Hi-sil 233-D	33	0.80	183
Aerosil	26	0.55	105

Comparing the silicas that gave poorer conversions in the benchmark reaction with Gasil, it is clear that their surface area is not a contributing factor as in most cases the surface area is very similar. Looking at the pore sizes, (Table 10), it becomes immediately apparent that while there is no trend in the total pore volume, there is a very clear trend in pore radius. The three materials with the lowest conversions in the benchmark reaction have much larger pore radii. A more detailed look into the pore radius distribution (Figure 16) revealed that the peak of the distribution curve, in all three cases, had a maximum between 200 Å and 300 Å but had a large distribution of pore radii suggesting that these materials are very disordered and may have a more uneven surface resulting in the larger pore radii. These materials will have very small particles with voids between them which will fill with nitrogen under porosimetry conditions, giving a wide range of apparent pore sizes. Compared with these silicas, K60 silica and Gasil have a narrower distribution of pore size. The radii range from approximately 20 Å to 60 Å with a sharp peak in the graph. These are ordered silicas and would most likely be more suitable as catalysts, as they would have lots of similar active sites available and would perhaps have the highest number of active sites.

In this investigation, total pore volume was not particularly helpful. As a parameter it did not help to highlight any trends and it gives very little information on the structure of the silica, *i.e.* whether the material contains lots of small pores or fewer large pores.
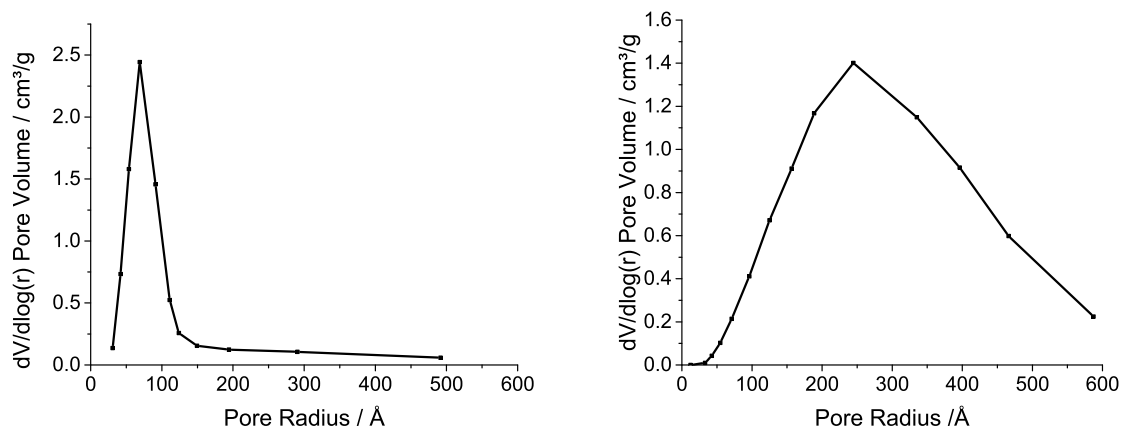
Figure 16: The pore distribution of Gasil and Hi-sil showing a very narrow distribution for Gasil (left) and a wide distribution of pore size for Hi-sil (right). These graphs are representative of the other materials as described in the text.

Logically, the pore size must be large enough to accommodate the substrate or, depending on the mechanism of the reaction, both substrates. The trend in pore radius, when examining the data for all catalysts tested, would suggest that smaller pores are more desirable for an active catalyst. However, as no materials with smaller pore sizes than the K60 silica have been tested, it is not possible to determine if there is an optimum pore size. From the data obtained, it could be envisaged that a larger surface area would, presumably, contain a larger number of isolated silanols available for catalysis and therefore would be desirable in a catalyst. All materials tested were mesoporous and contained no micropores.

Given that a variety of silicas with differing combinations of surface area and pore size have been examined, it may be prudent to conclude that there are many factors which affect the activity of these heterogeneous catalysts. It is likely that the isolated silanol content of the silica is important given that it is the proposed active site and the data presented above shows that the pore radius and the distribution of the pore radii may have a significant impact. In order to really test the significance of surface area and pore volume, it would be necessary to prepare silicas with identical (or very similar) surface areas and varying pore volumes and *vice versa*.

2.4.3 Solid-State NMR Analysis

In an attempt to investigate the active site of the silica catalyst, three silica samples were analysed by solid-state ^{29}Si MAS NMR. This shows the relative proportions of the different Si environments; Q2, a silicon atom attached to two hydroxyl groups; Q3, a silicon atom attached to one hydroxyl group, and Q4, a silicon atom with no hydroxyl groups attached (Figure 17).[45]
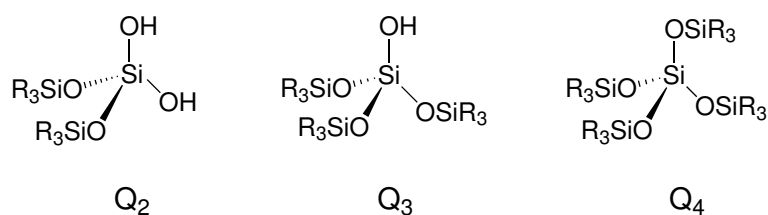
Figure 17: Three different silicon environments seen in ^{29}Si NMR.
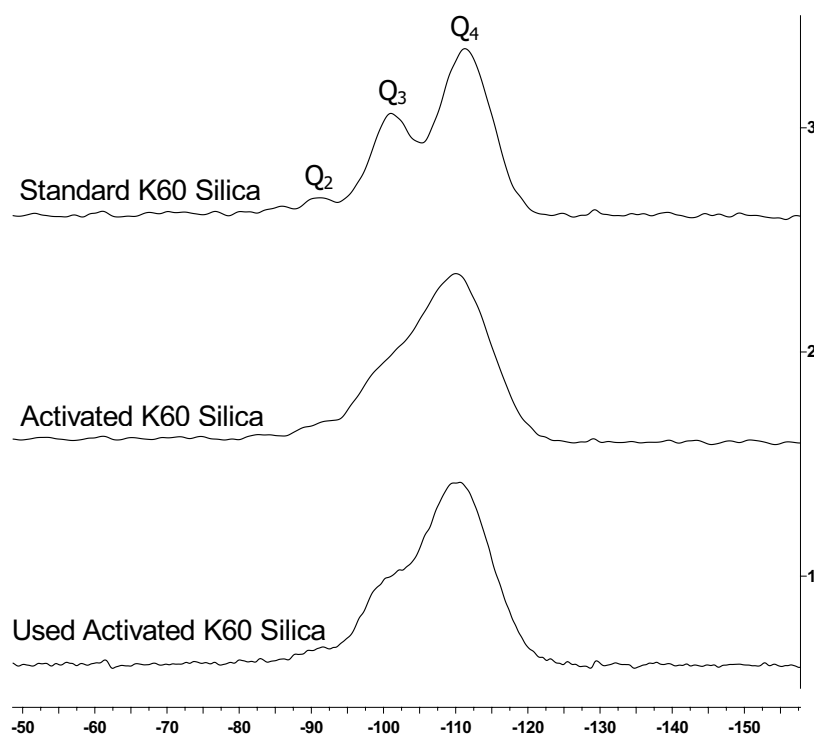
Figure 18: ^{29}Si NMR of three silica samples.

Table 11: The relative proportions of the different silicon environments in the three samples calculated after deconvolution of the NMR spectra.

Sample	Relative proportions of Si environments /%		
	Q2	Q3	Q4
Standard K60	4.1	29.4	66.5
Activated K60	1.8	25.0	73.2
Used K60	2.5	20.5	77.0

The results from this experiment do not give us much information. They suggest there is a drop in the number of Q2 environments upon activation of the silica which fits with both mechanisms proposed by Comerford.[38] There is also, however, a drop in the number of Q3 environments suggesting that, if no other properties affect the activity, unactivated K60 should have slightly higher activity. The number of Q4 environments is expected to increase as the OH groups are removed from the Q2 groups and the Q3 groups are surrounded by siloxanes. Interestingly, the proportion of Q3 groups drops again after the catalyst has been used, with the proportion of Q2 groups increasing. This perhaps suggests that the catalyst will deactivate over time. The proportion of Q4 groups does not drop after use which provide proof that the silica does not act as a desiccant. In such a case, the Q4 groups would be expected to decrease as the siloxanes were opened and the Q3 groups increase.

2.4.4   Thermal Gravimetric Analysis

It has been suggested that the silica catalyst acts as a desiccant in the condensation reaction between acid and amine. Following a large scale reaction, the spent silica catalyst was analysed by thermal gravimetry. The sample was heated to 300 $^\circ$C and the drop in mass measured. The balance showed a drop of 2.26% when the sample was heated. From a 50 mg sample, this means 1.13 mg water was adsorbed. Scaling this up to the full reaction, there would have been 0.1 g water adsorbed on to the silica, far less than the 1.48 g released in the reaction. This small amount suggests that the silica is not acting as a desiccant; however as there was a delay between reaction and analysis combined with the fact that the reaction

was done using a Dean-Stark apparatus which collected the water produced this result is not particularly reliable and more work is required to confirm this theory.

2.4.5 Conclusions

Examination of the reaction conditions for the silica-catalysed amide bond formation provided some insight into general conditions for amide bond formation and it was observed that measuring the level of the background reaction is important when looking at these catalytic reactions as temperature can affect the background reaction significantly. The use of a variety of silicas as catalysts, with the aim of making the catalyst even cheaper and more readily available, showed that K60 silica was by far the best catalyst, however, some of the other silica catalysts also gave promising, moderate yields. Infrared spectroscopy did not give any information as to the properties of an effective catalyst but porosimetry analysis did provide some information as to the desirable physical properties of a silica catalyst, particularly as the activated K60 silica has the largest surface area and smallest pore radius with a narrow distribution.

Analysis and testing of activated alumina balls as a catalyst using two reactions showed that they contained a significant amount of trace metal impurities which could contribute to catalytic activity. The background of the reported reaction between heptanoic acid **45** and 4-chloroaniline **46** using this catalyst was significant and in the benchmark reaction between phenylacetic acid **30** and aniline **48**, the catalyst was not as effective as the literature results indicated it should be.

A DRIFT spectroscopy study on the catalyst loaded with acetic acid or phenylacetic acid **30** allowed the observation of an acid carbonyl band. The spectra obtained suggest that a small amount of acetic acid may be bound to the silica surface however it was not possible to react it with ammonia gas *in situ*. Heating of the sample containing phenylacetic acid **30** to 100 °C resulted in loss of the acid.

Analysis of the activated silica catalyst by ^{29}Si NMR showed a small difference in the proportion of the Q2, Q3 and Q4 environments which confirms that the catalyst is changing upon activation and it also suggests that the catalyst does slightly deactivate over time. Ther-

mal gravimetric analysis showed very little water physisorbed on to the surface of the silica after use and provided a little evidence that the silica is acting as a catalyst and not a desiccant.

Chapter 3

Expansion of the substrate scope of silica-catalysed amide formation reactions

3.1 Introduction

The substrate scope of the silica-catalysed amide formation reaction has been investigated by Comerford *et al.*[21] A small number of amines and acids were tested in the reaction, shown in Figure 19. Generally, the catalysed reaction gave very good yields of amide product, though some of the substrates required 50 wt% silica catalyst. Compared to some metal-catalysed reactions (with a typical loading of 5-10 mol% catalyst) this reaction used a high catalyst loading, however as the catalyst is formed from cheap chromatographic silica and is easily recovered and reusable this may not be considered a significant limitation.

A further paper, published in 2012, detailed the use of structured silicas, called Santa Barbara Amorphous (SBA) as more efficient catalysts (Figure 20).[46] A lower catalyst loading was required and all catalysts could be used in a flow system, with the SBA catalysts significantly reducing the reaction time.
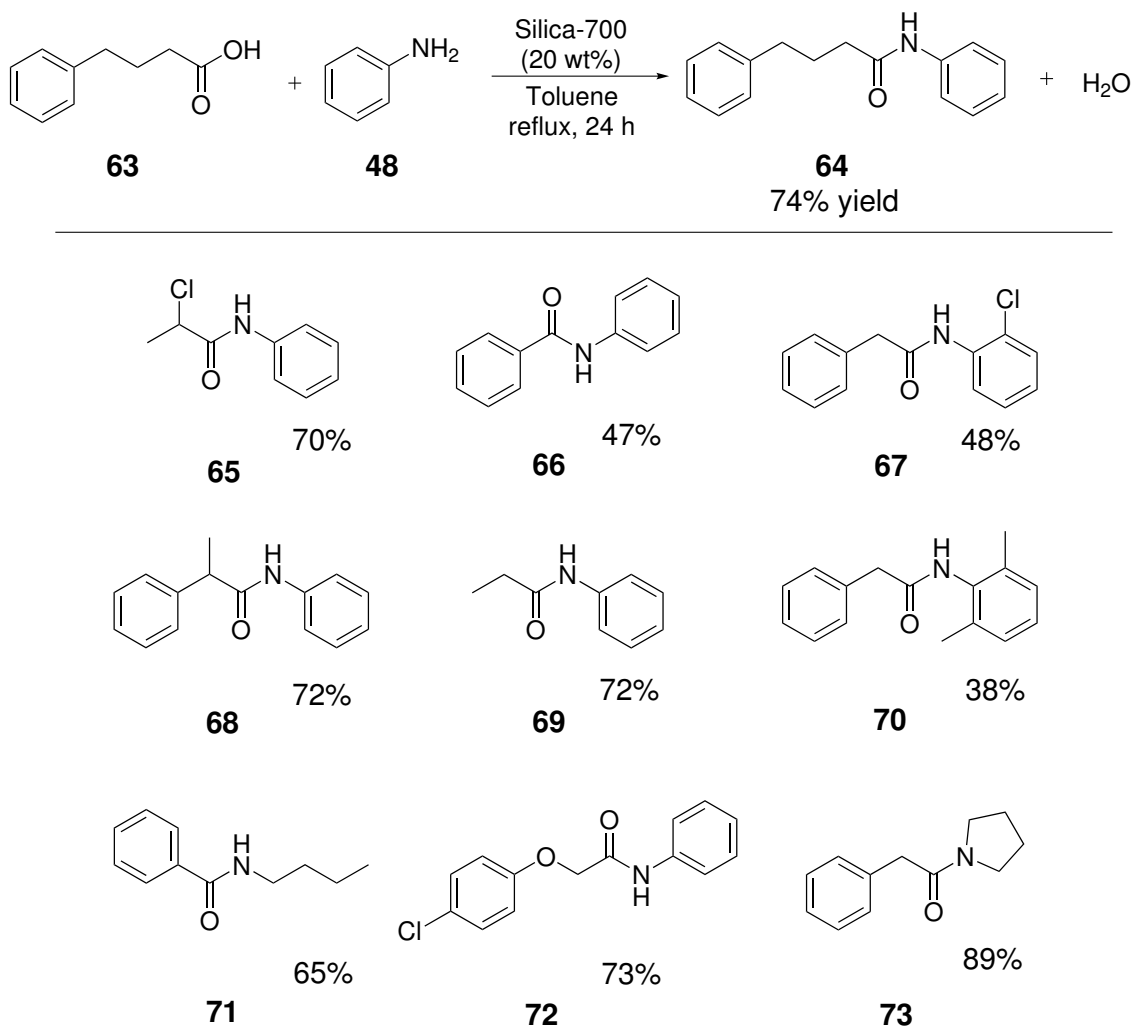
Figure 19: Example scheme of the silica-catalysed amide formation and previous substrate scope with yields of isolated compounds.[21]

The substrates tested, with both K60 silica and SBA, were all simple aromatic and aliphatic acids and amines. The initial aim of this project was to extend the scope of the silica-catalysed amide formation to target more complex acids and amines of interest to the pharmaceutical industry. The work was done in collaboration with Glaxo Smith Kline (GSK) and Pfizer and this chapter details the efforts made at the University of York to expand the substrate scope past these simple acids and amines. Care was taken to compare the catalysed reactions with their background reactions, that is with no silica catalyst present, to measure the thermal effect on the conversion of acid and amine to amide. It is important to measure these background reactions as surprisingly high conversions have been seen with no catalyst present.[47]
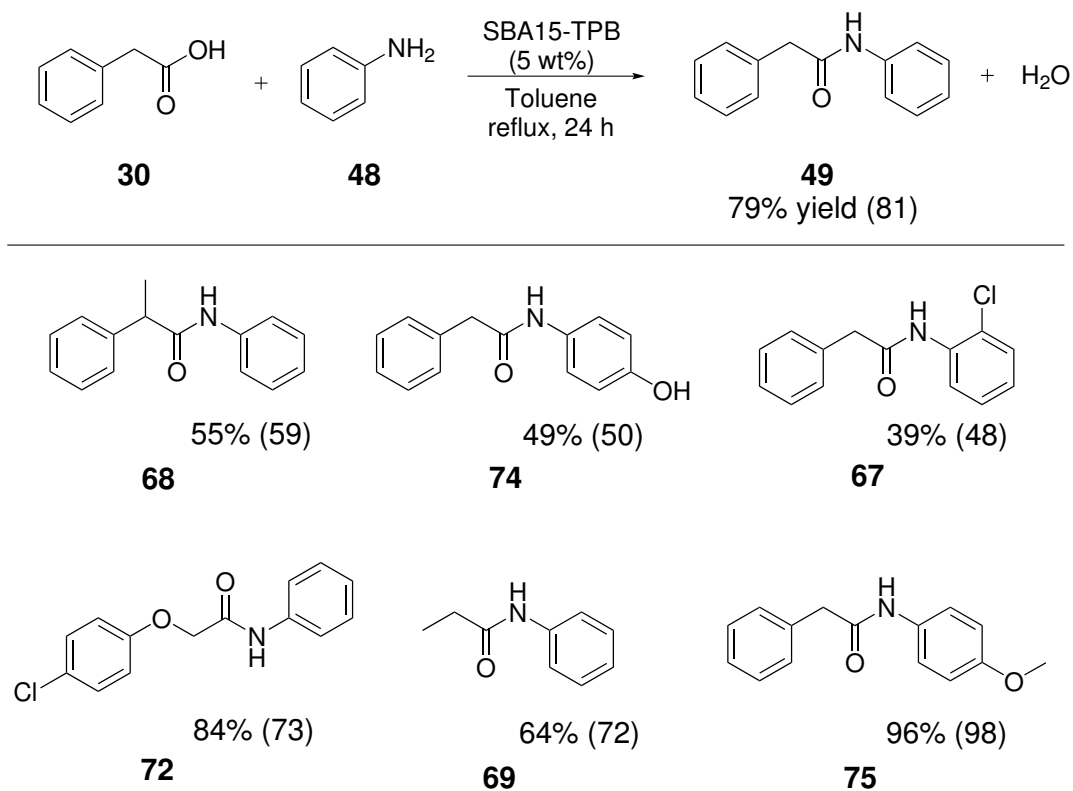
Figure 20: Example scheme of SBA-catalysed amide formation and substrate scope with yields of isolated compounds. Yields in parentheses are from reaction catalysed by K60 silica.

3.2   Synthesis of isoniazid by silica catalysis

Isoniazid **76** is an important drug for the treatment of tuberculosis (TB), a disease that is most prevalent in developing countries where access to medicines is difficult. Green, inexpensive processes for making the essential medicines required for these countries are needed to encourage pharmaceutical companies to manufacture these drugs at little gain to themselves. The sustainability of a process can quite often go hand-in-hand with the expense as waste disposal can add to the overall cost of a process.[48] Isoniazid is a prodrug that works by binding with the co-factor nicotinamide adenine dinucleotide (NAD), and this NAD-bound compound inhibits enzymes in the Mycobacterium tuberculosis.[49] It is proposed to inhibit two enzymes, InhA, an enoyl reductase enzyme,[50,51] and KasA, a ketoacyl synthase enzyme,[52] both of which are involved in the type II dissociated fatty acid biosynthesis pathway. Isoniazid inhibits the biosynthesis of mycolic acids, which are part of the bacterial cell

wall. Studies to determine the mode of action of isoniazid and the mode of drug resistance of the bacterium have involved compound **77** which is an isoniazid-NAD adduct that contains the head group of NAD and is shown to inhibit InhA *in vitro*.
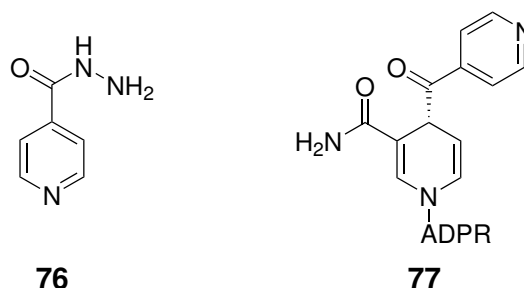
Figure 21: Isoniazid **76** and NAD-bound isoniazid **77**: the active drug.

Two procedures are reported in the literature for the synthesis of isoniazid **76**. The first, reported in 1912, begins with the oxidation of γ-picoline **78** followed by an acid chloride formation.[53] The acid chloride is then reacted to give an ester **80** which undergoes amidation with hydrazine monohydrate **81**. This is a five-step process to make a simple molecule. Currently, isoniazid is industrially synthesised from 4-cyanopyridine **82**, reacting with a base then hydrazine to give the final product **76** in two steps.[54]
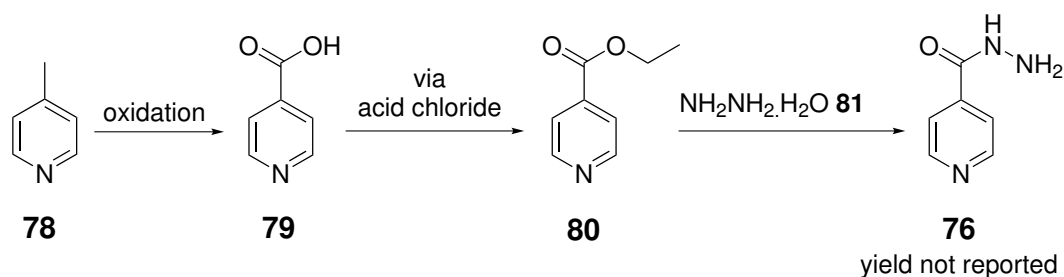
Scheme 22: Synthesis of isoniazid from γ-picoline **78**.[53,54]
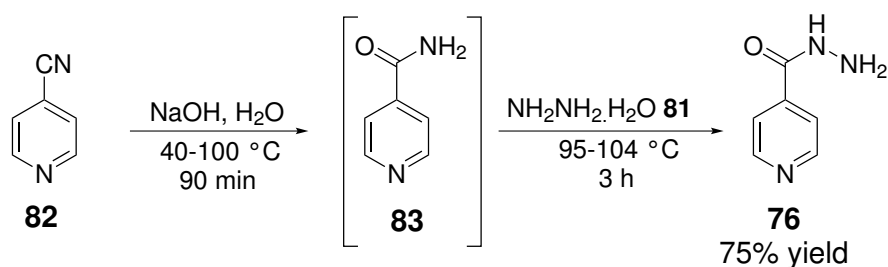
Scheme 23: Synthesis of isoniazid from 4-cyanopyridine **82**.[54]

The aim in this section of the project was to synthesise isoniazid **76** directly from isonicotinic acid **79** and hydrazine **81** using the activated silica catalyst (Scheme 24). This could then be compared to traditional methods of synthesis using green metrics. Beginning the synthesis with isonicotinic acid rather than 4-cyanopyridine would be slightly advantageous as the isonicotinic acid is slightly less hazardous (LD50 of 5000 mg/kg), labelled only as an irritant while 4-cyanopyridine is labelled as harmful (LD50 of 710 mg/kg).[55–57]
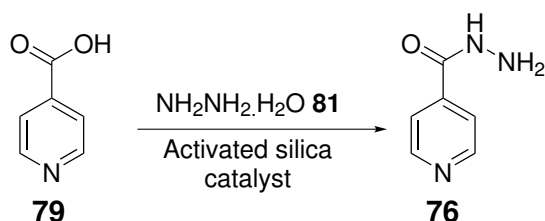
Scheme 24: Intended synthesis of isoniazid **76** from isonicotinic acid **79** and hydrazine **81** using an activated silica catalyst.

3.2.1 Optimisation of isoniazid synthesis

The first reaction used the standard conditions developed by Comerford *et al.*[21] with K60 silica activated at 700 °C at a loading of 20 mol% in toluene. This reaction gave a promising yield of 18% isoniazid with 78% purity by ^{1}H NMR spectroscopy. The product was contaminated with starting material, as the purification proved difficult due to the similar solubilities of the compounds. It was anticipated that increasing the conversion of the reaction would simplify the purification.
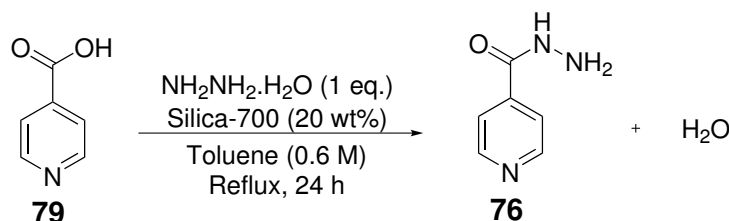
Scheme 25: Reaction conditions for the initial examination of silica-700 as a catalyst in the synthesis of isoniazid **76**.

The analysis of the reaction mixtures by ^{1}H NMR spectroscopy proved to be problematic. Solubility of both starting materials and products meant that only D_2O or DMSO could be

employed as solvents. It became apparent that the peaks corresponding to the pyridyl protons shifted depending on the amount of water contained within the NMR sample in DMSO and it was not possible to accurately identify the starting material and product peaks. The same problem was seen in D_2O when the starting material and product were doped with hydrazine. Following this realisation, it was decided that the most reliable way of analysing the reaction mixtures was by SFC (supercritical fluid chromatography). The starting material and product were both well resolved by this method and conversions are easily obtained. A repeat of the initial silica-catalysed isoniazid synthesis reaction gave a conversion by SFC of 17% so the method was considered reliable.

The background reaction for the isoniazid synthesis gave a conversion by SFC of 23% which certainly suggests the silica catalyst is not effective in this transformation. Conducting the background reaction without silica catalyst but with 4 Å molecular sieves gave only 5% conversion. Molecular sieves can be advantageous in amide formation reactions as the removal of water will push the equilibrium of the reaction towards the product. In this case they seem to be hindering the reaction; perhaps they are removing hydrazine as well as water.

The use of Dean-Stark apparatus in amide-bond forming reactions is common as the removal of water often pushes the reaction to completion.[58] When applying this technique to isoniazid formation using the silica catalyst, it was not successful. More than four species were observed by analysis of the ^{1}H NMR spectrum though these species have not been identified. The compounds have sets of two peaks with characteristic AA$'$XX$'$ coupling patterns in the aromatic region. It is possible, given that the boiling point of hydrazine monohydrate is 120 °C and its density is 1.02 g cm^{-3}, that some hydrazine could be removed along with the toluene and water and is then collected in the Dean-Stark. Taking into account the water in the hydrazine, 60 mmol of water was expected to be collected in the Dean-Stark receiver, assuming that the reaction (on a 30 mmol scale) went to completion. In total, 83 mmol of a water miscible liquid was collected in the reaction which suggests that there was either no starting material left (unlikely given the results seen throughout this section) or that the water collected also contained hydrazine. A lack of hydrazine in the reaction could cause undesired side reactions, such as the reaction of the product with another molecule of isonicotinic acid, as the product contains a reactive NH_2.

Optimisation of the reaction, to develop a method using a silica catalyst that would be effective and efficient in the synthesis of isoniazid, was begun by examining the catalyst loading of the silica-700 (Table 12). Increasing the catalyst loading from 20 wt% to 50 wt% almost doubled the conversion of isonicotinic acid while increasing the catalyst loading to 100 wt% caused a slight, but not notable, increase in the conversion. From these results it can be seen that the silica catalyst does make a difference in the reaction though the conversions are still modest.

Table 12: Effect of changing the catalyst loading of silica-700 on the conversion of isonicotinic acid **79** to isoniazid **76** run in toluene at 110 °C for 24 hours (Scheme 25).

Catalyst Loading /wt%	Conversion /%
20	17
50	33
100	38

While keeping the catalyst loading at 50 wt%, it was decided to focus on the solvent as isonicotinic acid is not particularly soluble in toluene. Solubility in toluene is not the only problem as toluene is considered as a solvent that green chemistry groups would prefer to replace. It has been labelled as problematic by the Chem21 consortium due to its reproductive toxicity and low flash point.[59] A selection of green solvents were chosen with boiling points ranging from 80 °C to 106 °C. Methyl tetrahydrofuran (Me-THF), water and DMSO were not suitable solvents in this reaction and gave no conversion. Water and DMSO are perhaps unsuitable due to the addition of water affecting the reaction equilibrium. *t*-Butyl acetate gave a modest conversion of 24% while cyclopentyl methyl ether (CPME) gave the best conversion of 41%. CPME has a boiling point close to toluene which perhaps explains the conversion seen. The lowest boiling point of the organic solvents was Me-THF which, similarly, perhaps explains the lack of conversion. Based on the results in Chapter 2, the conversions do not improve much past 8 hours so it is not thought that the conversion of the lower temperature reaction would improve with longer reaction times.
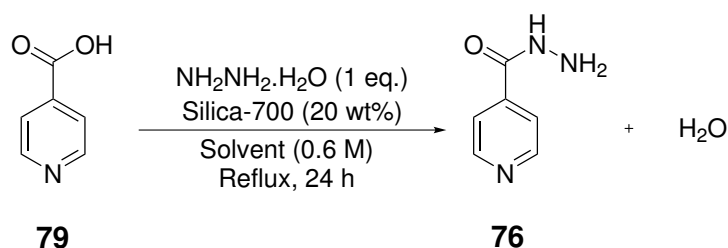
Scheme 26: Reaction conditions used for testing solvents in the synthesis of isoniazid **76**.

Table 13: Effect of changing the solvent on the conversion of isonicotinic acid to isoniazid under the conditions in Scheme 26.

Solvent	Conversion /%
Toluene	33
CPME	41
Me-THF	0
t-BuOAc	24
Water	0
DMSO	0
None	17

Given that temperature seemed to play an important part in the conversion of isonicotinic acid to isoniazid, it was thought that increasing the temperature above the boiling point of toluene may help to increase the conversion to a more useful level. A new solvent was again chosen, xylene, which would allow the reaction to be increased to 130 °C. Xylene has a structure similar to toluene but has a higher boiling point and can be a bio-based solvent.[60]

The temperature was first increased to 120 °C and analysis by SFC showed three peaks instead of the expected two. The third peak could be a diacylated product as isoniazid itself has a primary amine group available for reaction with a second equivalent of carboxylic acid. It was not possible to isolate and analyse this compound or to synthesise a pure diacylated product for comparison. The addition of two equivalents of hydrazine did not solve this problem and three peaks were again seen by SFC. Increasing the temperature to 130 °C produced a similar result. This could also explain the result seen with the Dean-Stark appa-

ratus as the reaction has to reflux vigorously. All of these results suggest that the temperature must be slightly below the reflux point of toluene in order to achieve selectivity in the reaction. This could be related to the retention of the hydrazine in the liquid at the bottom of the vessel to suppress side reactions as previously mentioned.

Hydrazine can be purchased at various concentrations and as a hydrochloric acid salt. Increasing the equivalency of hydrazine monohydrate to 1.5 with one equivalent of isonicotinic acid showed a slight increase in the conversion to 25% by SFC. Both the background and the silica-catalysed reaction were conducted in toluene at reflux using the HCl salt of hydrazine but neither provided any conversion and only isonicotinic acid was seen at the end of the reaction. All of these reactions, while showing some promise, only gave moderate conversions and a new strategy was needed if this method was to be viable from an industrial perspective.

To this end, a new catalyst was considered and Table 14 shows the results. It is immediately apparent that changing to a K60 silica catalyst activated at lower temperatures, in this case 300 °C, was promising. The use of K60 silica which was untreated gave a conversion of only 10%, lower than that of the background reaction.

As the activation temperature of the silica-300 is much lower than the standard silica catalyst and it is known that the activation process is much easier to reverse below 650 °C,[61,62] it was thought that the silica could possibly be acting as a desiccant, absorbing the water in the reaction mixture and returning to its untreated state. It was interesting then to see if the silica-300 could act as a desiccant while the silica-700 performed the work of a catalyst. To test this theory, a reaction was conducted using 25 wt% of silica-300 and 25 wt% of silica-700 which gave only 10% conversion of isonicotinic acid by SFC. This suggests that the silica-700 is not a suitable catalyst and that a high loading of silica-300 is required.
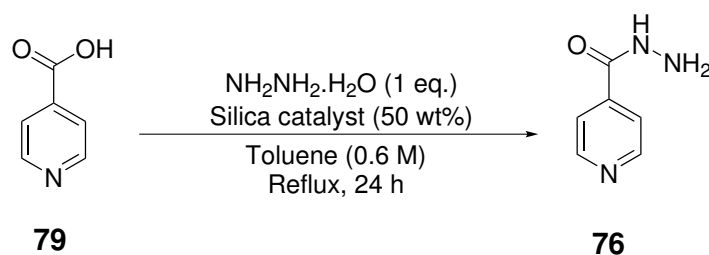
Scheme 27: Reaction conditions used for testing a variety of silica materials as catalysts in the synthesis of isoniazid.

Table 14: Use of K60 silica activated at different temperatures as catalysts in the reaction of isonicotinic acid **79** to form isoniazid **76** as in Scheme 27.

Catalyst system	Conversion /%
None	23
Silica-300	43
Silica-rt	10
Silica-300, 700[a]	10

[a] 25 wt% of silica-300 and 25 wt% of silica-700 used.

This investigation was continued by looking at the catalyst loading of the silica-300 (table 15). Between 10 and 50 wt% there was very little difference with the conversions being 46% and 44% respectively. A slight increase in conversion was seen both when the catalyst loading was increased to 100 wt% and when the reaction was conducted under a nitrogen atmosphere. The reason for testing the reaction under a nitrogen atmosphere was that using hydrazine in an industrial setting poses a significant risk due to its high toxicity and these reactions are usually carried out under inert conditions. The results show that the reaction could be carried out under an inert atmosphere without a reduction in conversion.
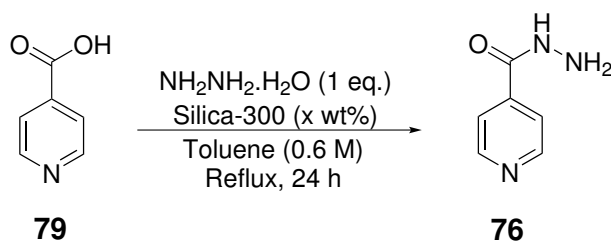
Scheme 28: Reaction conditions used for examining the catalyst loading of silica-300 in the synthesis of isoniazid **76**.

Table 15: Effect of increasing the catalyst loading of silica-300 on the conversion of isonicotinic acid to isoniazid under the conditions shown in Scheme 28.

Catalyst Loading /wt%	Conversion /%
10	46
20	39 [a]
50	44
50[b]	58 [a]
100	53

[a] These conversions are approximate as there were side products detected by SFC analysis that could not be quantified. [b] This reaction was conducted under a nitrogen atmosphere.

As the conversions in Table 15 do not vary a great deal, an investigation into the stability of the silica-300 catalyst was begun. Previous experiments had been carried out using silica that was activated and then kept in a desiccator for up to one week. If the silica-300 acts as a more efficient desiccant than the desiccant used to keep it dry, it may be deactivating faster than hoped. In order to test this theory, silica-300 was activated and used immediately after removal from the furnace. Three repeats of the reaction shown in scheme 29 were done in sealed microwave vials, which were heated conventionally as were previous reactions, to prevent moisture in the atmosphere from entering the reaction vessel. The results from the study (Table 16) show not only that the reaction is reproducible but that the catalyst is much better than previously seen. These results, when compared with previous reactions do suggest however that the catalyst is not particularly stable and would need to be freshly activated for each use. This theory was confirmed by the use of the freshly activated silica-

300 catalyst in a larger scale reaction in an ordinary reflux set-up open to the atmosphere. The catalyst used was the same batch, and at the same time, as that of the reactions in Table 16, however, the conversion dropped off significantly to 9% by NMR spectroscopic analysis so it can be assumed that the water in the atmosphere deactivates the catalyst very quickly. It is important to note that these reactions were not selective and other unidentified peaks were seen by both SFC and NMR spectroscopic analysis. For this reason, the conversions in Table 16 were calculated using the crude NMR spectra.
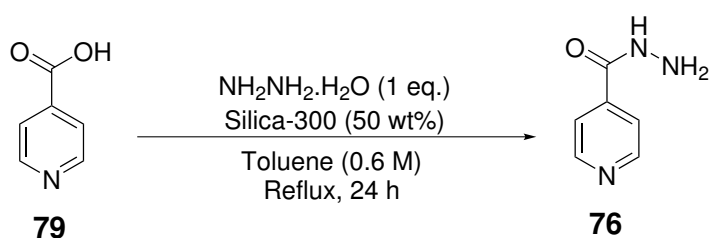
Scheme 29: Reaction conditions used for examining the stability and reliability of silica-300 as a catalyst in the synthesis of isoniazid **76**.

Table 16: Investigating the stability and reliability of the silica-300 catalyst in the synthesis of isoniazid **76**.

Repeat	Conversion[a] /%
1	77
2	80
3	75

The reaction conditions are shown in Scheme 29. [a] The conversions for these reactions were calculated by ^{1}H NMR spectroscopy.

Considering all of the data gathered on the silica-catalysed isoniazid formation, it is clear that the silica-300 catalyst is more effective than the silica-700 catalyst in this case, most likely because it acts as an efficient desiccant. It is deactivated quickly, by rehydration of the silica surface, so must be used immediately after activation. Further study of the catalyst, perhaps by examining rehydration by thermal gravimetric analysis (TGA) could give an insight into the mass of desiccant necessary for the reaction which could in turn give

information on the role of the silica. It would be interesting to investigate the activation temperature of the silica to see if it can be lowered without loss of conversion, as this could make the process simpler in a practical sense. Increasing the temperature of the reaction past 110 °C results in the formation of undesired side products, and similarly, decreasing the temperature results in decreased conversions. In order to see if the new method of synthesising isoniazid was more sustainable the than the literature method, the next step was to compare green metrics of both reactions.

3.2.2 Green metrics analysis of isoniazid synthesis

The aim in this project was to develop new, more sustainable routes to pharmaceutically relevant molecules and in order to do that, it was necessary to compare the reactions developed to the state of the art in the literature. The metrics tool kit described in Section 1.4 provides a good set of analytical methods, both quantitative and qualitative, to compare the processes.

The most recent literature preparation of isoniazid was selected for comparison against the new silica-catalysed method. In order to give a realistic comparison of the methods, only one step was chosen: the final isoniazid forming step. For the literature reaction, the 8% sodium hydroxide solution was considered purely as a reagent, with the solvent being the portion of water added at the beginning of the reaction.

The metrics of the work-up were not compared as, not only has the literature method likely been through extensive process development and is conducted on a much larger scale, but in an industrial setting these could be considered as very similar for both methods.
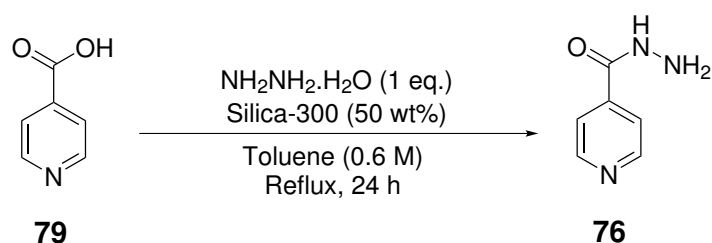
Scheme 30: Details of the silica-catalysed reaction used to calculate metrics for the synthesis of isoniazid **76**.
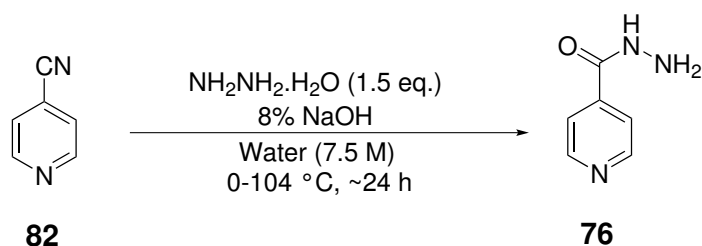
Scheme 31: Literature reaction used to calculate metrics for the synthesis of isoniazid **76**.

Table 17: Quantitative green metrics for the synthesis of isoniazid **76**: comparison of the literature synthesis from 4-cyanopyridine **82** and the silica-catalysed reaction from isonicotinic acid **79**.

Metric	*Via* Silica Catalysis	*Via* Literature Procedure
Yield	80%	75%
Conversion	80%	100%
Selectivity	100%	75%
RME	70.5	58.1
AE	88.4	89.0
Mass Intensity: Total	15.8	4.3
Mass Intensity: Reaction	15.8	2.8
Mass Intensity: Reaction chemicals	2.2	1.7
Mass Intensity: Reaction solvents	13.2	1.1

Table 17 shows the results of the metrics calculations. Using the best result obtained for the silica catalyst, the yield of the literature reaction has been improved upon and the silica-catalysed reaction is 100% selective. The literature reaction goes to full conversion of 4-cyanopyridine **82** but it produces 19% isonicotinic acid as a by-product. It could be envisioned that the remainder of the unconverted starting material in the silica-catalysed reaction could be isolated and fed back into the reaction mixture to increase the yield further. The atom economy is very similar for both reactions.

The reaction mass efficiency (RME) for the silica-catalysed reaction is much better than for the literature reaction, increasing from 58.13 to 78.37. This is perhaps a good measure to

compare the two processes as it takes into account both yield and stoichiometry. Not only is the yield of the silica-catalysed process higher but it uses only one equivalent of hydrazine. The increase in RME in the literature reaction is due to the use of sodium hydroxide, water and 1.5 equivalents of hydrazine. The reaction mass efficiency of the literature reaction is difficult to calculate as the amount of water used in the reaction is unclear. In this case the metrics were calculated using the water in the sodium hydroxide solution as a reagent, but as the reaction is conducted using water as a solvent, it is unclear just how much water is necessary for the reaction to take place. If the water were to be considered as a stoichiometric reagent (one equivalent per equivalent cyanopyridine), the reaction mass efficiency would improve to 60.52 but would still be much smaller than that for the silica-catalysed reaction.

The mass intensity on the silica-catalysed reaction is much higher than for the literature process and looking at the breakdown of this, it is clear that this is due to the solvent. At this early point in the research, this is not considered to be a problem. The literature reaction has been optimised and is conducted on a much larger scale. It is likely that if the silica-catalysed methodology was taken on through process chemistry that the solvent could be reduced significantly and this would bring it line with the literature procedure.

Table 18: Qualititative green metrics for the synthesis of isoniazid: comparison of the literature synthesis from 4-cyanopyridine and the silica-catalysed reaction from isonicotinic acid.

Metric	*Via* Silica Catalysis	*Via* Literature Procedure
Solvents	Toluene	Water
Health and Safety	H350, H410	H350, H400, H410,
Catalysts	Recovered	Reagents used catalytically
Reactor	Batch	Batch
Elements		
Energy	Above solvent BP$-5\,^\circ$C (110.0 $^\circ$C >105.0 $^\circ$C)	Above solvent BP$-5\,^\circ$C (100.0 $^\circ$C >95.0 $^\circ$C)

The qualitative measures of metrics (Table 18) are similar for both reactions. Health and safety both give a red flag which is to be expected and is currently unavoidable. To change this, it would be necessary to eliminate hydrazine from the reaction and find a more sustainable, safer alternative. Toluene is given a yellow flag in the Chem21 system, indicating that if possible, it should be changed to a more sustainable alternative. It should be possible in this reaction to swap toluene for cymene, which has very similar properties, but is more green due to its higher boiling point and its origin, from biomass. This would also improve the energy flag from red to green.

The silica catalyst is recovered, however, the metrics do not take into account that the silica catalyst would likely need to be reactivated before it could be used again. In the literature reaction there are no catalysts as such, but the sodium hydroxide is used in catalytic quantities, which in the Chem21 system gives a green flag.

Both reactor types are in batch for these reactions, with no rare elements in use and the energy for each is given a red flag due to the high temperatures used. It is possible that this could be improved upon for the silica-catalysed reaction as the solvent used is toluene. There are several alternatives that could be used in this reaction, including cymene which can be sustainably derived from limonene and has a much higher boiling point so the reaction temperature of 110 °C would not cause a problem in the metrics system. This would perhaps be a better alternative than the CPME tested as the energy of the reaction would be more favourable. The reactor type is a more difficult change to make. The silica-catalysed reaction is more of a slurry than a solution with a heterogeneous catalyst so the use of a fixed bed catalyst system would not be appropriate. It is possible to use a slurry flow system, however, some testing and analysis would have to conducted to prove that this was more sustainable than simply using a batch system. From a health and safety perspective, a flow system would be advantageous because there is less solvent and, in this case, hydrazine in the hot zone at one time.

Considering the metrics tool kit as a whole, it is evident that changes to the new process can be recommended. A change of solvent to cymene would improve the process from both an energy and health and safety perspective as long as the conversion and selectivity remained high. A decrease in the volume of solvent used, most likely along with an increase in

reaction scale would improve the mass intensity of the process, and converting the reaction to a flow process would likely be a positive step. The current set of metrics results suggest that the new process developed would be more sustainable that the current method in the literature.

3.3   Initial expansion of substrate scope

The investigation of substrate scope began with a small screen using two acids with different properties. *N*-Boc proline **84** was chosen because of its biological relevance as an amino acid and its potential use in a medicinal chemistry situation.[63] It is relatively polar compared with the substrates already published in this chemistry and would extend the substrate scope into heterocycles. Adamantane carboxylic acid **88** was chosen due to its steric bulk and its non-polar property. These were paired with both aniline **48** and benzylamine **85** because of the results previously published by Comerford[21] where aniline was seen to be a suitable substrate for this catalyst. The slightly more nucleophilic benzylamine was chosen as a comparison with aniline and as an amine candidate that was more likely to react.
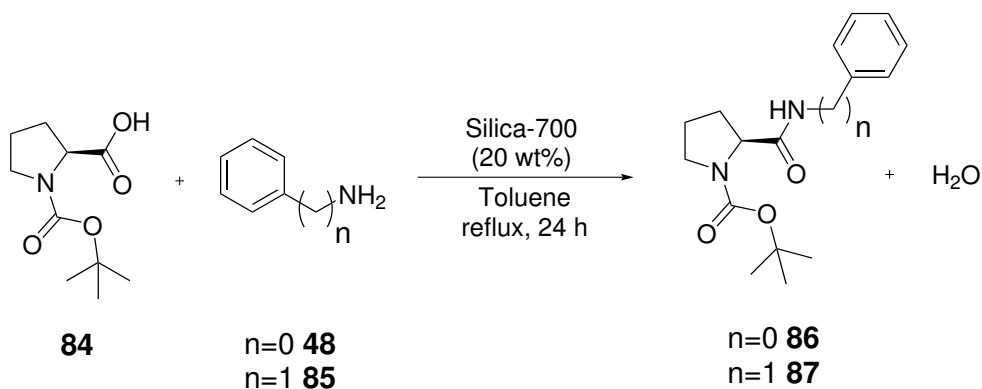
Scheme 32: Reaction of *N*-Boc proline with aniline and benzylamine using an activated silica catalyst.
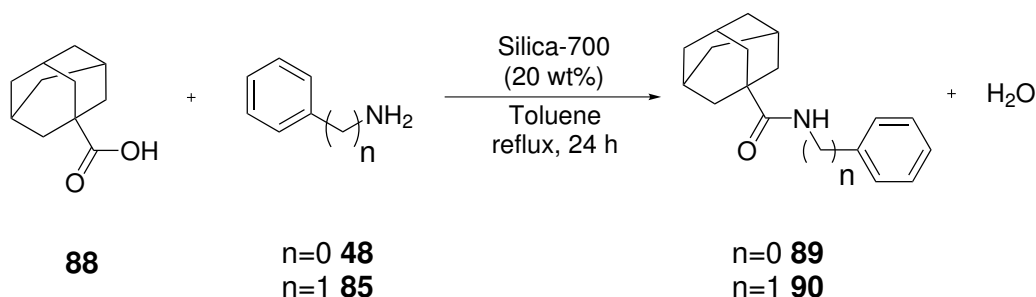
Scheme 33: Reaction of adamantane carboxylic acid with aniline and benzylamine using an activated silica catalyst.

As can be seen from Table 19, adamantane carboxylic acid **88** gave no positive results. In both cases only acid starting material was isolated from the reaction mixture. It is thought that the reason for the lack of reaction when using adamantane carboxylic acid **88** is due to its steric bulk which could be hindering the acid from reaching the active site of the catalyst, particularly if the active sites are within the silica pores. The other possible reason is that the adamantane carboxylic acid **88** is reaching the active site but is so bulky that it blocks the amine which is then unable to react.

Table 19: Conversion and yield of the reactions of *N*-boc proline **84** and adamantane carboxylic acid **88** with aniline **48** and benzylamine **85** under the conditions shown in Schemes 32 and 33.

Acid	Amine	Conversion by GC[a]/%	Isolated Product Yield /%
N-boc Proline **84**	Aniline **48**	35	14
	Benzylamine **85**	83	78
Adamantane Carboxylic acid **88**	Aniline **48**	No Reaction	
	Benzylamine **85**	No Reaction	

[a] GC conversion was measured using tetradecane as an internal standard.

The results for the proline substrate **84** were more promising. The initial reactions gave 35% and 83% conversion by GC with aniline **48** and benzylamine **85** respectively with the yields of isolated product slightly below that. Background reactions, omitting the silica, were measured (Table 20) which unfortunately showed that the reaction with benzylamine

as the amine was not significantly improved upon by the use of a catalyst. The background seen for the aniline reaction was higher than expected (23%) but could be improved upon by the use of the silica-700 catalyst.

As the *N*-boc proline used was enantiomerically pure, it was interesting to see if the use of the silica catalyst caused any racemisation. This was examined by the use of optical rotation measurements. In both cases the α_D values obtained were similar to literature values so it can be assumed that the silica catalyst does not cause racemisation of the substrates. It would be interesting if, following these results, an enantiomerically-pure amine was used in this chemistry to see if this result would extend to the amine substrate as well.

Table 20: Optical rotation measurements of the amide products of the reactions between *N*-boc proline **84** and aniline **48**/benzylamine **85**, conducted in CHCl$_3$.

Amine	Background Conversion /%	Catalysed Conversion /%	Isolated Yield /%	α_D (Lit)
Aniline **48**	23	35	14	-142.03°(c=1.0) (-140.9°) (c=0.86)
Benzylamine **85**	78	83	78	-90.36°(c=1.0) (-80.2°) (c=0.6)

3.4   Extending the scope

3.4.1   High-throughput substrate screen

Once the initial substrate results were obtained, it was decided that in order to produce a wide substrate scope, a high-throughput screening method would be useful. The aim of this screen was to select seven acids and seven amines which could be reacted against each other in a set of 49 reactions. The reactions could be carried out using a ChemSpeed® robotic system and analysed *via* liquid chromatography-mass spectrometry (LC-MS). Figure 22 shows the acids and amines selected.
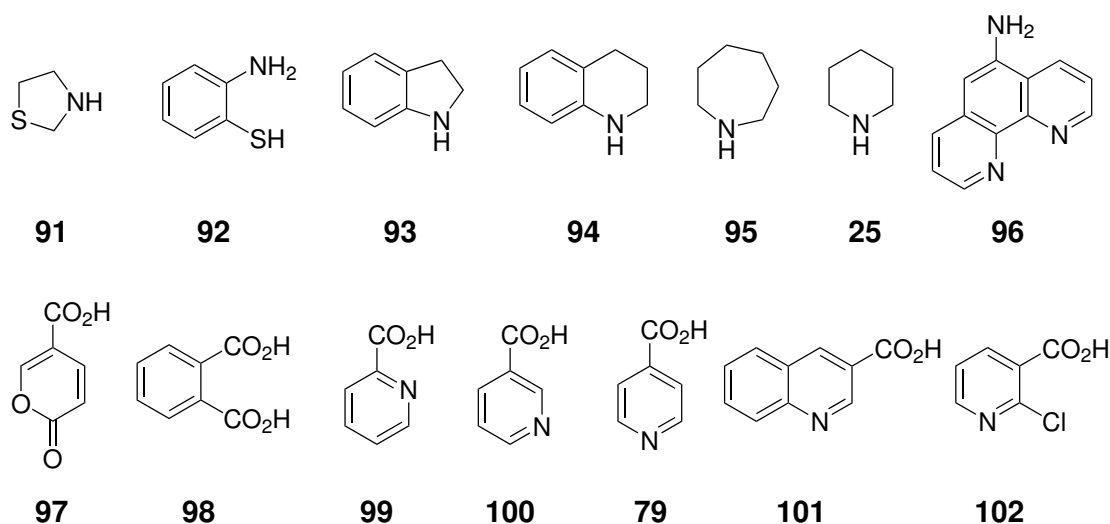
Figure 22: Acids and amines used in the ChemSpeed® substrate screen.

Coumalic acid **97**, quinoline-3-carboxylic acid **101** and 2-chloropyridine-3-carboxylic acid **102** were chosen as these are slightly more complex aromatics than previously reported substrates,[21] introducing heteroaromatics and slightly more steric bulk. Picolinic acids **99**, **100** and **79** with the nitrogen in positions 2, 3 and 4 would give information on whether the position of a heteroatom in the aromatic ring affects the catalysis. Phthalic acid **98** was chosen because it contains two identical reactive acid groups, and would provide an interesting study on the reactivity and selectivity of these acid groups with a variety of amine nucleophiles.

Five cyclic aliphatic amines were chosen containing 5, 6 and 7-membered rings. Piperidine **25** and azepane **95** were chosen for their simplicity; tetrahydroquinoline **94** and indoline **93** provided 6 and 5-membered rings with some steric bulk attached, and thiazolidine **91** provided an extra sulfur atom within the ring. Two aromatic amines were chosen; 2-aminothiophene **92**, containing a possibly reactive thiol group, and 1,10-phenanthrolin-5-amine **96**, increasing the steric bulk and with potentially interesting properties for use as a ligand.
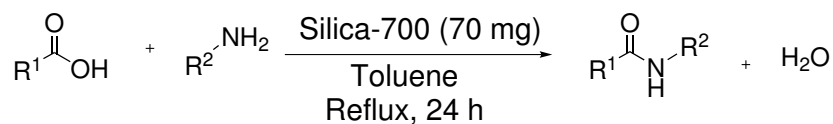
Scheme 34: Reaction conditions for the high-throughput screen of substrates carried out using a ChemSpeed® robotic system.

Each reaction was carried out on a 0.5 mmol scale in a sealed GC vial. The ChemSpeed® was used to weigh each solid substrate and measure by volume each liquid substrate into the appropriate vial along with 70 mg silica-700 catalyst and 0.83 mL toluene. The set of vials were stirred by mechanical shaking and heated to 120 °C for 24 hours.

The initial aim was to analyse these reactions by LC-MS and so each substrate was dissolved in an MeCN:H_2O 50:50 mix in order to find a suitable method. Three high performance liquid chromatography (HPLC) columns were used in these tests. The first was an Acclaim RSLC Polar Advantage II which is used for the analysis of both acidic and basic compounds. Each amine was run through this column with a variety of gradient mobile phases and the resulting chromatograms examined. Most of the amines were seen to have significant tailing due to high affinity with the silica and the addition of either formic acid or ammonium hydroxide was not able to overcome this problem. The second column tested was a C18 Sunfire which eluted the amine compounds with acceptable retention times. This looked more promising, however analysis of the acid compounds by this column was unsuccessful as the acids were eluted at the same retention time as the amines. Altering the mobile phase to try to alter some of the retention times was ineffective. The third column tested was a Dionex WCX-1 which is a versatile column in which the selectivity can be changed by tuning the mobile phase. The amines, when tested, were retained on the column with three MeCN:H_2O mobile phases, one with ammonium acetate, one with formic acid and one with no additives.

At this point it was decided that the most time efficient way to give an indication as to whether the reactions were successful or not was to simply analyse directly by mass spectrometry (MS) to see if the amide was present. The successful reactions could then be scaled up and analysed fully.

Coumalic Acid 97
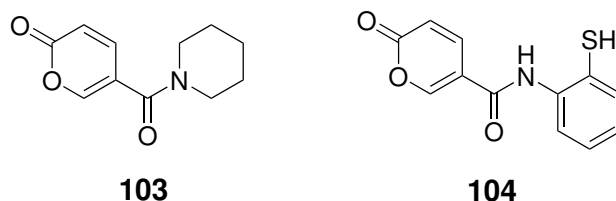
Figure 23: Amides synthesised from coumalic acid *via* silica catalysis.

Only two amines were reacted successfully with coumalic acid. Figure 23 shows the products from these reactions. One amine was in a 6-membered aliphatic ring, the other was attached to a 6-membered aromatic ring. There are two other amines in or attached to 6-membered rings which were unsuccessful so these seem to be isolated results.
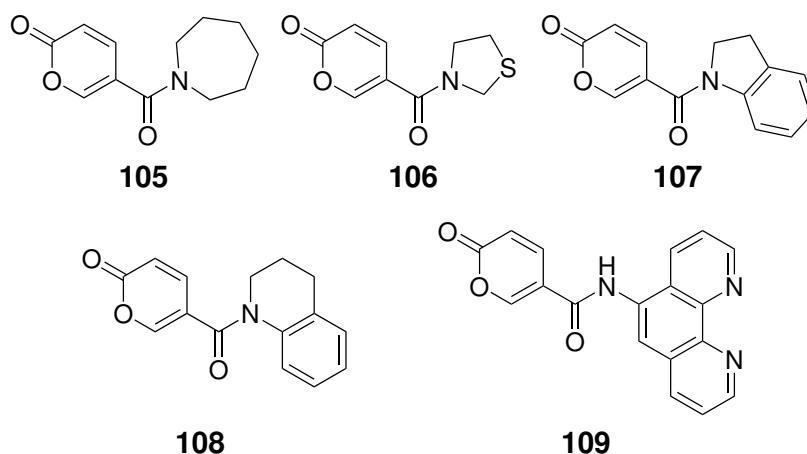
Figure 24: Structures of amides not detected from reactions involving coumalic acid *via* silica catalysis.

The amides shown in Figure 24 were not detected when their corresponding reactions were analysed by MS. It was assumed that these reactions were unsuccessful. This is, perhaps, quite unsurprising as the pyrone ring could be donating electrons to the carboxylic acid group making it less electrophilic. Three of the amines used are quite bulky and could be unable to reach the proposed activated carboxylic acid site.

3-Quinoline carboxylic acid 101 and 2-chloropyridine-3-carboxylic acid 102

110   **111**   **112**   **113**

114   **115**   **116**
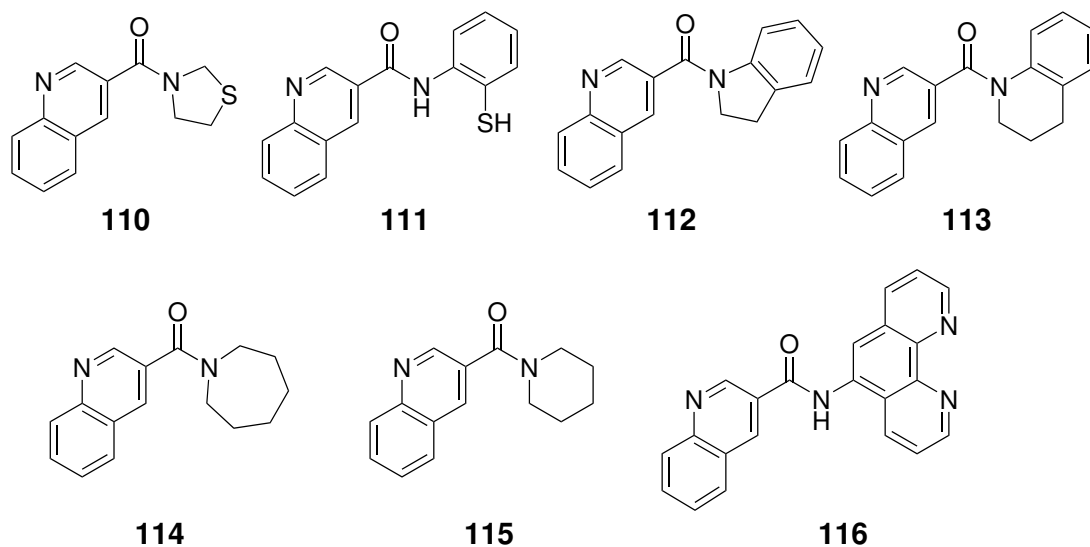
Figure 25: Structures of amides not detected by MS from reactions involving 3-quinoline-carboxylic acid *via* silica catalysis.

The reactions involving 3-quinoline carboxylic acid and 2-chloropyridine-3-carboxylic acid were unsuccessful. With 3-quinoline carboxylic acid, it may be that the substrate bulk hinders access to the active sites of the catalyst as was seen with adamantane carboxylic acid. It is also possible that the nitrogen causes the carboxyl carbon to be unreactive.

With the 2-chloropyridine-3-carboxylic acid, having a chlorine atom *ortho* to the carboxylic acid group could be stopping the carboxylic acid from interacting with the catalyst. Alternatively, it could be the polarity of the molecule and the hydrophobicity of the catalyst that is preventing any reaction taking place. These compounds were both taken on to a further study (Section 3.4.2).
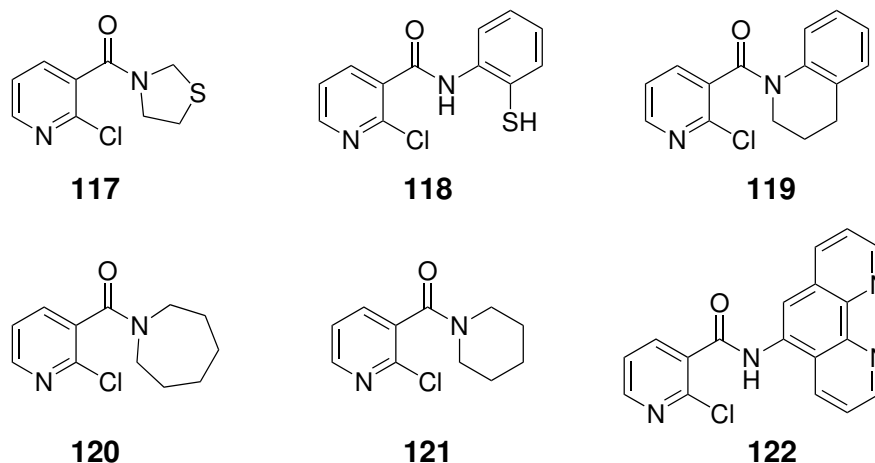
Figure 26: Structures of amides not detected from reactions involving 2-chloropyridine-3-carboxylic acid *via* silica catalysis.

Picolinic Acids 99, 100 and 79
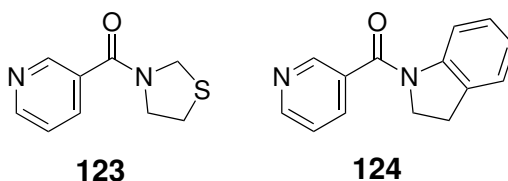
Figure 27: Amides synthesised from 3-picolinic acid **100** *via* silica catalysis. These are representative of the results obtained with 2-picolinic acid **99** and 4-picolinic acid **79**.

The two amides that were detected in the screen using the picolinic acids (Figure 27) were both using amines with the nitrogen in a 5-membered ring. These could be considered as reactive amines with the C-N-C angle allowing the most space for the reaction to take place. There was no difference in the reactivity, in the sense of reaction or no reaction, of any of the picolinic acids. This would need to be probed further with the scale-up and proper analysis of the successful reactions before any true conclusions could be drawn but the initial results suggest that the position of the nitrogen in the aromatic ring does not affect the reaction. None of the amides shown in Figure 28 were detected by MS so it was assumed that these combinations did not react. Attempts to TLC these reaction mixtures proved unsuccessful due to the high affinity of the amines for the stationary phase.
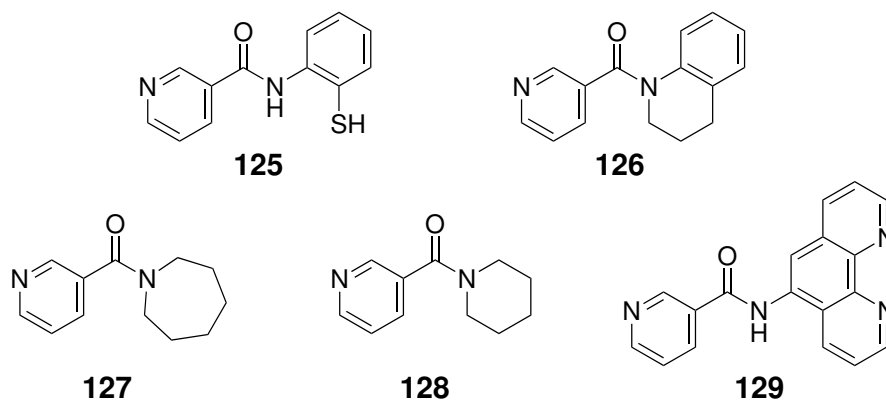
Figure 28: Structures of amides not detected from reactions involving 3-picolinic acid **100** *via* silica catalysis.
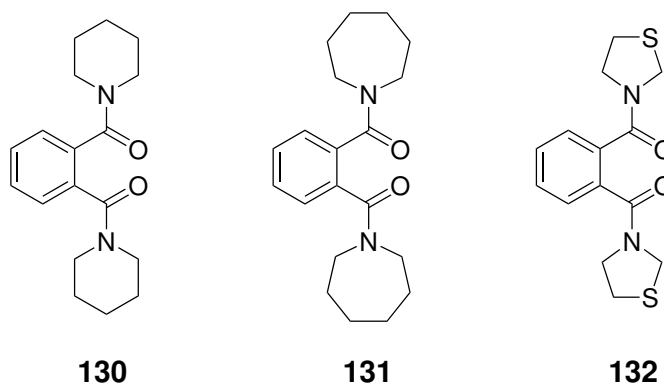
Phthalic Acid 98

Figure 29: Diamides synthesised from phthalic acid *via* silica catalysis.

Phthalic acid **98**, was the most successful acid used. The outcome of this set of reactions depended on the amine used, with some di-amidation taking place as well as some ring closing imide-formation. Di-amidation occurred with piperidine **25**, azepane **95** and thiazolidine **91** while imide **135** was formed when 1,10-phenanthrolin-5-amine **96** was used as the amine. This is likely due to the bulky nature of the amine so the intermediate would be too sterically hindered for a second amine to attack. This imide could be potentially interesting as a ligand in organometallic reactions as there are two nitrogen atoms available for co-ordination and the properties of the imide would likely be different from the amine which is commonly used. The use of 2-aminothiophenol **92** as the amine was interesting due to the presence of a second nucleophile on the amine. This resulted in a cyclic product being formed which

indicates that the catalyst could possibly be used for the formation of thioesters. Comerford investigated the used of alcohols and thiols in the reaction and found that esterification was possible but the formation of thioesters was more difficult which he suggests could be due to the increased acidity of the thiol or the susceptibility of the thioester to hydrolysis.[38]

133   **134**   **135**
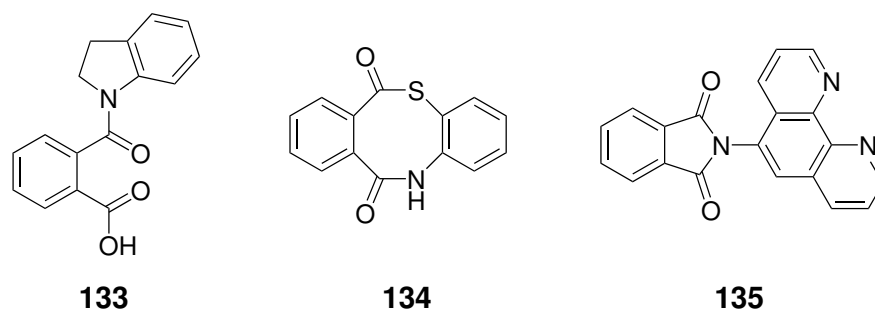
Figure 30: Amides and imide synthesised from phthalic acid *via* silica catalysis.

If the results are considered by amine rather than by acid, then indoline **93** and thiazolidine **91** were the most successful. This would suggest the 5-membered rings are better than the non-cyclic, or 6- or 7-membered rings, possibly due to the bond angle around the nitrogen. However, this could be a false result as three of the positive substrates were picolinic acids and these amines would need to be tested with a wider variety of substrates. Setting aside the results with phthalic acid, the only other amines that produced amide products were 2-aminothiophenol **92** and piperidine **25**, both when paired with coumalic acid **97**.

Scale-up of the phthalic acid reactions

Each of the reactions with phthalic acid as one of the substrates was repeated on a larger scale (1.5 mmol). The reactions which showed double amidation were treated with two equivalents of amine. Some difficulties were encountered when trying to separate the re-action mixture from the silica catalyst due to the solubilities of the starting materials and products. For this reason it was not possible to obtain crude conversions of the reactions. Similarly, the attempts made to isolate the products from the reaction mixtures encountered problems. Both acid/base washes and flash column chromatography were used but neither gave pure products. It is thought the acid/base washes may have caused degradation of product in some cases as the material that was isolated gave a ^{1}H NMR spectrum with many

more peaks than expected, some of which were very broad. No product was isolated from the reaction mixtures that were subjected to column chromatography. It is possible that the compounds were degrading on the silica but this could not be confirmed. Unfortunately, due to time constraints, this work could not be investigated any further.

These preliminary results suggest that the scope of the silica-700 catalyst could be expanded slightly but more investigation would be required, including scale-up reactions and background reaction measurements. What is revealed in these results is that there is a limited substrate scope for this chemistry. Further work to expand the current scope might only be beneficial if the origin of the limited substrate scope can be deduced.

3.4.2 Investigating the use of aniline as the amine

In amidation reactions, aniline is considered to be a particularly tricky substrate due to its lack of nucleophilicity. The results from Comerford *et. al.*[21] indicated that the silica catalyst may be very efficient at catalysing reactions using aniline as the amine and so it was decided to investigate this further by screening aniline with a selection of 6 acids. As the isoniazid synthesis study showed that the silica-300 could be a more effective catalyst than silica-700, it was decided to test both catalysts in these reactions.
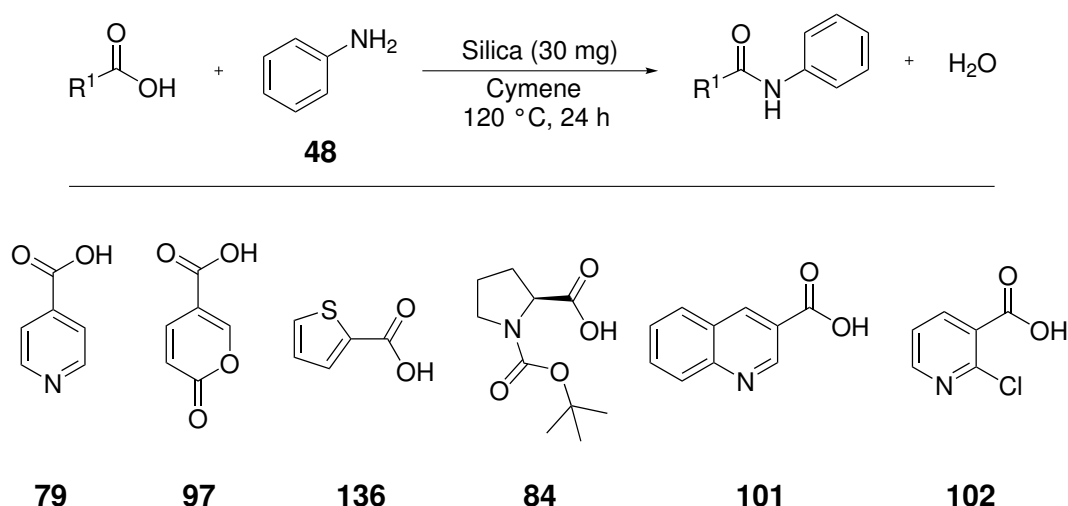
Figure 31: Acids chosen to be screened with aniline in the silica-catalysed amide formation.

Isonicotinic acid **79** and coumalic acid **97** were chosen as these had given some positive results in the ChemSpeed® screen. 2-Thiophene carboxylic acid **136** was chosen to introduce

a different kind of heteroaromatic compound, as previously only nitrogen-based heteroaromatics had been tested. *N*-Boc proline **84**, used previously in this reaction, was brought back to test with the more hydrophilic silica-300 catalyst. 3-Quinoline carboxylic acid **101** and 2-chloropyridine-3-carboxylic acid **102** were chosen as these were the least successful in the ChemSpeed® screen and would likely present more of a challenge.

As can be seen from Table 21 only two of the acid substrates tested were successful in reactions with aniline. Coumalic acid **97**, which did show some promise in the screen using the ChemSpeed® robotic system, gave no conversion with either catalyst. This was a little surprising as one of the amines it had previously reacted with was 2-aminothiophenol **92** which is very similar in structure, though perhaps it is a little more reactive due to the electron donating thiol group. 3-Quinoline carboxylic acid **101**, 2-chloropyridine-3-carboxylic acid **102** and 2-thiophene carboxylic acid **136** were also unsuccessful, confirming that the activated silica catalysts are limited when it comes to more bulky, polar and less electrophilic substrates.

Table 21: Conversion of aniline after reaction with various carboxylic acids using two silica catalysts.

Carboxylic Acid	Catalyst	Conversion /%
Isonicotinic acid **79**	Silica-700	7
	Silica-300	10
	None	No product detected
Coumalic acid **97**	Silica-700	No product detected
	Silica-300	No product detected
	None	No product detected
2-Thiophene carboxylic acid **136**	Silica-700	No product detected
	Silica-300	No product detected
	None	No product detected
N-boc L-proline **84**	Silica-700	10
	Silica-300	20
	None	4
3-Quinoline carboxylic acid **101**	Silica-700	No product detected
	Silica-300	No product detected
	None	No product detected
2-chloropyridine-3-carboxylic acid **102**	Silica-700	No product detected
	Silica-300	No product detected
	None	No product detected

As seen previously (Section 3.3), *N*-boc proline **84** is a suitable substrate for these catalysts, though in this study the conversion was slightly lower. It seems that using the silica-300 catalyst improves on the conversion seen with the silica-700 catalyst. As described in Section 3.2 it is likely that this is due to the more polar nature of the silica-300 catalyst being more suitable for polar substrates. This is also likely the reason for the slight increase in the conversion when silica-300 is used with isonicotinic acid **79**.
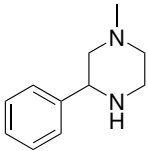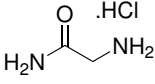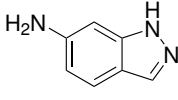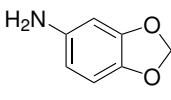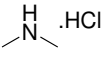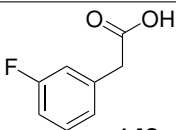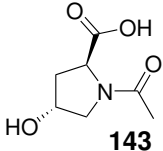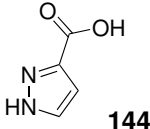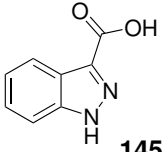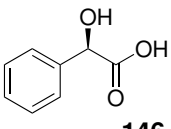
If it is possible to find a way to keep the silica-300 catalyst from deactivating, perhaps by activating it *in situ* prior to the reactants being added, then it would be interesting to repeat

the two successful reactions in this study to see if the conversions could be improved upon.

3.4.3 Mandelic acids as substrates

This project is part of a large consortium and as such the sharing of resources and data gave direction to the work that was carried out. Table 22 shows the results of a screen using the silica-700 catalyst conducted by researchers at GSK.[64]

Table 22: Screening results obtained by Dr Lee Boulton and Janette McKnight at GSK using the activated silica-700 catalyst.[64]

	137	138	139	140	141
142	<5%	<5%	14%[a]	67%[a]	<5%
143	<5%[b]	<5%[b]	12%[c]	13%[c]	<5%[b]
144	<5%[b]	<5%[b]	<5%	<5%	<5%[b]
145	<5%[b]	<5%[b]	<5%	<5%	<5%[b]
146	<5%	<5%	55%[a]	89%[a]	<5%

[a]Yield of isolated product. [b]Reaction run on 20-25 mg input. [c]Yield of isolated product following mass-directed autoprep due to very low solubility of compound and crude mixture.

From these results it can be seen that (*R*)-mandelic acid **146** gave very promising results with two of the aromatic amines. It was decided to probe this substrate further by reacting (*R*)-mandelic acid with aniline, the previously successful amine.

Scheme 35: Reaction of mandelic acid with aniline using a silica catalyst activated at 700 °C.

An initial reaction was conducted using the conditions shown in Scheme 35 at reflux. A conversion of 61% was obtained and so the background reaction was measured. Unfortunately the background reaction of (*R*)-mandelic acid and aniline gave an improved yield of 73% so it appeared that the catalyst was actually hindering the reaction.

The decision was taken to continue with this study by lowering the temperature of the reaction. It was expected, based on the results in Chapter 2, that the conversion of the background reaction would decrease as the temperature decreased and it was anticipated that the catalyst could then begin to be effective.

Table 23: Yield of silica-catalysed and uncatalysed reactions between mandelic acid **146** and aniline **48** at various temperatures.

Temperature / °C	Yield /%	
	Silica-Catalysed	Uncatalysed
20	0	0
40	0	0
60	9	9
70	26	32
80	48	53
120	61	73

Table 23 shows the results of this study. Below 60 °C there was no conversion seen in either the silica-catalysed or uncatalysed reactions. From 60 °C upwards there was a steady increase in the yield of the uncatalysed reaction which was mirrored in the catalysed reactions. As the high background reaction is not seen with phenylacetic acid as the substrate, it can be concluded that the hydroxyl group of mandelic acid is important and may be hydrogen bonding with the amine in the reaction, bringing it into the correct position for a reaction to easily take place. It is evident from the results obtained that the catalyst does not help this reaction and there is no indication as to why the catalyst seems to hinder the reaction. One possible explanation is that the catalyst selectively adsorbs the mandelic acid, with the hydroxyl group helping it to bind, which reduces the concentration of the acid in the solution thereby reducing the conversion. The study would not help to extend the substrate scope of this amidation catalyst.

There was one factor left to examine in this reaction and that was the use of an enantiopure substrate. It was useful to check that the silica catalyst was not causing any epimerisation of the chiral centre during reaction, confirming the earlier results with *N*-boc proline **84**. In order to do this, products from both the catalysed and uncatalysed reaction were analysed by optical rotation.

Table 24: Optical rotation measurements of the (*R*)-2-hydroxydiphenylacetamide **147** synthesised with and without a silica-700 catalyst. Measurements recorded in $CHCl_3$, c = 1.0.

	Silica-Catalysed	Uncatalysed
α_D	-74.5°	-70.6°

The products from both reactions gave similar optical rotations suggesting that the chiral centre is not affected in either reaction. Comparison with literature data shows that the optical rotations obtained are double that of the literature data (-34°, c = 1.0 in acetone), but as there is only one value reported in the literature, there is no evidence to suggest that either value is incorrect or unreliable.[65] These data, along with the data obtained for the *N*-boc proline-based products **86** and **87** in section 3.3 confirm that the catalyst does not affect chiral centres.

3.5 Conclusions

The results obtained in this chapter demonstrate that activated silica catalysts have limitations in amidation reactions. Low product conversions were seen with two of the more complex substrates tested, **79** and **84**, but the vast majority of them were unsuccessful.

Out of the eleven acids, **79**, **84**, **88**, **97**, **98**, **99**, **100**, **101**, **102**, **136** and **146**, tested in this chapter, **79**, **84**, **97**, **98**, **99** and **100** showed promise as substrates. The results suggest that bulky or particularly polar acids are not suited to this type of catalysis. It is also likely that the acids need to be quite electrophilic for the catalyst to be effective. This would be supported by the mechanisms proposed, particularly the chemically-bound intermediate, as the acid would be need to be sufficiently electrophilic to react with the silanols on the silica.

Phthalic acid **98** gave positive results with all the amines it was screened against, giving a variety of cyclic products depending on the amine used, though it was not possible to scale these reactions up and isolate the products. A silica catalyst activated at 300 °C was found to be more effective than silica-700 in a screen of aniline against carboxylic acids containing heteroatoms.

Mandelic acid **146** was tested as a potentially promising substrate but it was found that the background reaction was high and could not be improved upon with the use of a silica catalyst. This study highlighted the importance of measuring the background reaction when examining direct amide formation using catalysts at high temperatures. The products from these reactions, along with the products from reactions involving *N*-boc proline show that no epimerisation takes place when chiral centres are present in the acid starting materials.

Aniline **48** is seen to be a reactive amine in these reactions when paired with appropriate acids. The small number of amines tested in a high-throughput screen showed that amines with the nitrogen contained in 5-membered rings were the most effective nucleophiles though the success of any amine tested in the silica-catalysed amide formation depended on the carboxylic acid used.

The most positive result in this work was the synthesis of the anti-TB drug, isoniazid **76**. A number of conditions and catalysts were tested in the reaction between isonicotinic acid **79**

and hydrazine **81**. The silica-300 catalyst was the most effective catalyst for this transformation, giving an average conversion of 77% over three reactions. Green metrics analysis showed that this new process could be a greener alternative to the current literature procedure. It is anticipated that this work could now be scaled up in a process flow chemistry laboratory and provide a new route to isoniazid.

Chapter 4

Palladium-catalysed oxidative C–H bond functionalisation in the synthesis of amide-containing aromatics

4.1   Introduction

Two of the most atom economical forms of Pd catalysis are direct C–H functionalisation, which releases HX as a by-product, and double C–H functionalisation, which involves the formal loss of 'H$_2$'. This chapter focuses on the use of simple diphenyl amides as substrates in intramolecular oxidative C–H functionalisation reactions.
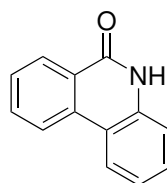
148

Figure 32: Phenanthridinone, a PARP inhibitor.

With the amide bond motif present in 25% of drug molecules, this project began to focus on the synthesis of a more complex amide-containing system.[3] Phenanthridinones are an important structural motif in medicinal chemistry. Compound **148**, 6-(5H)-phenanthridinone, is used in cancer treatment, as a poly ADP ribose polymerase (PARP) inhibitor and has some effect as an immunosuppressant.[66] PARP is a chromatin bound enzyme used for modifying nuclear proteins after translation and it is involved in cytotoxic processes effected by immune cells. The synthesis of this inhibitor is reported with four main methods in the literature. The first method was a traditional Suzuki cross-coupling.[67] This was a robust method working on a range of substrates, the exception being an NO$_2$ group, which gave a disappointing yield of 24%.
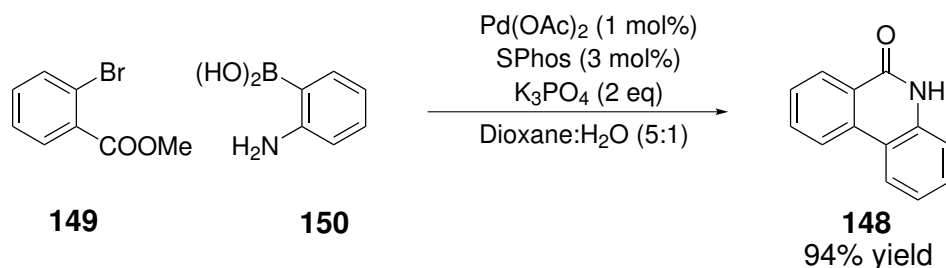
Scheme 36: Synthesis of phenanthridinone *via* Suzuki coupling.[67]

The second began with 2-aminobiphenyl **151** and utilised a Pd-catalysed carbonylation approach to form the phenanthridinone **148** where $Cu(TFA)_2$ was used to re-oxidise the Pd(0) back to Pd(II).[68] The scope of this reaction was good, with both protected and unprotected amines affording product in moderate to good yields. A downside to this method was that electron withdrawing substituents tend to decrease the yield.
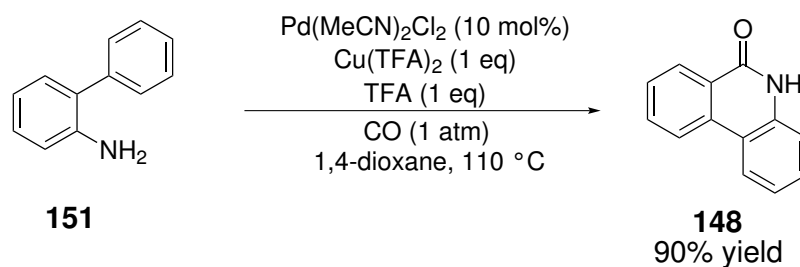
Scheme 37: Synthesis of phenanthridinone *via* aminocarbonylation.[68]

The third method involves single C–H functionalisation of a brominated compound using $Pd_3(OAc)_6$, phosphine and base in a polar aprotic solvent. In 1984, Ames reported the synthesis of phenanthridinone using $Pd(OAc)_2$ and sodium carbonate in DMA with modest yields.[69] The essential point of this synthesis was that the halide had to be on the amine side of the benzamide or the reaction did not occur as expected. Instead of oxidative C–H functionalisation, the Pd co-ordinated to the nitrogen. If the halide was on the benzoyl side of the benzamide, the nitrogen had to be protected for the desired cyclisation to occur.
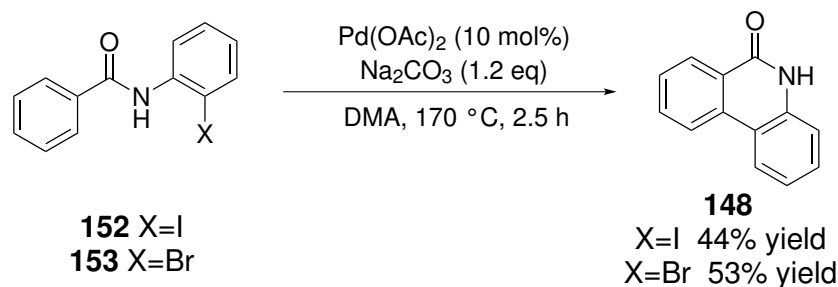
Scheme 38: Synthesis of phenanthridinone *via* direct C–H functionalisation.[69]

In 2008, this work was expanded by Sferrazza *et al.* who reported the synthesis of a range of *N*-protected phenanthridinones (Scheme 39) in good yields, again using Pd(OAc)$_2$ but also with a bidentate phosphine ligand at the lower temperature of 100 °C in 30 minutes.[70]
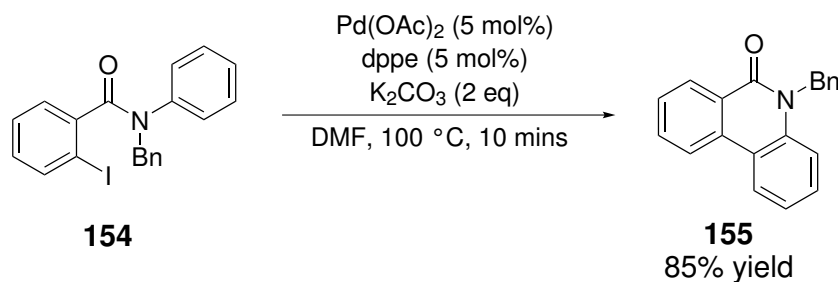
Scheme 39: Improved synthesis of phenanthridinone *via* direct C–H functionalisation.[70]

The final method, which is the basis of the work in this chapter, involves oxidative C–H functionalisation of *N*-phenylbenzamide **66** using Pd(TFA)$_2$ and molecular oxygen.[71] There is a small substrate scope using this chemistry with yields ranging from 57% to 89% but the authors report that bromo- and cyano- substituents were not tolerated. The drawback to this reaction is that it is conducted in molten benzoic acid, which makes it experimentally awkward, particularly if it was put into flow.
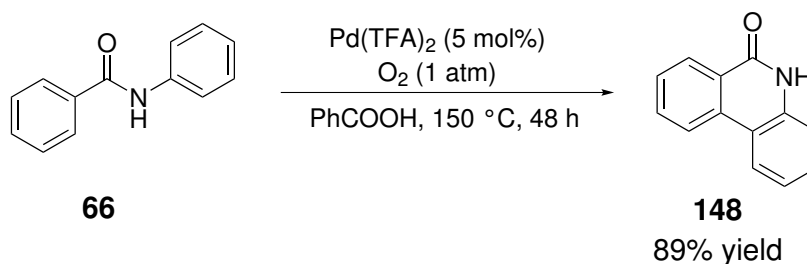
Scheme 40: Synthesis of phenanthridinone *via* oxidative C–H functionalisation performed by Ishida *et al.*[71]

The aim of the work in this chapter was to investigate the use of alternative catalysts in the oxidative C–H functionalisation reaction of *N*-phenylbenzamide **66** and to examine the possibility of a one-pot synthesis of phenanthridin-6(5*H*)-one **148** from benzoic acid and aniline using the Pd(TFA)$_2$ catalyst. It was anticipated that, if successful, this work could be extended to use a recoverable catalyst for the one-pot synthesis, further improving its green credentials.

4.2 Phenanthridinone synthesis *via* an oxidative double C–H functionalisation

4.2.1 Synthesis of the amide starting material

Following on from the results in chapter 3, it was desirable to be able to synthesise the starting materials for the C–H functionalisation reaction in a clean and sustainable reaction. To this end, the starting material was synthesised by two methods. Firstly for comparison, benzoyl chloride **156** was reacted with aniline **48** to form the desired amide **66** (Scheme 41). The second method was the silica-catalysed direct amide formation (Scheme 42).[21]
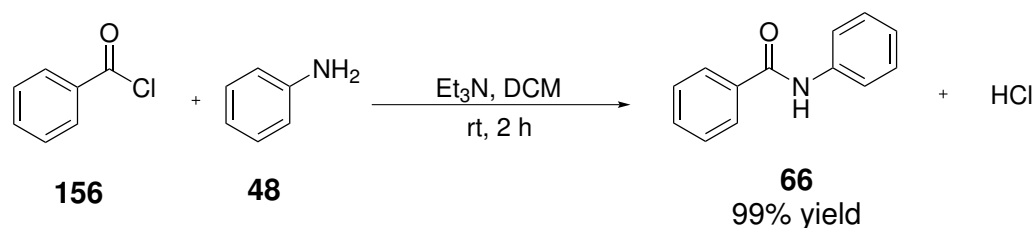
Scheme 41: Synthesis of *N*-phenylbenzamide *via* an acid chloride intermediate.

The acid chloride method, as expected, provided a excellent yield of 99% product. The high yield led to a good RME (83.13) and atom economy (84.40). The mass intensity for this reaction was quite high (96.35) due to the aqueous work-up to remove the triethylammonium salt formed. These metrics do not take into account the formation of the acid chloride, however they do give a good control for comparison with the silica-catalysed method.

Scheme 42: Synthesis of *N*-phenylbenzamide *via* silica catalysis.

The silica-catalysed reaction was conducted in toluene initially but this did not give any conversion to product. The solvent was changed to xylene so that the temperature could be increased from 110 °C to 130 °C. This was successful and a yield of 70% was obtained. Though the yield was modest and therefore the RME was lower (64.06) than the acid chloride reaction, the atom economy was improved (91.63) and the mass intensity slightly lower (88.39), a result of the simplified work-up of a filtration and recrystallisation from ethyl acetate and hexane.

4.2.2 Oxidative C–H functionalisation of *N*-phenylbenzamide

The amide **66**, synthesised in Scheme 41, was subjected to the reaction conditions[*] published by Ishida *et al.* (shown in Scheme 43).[71] A yield of 81% phenanthridin-6-(5*H*)-one **148** was obtained and so efforts were begun to make this synthesis more sustainable.
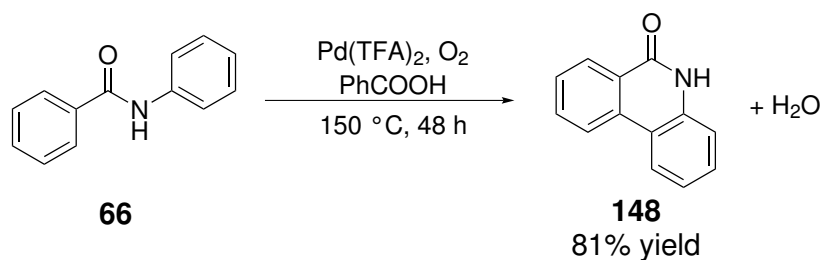
Scheme 43: Synthesis of phenanthridin-6-(5*H*)-one using Pd(TFA)$_2$ as a catalyst.

---

[*]Oxygen gas which is labelled 'may cause or intensify fire; oxidiser' was used in this experiment. Safety precautions were taken including training on compressed gas cylinders and the exclusion of oil baths from the working area. The cylinder was kept sealed at all times when not in use and the pressure monitored to ensure no leaks occurred. Oxygen gas was transferred to the reaction vessel with the use of balloons.

The first experiments undertaken were the screening of new Pd catalysts in the reaction. The first catalyst tested had been previously synthesised by a student (Jonathan Reeds) in the Fairlamb group and so the method used for synthesis was already developed (Scheme 44).[72] The catalyst **160** is a Pd complex bearing two tetrafluorosuccinimide ligands and two co-ordinated acetonitrile ligands. Imidate ligands have similar σ accepting and π donating properties to pseudohalide ligands, such as acetate and triflate.[73] They can stabilise Pd^0L_n complexes, preventing the formation of metallic palladium[74] and have the possibility of stabilising catalytic intermediates through their four co-ordination modes made possible by the nitrogen and carbonyl oxygens.[75]

The tetrafluorosuccinimide ligand **159** was synthesised *via* a condensation reaction of commercially available tetrafluorosuccinamide and purified by sublimation. The catalyst was then synthesised from the ligand and $Pd_3(OAc)_6$ **158** in acetonitrile at room temperature (Scheme 44). Precipitation from an acetonitrile/diethyl ether/petroleum ether mixture yielded the active catalyst **160**, a yellow powder, in 67% yield.
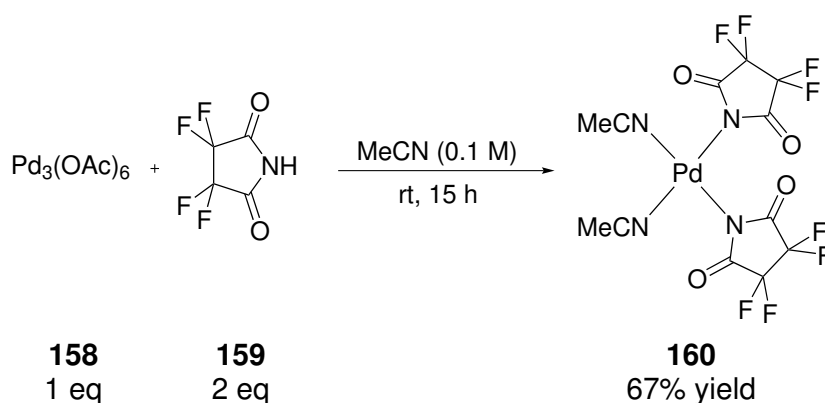
Scheme 44: Synthesis of $Pd(tfs)_2(MeCN)_2$.

Comparison of the data obtained from analysis of $Pd(tfs)_2(MeCN)_2$ **160** with that previously reported by Reeds showed a few differences.[72] The most notable difference was the appearance of the catalyst. Reeds described the catalyst as a grey/white powder, but the catalyst isolated was yellow in colour. It was not possible to obtain liquid-state NMR due to the insolubility of the complex in suitable solvents. Succinimide complexes containing acetonitrile ligands are known to be insoluble and therefore difficult to crystallise.[76] Solid-state cross polarisation magic angle spinning (CPMAS)-NMR spectra were obtained for the

compound at two spin rates, 10000 and 12000 Hz, with both ^{1}H and ^{19}F decoupling. Reeds obtained only ^{13}C NMR data, which is close but not identical to the data obtained for the new batch of catalyst.
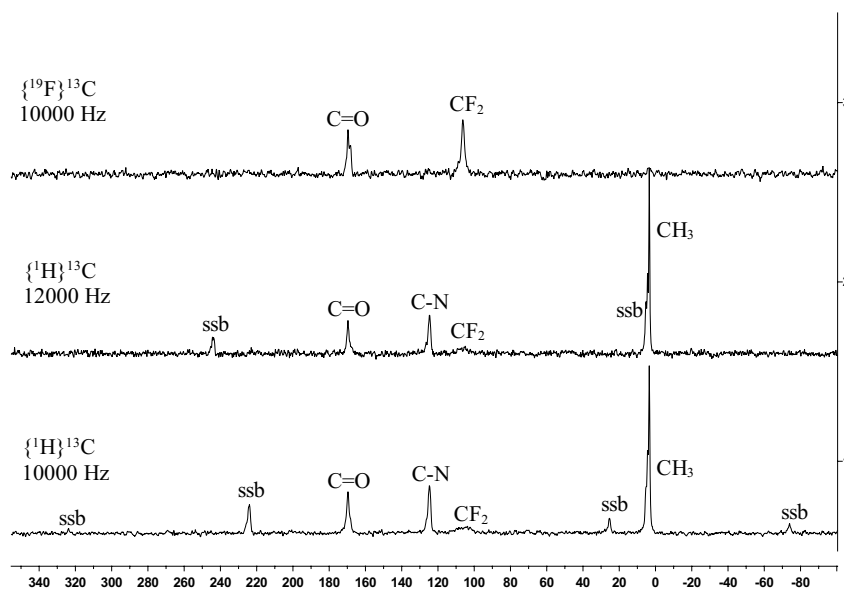
Figure 33: ^{13}C CPMAS-NMR spectra of Pd(tfs)$_2$(MeCN)$_2$ **160**. Spectrum 1: $\{^1\text{H}\}^{13}$C CPMAS spectrum at 10 kHz. Spectrum 2: $\{^1\text{H}\}^{13}$C CPMAS spectrum at 12 kHz. Spectrum 3: $\{^{19}\text{F}\}^{13}$C CPMAS spectrum at 10 kHz.

The carbon spectra are perhaps the most interesting and informative. Reeds reported two peaks at 169 and 168 ppm, corresponding to the carbonyls, which are both seen in the $\{^{19}\text{F}\}^{13}$C spectrum (Spectrum 3, Figure 33). The C–N peak at 125 ppm was also seen with spinning side bands at 244 and 5 ppm with a 12 kHz spin rate (spectrum 2) and at 323, 224, 25 and -74 ppm with a 10 kHz spin rate (spectrum 1). The broad peak reported at 106 ppm for the CF$_2$ was seen in the ^{13}C spectrum and when this spectrum was ^{19}F-decoupled the peak resolved from a full width at half peak height (FWHM) of 875 Hz to 195 Hz. The final peak seen by Reeds was the Me peak at 4.5 ppm, seen in the new spectrum at 4.3 ppm. There was one peak in the new spectrum not previously reported, which was a Me peak at 3.4 ppm. It is thought this could be either free acetonitrile in the sample, which in the liquid-state ^{1}H NMR spectrum gives a signal at approximately 2.05 ppm,[77] or perhaps the complex is found in both *cis* and *trans* configurations.
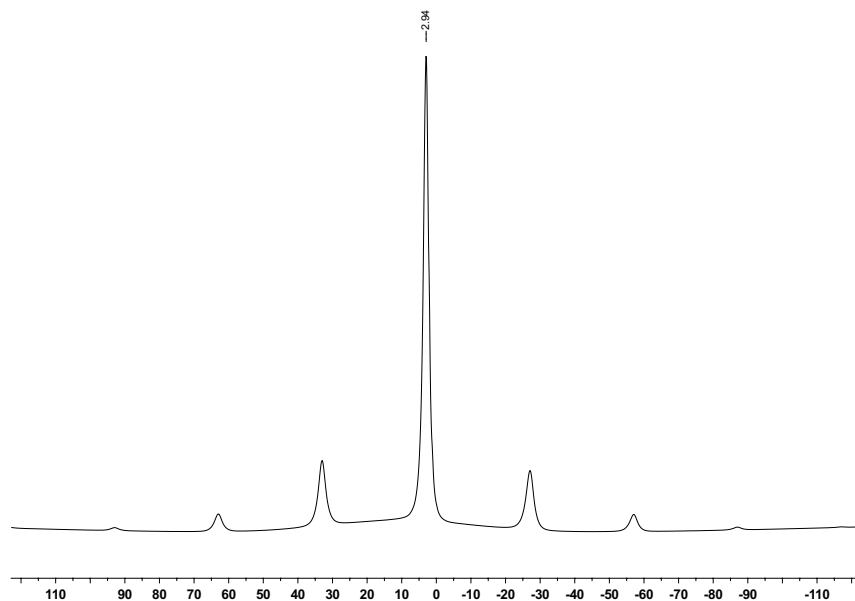
Figure 34: ^{1}H MAS NMR spectra of Pd(tfs)$_2$(MeCN)$_2$ **160**.
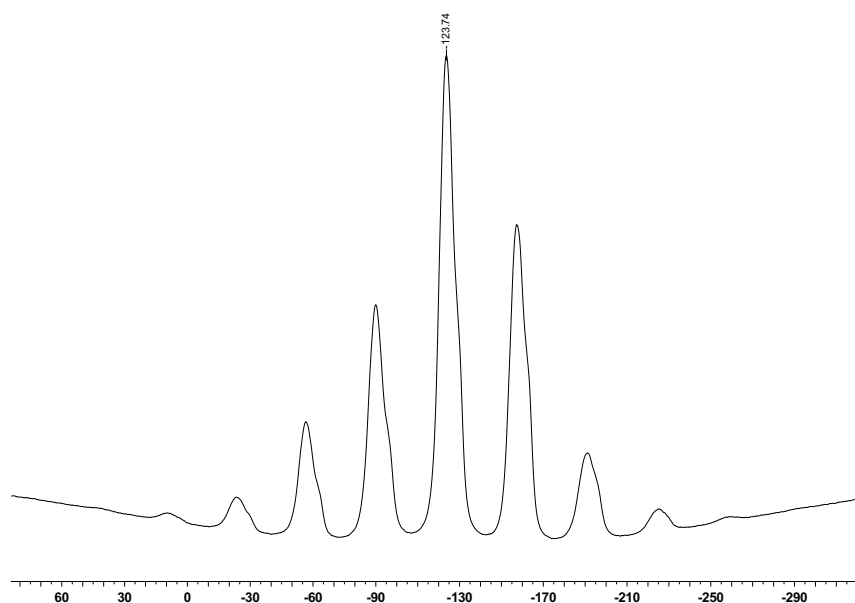
Figure 35: ^{19}F MAS NMR spectra of Pd(tfs)$_2$(MeCN)$_2$ **160**.

The ^{1}H NMR spectrum shows only one singlet peak, as expected, at 2.94 ppm with three sets of spinning side bands, while the ^{19}F NMR spectrum shows one singlet peak at -123.7 ppm with four sets of spinning side bands. The ^{19}F spectrum (shown in Figure 35) is not completely symmetrical but the sample was shimmed as best as possible. Lower spin rates resulted in worse phasing and applying spectral weighting functions, Gaussian, Sine Bell or

Sine Square, did not improve these.
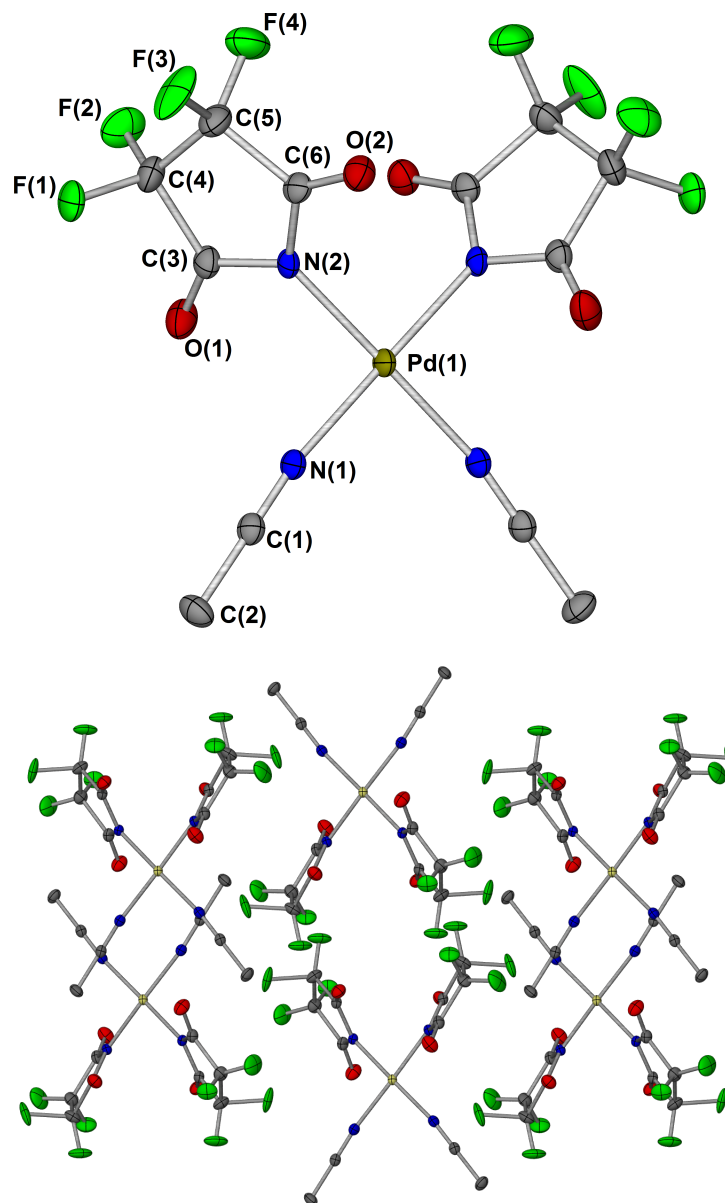
Figure 36: Single crystal X-ray diffraction structure of Pd(tfs)$_2$(MeCN)$_2$ **160**. Hydrogen atoms were removed for clarity. Thermal ellipsoids shown with probability of 50%. The fluorine atoms exhibited disorder and this was modelled with refined occupancies of 0.78:0.22(4). Selected bond lengths (Å): Pd(1)-N(1): 1.9826(14), Pd(1)-N(2): 1.9929(15). Selected bond angles (°): N(1)-Pd(1)-N(1): 88.23(8), N(1)-Pd(1)-N(2): 92.03(6), N(2)-Pd(1)-N(2): 87.93(8).

Isolation of **160** by precipitation from the acetonitrile, diethyl ether and petroleum ether mix reported in the literature[72] proved to be quite challenging and in the first instance the com-

plex crystallised out of the reaction mixture and the single crystal structure was determined by X-ray diffraction (Figure 36). Similar crystal structures of Pd complexes with imidate and solvent ligands have been reported as being in *trans*-configurations with *cis*-complexes only seen when bidentate ligands are introduced.[76] Instead of the anticipated *trans*-complex due to the bulky tfs ligands, a *cis*-complex prevailed, showing that there is a strong *trans*-effect in the complex due to the donating acetonitrile ligands and the withdrawing tfs ligands. The complex had a C_2 axis of symmetry through the Pd atom and therefore had equivalent imidate ligands in the solid state. The molecules were packed in rows, with the acetonitrile ligands alternating up and down. The rows then alternated so that the fluorine atoms of molecules in adjacent rows were close together and the acetonitrile ligands of molecules in adjacent rows crossed (shown in Figure 36).

Comparison with single crystal structures in the literature suggested that the bond lengths seen are typical of acetonitrile Pd complexes. *Tetrakis*(acetonitrile)palladium(II) tetrafluoroborate has Pd–N bonds lengths of 1.956(8) and 1.956(7) Å. These are slightly shorter than the Pd(1)–N(1) bond length of 1.9826(14) Å in complex **160**. The angles reported in the literature for N(1)-Pd(1)-N(2) and N(1)D-Pd(1)-N(2)D are 89.3(4)$^\circ$ and 90.7(4)$^\circ$ respectively, close to the 88.23(8)$^\circ$ seen in complex **160**.[78] Similarly, [Pd(acac)(MeCN)$_2$]BF$_4$ had Pd–N bond lengths of 1.991(12) and 1.994(13) Å and a N(1)-Pd(1)-N(2) angle of 87.4(5)$^\circ$.[79]

An attempt was made to undergo ligand exchange of the acetonitrile ligands with triphenylphosphine. This was unsuccessful and no such complex could be isolated. It is concluded that complex **160** may not have the ability to readily undergo ligand exchange, and could therefore be limited in its use as a catalyst. *Bis*-imidate Pd complexes have been known to undergo ligand exchange of solvents with phosphines when the solvent used was SMe$_2$ but no such reactions are reported for acetonitrile-containing imidate complexes.[76]

The second catalyst that was tested was an 8-methylquinoline palladium acetate dimer **161** (Figure 37) that has been previously used in the Fairlamb group.[80] Apart from its use as a starting material for the synthesis of other palladacyclic complexes, it is catalytically competent in oxidative C–H functionalisation reactions.[81,82]

161
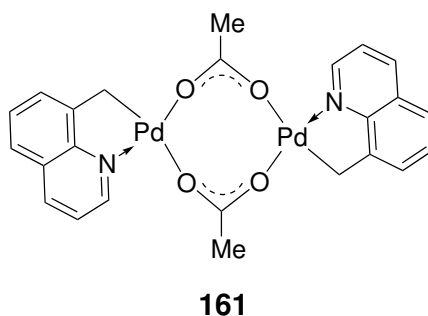
Figure 37: Acetate-bridged 8-methylquinoline palladium (II) dimer **161**, previously used as a catalyst in oxidative C–H functionalisation reactions.[80]

As can be seen in Table 25, the new Pd catalysts **160** and **161** were successful in this reaction though not as efficient as Pd(TFA)$_2$. A repeat of the reaction with the tetrafluorosuccinimide catalyst **160** gave a yield of 52%. Some optimisation of these reactions may provide better yields with these catalysts but for the purpose of the project, the work was not carried on. Due to the high yield already provided by the simple Pd(TFA)$_2$ catalyst, it was necessary to look at other ways to modify this reaction.

Table 25: Conversions of *N*-phenylbenzamide to phenanthridin-6-(5*H*)-one by various Pd based catalysts. Yield of isolated product shown in parentheses.

Catalyst	Conversion /%
Pd(TFA)$_2$	71
Pd(tfs)$_2$(MeCN)$_2$ **160**	42 (52)
Pd dimer **161**	29
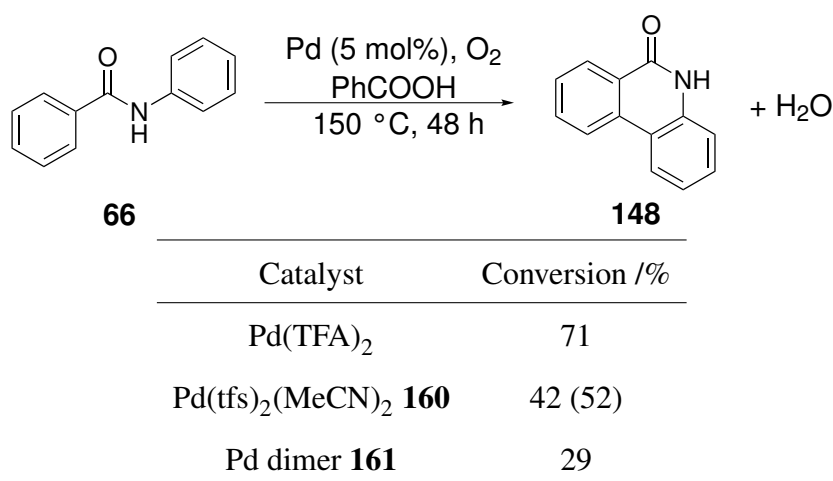
4.2.3   Study of the one-pot synthesis of phenanthridinone

Lewis acids are well known to be effective catalysts in amide formation reactions[83,84] and as the catalyst for the second step of the reaction (Scheme 43) was a Pd-based Lewis acid, it

was envisaged that the entire two-step reaction could be performed in one-pot with a single catalyst starting with benzoic acid **157** and aniline **48**. For the reaction shown in Scheme 45, this would be fairly simple as the solvent used is molten benzoic acid and so the reaction could be conducted with aniline in an excess of benzoic acid (Scheme 45).
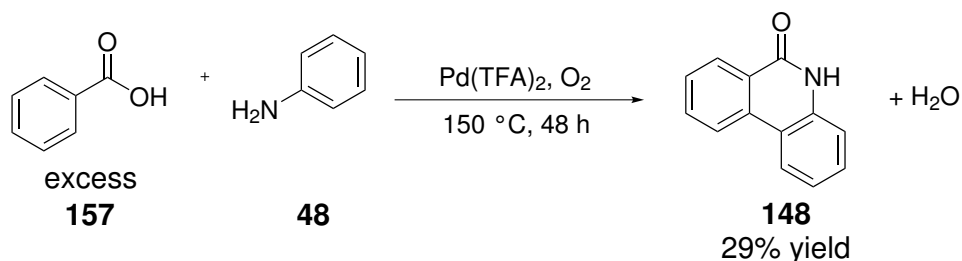
Scheme 45: The reaction of benzoic acid **157** and aniline **48** to form phenanthridin-6-(5*H*)-one **148** using Pd(TFA)$_2$ as a catalyst.

The first one-pot synthesis was successful, giving a yield of 29% of phenanthridin-6-(5*H*)-one **148**. Successive attempts to increase the conversion were not. Table 26 shows the results of a screen of different conditions tested in order to increase the conversion. These conditions were mainly based on the vessel used and how it was heated.

Entries 1 and 2 are repeats of the reaction shown in Scheme 45 which gave a yield of 29%. The conversions can be seen to decrease. Entry 3, using freshly distilled aniline, also gave a poorer conversion. It was noticed during the reaction that the benzoic acid was subliming in the microwave vial, and sometimes appeared that the reaction mixture had sublimed with it. This could have been preventing the reaction taking place as the top of the vial was much cooler than the reaction temperature (150 °C). In order to prevent this problem, a few variables were changed. Reducing the temperature to 130 °C (entry 4) did not improve the conversion, neither did changing the vial cap for a Suba-seal or completely sealing the reaction vessel (entries 5 and 6). In all of these reactions the intermediate was formed in high yields but the conversion to phenanthridinone **148** was very poor.

Fully immersing the reaction vessel in a graphite bath to ensure the entire vessel was heated to 150 °C (entry 7) did not lead to an increase in product conversion, neither did changing the reaction vessel type. Both a round-bottomed flask and Schlenk tube were used but neither showed formation of phenanthridinone product **148**. In the case of the round-bottomed flask,

only decomposition was seen as the benzoic acid quickly sublimed and left Pd(TFA)$_2$ and aniline at the bottom of the flask. The reaction in the Schlenk tube could be improved by the addition of 4 Å molecular sieves, where 13% conversion to product was seen and there was no aniline left in the reaction flask. This suggested that the water that is produced in the amide forming reaction is somehow hindering the oxidative C–H functionalisation reaction.

Table 26: Varying the conditions of the one-pot procedure to synthesise phenanthridin-6-(5*H*)-one **148**. Results are given as a ratio of product:intermediate:aniline calculated by crude ^{1}H NMR spectroscopy.

Entry	Vessel	+ve O$_2$	Experimental Detail	**148**:66:48 (ratio by ^{1}H NMR)
1	Vial	Yes	-	30:70:0
2	Vial	Yes	-	30:60:10
3	Vial	Yes	Freshly distilled aniline	4:87:9
4	Vial	Yes	130 °C	0:84:16
5	Vial	Yes	Subaseal, no vial cap	5:95:0
6	Vial	No	-	0:100:0
7	Vial	Yes	Fully immersed in graphite bath	5:80:15
8	Round-bottomed flask	No	-	Decomp
9	Schlenk tube	No	-	0:100:0
10	Schlenk tube	Yes	4 Å molecular sieves	13:87:0

The problems resulting from the sublimation of the benzoic acid were a major hurdle to a successful reaction. One of the easiest ways to avoid the problem would be a solvent change. Use of benzoic anhydride instead of benzoic acid provided 15% conversion to product but isolation proved difficult as the product was contaminated with benzoic anhydride. A 1:1 mixture of benzoic acid with benzoic anhydride, methyl benzoate or propylene carbonate

gave full conversion to intermediate amide **66** but no conversion to oxidative cyclisation product **148**.

Table 27: Solvent screening of the one-pot procedure to synthesise phenanthridin-6-(5*H*)-one **148**. Results are given as a ratio of product:intermediate:aniline calculated by crude ^{1}H NMR spectroscopy.
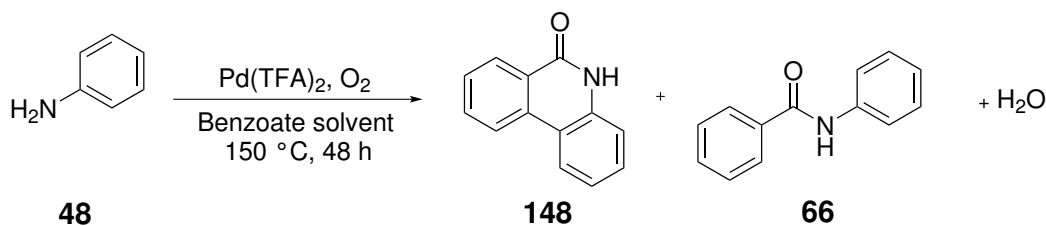
Entry	Vessel	+ve O_2	Solvent	**148**:**66**:**48** (ratio by ^{1}H NMR)
1	Vial	Yes	PhCOOCOPh	15:85:0[a]
2	Vial	Yes	1:1 PhCOOH: propylene carbonate	0:1:0
3	Vial	Yes	1:1 PhCOOH: PhCOOCOPh	0:1:0
4	Vial	Yes	1:1 PhCOOH: PhCOOMe	0:1:0

[a] ~5% yield phenanthridinone **148** determined by ^{1}H NMR spectroscopic analysis as product was still contaminated with benzoic anhydride after purification by column chromatography on silica gel.

The use of microwave radiation is known to be an effective way of conducting a reaction due to the even heating of the sample.[85] It was therefore possible that the use of a microwave as the heat source would prevent the sublimation of the benzoic acid and allow the reaction to take place. This did seem to be the case, though longer reaction times than expected were necessary and increasing the reaction time from 4 to 6 h had a negative impact on the amount of product formed though no decomposition was seen.

Table 28: Screening of microwave heating in the one-pot procedure to synthesise phenanthridin-6-(5*H*)-one **148**. Results are given as a ratio of product:intermediate:aniline calculated by crude ^{1}H NMR spectroscopy.
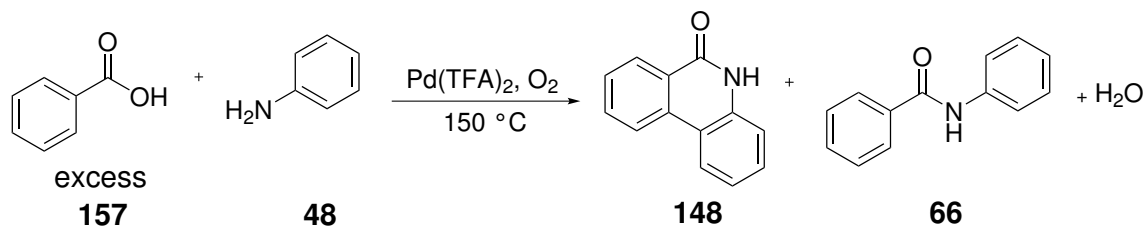
Entry	Vessel	+ve O_2	Time /h	**148**:**66**:**48** (ratio by ^{1}H NMR)
1	Vial	No	1	0:20:80
2	Vial	No	2	0:90:10
3	Large vial	No	2	0:17:83
4	Vial	No	4	10:80:10
5	Vial	No	6	5:85:10

The majority of the reactions had a positive pressure of oxygen to ensure that enough reached the necessary sites within the reaction. This was not possible with the microwave reactions due to the use of the pressure head and so it could be limiting the conversion to the final product. Most of these reactions were conducted in 10 ml microwave vials. Assuming the benzoic acid fills approximately 0.8 mL, this leaves 9.2 mL oxygen, which is 0.38 mmol, 1.8 equivalents per aniline. This means there is plenty of oxygen in the vial, though due to the unusual use of benzoic acid as a solvent, it is unknown how much of this will be dissolved throughout the course of the reaction. To encourage conversion to product, the vials were refilled with oxygen every 1-2 hours.

In order to check that it was not purely the amide bond forming reaction hindering the oxidative C–H functionalisation, the original reaction (Scheme 43) using amide **66** as starting material was re-tested. The yield dropped to 47% and performing the reaction in a heated, sealed metal reactor vessel, which should have been able to solve the problem of the sublimation, was unsuccessful, with no product detected.

Table 29: Repeats of the reaction in Scheme 43 to investigate decreased product yields.
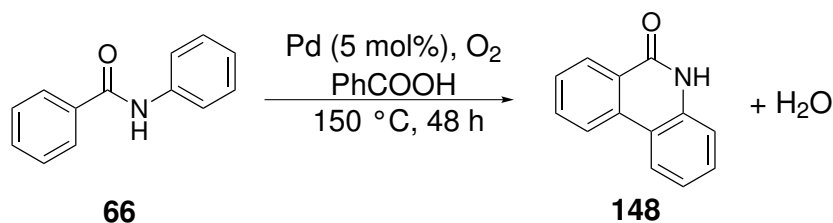
Entry	Vessel	Yield /%
1	Vial	81
2	Vial (repeat)	47
3	High pressure metal reactor	0

While some of the results obtained in this one-pot synthesis of phenanthridinone **148** from benzoic acid **157** and aniline **48** looked promising, it was not possible to develop a robust, reliable method that could be used to test other Pd catalysts, including solid-supported systems. It was decided to focus on a direct C–H functionalisation approach (Chapter 5).

4.3   Conclusions

The use of new Pd catalysts in the oxidative C–H functionalisation of *N*-phenylbenzamide **66** was successful with two new catalysts tested. One of the catalysts, Pd(tfs)$_2$(MeCN)$_2$ **160** has been fully characterised and a single crystal structure obtained. Further work with this catalyst could include a screen of different oxidative C–H functionalisation reactions to test its activity across a range of substrates.

Efforts to develop a one-pot, single catalyst reaction to phenanthridin-6(5*H*)-one **148** from aniline **48** and benzoic acid **157** were unsuccessful which was thought to be due to the sublimation of the benzoic acid under the conditions used and possibly the effect of water in the system after the initial amide formation step. A range of reaction conditions were tested, including microwave heating and changing vessel type. The challenges encountered meant that solid supported catalysts for this reaction could not be developed and tested.

Chapter 5

Phenanthridinone synthesis *via* direct C–H bond functionalisation

5.1   Introduction

The initial aim of this work was to form phenanthridin-6(5*H*)-one **164** *via* a single C–H functionalisation reaction of 2-bromo-*N*-phenylbenzamide **163**. The reaction conditions chosen are given in Scheme 46; Reaction 2, and are based on the reaction of a similar substrate with the N–H protected by a benzyl group and the halide on the other phenyl ring (Scheme 46; Reaction 1).[70] This aim was altered when the first reaction was analysed and found to have produced 5-phenylphenanthridin-6(5*H*)-one as the product. Scheme 46 shows the reaction that this chapter of work is based on in which two moles of substrate react to from one mole of product which contains one extra phenyl ring compared with the amide starting material and a by-product based on phenyl isocyanate.

This reaction has been previously reported by Furuta *et al.*, with the same substrate, giving a yield of 23% (Scheme 47).[86] The reaction involved the use of a special biaryl phosphine ligand to give 5-phenylphenanthridin-6(5*H*)-one **164** in a 23% yield.

Reaction 1:

162

155
85% yield

Reaction 2:

2 x

163

164
64% yield

165

148
Expected product
(not observed)
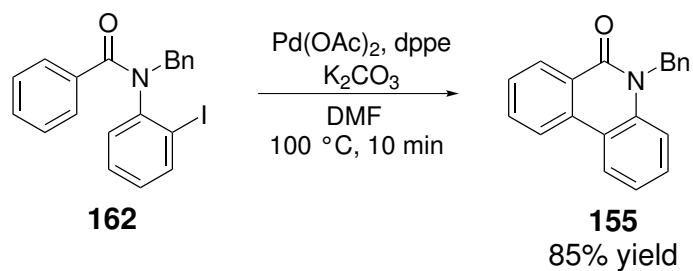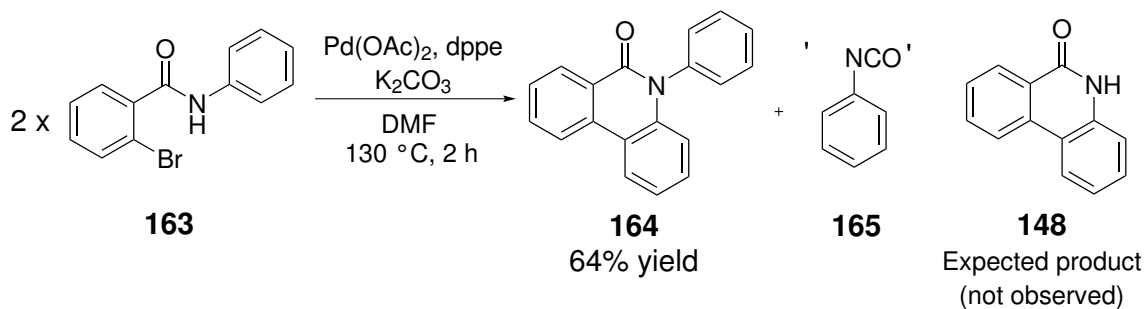
Scheme 46: Preliminary conditions for the direct C–H functionalisation reaction of 2-bromo-*N*-phenylbenzamide **163** to afford 5-phenylphenanthridin-6(5*H*)-one **164**.

2 x

163

164
23% yield

Ligand 1

166
37% yield

167
45% yield

168
81% yield
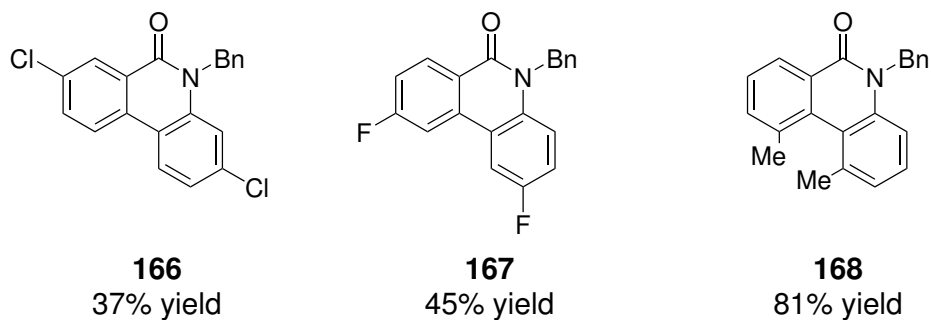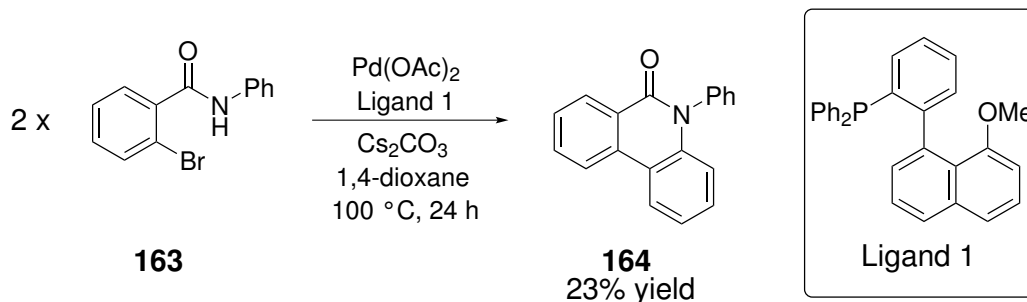
Scheme 47: Synthesis of 5-phenylphenanthridin-6(5*H*)-one **164** and derivatives by Furuta *et al.*[86]

Catellani *et al.* also reported this type of reaction with a methyl group in the 5 position of the phenanthridinone, and with a selection of heteroaromatic substrates (Scheme 48).[87] The heteroaromatic substrates gave much higher yields (generally 50-80%) than the simple phenyl substrate. Catellani proposed a mechanism for the reaction (shown in Scheme 48), which involved the formation of a C–N palladacycle **171**, followed by cross-coupling with a second molecule of starting material to give intermediate **172**, then loss of the second amide group as CO_2 and aniline.
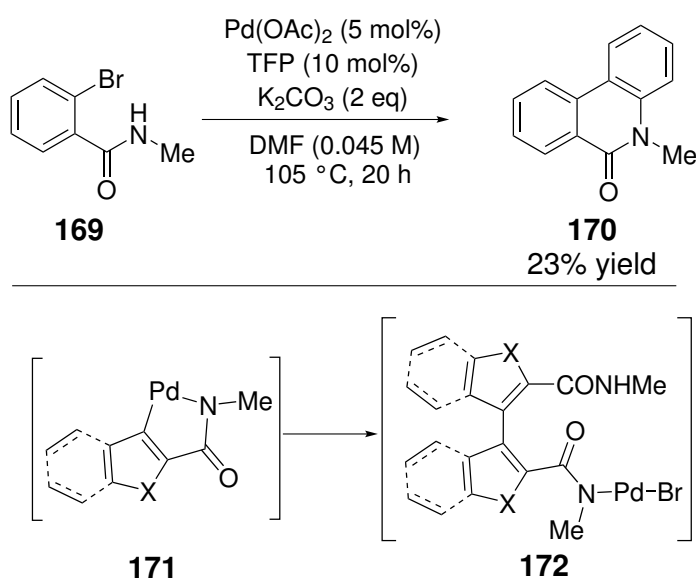
Scheme 48: Synthesis of 5-methylphenanthridin-6(5*H*)-one **170** and proposed intermediates by Catellani *et al.*[87]

Recently, Chen *et al.* reported a phosphine free, Pd-catalysed reaction using less reactive aryl chlorides as substrates.[88] The reaction used a $PdCl_2(PhCN)_2$ catalyst with 4 equivalents of CsF as base. Trace water was required, though the authors do not comment on its role. In general, the reaction gave good to excellent yields for a variety of substrates with a reaction time of 24 hours at 140 °C.
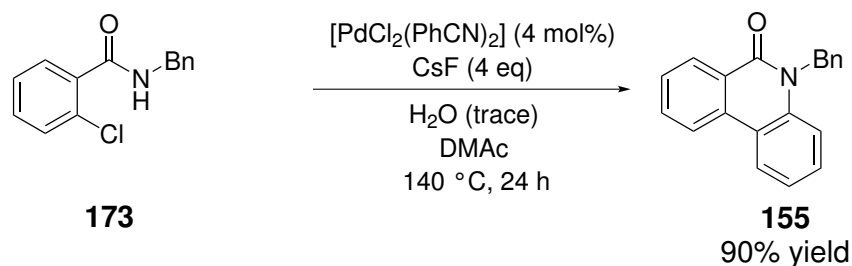
Scheme 49: Synthesis of 5-benzylphenanthridin-6(5*H*)-one **155** by Chen *et al.*[88]

Porée *et al.* have also studied this reaction.[89] They tested a variety of reaction conditions to change the selectivity between two different products and found that changing the solvent and base could result in a switch in selectivity. The mechanism they proposed for the reaction to form the phenanthridinones discussed in this chapter is presented in Figure 38 and was supported by analytical data and computational calculations using DFT methods. It began with the oxidative addition of the substrate followed by deprotonation to give complex **175**. A second oxidative addition occured giving complex **175** which then underwent a reductive elimination to give complex **176**. They then proposed that elimination of methylisocyanate occurred before deprotonation of the nitrogen to give complex **177**. They provided evidence of complex **175** by ESI-MS.
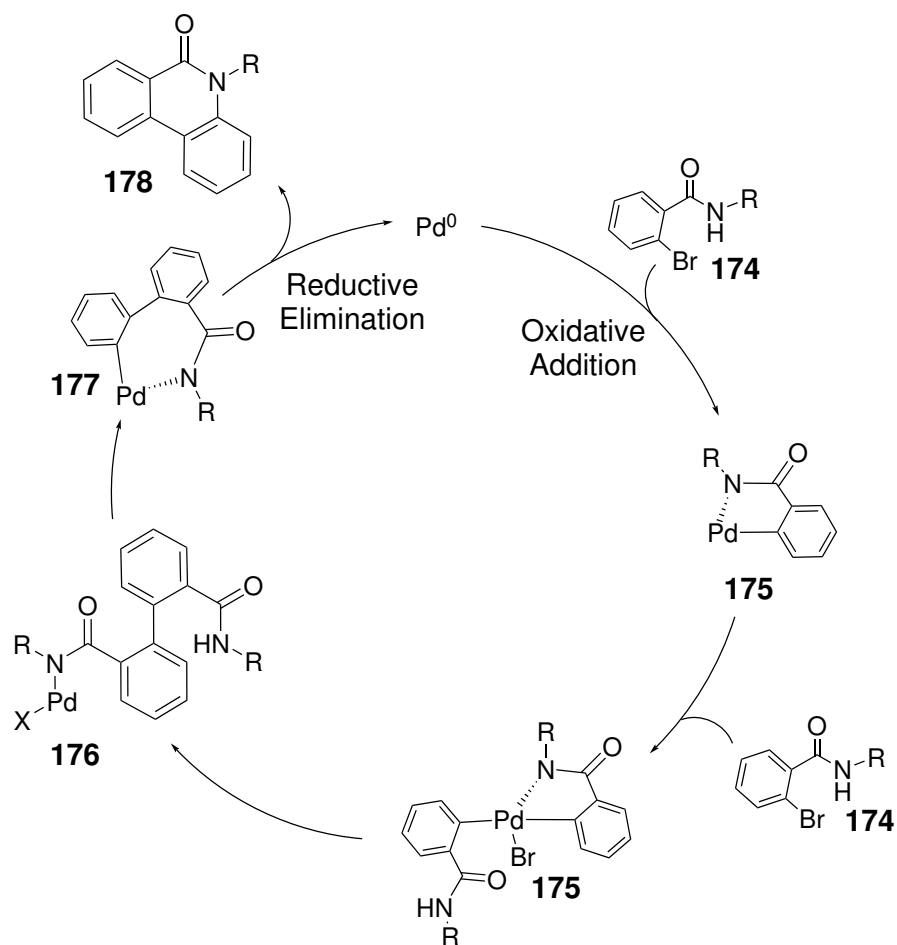
Figure 38: Mechanism proposed by Porée *et al.* for the synthesis of 5-substituted phenanthridinones.

The aim of the work in this chapter was to examine simple catalytic systems in the reaction and to measure the green metrics of the reaction against different literature routes to 5-phenylphenanthridin-6(5*H*)-one **164**. The second aim was to probe the mechanism of the reaction using chemical and analytical methods. The objective of the mechanistic work was to gather more experimental evidence to either support or disprove the mechanism proposed by Porée. The work in this chapter was supported in the laboratory by two undergraduate students, Rebecca Campbell and Alex Pagett.

5.2 Synthesis of the amide starting material 163

As with the previous chapter, the amide starting material **163** for this study was synthesised *via* two methods. The first was the traditional acid chloride synthesis using oxalyl chloride

and the second was the silica synthesis.

Both methods were successful in synthesising 2-bromo-*N*-phenylbenzamide **163**. The acid chloride route gave a yield of 96% and green metrics analysis showed that the atom economy was 65.58, the RME 55.42 and the mass intensity 137.32. Unlike the previous acid chloride reaction outlined in chapter 4 this one takes into account the formation of the acid chloride which is reflected in the significantly lower RME and the higher mass intensity.

Scheme 50: Synthesis of 2-bromo-*N*-phenylbenzamide **163** *via* an acid chloride intermediate.

Synthesising the amide *via* silica catalysis required the harsher conditions used previously in section 4, the use of xylene and a temperature increase to 130 °C. A yield of 59% product was isolated and the green metrics analysis showed a much improved atom economy of 93.88 and mass intensity of 107.1. The RME (54.98) was close to the acid chloride reaction. Compared with the metrics shown in Chapter 3, the mass intensity is high. The reason for this is the amount of solvent used in work-up. For the silica-catalysed reaction, this is purely the recrystallisation, which is unavoidable. For the acid chloride reaction, as explained before, the extra 30 units come from an aqueous work-up which is needed to remove the salt formed, proving that the silica-catalysed method is greener and would be a better alternative if the yield could be improved.
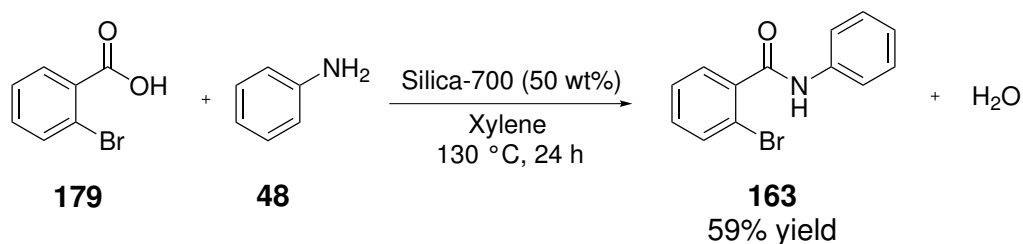
Scheme 51: Synthesis of 2-bromo-*N*-phenylbenzamide **163** *via* silica catalysis.

With the possibility of synthesising the amide starting material **163** through two different routes, one of which could be an excellent green alternative, it was possible to focus on the C–H functionalisation reaction of this amide to form 5-phenylphenanthridin-6-(5*H*)-one **164**, using Pd catalysis.

5.3 Investigation of the reaction conditions in the synthesis of 5-phenylphenanthridin-6(5*H*)-one 164
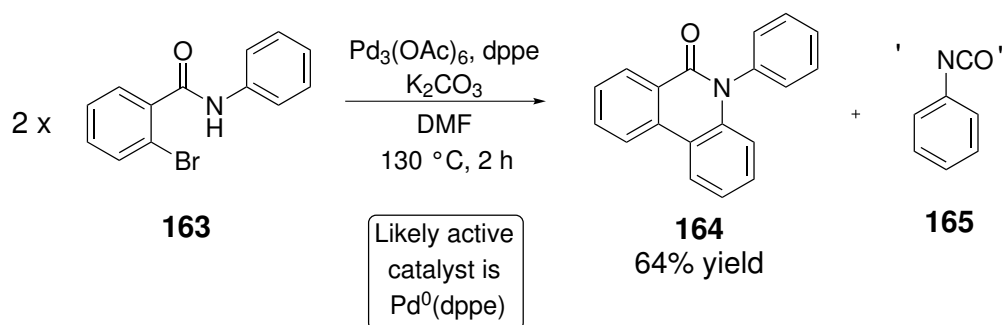
Scheme 52: Pd-catalysed reaction of 2-bromo-*N*-phenylbenzamide **163** for the synthesis of 5-phenylphenanthridin-6(5*H*)-one **164**.

Following analysis of the reaction shown in scheme 52, the structure of the product was confirmed by X-ray diffraction (XRD) analysis of a single crystal (Figure 39). The unit cell contained four molecules which were aligned in rows with the anilide phenyl ring perpendicular to the rest of the molecule. Short contacts were seen between the edge of the anilide phenyl ring and the top face of the phenanthridinone core of the adjacent molecule.
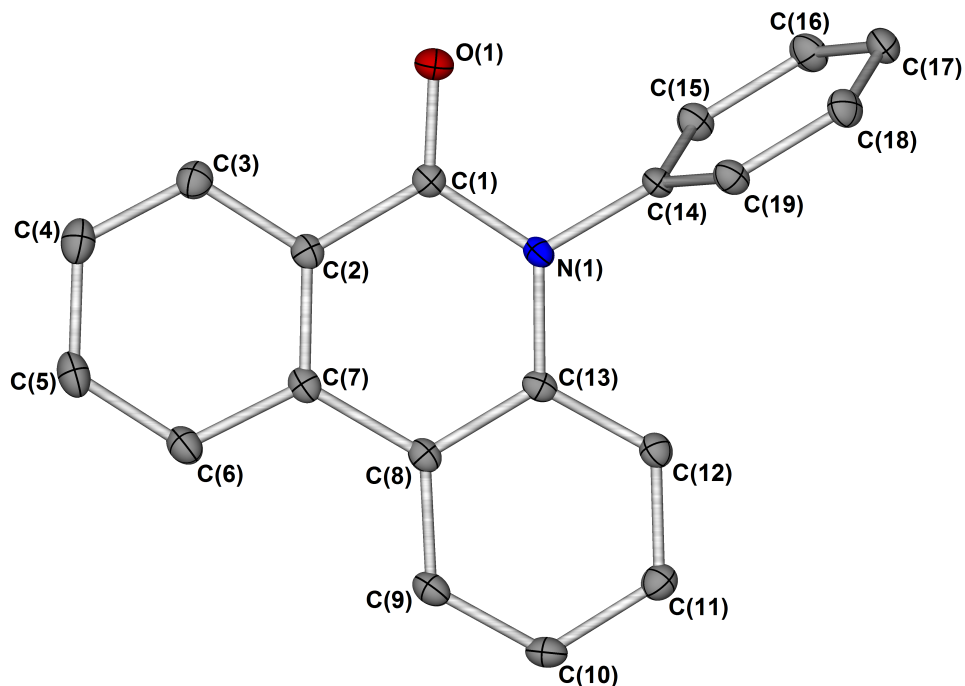
Figure 39: Single crystal X-ray diffraction structure of 5-phenylphenanthridin-6(5*H*)-one **164**. Hydrogen atoms removed for clarity. Thermal ellipsoids shown with probability of 50%. Selected bond lengths (Å): C(1)–N(1): 1.225(1), C(1)–O(1): 1.380(1), C(13)–N(1): 1.405(1), C(14)–N(1): 1.441(1).

A reaction performed with partially-deuterated starting material **163-d$_5$** revealed that the third phenyl ring came from the benzoyl side of the starting material and attached between the benzoyl ring and the nitrogen atom (Scheme 53).
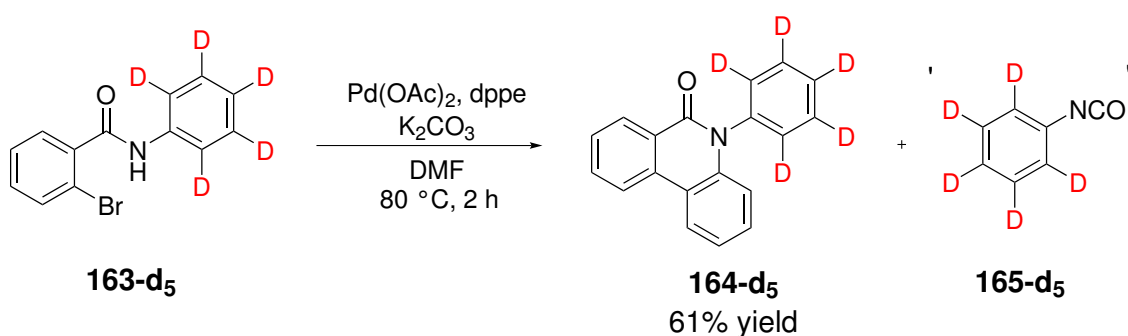
Scheme 53: Reaction of 2-bromo-*N*-d$_5$-phenylbenzamide **163-d$_5$** to give the corresponding 5-d$_5$-phenylphenanthridin-6(5*H*)-one **164-d$_5$** product with one deuterated phenyl ring.

This finding was confirmed by literature data from Furuta *et al.* who carried out the reaction

with a variety of substituents on the benzoyl ring of this type starting material that were seen on the third phenyl ring of the product (Scheme 47).[86]

This was quite an unusual reaction due to the loss of half of one molecule of the starting material and so there was potential for the mechanism for the reaction to be interesting and complex. An examination of the literature revealed that there was very little investigation into the ligand used for the reaction. Many reactions were conducted ligand-free or with phosphine containing pre-formed catalysts.[88–91] Furuta *et al.* tested $Pd(OAc)_2$ as precatalyst with four ligands: BINAP, MOP and two specially synthesised monodentate phosphine ligands.[86] These ligands are all bulky, and contain biaryl groups. A variety of palladium sources have been used in the literature for this reaction, including $Pd(OAc)_2$, Pd_2dba_3 and some preformed $PdCl_2$ based pre-catalysts.[87,88,90,91] This section will focus on $Pd_3(OAc)_6$(99% purity)* and $Pd_2dba_3 \cdot CHCl_3$ (86% purity) as precatalysts in the reaction as these are well defined palladium sources, particularly Pd_2dba_3,[94] and they produced some interesting results.

_____

*Palladium acetate (commonly written as $Pd(OAc)_2$ is know to exist as trimer $Pd_3(OAc)_6$ in the solid state. Some commercial $Pd_3(OAc)_6$ has been shown to contain $Pd_3(OAc)_5(NO_2)$ and polymeric, insoluble $[Pd(OAc)_2]n$.[92,93] The palladium acetate used in this study was high purity $Pd_3(OAc)_6$.
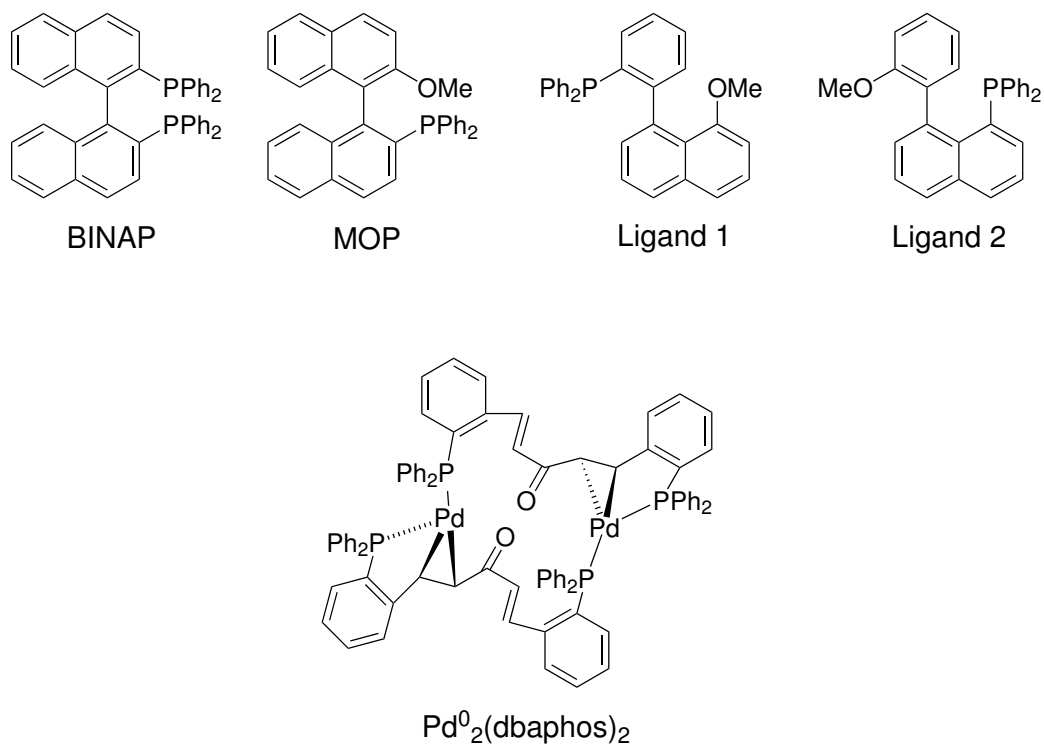
Figure 40: Ligands examined by Furuta in the synthesis of phenanthridinones[86] and the structure of Pd$_2$(dbaphos)$_2$ used in this study.[95]

As this study began with 1,2-bis(diphenylphosphino)ethane (dppe) as the bidentate phosphine ligand, it was decided to examine a variety of similar bidentate ligands to identify the optimum bite angle at Pd. The 1,3-bis(diphenylphosphino)propane (dppp) ligand gave the highest yield of 83% (Table 30). It is clear that there is a sweet spot, possibly around 90 $^\circ$, for the bite angle as having a bite angle too small or too big is detrimental to the yield.[96] In addition to this Pd$_2$(dbaphos)$_2$, developed within the Fairlamb group, was examined. Dbaphos ligands contain multiple binding sites due to the two phosphines and the two alkenes and the Pd$_2$(dbaphos)$_2$ complex (shown in Figure 40) contained bridging ligands between two Pd atoms.[95] An oxidative addition product of Pd$_2$(dbaphos)$_2$ with iodobenzene contained the dbaphos sitting in a *trans*-configuration and it was clear from the lack of conversion in this reaction that it must be necessary for the active catalyst to be in a *cis*-configuration.

Table 30: Yields of 5-phenylphenanthridin-6(5H)-one **164** in reactions using a variety of bidentate phosphine ligands with a Pd$_3$(OAc)$_6$ catalyst.
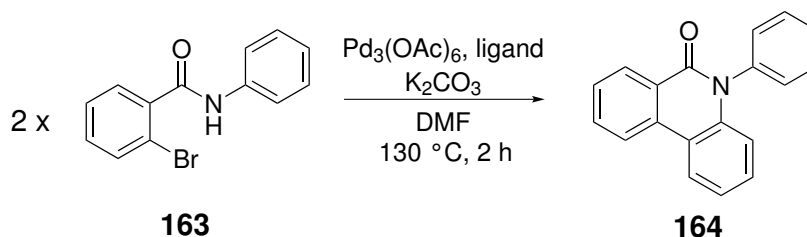
Ligand	Yield /%
dppm	52
dppe [a]	64
dppp [a]	83
dppb [a]	71
dppf [a]	58
dbaphos[b]	0

[a] These reactions were carried out by Alex Pagett. [b] Dbaphos was introduced to the reaction as the preformed catalyst Pd$_2$dbaphos$_2$.

The first set of reactions utilising Pd$_3$(OAc)$_6$ and Pd$_2$dba$_3 \cdot$ CHCl$_3$ as precatalysts highlighted a possible avenue for investigation. The use of Pd$_2$dba$_3 \cdot$ CHCl$_3$ in the absence of air lead to no reaction occurring, contrasting with the use of Pd$_3$(OAc)$_6$ in the absence of air in which the reaction proceeded with good yield. The addition of air into the reaction was tolerated with both catalyst systems, but absolutely necessary for Pd$_2$dba$_3$.

In order to investigate this phenomenon, the direct C–H functionalisation reaction using 2-bromo-N-phenylbenzamide **163** was carefully conducted in the presence and absence of air using Pd$_3$(OAc)$_6$ and Pd$_2$dba$_3 \cdot$ CHCl$_3$. The reactions performed in the absence of air were set up using anhydrous starting materials and catalysts under nitrogen, adding both the dry, degassed DMF (<50 ppm H$_2$O) and substrate in the glovebox. The sealed Schlenk tube was then removed from the glovebox and heated to 80 °C. The reaction vessel was left sealed and stirred for 2 hours, cooled and only then opened to the atmosphere to undergo an aqueous workup. The reactions involving air were set up using Schlenk techniques and 5 ml of air was then injected into the Schlenk tube. The results of these four reactions are detailed in

Table 31, along with the use of PdCl$_2$ as a precatalyst.

Using Pd$_2$dba$_3 \cdot$ CHCl$_3$, air plays a important role, while with Pd$_3$(OAc)$_6$ air gave little difference in yield of product. It is possible then that there is an oxidative process during the reaction in which the acetate or air takes part. Another palladium(II) source, PdCl$_2$, was tested in the air-free reaction and this was successful with a 41% yield obtained. As the only difference in the reaction was the pre-catalyst, this suggests that acetate can be substituted for chloride in the reaction.

Table 31: Yields of isolated 5-phenylphenanthridin-6(5*H*)-one **164** when the reaction was conducted with a variety of pre-catalysts and dppe in the presence and absence of air.
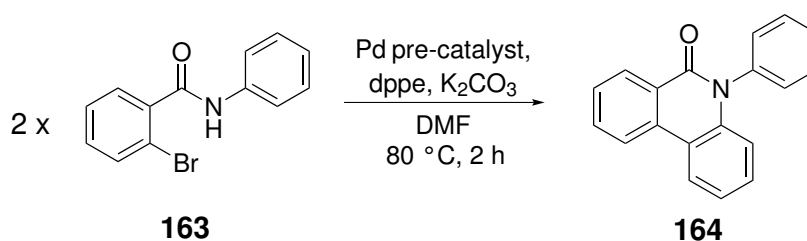
Pd pre-catalyst	Yield /%	
	With Air	Without Air
Pd$_2$dba$_3 \cdot$ CHCl$_3$	73[a]	0
Pd$_3$(OAc)$_6$	58[b]	54
PdCl$_2$	-	41[c]

[a] Reaction conducted in DMAc at 130 °C using dppp as a ligand. Air was bubbled through DMAc for 5 minutes before use.

[b] 5 mL air added after reaction started.

[c] These results were obtained by Alex Pagett.

As the use of dimethylformamide (DMF) and dimethylacetamide (DMAc) are discouraged due to their teratogenic properties,[97,98] a new solvent was desirable in this reaction. Dipolar aprotic solvents do not have a wide range of replacements, although new solvents are emerging in the literature.[99,100] Ethylene carbonate **180** and propylene carbonate are commonly thought of as a replacement for DMF and NMP.[101] Both are reasonably water soluble so can be removed by an aqueous work-up making them practically similar to the traditional dipolar aprotic solvents.[99] Cyrene **181** is a new bio-based solvent that was reported by Sher-

wood *et al.* in 2014.[100] It is produced in two steps from cellulose and has shown promise as a replacement for NMP and other polar aprotic solvents. Various solvent property parameters, such as the Kamlet-Abboud-Taft and Hansen solubility parameters, have shown very similar values to NMP and the solvent has been tested in two simple organic reactions, a fluorination and a Menschutkin reaction, with promising results.
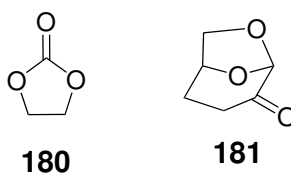
Figure 41: Structures of ethylene carbonate **180** and cyrene **181**: alternative solvents to dipolar aprotics.

Introducing a change of solvent to the reaction shown in Scheme 46, ethylene carbonate gave an approximate yield of 56% by ^{1}H NMR analysis. The product was contaminated with starting material and as all reactions conducted in DMF showed complete conversion of starting material, this suggests that the reaction may be a little slower in ethylene carbonate. The use of $Pd_2dba_3 \cdot CHCl_3$ as the pre-catalyst resulted in a much lower 20% yield which is thought to be linked to the amount of air in the reaction. Unfortunately, cyrene did not show any promise as a solvent in this reaction. The reaction mixture turned from liquid to solid during the reaction which, at first, was though to be some type of polymerisation reaction of the solvent occurring. NMR and MS analysis of the solvent did not provide any useful data and suggested, from the complexity, that the solvent may have degraded. Watson *et al.* reported the formation of aldol products when cyrene is used in the presence of a base.[102] Comparison of the reported NMR spectroscopy data with that obtained experimentally revealed several overlapping peaks suggesting that an aldol reaction is taking place under the reaction conditions shown in 52. The reaction was repeated without the amide substrate and the result was identical so it is clear that cyrene is not compatible with this Pd catalytic system and therefore may be unsuitable for other Pd-catalysed reactions.

5.4 Green metrics analysis of the synthesis of 5-phenylphenanthridin-6(5*H*)-one

Green metrics have been calculated for two literature reactions along with the reaction developed in this chapter. The literature reactions will be considered separately along side the Pd-catalysed phenanthridinone synthesis from 2-bromo-*N*-phenylbenzamide. The first reaction comparison was using the oxidative arylation reaction reported by Liang *et al.* (Method 1 shown in Scheme 54).[103] This reaction is a two step process both of which are catalysed by Pd(OAc)$_2$.

Method 1:
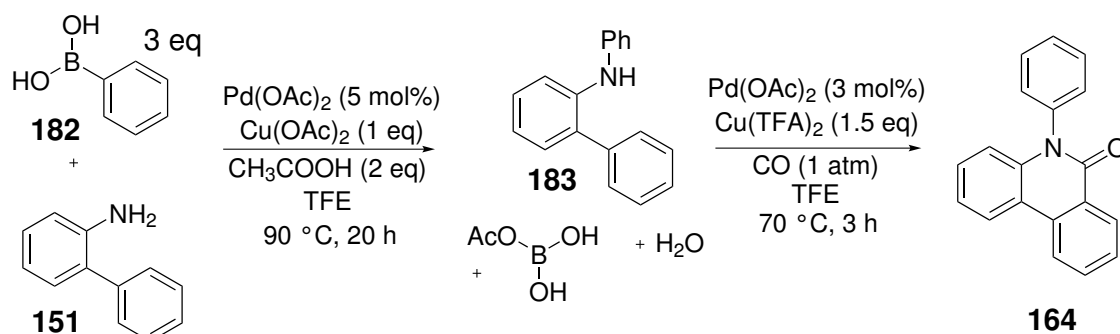
Method 2:
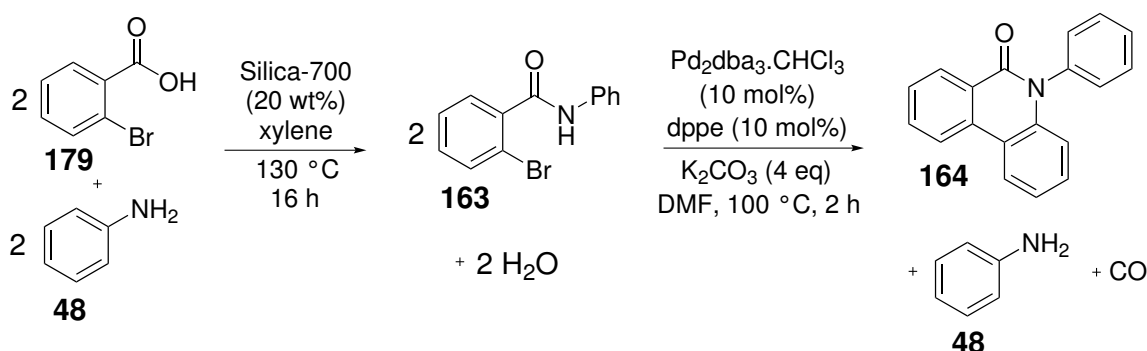
Scheme 54: Details of the reactions used to calculate metrics for the synthesis of 5-phenylphenanthridin-6(5*H*)-one. All values are given with respect to the formation of one equivalent of product.

In order to compare this process to the reaction developed in this chapter it was necessary to calculate the metrics of both steps as shown in Scheme 54. Some assumptions had to be made regarding the literature reaction where the experimental information was not detailed

enough for metrics calculations. Firstly, the oxidative arylation step did not include a yield so this was assumed to be approximately 90%. This first step was scaled down in order to provide the correct amount of starting material for the second step of the reaction. Solvent volumes for purification are generally not included in experimental details and so for each column, 100 mL solvent and 40 g silica were assumed to be used. For the carbonylation step, the carbon monoxide needs to be counted as a reagent in excess and the total volume is unknown. Therefore, the carbon monoxide was considered as being in two equivalents compared to starting material. These assumptions, particularly with the yield, mean that the metrics are only approximate and can only be used to give an indication of the sustainability of the reaction. The results of the metrics calculations are shown in Tables 32 and 33.

Table 32: Quantitative green metrics for the synthesis of 5-phenylphenanthridin-6(5*H*)-one **164**: comparison of the literature synthesis from biphenyl-2-amine **151**[103] (Method 1) and the silica-catalysed reaction from 2-bromobenzoic acid **179** (Method 2).

Metric	Method 1	Method 2
Yield	47% 🚩	47% 🚩
Conversion	100%	100%
Selectivity	47 % 🚩	47% 🚩
RME	18.2	21.6
AE	71.6	46.1
Mass Intensity: Total	4365.6	7465.2
Mass Intensity: Reaction	61.7	136.6
Mass Intensity: Reaction chemicals	10.1	10.3
Mass Intensity: Reaction solvents	51.6	126.3

The quantitative metrics clearly indicate differences between the two processes. The overall yields for both processes are similar, as are the selectivity values. The reaction mass efficiency is slightly higher for method 2, which must be due to the stoichiometry used in the reaction as the atom economy is significant lower. The atom economy would be expected to be low for method 2 due to the loss of aniline and CO from the starting material. The boron reagent that is used in method 1 is relatively small in mass and so does not contribute to

the atom economy too much. The mass intensity of the reaction shows the biggest problem with method 2 is the solvent used. The overall mass intensity is large due to the work-up including chromatography, however, when broken down to look at the mass intensity of the reaction, the chemicals contribute 10.3 in method 2 compared to 10.1 in method 1. This shows that the reactions are more similar than the AE suggests. Solvents contribute the most to the mass intensity of all the reactions examined. An increase in concentration could lead to aggregation of the palladium in solution and inactivity but if the increase in concentration could be coupled with a decrease in the catalyst loading, this may lead to improved metrics.

Table 33: Qualititative green metrics for the synthesis of 5-phenylphenanthridin-6(5*H*)-one **164**: comparison of the literature synthesis from biphenyl-2-amine **151** (Method 1) and the silica-catalysed reaction from 2-bromobenzoic acid **179** (Method 2).

Metric	Method 1	Method 2
Solvents	TFE 🏴	diethyl ether 🏴
Health and Safety	H360, H372, H400 🚩	H360, H372, H400 🚩
Catalysts	Not recovered 🏴	Not recovered 🏴
Reactor	Batch 🏴	Batch 🏴
Elements	B, Pd 🏴	P, Pd 🏴
Energy	Above solvent BP 🚩	🏴

The qualitative metrics for methods 1 and 2 are very similar. Both methods involved the use or production of CO which lead to health and safety concerns. The only differences between the two methods are the solvents and energy used. Method 1 used trifluoroethanol as the solvent for both reactions which is given a green flag under the Chem21 system. Method 2 used diethyl ether in the work-up of the amide formation reaction which is given a black flag due to its vapour pressure and flammability. This solvent could easily be changed but the phenanthridinone forming step uses DMF as a solvent, which is given a red flag. Initial studies suggest that ethylene carbonate could be a good alternative for the DMF in this reaction which would improve the metrics. The energy used in method 2 is given a green flag as the first reaction is conducted at room temperature and the second is well below the boiling point of DMF. For method 1, the energy is given a red flag. The second reaction was

conducted at 90 °C with is 10 °C above the boiling point of trifluoroethanol.

The second reaction from the literature that was used for metrics comparison is shown as method 3 in Scheme 55.[104] This reaction is a concerted, annulation reaction involving 2-trimethylsilylphenyltriflate as a benzyne source which reacts with the iodo-amide. For this calculation it was decided to use just the second step for comparison because the starting materials were similar. As with the first literature reaction,[103] assumptions had to be about the purification of the compound. The column was assumed to use 140 mL solvent and 40 g silica. For the purpose of the metrics calculation, the by-products of the reaction are considered to be triflic acid and trimethylsilyliodide.

Method 3:
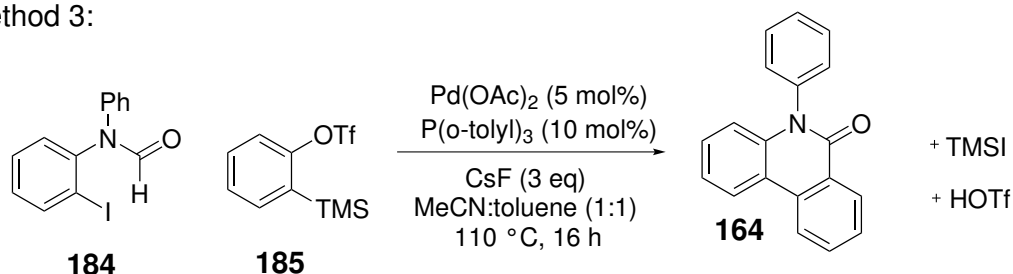
Method 4:
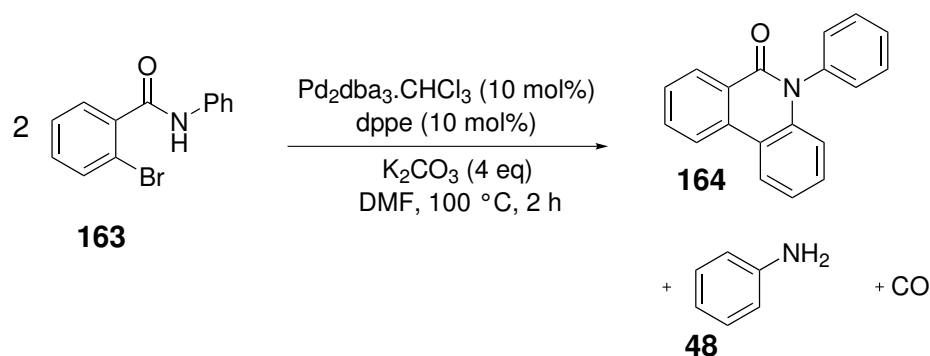
Scheme 55: Details of the reactions used to calculate metrics for the synthesis of 5-phenylphenanthridin-6(5H)-one **164**.

The quantitative metrics were measured first and the yield and selectivity for method 4 were considerably higher than for method 3. Atom economy for both reactions was close; in method 4 the amide is lost and in method 3 the TMS-I and triflic acid contribute a significant mass to the AE. The RME of the literature reaction is lower than that of method 4, which in this case can be attributed to the lower yield. Once again, the mass intensity was higher for method 4, most of which could be attributed to the work-up and to solvents in the reaction. Focussing only on the reaction chemicals, method 4 has a lower value of 5.5 compared to 7.3

for method 3. The reason for this is the higher yield of product as $Pd_2dba_3 \cdot CHCl_3$ is much higher in mass than $Pd_3(OAc)_6$ and method 3 uses less base than method 4 so the opposite outcome would be expected. In spite of the lower mass intensity for the reaction chemicals, the results do highlight the potential for optimisation of catalyst loading and reduction in base.

Table 34: Quantitative green metrics for the synthesis of 5-phenylphenanthridin-6(5*H*)-one **164**: comparison of the literature synthesis from *N*-(2-iodophenyl)-*N*-phenylformamide **184**[104] (Method 3) and the silica-catalysed reaction from 2-bromo-*N*-phenylbenzamide **163** (Method 4).

Metric	Method 3	Method 4
Yield	60%	80%
Conversion	100%	100%
Selectivity	60%	80%
RME	23.9	39.4
AE	43.7	49.1
Mass Intensity: Total	3580.1	6946.0
Mass Intensity: Reaction	41.1	109.6
Mass Intensity: Reaction chemicals	7.3	5.5
Mass Intensity: Reaction solvents	33.9	104.1
Mass Intensity: Work-up	3538.9	6836.4
Mass Intensity: Work-up chemicals	1024.6	801.8
Mass Intensity: Work-up solvents	2514.3	6034.6

Table 35 provides the qualitative metrics for methods 3 and 4. The solvent system used in method 3 (MeCN/toluene) is more sustainable than that of method 2 which uses DMF. The qualitative metrics highlight the use of sulfur and iodine in method 3 in addition to phosphorus and palladium. These are all considered yellow flag elements so not of immediate concern. The reaction temperature of method 3 is within 5 °C of the boiling point of toluene which triggers a red flag while method 4 is conducted well below the boiling point of DMF. The remaining qualitative metrics are identical for both reactions.

Table 35: Qualititative green metrics for the synthesis of 5-phenylphenanthridin-6(5*H*)-one **164**: comparison of the literature synthesis from *N*-(2-iodophenyl)-*N*-phenylformamide **184** (Method 3) and the silica-catalysed reaction from 2-bromo-*N*-phenylbenzamide **163** (Method 4).

Metric	Method 3	Method 4
Solvents	MeCN/toluene 🚩	DMF 🚩
Health and Safety	H360, H372, H400 🚩	H360, H372, H400 🚩
Catalysts	Not recovered 🚩	Not recovered 🚩
Reactor	Batch 🚩	Batch 🚩
Elements	P, S, Pd, I 🚩	P, Pd 🚩
Energy	Above solvent BP 🚩	🚩

After studying the green metrics data, it was not possible to declare that one reaction is greener than another. For methods 1 and 2, the metrics data are very similar for both processes. Between methods 3 and 4, overall method 4 looks slightly greener with the better RME, however, this is mainly due to the higher yield obtained which improves the other metrics. The reaction developed in this chapter could be further optimised to allow both quantitative and qualitative metrics to improve. One such optimisation would be further work on reaction solvents, both to use a greener alternative to DMF and to increase the concentration of the reaction to improve the mass intensity. It would be beneficial to look further at purification methods. These metrics highlight the mass intensity of using chromatography for purification, which is particularly apparent in method 4. Out of all of the steps examined using green metrics, this reaction showed the highest mass intensity for work-up solvent. This is due to the number of side products produced in the reaction making separation by column chromatography challenging. Increasing the selectivity of the reaction, and therefore the yield, may make this easier and would allow a reduction in the volume of solvent used in purification.

5.5 Mechanistic investigations of the synthesis of 5-phenyl phenanthridin-6(5*H*)-one 164

The most interesting feature of the reaction forming 5-phenylphenanthridin-6(5*H*)-one **164** was the mechanism involved in the addition of the third phenyl ring. Standard cross-coupling reactions involving C–H activation begin with the oxidative addition of the Ar–X to a Pd^0 centre, followed by the activation of the C–H bond and the elimination of HX from the cycle, ending with reductive elimination of the cross coupled product. The phenanthridinone forming reaction is more complex, and from looking at the product, can be formed by several possible pathways, shown in Figure 42. One potential route (shown in red) would be an Ullmann-type coupling between the two C–Br bonds, with the second reaction between the N–H and the C–C highlighted in blue. Another is a Buchwald-Hartwig cross-coupling (in purple) between the N–H and C–Br followed by a cross-coupling between the remaining C–Br and the C–C bond highlighter in red. The third option (shown by the blue arrow) would be a standard C–H functionalisation reaction between the C–Br and C–H highlighted in red followed by the decarbamoylation and coupling to the N–H to form intermediate **186**. This would then need to be followed by a hydrodebromination (shown in green) to obtain the final product **164**.
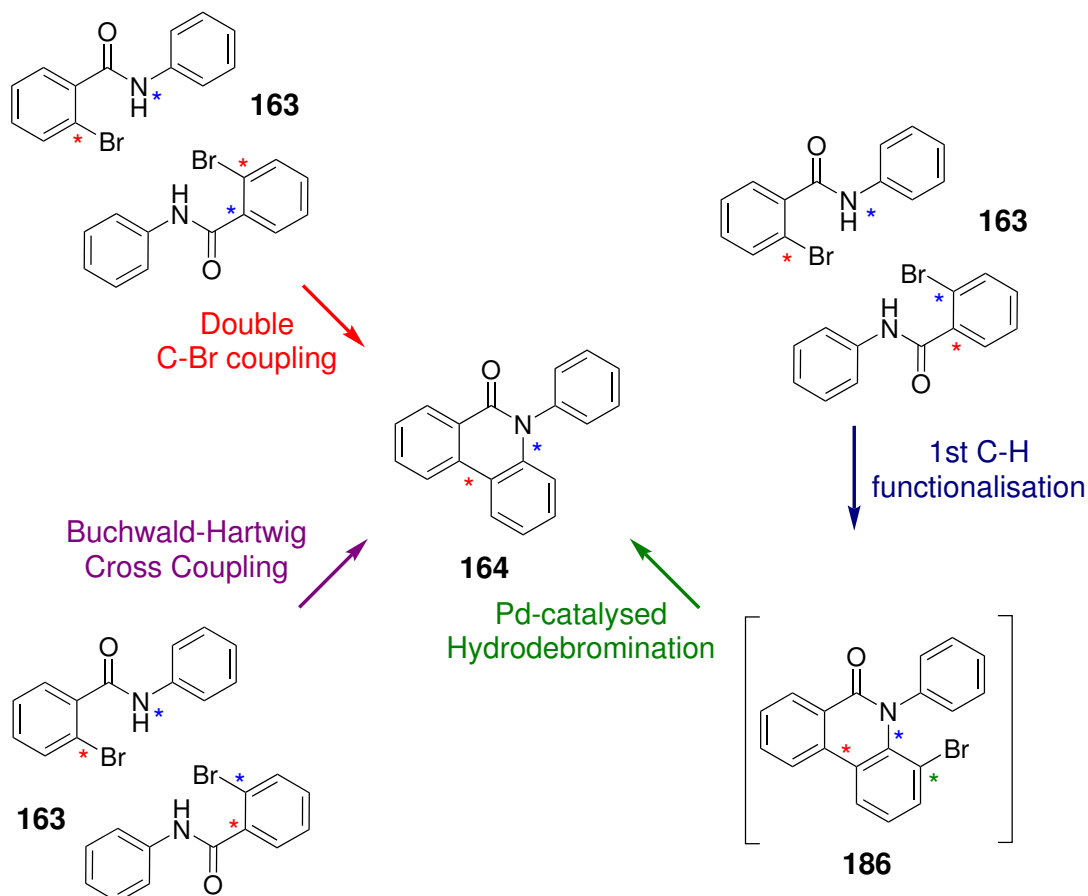
Figure 42: Three possible routes to 5-phenylphenanthridin-6(5*H*)-one **164** from 2-bromo-*N*-phenylbenzamide **163**.

The other possibility is that the Pd catalyst helps to produce some type of benzyne intermediate which is then coupled to the starting material in a concerted fashion. One way of detecting this type of intermediate is to introduce tetraphenylcyclopentadienone **187** to the reaction which can trap the benzyne, releasing CO and forming tetraphenylnaphthalene **188**.
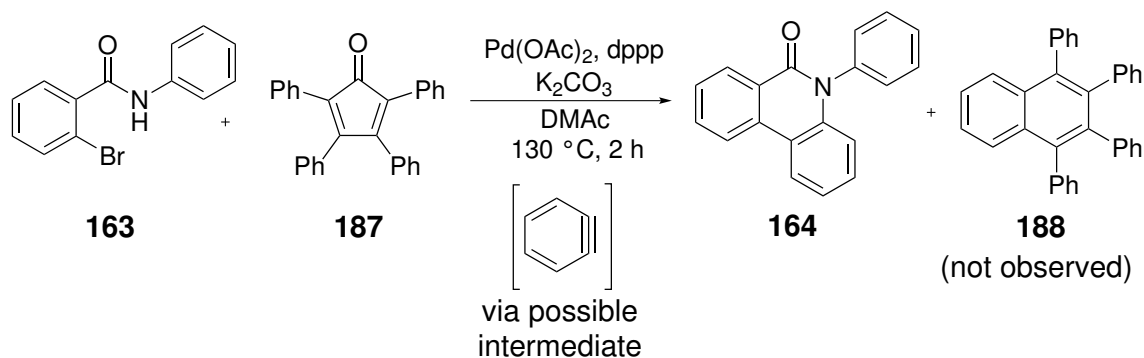
Scheme 56: Addition of 0.5 eq. tetraphenylcyclopentadienone **187** to the reaction of 2-bromo-*N*-phenylbenzamide **163** in order to trap any benzyne present.

The reaction shown in Scheme 56 was conducted on a 0.5 mmol scale and the crude mixture analysed by ^{1}H NMR spectroscopy and mass spectrometry. ^{1}H NMR analysis showed peaks at 6.90–6.94, 7.14–7.19 and 7.21–7.23 with integrals corresponding to the dienone **187** suggesting that most of the dienone was still present. The complexity of the ^{1}H NMR spectrum meant that small traces of tetraphenylnaphthalene would not be visible. No evidence was seen of the naphthalene derivative by mass spectrometry so although a benzyne intermediate could not be ruled out, it seemed unlikely. Furthermore, benzyne is known to react with aniline[105] which is released as a by-product so if a benzyne intermediate were present in the reaction, it is likely that diphenyl amine would be formed and this has not been detected by either ^{1}H NMR or MS analysis in any of the studies conducted. Further mechanistic work concentrated on an alternative mechanism.

5.5.1 Use of a methyl-substituted amide as a substrate

To gain mechanistic information, the reaction to form phenanthridinone **164** was conducted with 2-bromo-4-methyl-*N*-phenylbenzamide **189** as substrate (Scheme 57). The methyl group can act as a mechanistic handle, which can, in principle, give rise to the formation of two regioisomeric products **190** and **191**, shown in the scheme. Compound **190** has the methyl group in the 2-position, and compound **191** in the 3-position. If the product formed possessing the methyl in the 2-position, it would indicate that the mechanism goes *via* a double C–Br coupling and would eliminate the other mechanisms from enquiry.
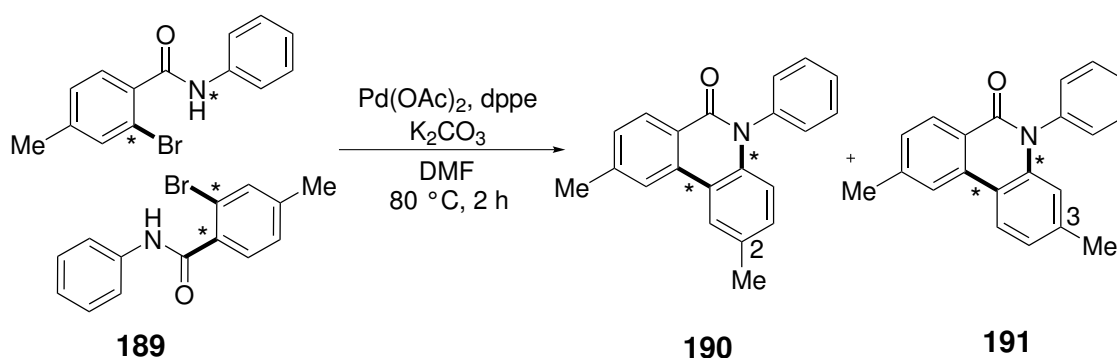
Scheme 57: Reaction conditions for the synthesis of a dimethyl-substituted 5-phenylphenanthridinone with the two possible products **190** and **191** shown. The bonds that are broken and formed during the reaction are highlighted in bold.

The reaction, conducted on a 0.25 mmol scale, was successful and a single regioisomeric product was isolated in 39% yield. ^{1}H and ^{13}C NMR analysis revealed the product to contain the methyl group in position 2 (**190**), as shown in Figure 43. As the two structures are similar, it required selective NOE experiments to distinguish between the two possible regioisomeric structures.
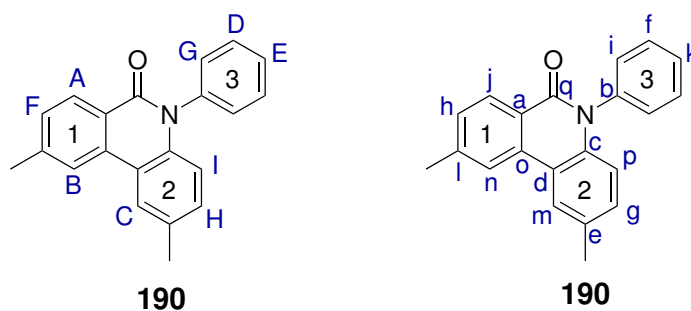
Figure 43: Structure of product formed using methyl-substituted amide starting material.
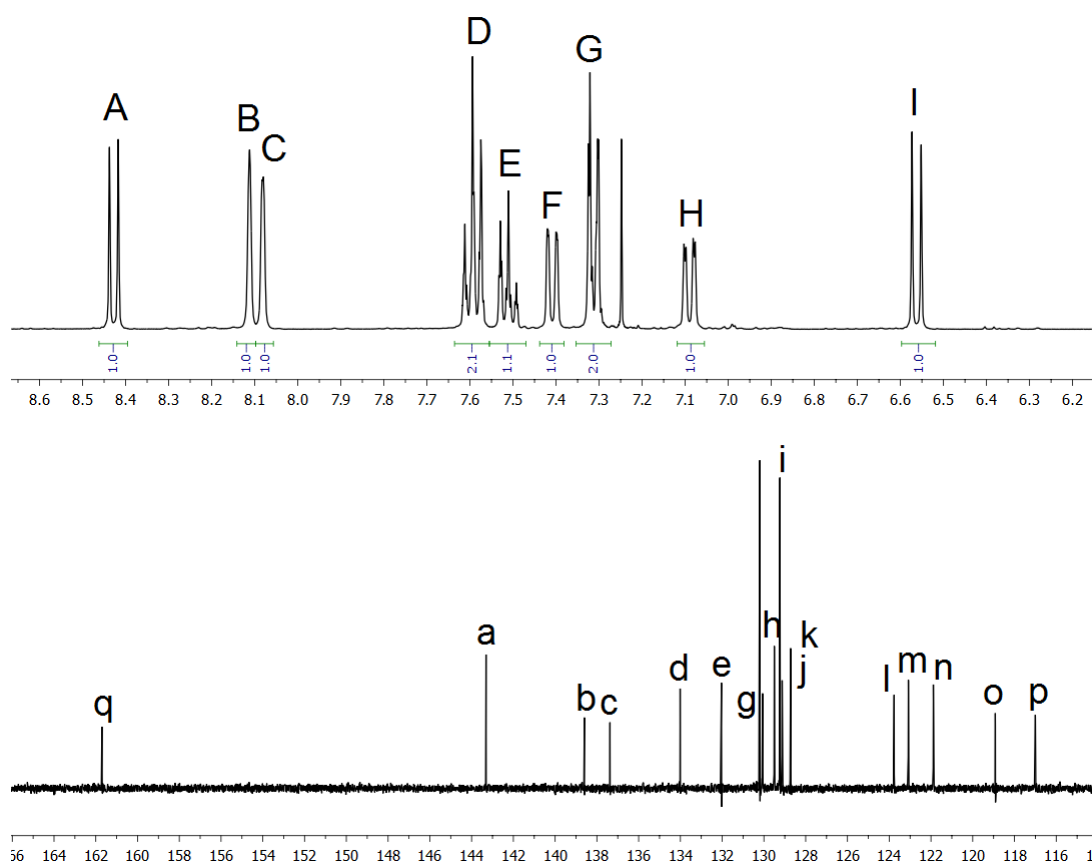
Figure 44: ^{1}H and ^{13}C NMR spectra of 2,9-dimethyl-5-phenylphenanthridin-6(5*H*)-one **190**.

For clarity, the proton signals have been allocated upper-case letters and the carbon signals lower-case letters (Figure 44).

The 2D-^{1}H correlation spectroscopy (COSY) spectrum (Figure 45) provided information on all of the H-H correlations and divided the ^{1}H signals into three ring systems: 'A-F-B', 'C-H-I' and 'G-D-E'. From the integration of the ^{1}H NMR spectrum, it was clear that the anilide ring 3 contains protons G, D and E.

The 2D-^{1}H-^{13}C heteronuclear multiple-quantum correlation spectroscopy (HMQC) spectrum (Figure 46) allocated each of the protons to a carbon signal and therefore some of the carbon signals could be divided into the three ring systems. Protons B and C could be allocated to carbons n and m, respectively.

2D-^{1}H-^{13}C Heteronuclear multiple-bond correlation spectroscopy (HMBC) analysis (Figure 47) enabled remaining carbon signals to be placed and the order of proton signals around the rings to be determined. Signals B and C were the most useful here as they were the protons on each ring that only coupled weakly to other protons, and so were likely to be next to the methyl groups. The HMBC spectrum confirmed that B was on ring 1 as it coupled to the carbonyl, which left C as the proton on ring 2 ortho to the methyl group. There was still, at this point, some ambiguity as to the order of protons on ring 2; proton C could either be close in space to proton B or to proton G as it coupled to proton H and the adjacent methyl group and to both of the quaternary carbons on ring 2 but none of the carbons on rings 1 or 3.
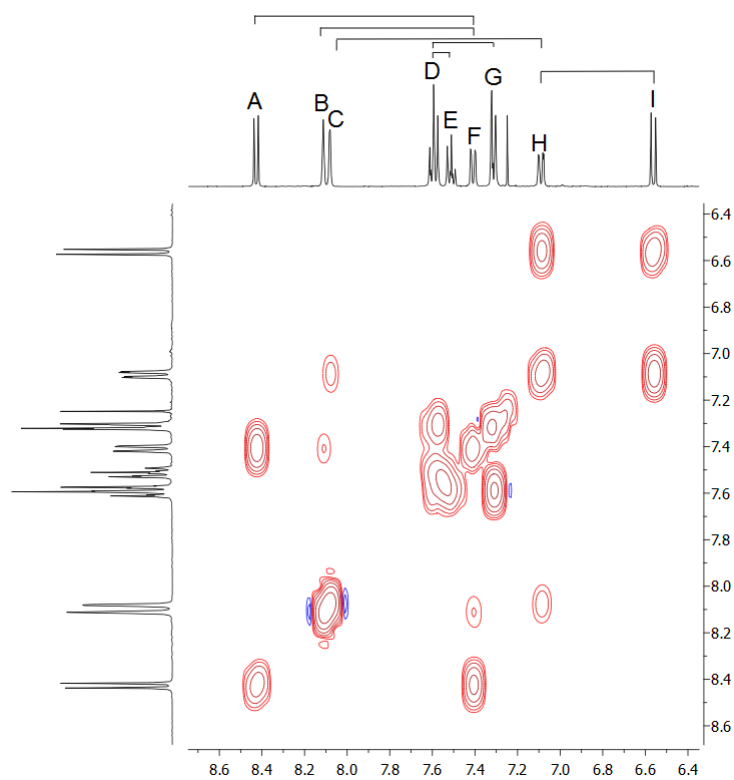
Figure 45: ^{1}H-^{1}H COSY NMR spectrum of 2,9-dimethyl-5-phenylphenanthridin-6(5*H*)-one **190**.
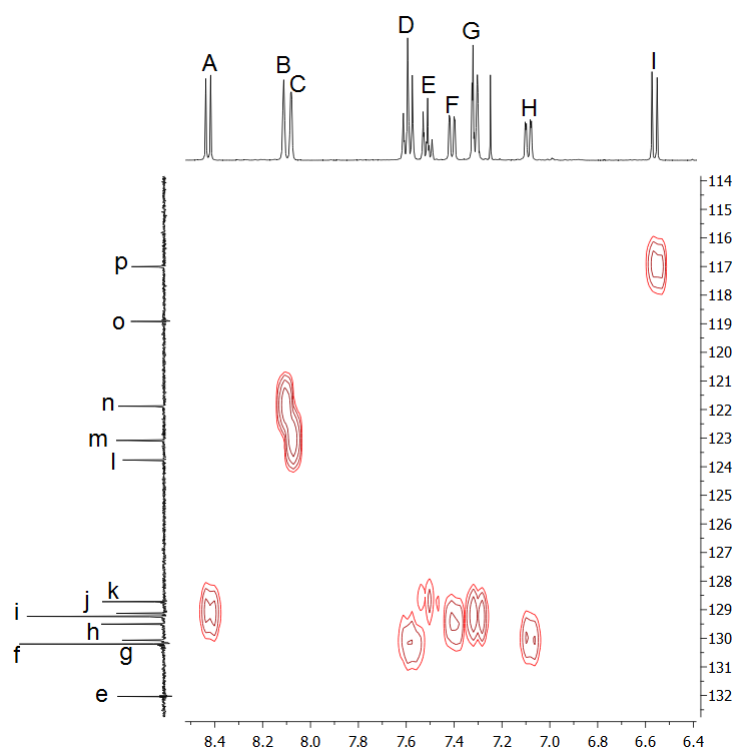
Figure 46: ^{1}H-^{13}C HMQC NMR spectrum of 2,9-dimethyl-5-phenylphenanthridin-6(5*H*)-one **190**.
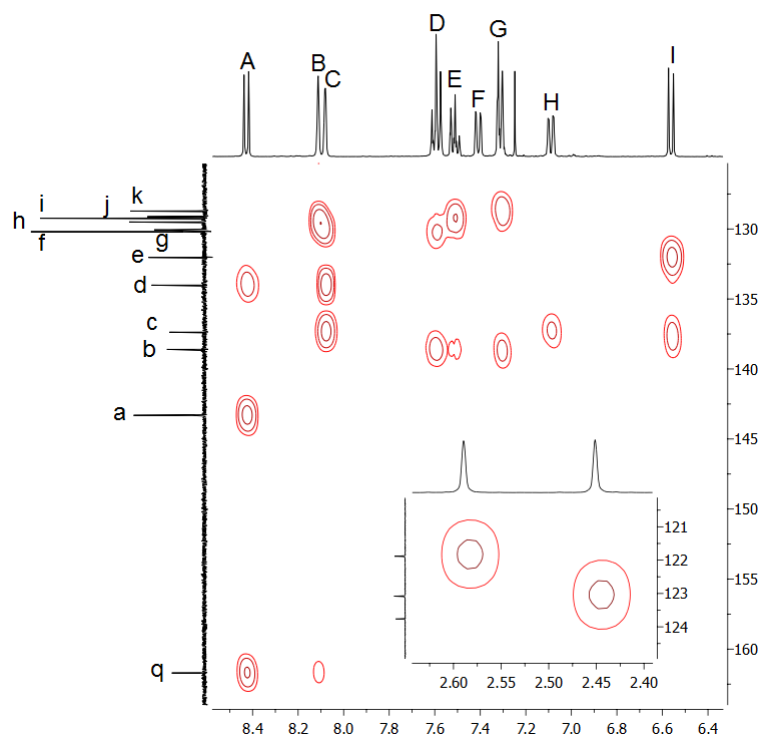
Figure 47: ^{1}H-^{13}C HMBC NMR spectrum of 2,9-dimethyl-5-phenylphenanthridin-6(5*H*)-one **190**. The inset shows the correlation of the methyl protons with the carbons adjacent.

Selective ^{1}H NOE spectroscopy was the perfect tool to allow placement of proton C and the methyl group, as irradiation of proton B would give information on which protons were close in space. A signal was seen for protons C, F and both methyl groups in this experiment which confirmed the structure in Figure 43. Further NOE experiments on proton C and the methyl groups provided similar information to support the assignment. Furthermore, when signal I was irradiated an NOE signal was seen for proton G on ring 3 confirming that proton I was on the right hand side of ring 2.
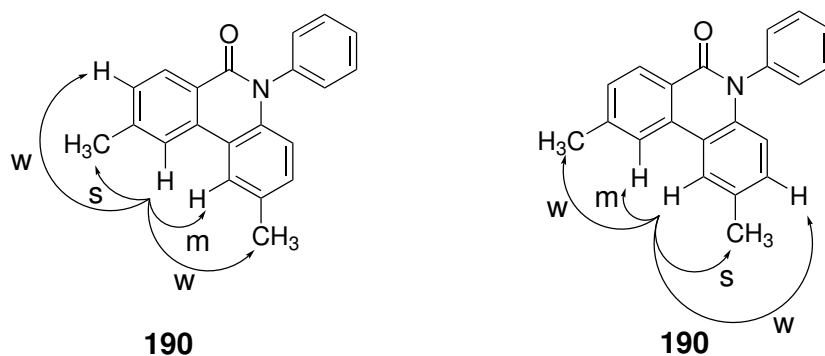
Figure 48: NOE interactions of selected protons in 2,9-dimethyl-5-phenylphenanthridin-6(5H)-one. 'w', 'm', 's' denotes weak (∼0.2%), medium (∼1%) and strong (∼2%) interactions. Spectra were recorded with 32 scans and a 5 second relaxation delay.

Further support for the structure of compound **190** shown in Figure 43 was obtained from XRD analysis of a single crystal (Figure 49) which showed the methyl in position 2. Four molecules were seen per unit cell along with four molecules of $CHCl_3$ which were located in the pocket created between the two methyl groups of one molecule and the carbonyl of another molecule. The crystals were analysed by ^{1}H NMR spectroscopy to confirm that the crystals were representative of the bulk material.
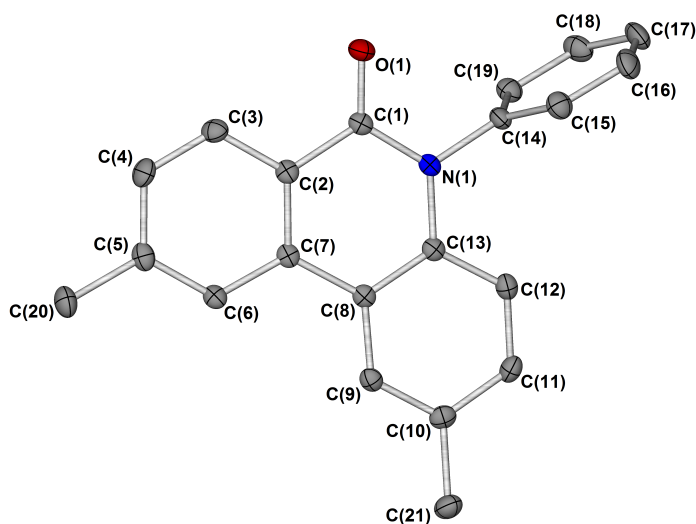
Figure 49: Single crystal X-ray diffraction structure of 2,9-dimethyl-5-phenylphenanthridin-6(5H)-one **190**. Hydrogen atoms removed for clarity. Thermal ellipsoids shown with probability of 50%. Selected bond lengths (Å): C(1)–N(1): 1.377(2), C(1)–O(1): 1.231(2), C(13)–N(1): 1.410(2), C(14)–N(1): 1.450(2).

This result is consistent with a mechanism involving a double C–Br cross-coupling and a decarbamoylation/C–N bond formation. The reaction could occur in two steps, with two different intermediates possible. Figure 50 shows the two possible intermediates in the reaction. Intermediate **192** would be formed when the intermolecular double C–Br coupling has taken place first. Intermediate **193** would be formed when the decarbamoylation has taken place first with a subsequent coupling to the nitrogen. The complete selectivity of this reaction also helped to rule out benzyne intermediacy as that would give two regioisomers.
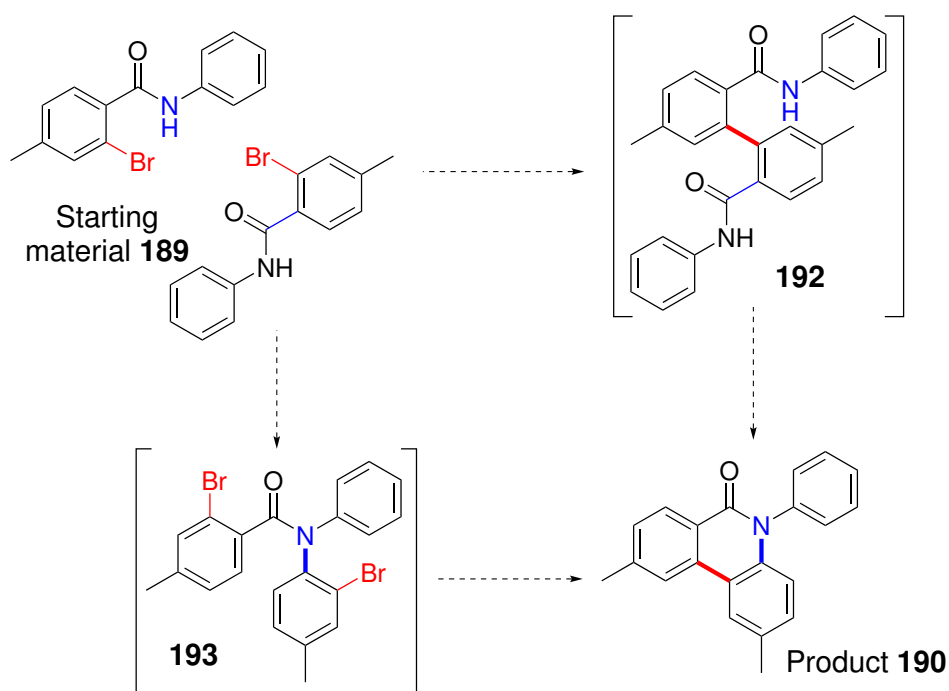
Figure 50: Possible intermediates of the reaction involving the methyl substituted amide starting material **189**.

A reaction performed by Porée *et al.* with a 3-methyl substituted amide **194** corroborated the findings in this study.[89] Their reaction produced the phenanthridinone product **195** with the methyl group in the 1 position of the ring, which is in agreement with the way that the third ring attaches in the product shown in Figure 43. Porée *et al.* examined a series of substrates that are consistent with the broad mechanism described in Figure 50 and their proposed mechanism is shown in Figure 38.
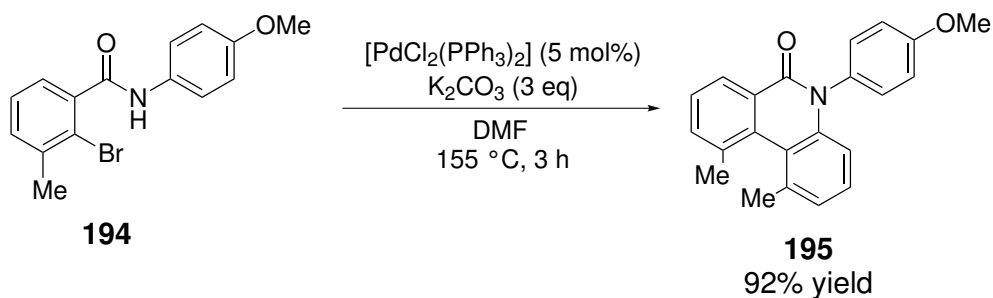
Scheme 58: Reaction of 2-bromo-3-methyl-*N*-(4-methoxyphenyl)benzamide **194**.[89]

5.5.2 Side products in the synthesis of 5-phenylphenanthridin-6(5*H*)-one 164

It was noted in these reactions that the crude ^{1}H NMR spectrum was quite complex and analysis by TLC showed far more compounds than expected. Isolation and identification of these compounds could be useful in proposing a mechanism for the reaction as they may give information on possible intermediates. This information could then be used to improve the selectivity of one compound over the rest, thereby improving the green credentials of the reaction. Figure 52 shows the side products identified by MS and discussed in this section.
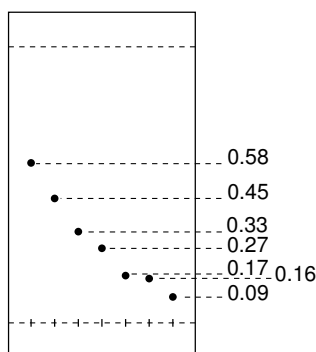
Figure 51: Example TLC plate of the reaction to produce 5-phenylphenanthridin-6(5*H*)-one **164**.

196
MNa+ 291

202
MNa+ 236

204
MNa+ 296

66
MNa+ 220

201
MNa+ 415

210
MNa+ 413

208
MNa+ 489

207
MNa+ 235
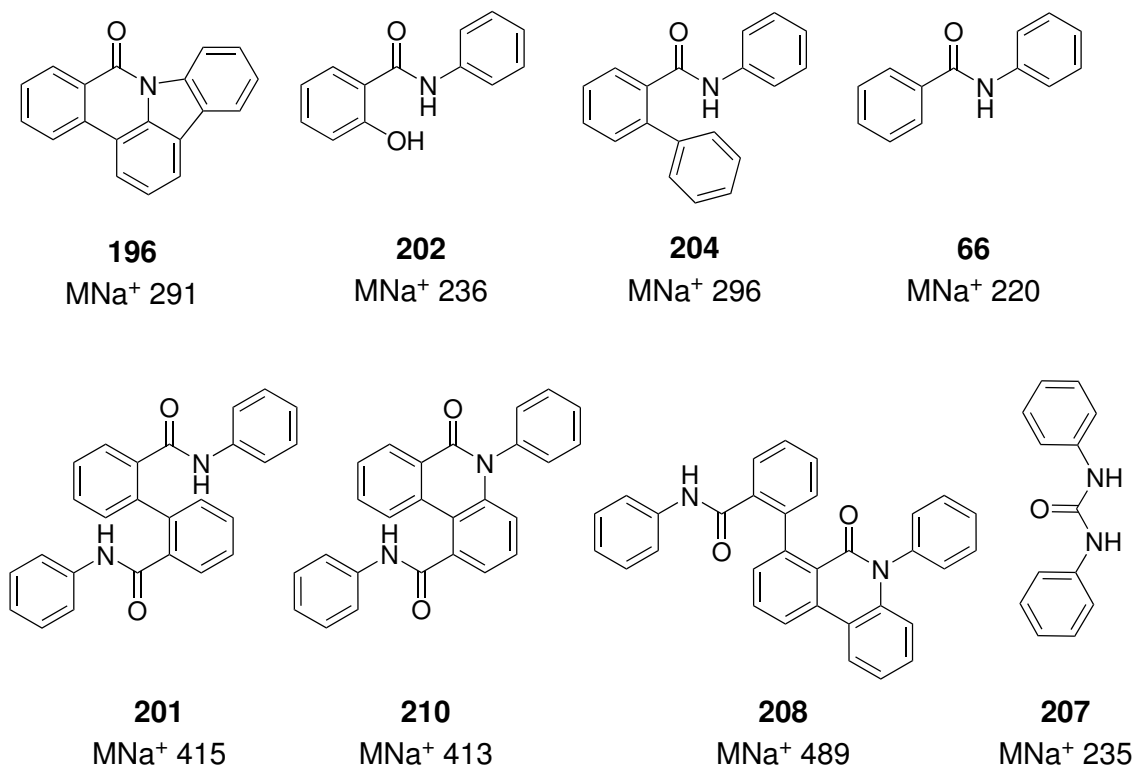
Figure 52: Eight side products identified by MS

A reaction of **163** was performed on a 1.25 mmol scale (Scheme 59) and seven fractions were obtained by column chromatography on silica gel. As there were many compounds and they were produced in small quantities, only two fractions obtained were pure by ^{1}H NMR analysis. In most cases the fractions were mixtures of compounds with the same (or very similar) R_f.

163

Pd(OAc)$_2$ (5 mol%)
dppe (5 mol%)
K$_2$CO$_3$ (2 eq)
DMF
80 °C, 2 h

164
28% yield
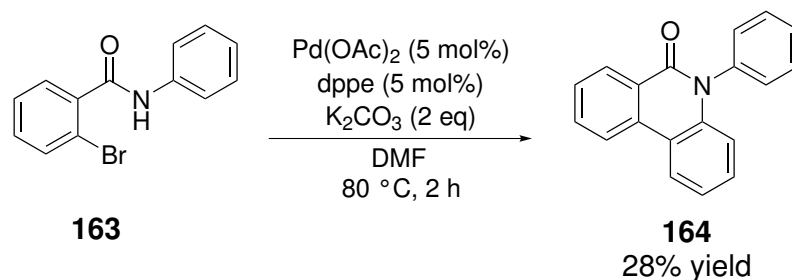
Scheme 59: Reaction at 1.25 mmol scale used for the isolation of side products.

The reaction was repeated with the deuterated substrate **163-d$_5$** mentioned previously, in order to compare the products obtained (Scheme 60). It was anticipated that the deuterated ring would help to identify how some of the compounds were formed. Likewise, the reaction

conducted with the methyl-substituted amide **189** shown in Scheme 57 was scaled-up to 1.25 mmol and analysed by mass spectrometry to provide similar structural information which could be used to suggest an origin for the compounds.
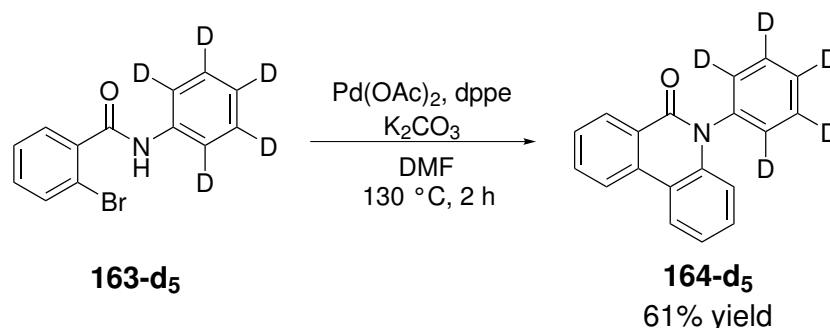
Scheme 60: Reaction of 2-bromo-*N*-d$_5$-phenylbenzamide **163-d$_5$** at 0.63 mmol scale for obtaining structural information about other side products.

The first compound identified, which was isolated from the larger scale reaction and fully characterised, was 8*H*-indolo[3,2,1-*de*]phenanthridin-8-one **196** which contains the phenanthridinone core. This compound was likely formed *via* a double C–H, dehydrogenative functionalisation reaction of 5-phenylphenanthridin-6(5*H*)-one, the main product of the reaction.
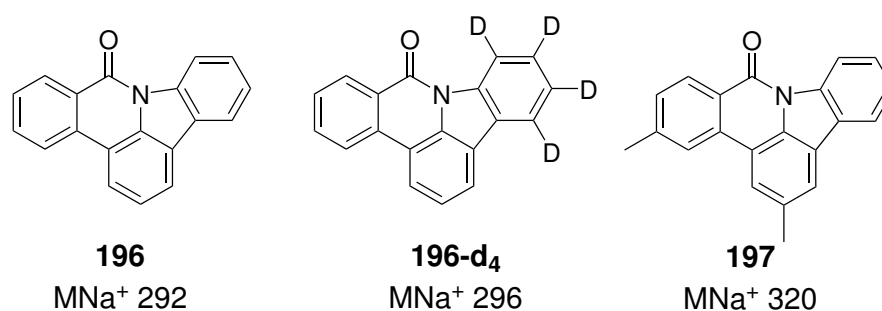
Figure 53: Structure of the first phenanthridinone-based side product, 8*H*-indolo[3,2,1-*de*]phenanthridin-8-one. Corresponding deuteratured **196-d$_4$** and methylated **197** compounds are also shown.

It is a known compound in the literature and had been previously synthesised *via* intramolecular photochemical reactions and Bu$_3$SnH-mediated reactions.[106,107] More recently it has been synthesised *via* an intermolecular Suzuki reaction and an intramolecular Heck reaction followed by an oxidation.[108,109]
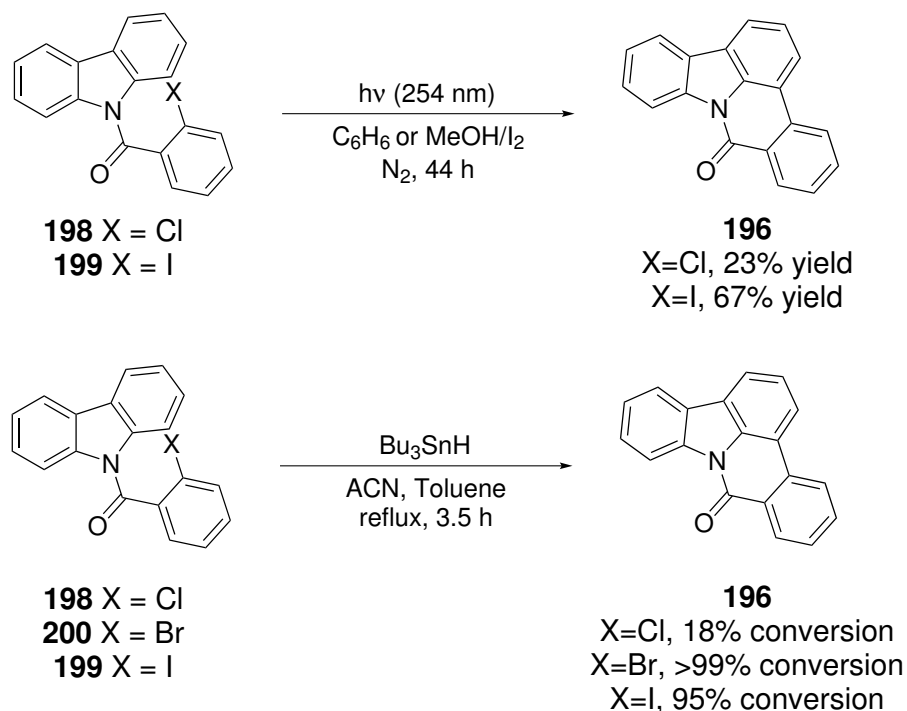
Scheme 61: Synthesis of 8*H*-indolo[3,2,1-*de*]phenanthridin-8-one **196** *via* photochemical reactions and Bu$_3$SnH-mediated reactions.[106,107]

The corresponding compounds were also detected in the reactions conducted with deutero-amide **163-d$_5$** and methyl-amide **189** (Figure 53). The synthesis of compound **196-d$_4$** must involve both C–H and C–D functionalisation, while compound **197** would be formed from the same double C–H functionalisation reaction of compound **196**. Both of these compounds confirm that compound **196** is formed *via* a similar reaction pathway to the main product as it is observed that the phenyl rings have the same origin.

The structure of compound **196** has been confirmed by XRD analysis of a single crystal (Figure 54). There were four molecules to a unit cell. No pi-stacking was observed though expansion from the unit cell revealed that the molecules were stacked off-centre in pairs.
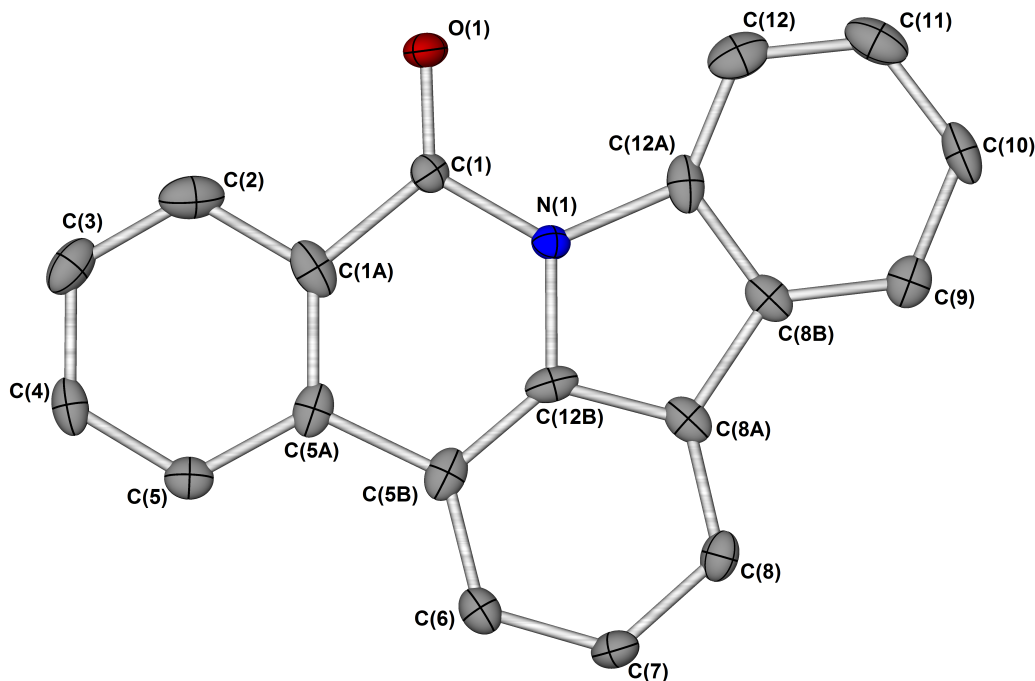
Figure 54: Single crystal X-ray diffraction structure of the phenanthridinone-based side product, 8*H*-indolo[3,2,1-*de*]phenanthridin-8-one **196**. Hydrogen atoms removed for clarity. Thermal ellipsoids shown with probability of 50%. The molecule can adopt two different orientations and this has been modelled by placing the amide in two positions with the refine occupancy 0.708: 0.292(3). Selected bond lengths (Å): C(1)-N(1): 1.219(4), C(1)-O(1): 1.383(3), C(12B)-N(1): 1.412(3), C(12A)-N(1): 1.458(3).

The second compound detected was a biaryl diamide compound **201** which was formed from homocoupling of the starting material **163**. The deuterated analogue **201-d$_{10}$** of the homocoupled starting material was also detected by MS in the deuterated reaction. Compound **201** and its analogues have been reported in these types of reactions before as the main product of the reaction[110] and as a side product of it.[69,87] ^{1}H and ^{13}C NMR data obtained for compound **201** supported the assignment. Eleven ^{13}C peaks were seen with ten in the aromatic region and one carbonyl which matched well with the literature.[110] The proton NMR spectrum showed seven peaks, three of which were double the integral ratio. The compound contains twenty protons, in seven environments. The upfield area of the aromatic region matched well with the literature, however the downfield region (above 7.2 ppm) was less clear. Three distinct signals were seen in the ^{1}H NMR spectrum compared to the reported multiplet for eight hydrogens.[110] Three of the proton signals were absent in the

^{1}H NMR spectrum of compound **201-d₁₀** confirming the presence of the anilide ring.
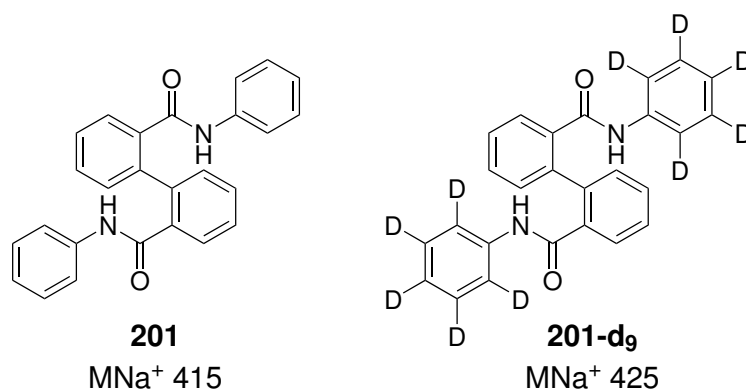
Figure 55: Structure of homocoupled starting material, *N*2,*N*2′-diphenyl[1,1′-biphenyl]-2,2′-dicarboxamide **201** with its deuterated version.

The structure of compound **201** has also been confirmed by XRD analysis of a single crystal. The crystal structure obtained for this compound shows intramolecular hydrogen bonding between the N–H of one amide and the carbonyl oxygen of the other amide, graph set S(9), N···O 2.8264(18) Å which is similar to the distance reported by Goswami *et al.* of 2.857(6) Å.[110] Goswami *et al.* also reported two intermolecular hydrogen bonds between the amide N–H or ortho C–H of one molecule and the carbonyl oxygen of another molecule which creates a 6-membered ring with 2 hydrogen bonds. This can be seen in the crystal structure obtained in Figure 56. The data reported for the intermolecular N···O bond, 2.857(6) Å and C···O bond, 3.313(8) Å are close to the 2.8739(18) Å and 3.287(2) Å obtained.[110] The hydrogen bond lengths seen in the XRD analysis are fairly typical of hydrogen bonding within amide-containing systems.[111–113] The detection of this compound suggests that the mechanism for the main reaction proceeds through a double C–Br coupling followed by a decarbamoylation and compound **201** is released halfway through the cycle.
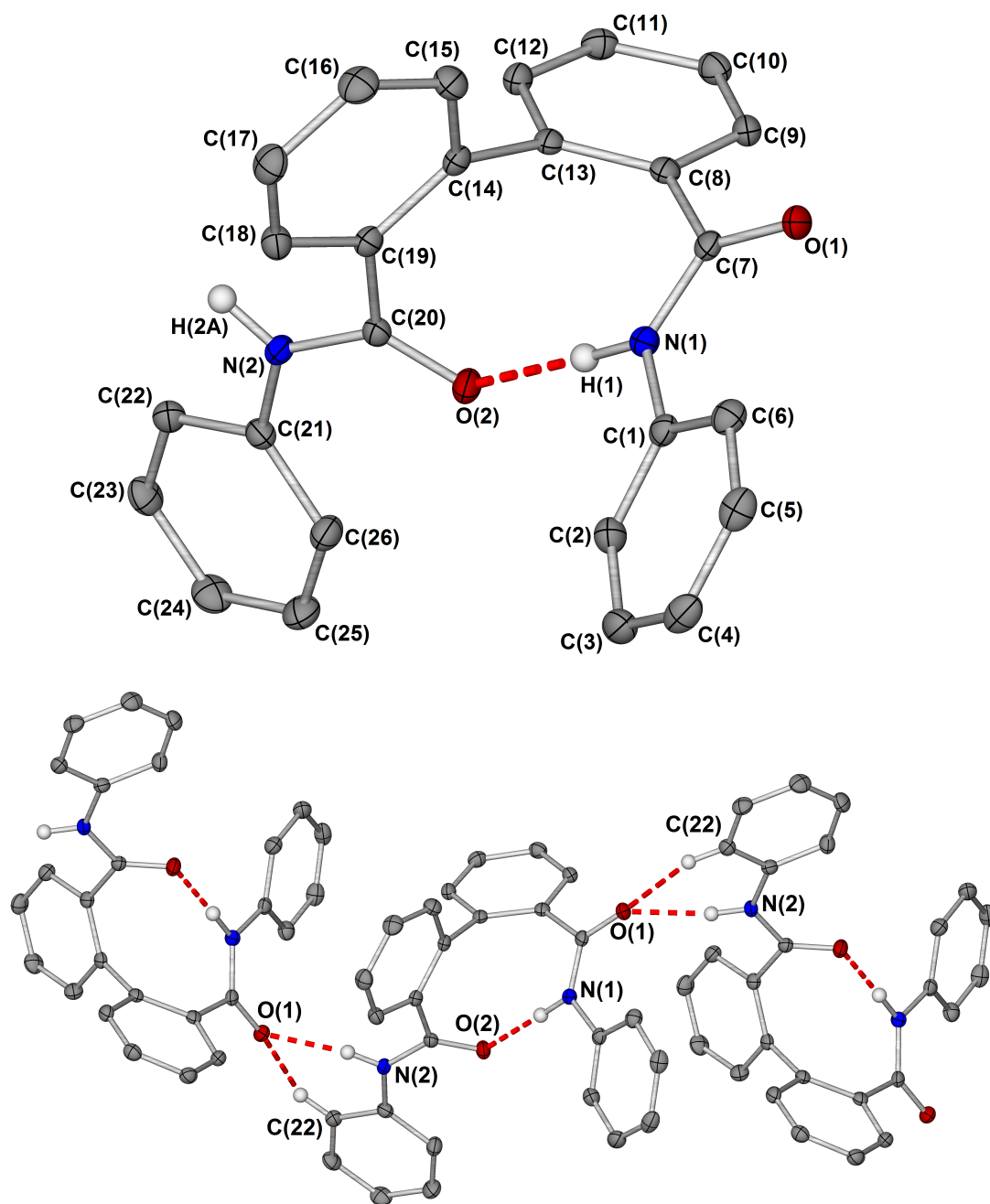
Figure 56: Single crystal X-ray diffraction structure of homocoupled starting material, *N*2,*N*2′-diphenyl[1,1′-biphenyl]-2,2′-dicarboxamide **201**. Top: Hydrogen atoms removed for clarity. Thermal ellipsoids shown with probability of 50%. Selected bond lengths (Å): C(7)–N(1): 1.353(2), C(7)–O(1): 1.233(2), C(20)–N(2): 1.352(2), C(20)–O(2): 1.237(2). Bottom: View of the interactions with the 6-membered hydrogen bond ring shown.

The second fraction from the column was a mixture of three compounds which were insep-arable by TLC. The compounds shown in Figure 57 are proposed structures based on data

obtained by mass spectrometry.

202*
MNa⁺ 236

203
MNa⁺ 250

204
MNa⁺ 296

204-d₅*
MNa⁺ 301

205*
MNa⁺ 310

66
MNa⁺ 220

66-d₅
MNa⁺ 225

206
MNa⁺ 234
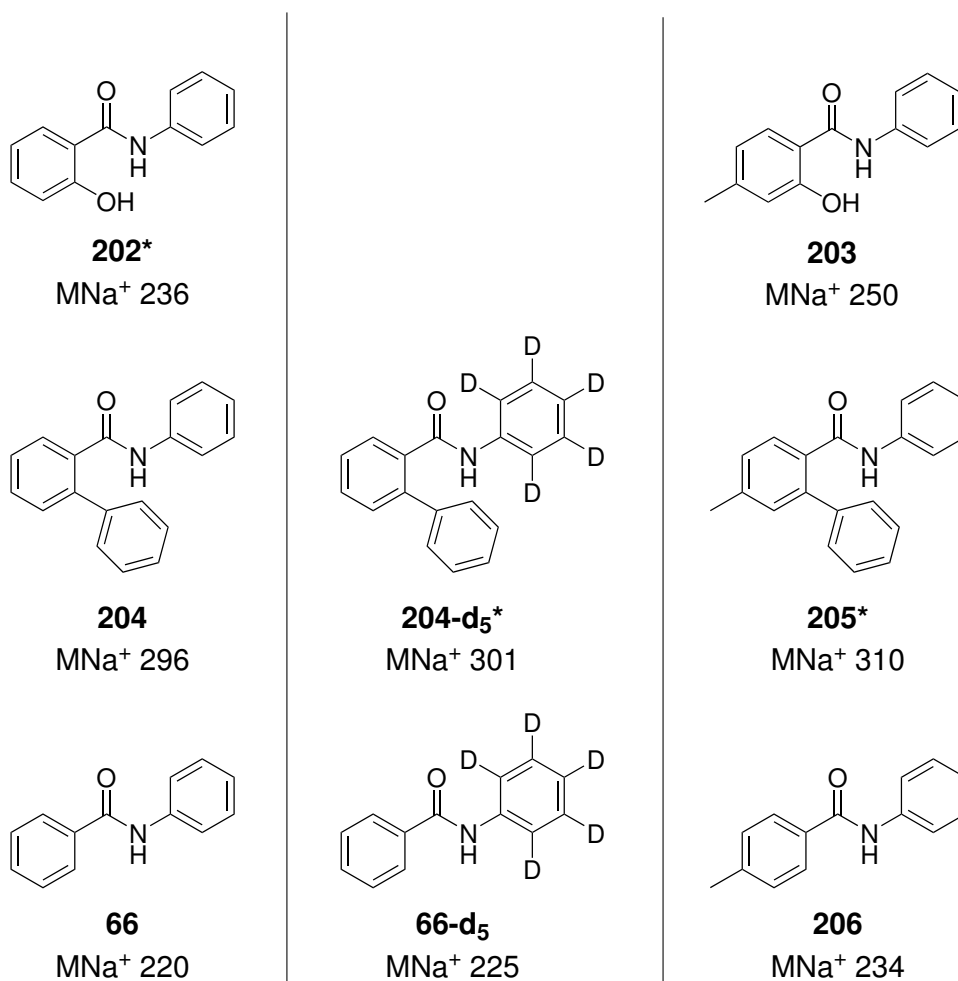
Figure 57: Proposed structures of side products based on MS data of the second fraction from silica column chromatography. * indicates that this compound was the main component in the fraction collected from the silica column.

2-Hydroxy-*N*-phenylbenzamide **202** results from the replacement of the bromine in the starting material with a hydroxyl group. The mass spectrum displayed a high intensity peak at 236 m/z which is the sodium adduct of this compound. The aromatic region of the ^{1}H NMR spectrum was complex making analysis difficult, however comparison with the literature data clearly showed that the assignment of 2-hydroxy-*N*-phenylbenzamide was correct and that this compound was the main component of fraction two. The ^{1}H NMR spectrum contained 8 proton environments corresponding to 10 protons with similar chemical shifts and integrations to the literature.[114] This compound was not seen in the deuterated reaction but compound **203** was detected by MS in the reaction with the methylated started material.

This type of reaction has been reported in the literature by Buchwald *et al.* using KOH as the hydroxide source.[115] Since then, various papers have been published on Pd-catalysed hydroxylation of aryl halides, many using hydroxide bases. Beller *et al.* reported the investigation of ligands in this reaction and isolated an oxidative addition product (Figure 58).[116] They attempted to synthesise the hydroxo complex, but only isolated the aryl hydroxide and suggested that the reductive elimination from the hydroxo complex occurred quickly. In the case the phenanthridinone reaction, the hydroxide needed to form the hydroxo-Pd complex could originate from the reaction of the K_2CO_3 base with any residual water in the reaction.
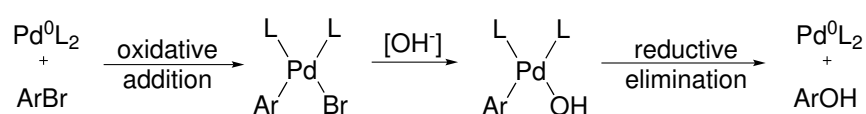
Figure 58: Proposed mechanism for the Pd-catalysed formation of 2-hydroxy-*N*-phenylbenzamide **202**.

204	**204-d$_5$***	**205***
MNa$^+$ 296	MNa$^+$ 301	MNa$^+$ 310
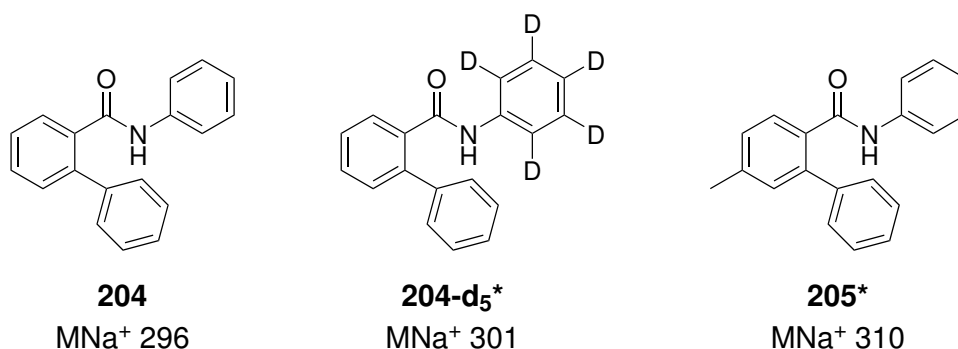
Figure 59: Proposed structures, **204**, **204-d$_5$** and **205** of side products based on MS data of the second fraction from silica column chromatography.

The next structure proposed from the MS data is *N*-phenyl[1,1-biphenyl]-2-carboxamide **204**, a possible intermediate of the reaction. One new phenyl ring has been coupled to the starting material, possibly in a C–H functionalisation reaction. From this reaction is it difficult to say definitively from where the new ring has originated. Given the main reaction involves the coupling of a phenyl ring from another molecule of starting material, it would be likely that this compound is made in the same way. The deuterated starting material does not help to solve this as only one ring in the product **204-d$_5$** is deuterated, which is to be expected. When the reaction is conducted with a methyl substituent attached to the ring that

is transferred, a methyl substituent is only seen on one ring in compound **205**, proving that this compound is not formed from an intermediate in the main reaction but is, in fact, a side reaction. It is possible that the new ring could have come from the phosphine, which contains 4 phenyl rings. This reaction has been reported by Hartwig who saw biaryls made partly from phosphine phenyl rings in a reaction designed to form aryl sulfides.[117] This reaction used the dppe ligand which suggests it is possible that this aryl exchange could have taken place in the phenanthridinone synthesis. Using mechanistic studies and deuterium labelling, Novak suggested that this exchange occured *via* a phosphonium salt which was made from the reductive elimination of one of the phenyl groups of the phosphine.[118,119]
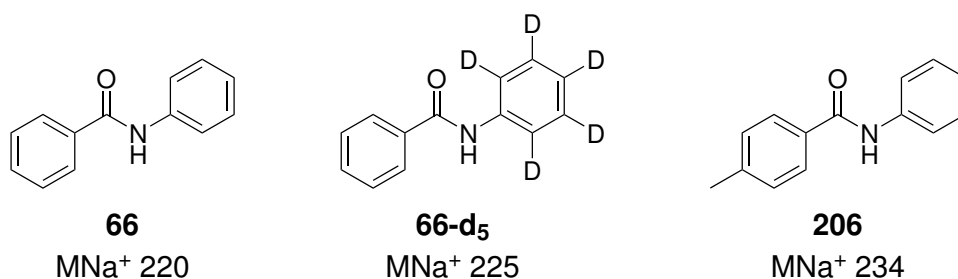
Figure 60: Proposed structures, **66**, **66-d₅** and **206** of side products based on MS data of the second fraction from silica column chromatography.

N-Phenylbenzamide **66** is the result of hydrodebromination of the starting material. This reaction is seen with all three substrates, giving the products **66**, **66-d₅** and **206**. This is a well known reaction in palladium-catalysed reactions in DMF, particularly at high temperatures. This is due to the instability of DMF that decomposes at high temperatures to carbon monoxide and dimethylamine.[120] The dimethylamine is then able to act as a hydride source for the hydrodebromination reaction. The hydrodebromination is thought to occur *via* oxidative addition of the substrate, followed by exchange of the halide for dimethylamine. This complex then undergoes β-hydride elimination followed by reductive elimination to give the dehalogenated compound.[120]

The sixth compound seen in the reaction has a mass that matches diphenylurea **207**. This urea could be formed from the remainder of the second equivalent of starting material.[87] If the remainder of the starting material is phenyl isocyanate, it would be feasible for the isocyanate to break down into CO_2 and aniline. This molecule of aniline could then react

with another phenyl isocyanate to form the diphenylurea. When the starting material used contains a deuterated anilide ring, the MS analysis suggests that the urea formed has two deuterated rings, **207-d₁₀**, which confirms the reaction described above. Urea **207** is formed when the methylated starting material is used which is to be expected as the aniline ring is not substituted. Ureas have been reported in this reaction previously. Catellani *et al.* reported that aniline had been seen in the ^{1}H NMR analysis of the crude product which was trapped with an isocyanate compound to produce an isolable urea.[87] They also reported that symmetrical ureas were detected if the amine part of the amide starting material was particularly nucleophilic. Furuta *et al.* isolated 1,3-bis(4-methoxyphenyl)urea in 40 % yield. This was likely isolated in such a high yield due to the higher nucleophilicity of the amine from the electron donating nature of the methoxy group.[86] Compound **207** is discussed further in section 5.5.3.

The ^{1}H NMR data collected for the column chromatography fraction containing urea **207** could not be used to confirm the urea structure proposed due to the complexity of the spectrum obtained. It is evident that the compound was not cleanly isolated and that there is product and at least one other aromatic compound contaminating the urea. Attempts to separate these compounds were unsuccessful. COSY NMR analysis did not help to identify possible urea peaks as the coupling between peaks does not match that seen in the literature.[121] It is concluded from the combination of NMR and MS data that the main component of fraction four is an unknown aromatic compound while the urea, which is easily seen by MS is only present in a very small amount.

207
MNa$^+$ 235

207-d₁₀
MNa$^+$ 245
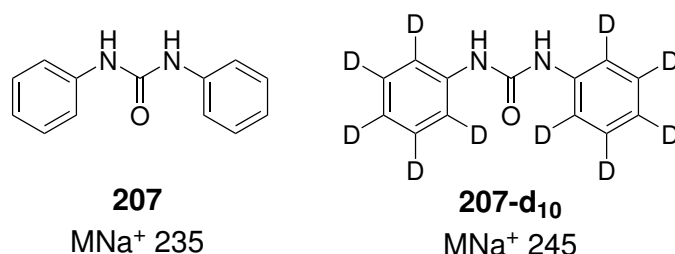
Figure 61: Proposed structures of side product based on MS data of the fourth fraction collected in column chromatography.

Compound **208** was detected in the fifth fraction of the column (Figure 62). This fraction also contained *N*2,*N*2′-diphenyl[1,1′-biphenyl]-2,2′-dicarboxamide **201** and so these peaks

were disregarded in the ^{1}H NMR spectrum. Compound **208** is essentially one molecule of 5-phenylphenanthridin-6(5*H*)-one **164** with a molecule of amide **163** attached. The molecule of amide **163** could be attached at any point except around the anilide ring. The reason for this is that the reaction using deuterated amide **163-d$_5$** produced compound **208-d$_{10}$** which contains 10 deuterium atoms and so both anilide rings must remain unsubstituted. A methyl derivative **209** similar to compound **208** (Figure 63) has been reported by Catellani *et al.* which they report as the main product of the reaction of 2-bromo-*N*-methylbenzamide.[87] They suggest that this compound is formed *via* homocoupling of the starting material followed by a direct arylation type reaction with the amide as a directing group for Pd.

208
MNa$^+$ 489

208-d$_{10}$
MNa$^+$ 499
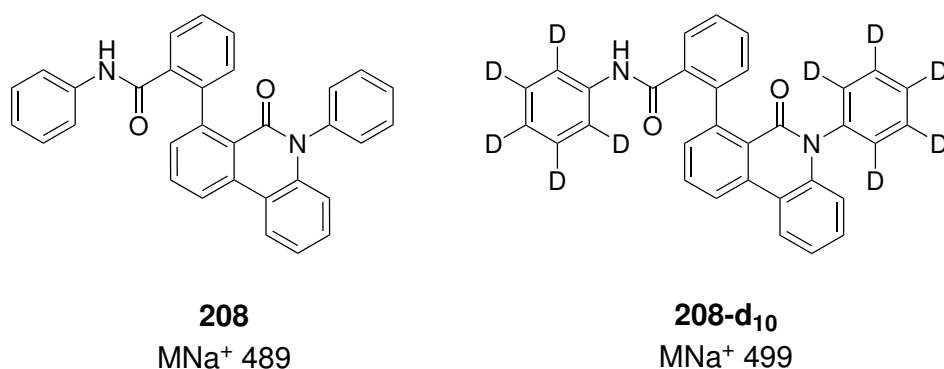
Figure 62: Proposed structures of side product detected by MS, 2′-(6-oxophenanthridin-5(6*H*)-yl)-*N*-phenyl[1,1′-biphenyl]-2-carboxamide.

Analysis of the ^{1}H NMR spectrum of the fraction provided support for the proposed structure of compound **208**. The two extra phenyl groups compared with the literature compound (which contains two methyl groups instead) make the aromatic region of the ^{1}H NMR more complex but some peaks can be clearly compared with literature. A doublet at 8.35 ppm and a doublet of doublets at 8.32 ppm are close to the literature values of 8.35 and 8.37 ppm. A multiplet between 6.60 and 6.67 ppm is also seen, with the Catellani *et al.* reporting a broad quartet at 6.65 ppm.[87] The remainder of the peaks are located between 6.90 and 7.75 ppm as doublets, triplets or multiplets. Comparing the spectrum of this product to that of 5-phenylphenanthridin-6(5*H*)-one, the peak corresponding to the most deshielded proton nearest to the carbonyl is missing which, if replicated in the literature data, would explain the assignment by Catellani *et al.*, logically suggesting that the C–H activation has taken place ortho to the carbonyl of the amide.[87]

209
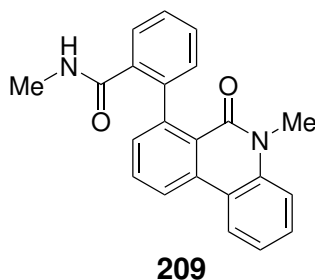
Figure 63: *N*-methyl-2-(5-methyl-6-oxo-5,6-dihydrophenanthridin-7-yl)benzamide **209** detected by Catellani *et al.*[87]

Compounds **210** and **211** are possible structures based on the mass of 413 m/z detected in fraction seven from the column. Compounds with corresponding masses were not detected in other reactions. Compound **211** seems the more likely of the two as it involves two Buchwald-Hartwig amination reactions which are well documented. Typical reaction conditions for this type of reaction are similar, using palladium-phosphine complexes and inorganic bases in solvent such as toluene at high temperatures.[122–124] However, derivatives of compound **210** have been reported by Porée *et al.* as the main product of the reaction of 2-bromo-*N*-phenylbenzamide analogues when 1,4-dioxane was used as a solvent.[125]

The ^{1}H NMR spectrum for fraction seven contained eight peaks corresponding to single inequivalent protons on the proposed product in addition to an N–H proton which lends support to compound **210**, which has nine inequivalent single C–H protons, as the structure. The other proton peaks were overlapping with impurity peaks and therefore were not well resolved. Comparison of the ^{1}H NMR data with the benzyl analogue synthesised by Porée *et al.* show similarities in terms of coupling constants and peak splitting but very different chemical shifts. Their peaks are more downfield, particularly the single C–H peaks on the phenanthridinone core and they see only two aromatic protons below 7.0 ppm, in contrast with the 4 aromatic C–H protons in the phenyl compound.
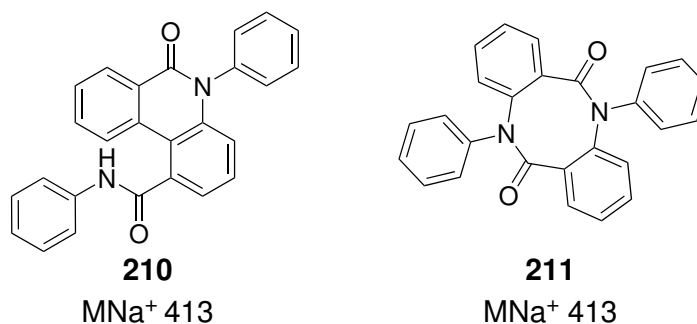
Figure 64: Two possible structures of side product detected by MS at 413 m/z.

5.5.3 The by-product of the synthesis of 5-phenylphenanthridin-6(5*H*)-one 164

The urea **207** which was proposed to be detected in the reaction in Scheme 59 could form *via* reaction of an isocyanate and aniline. As these compounds both originate from the by-product of the reaction, and would hence be in small quantities (a maximum of 25% of each would be theoretically possible; the urea was detected in 2.6% yield), it was decided to try adding phenylisocyanate **165** into the reaction to trap the aniline formed and encourage formation of the urea (Scheme 62). This could help to confirm what the by-product of the reaction was, particularly when using the deuterated substrate (Scheme 63).
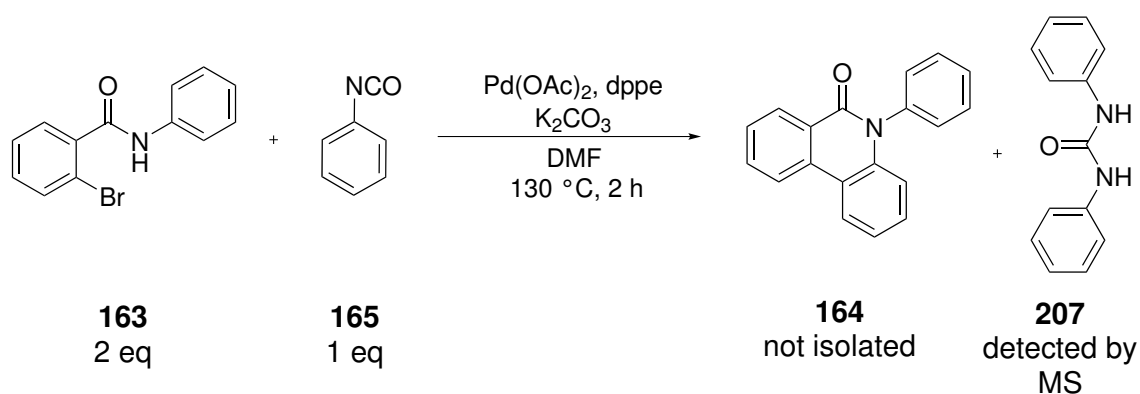
Scheme 62: Scheme showing the addition of 1 eq. phenylisocyanate to the phenanthridinone synthesis to trap the by-product.

Analysis of the crude reaction mixture (Scheme 62) by high resolution mass spectrometry (HRMS) showed evidence of diphenylurea **207** at 235.0837 m/z. Performing the reaction

with the partially deuterated substrate (Scheme 63) in the presence of phenyl isocyanate should result in the formation of a mixed urea **207-d$_5$**. This urea was detected by HRMS at 240.1157 m/z. It should also be noted that in this reaction, the non-deuterated diphenylurea **207** was also detected by MS showing that under the reaction conditions, the phenyl isocyanate is reacting with itself or its degradation product to give the symmetrical urea. The addition of isocyanate did make detection of urea by-products easier but it was not selective and so several different urea-based compounds could be formed in one reaction. The detection of mixed and symmetrical compounds in crude reaction mixtures provide further support for the urea structures proposed in section 5.5.2.
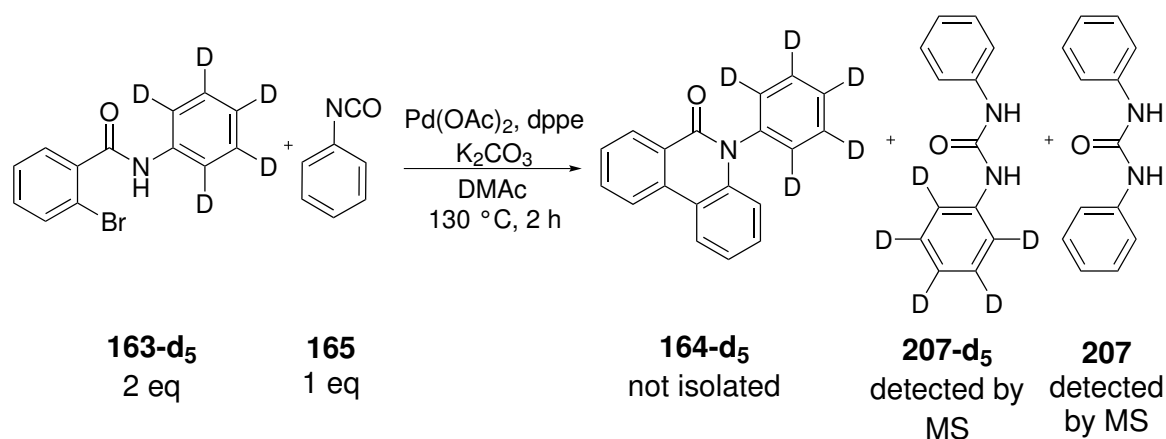
Scheme 63: Scheme showing the addition of 1 eq phenylisocyanate to the partially deuterated phenanthridinone synthesis to trap the by-product.

As mentioned previously, Furuta *et al.* reported the isolation of symmetrical urea **214** in 40% yield from the reaction shown in Scheme 64. They suggested that the urea is formed from dimerisation and decarboxylation of the corresponding isocyanate. This hypothesis is supported by the detection of benzyl isocyanate by gas chromatography-mass spectrometry (GC-MS) in a related reaction.[86]
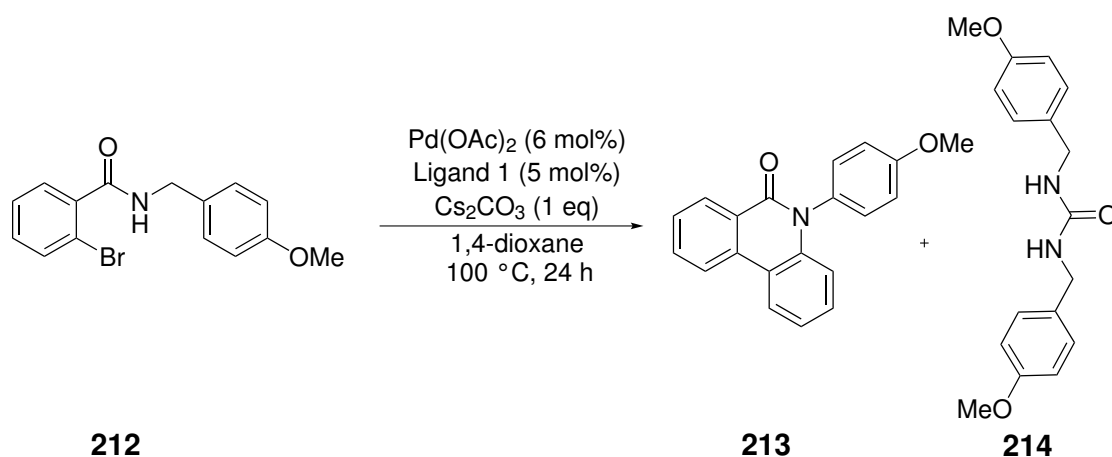
Scheme 64: Literature reaction of 2-bromo-*N*-(p-methoxybenzyl)benzamide **212** in which urea byproduct **214** was isolated.

Ferraccioli *et al.* observed the production of aniline in the reaction of 3-bromo-*N*-phenyl-1-benzothiophene-2-carboxamide which they were able to isolate as a urea after the addition of p-methoxybenzylisocyanate. They believe the symmetrical urea can form if the amine produced is sufficiently nucleophilic but given the detection of diphenylurea **207** in the reactions in Schemes 59 and 62, it is possible to form symmetrical ureas from less nucleophilic amines as well.

5.5.4 Use of ^{31}P NMR spectroscopic analysis and mass spectrometry to identify potential intermediates

^{31}P NMR spectroscopy is commonly used to examine catalytic Pd species involving phosphine ligands. This section details the efforts made to identify the active catalyst species in the reaction and to monitor the progress of the reaction by ^{31}P NMR, using the data to propose potential intermediates in the catalytic cycle. Mass spectrometry was also used to try to identify the proposed intermediates in a series of experiments.

Firstly, using dppp as a ligand, an experiment was carried out with samples taken at 2, 5, 10 and 15 minutes into the reaction. These samples then had the solvent removed *in vacuo* before being diluted in acetonitrile and analysed by electrospray ionisation mass spectrometry (ESI-MS). The reaction was conducted on a 0.5 mmol scale with 5 mol% of catalyst.

Pd$_3$(OAc)$_6$ was chosen as the pre-catalyst to avoid any potential issues with the presence or absence of air. Scheme 65 shows the reaction and compounds detected in the experiment.
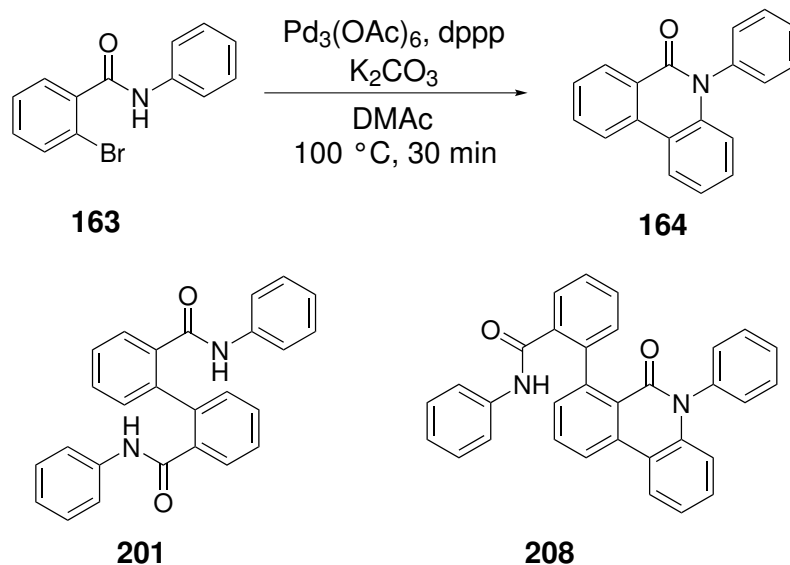
Scheme 65: Phenanthridinone reaction studied by mass spectrometry and the two additional compounds detected.

The sodium adducts of four compounds were seen in the mass spectrometry study. The starting material (m/z 298) was present throughout the 15 minute period, with the intensity decreasing as expected with complete consumption within 15 minutes. This was accompanied by a peak corresponding to two molecules of starting material with a sodium ion (m/z 575), formed during MS analysis which was visible in the first three samples. Similarly, 5-phenylphenanthridin-6(5*H*)-one **164** was observed (m/z 294), with the intensity of the peak increasing throughout the reaction. The other two compounds seen were compound **201**, the homocoupled starting material (m/z 415), that is possibly an intermediate in the reaction, and compound **208** (m/z 489), one of the main side products in the reaction, which increases steadily over the 15 minute period. Compound **201** forms immediately in the reaction mixture and increases over the first 10 minutes of the reaction at which point its formation appears to slow, suggesting that it could be a steady state intermediate in the catalytic cycle.

Unfortunately, no Pd species were seen in the MS analysis. This is most likely due to the high concentration of substrate, combined with the low concentration of Pd catalyst which meant that any Pd species were in too low a concentration to be detected.

Before any more MS studies were carried out, it was advantageous to examine the catalyst systems and the overall reaction by ^{31}P NMR spectroscopic analysis. This could help to pin-point the presence of any likely Pd species so the MS studies could be targeted. At this point, it was decided to use dppe as the ligand in these studies as it is well defined in the literature and has a lower mass than dppp which could be an advantage for mass spectrometry analysis.

The first NMR study was undertaken on the catalyst system. The aim of this study was to identify the active palladium species entering into the catalytic cycle. Palladium-phosphine catalytic systems are well defined in the literature and so the reaction conditions used in Scheme 65 could be easily compared to literature. Three experiments were conducted as shown in Scheme 66 using the two main pre-catalysts from this project with dppe. The catalyst systems were prepared by dissolving Pd pre-catalyst (10 mg) and phosphine (1:1 Pd:P^P) in 1 mL DMF, before a 0.5 mL aliquot was added to 0.2 mL acetone-d_6 for analysis.
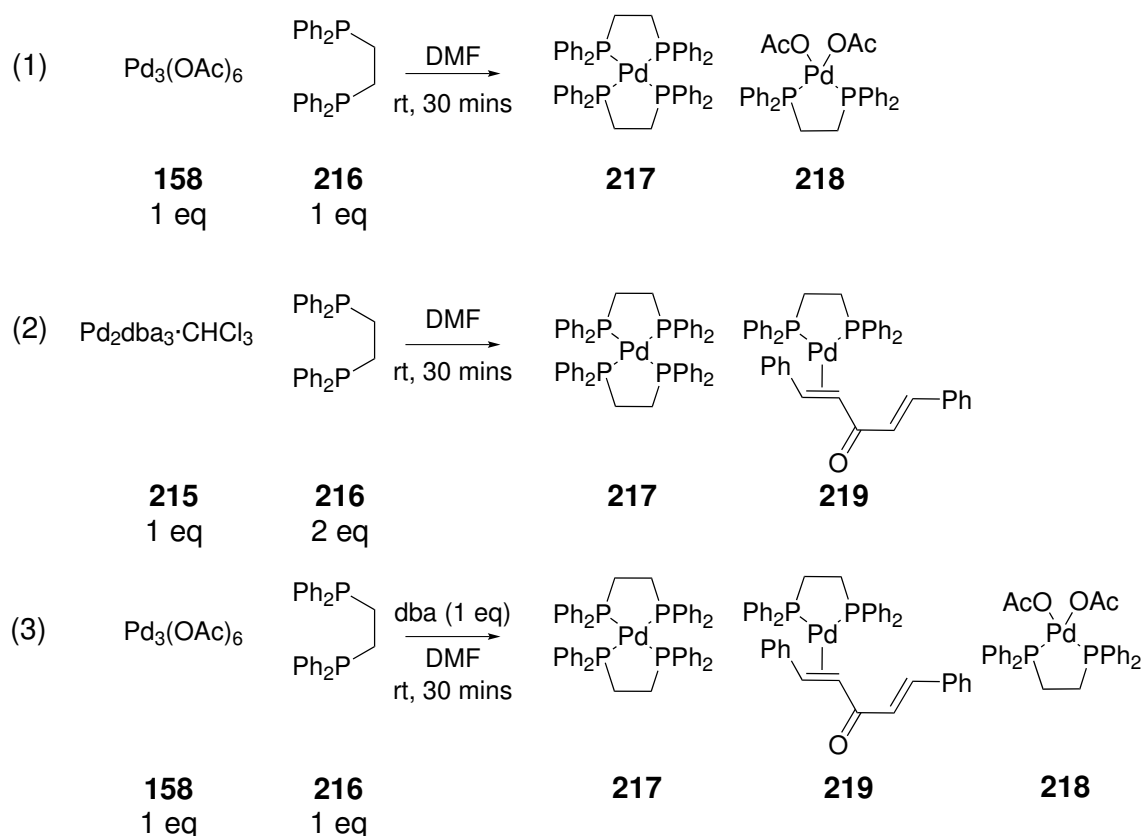
Scheme 66: Catalyst investigation by ^{31}P NMR analysis.

Reaction (1) was the mixing of Pd$_3$(OAc)$_6$ and dppe (reaction 1 in Scheme 66). The NMR

spectrum can be seen in Figure 65 and the species identified in the reaction scheme. There are two singlet peaks at 30.1 and 30.0 ppm. As these are both singlets, the phosphorus atoms must be equivalent. One of these peaks can be assigned to Pd(dppe)$_2$ **217** which is reported in the literature as a singlet peak at 30.46 ppm in THF.[126] The other peak could possibly be oxidised phosphine ligand which in the literature is reported at 33.2 ppm in CDCl$_3$.[127] The peak at 59.07 ppm is assigned to Pd(dppe)(OAc)$_2$ **218**. This compound has been synthesised by Bianchini *et al.* and analysed in CH$_2$Cl$_2$, showing a peak at 58.9 ppm.[128]

Reaction (2) involved the mixing of Pd$_2$dba$_3 \cdot$CHCl$_3$ (86% purity by ^{1}H NMR spectroscopic analysis) with dppe to compare the resulting ^{31}P NMR spectra. Two broad singlets (most likely two unresolved doublets) can be seen in the ^{31}P NMR spectrum at 35.5 (FWHM = 28.6 Hz) and 37.0 (FWHM = 28.3 Hz) ppm. These signals correspond to compound **219** in Scheme 65. This compound is well documented in the literature with ^{31}P NMR peaks reported at 37.8 and 36.4 ppm in DMSO-d$_6$[129] and 34.41 and 36.63 ppm in THF.[126]

Reaction (3) aimed to bring the previous two reactions together by the addition of dba to Pd$_3$(OAc)$_6$ and dppe (reaction 3). The aim was to trap any catalytically active Pd species formed from Pd$_3$(OAc)$_6$ and dppe with a dba ligand. This was successful with the two broad singlets seen at 35.5 (FWHM = 26.4 Hz) and 37.0 (FWHM = 27.9 Hz) ppm (spectrum 3 in Figure 65). A peak at 59.11 ppm was also seen for compound **218**.
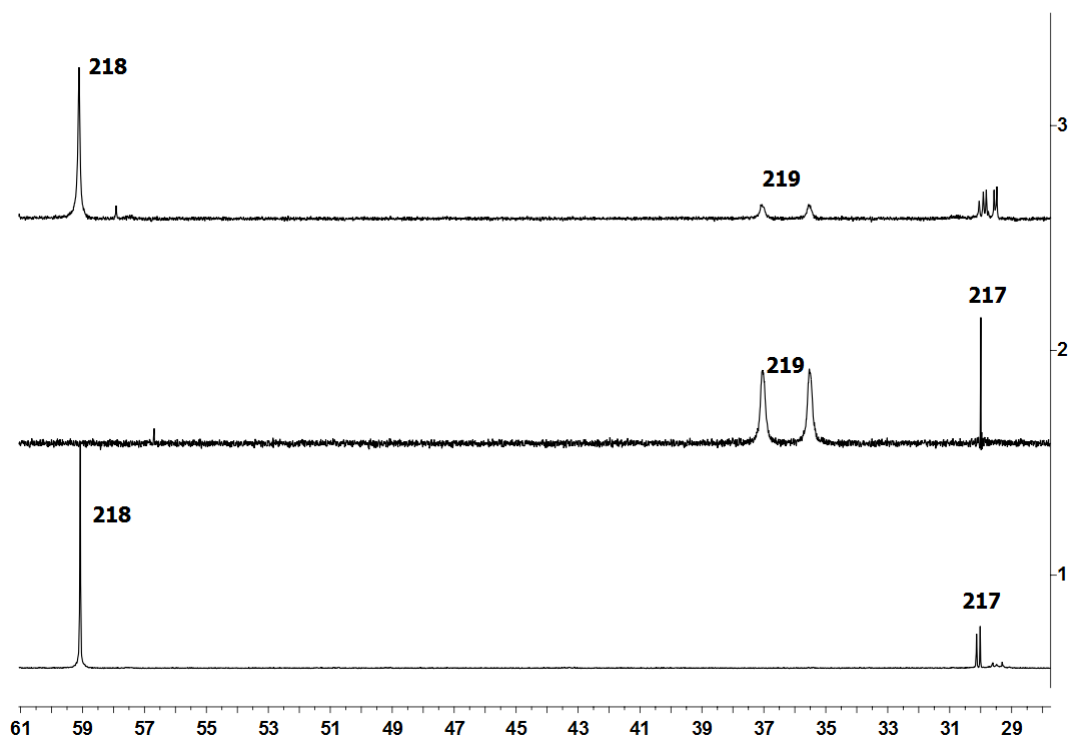
Figure 65: ^{31}P NMR (162 MHz, DMF/$(CD_3)_2$CO-lock solvent) spectra of catalytic species formed from mixing of precatalysts and ligands: (1) spectrum of reaction 1 between $Pd_3(OAc)_6$ and dppe; (2) spectrum of reaction 2 between $Pd_2dba_3 \cdot CHCl_3$ and dppe; (3) spectrum of reaction 3 between $Pd_3(OAc)_6$, dppe and dba. Laboratory work performed by Rebecca Campbell.

From this it could be deduced that the likely active catalyst is the Pd^0 complex **220**. This complex could be released from the complexes detected in the NMR spectra above.
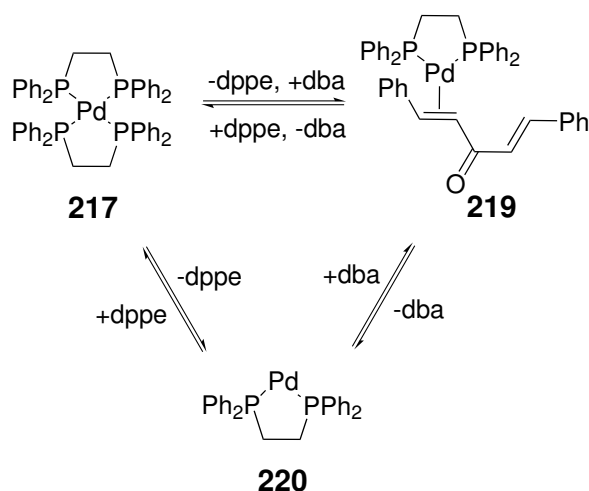
Figure 66: Proposed active Pd complex **220** and route towards it from complexes **217** and **219**.

The second NMR study was similar to the first but instead examined the effect of adding in the substrate. It was anticipated that performing the reaction stoichiometrically without base would result in the formation of an intermediate that could be observed by NMR spectroscopy. This reaction was conducted in DMF-d$_7$ with Pd$_2$dba$_3 \cdot$ CHCl$_3$ as the precatalyst. All manipulations were performed in a glove-box to ensure a rigorous nitrogen atmosphere was maintained, though the solvent was only degassed and not dried. The catalyst system was mixed in DMF-d$_7$ and analysed by NMR spectroscopy before the substrate was added and a second NMR spectrum recorded. The reaction mixture was then heated at 80 °C for 45 minutes and a third spectrum recorded. The fourth spectrum shown in Figure 67 was recorded after 16 hours heating at 80 °C to determine if any degradation was taking place.
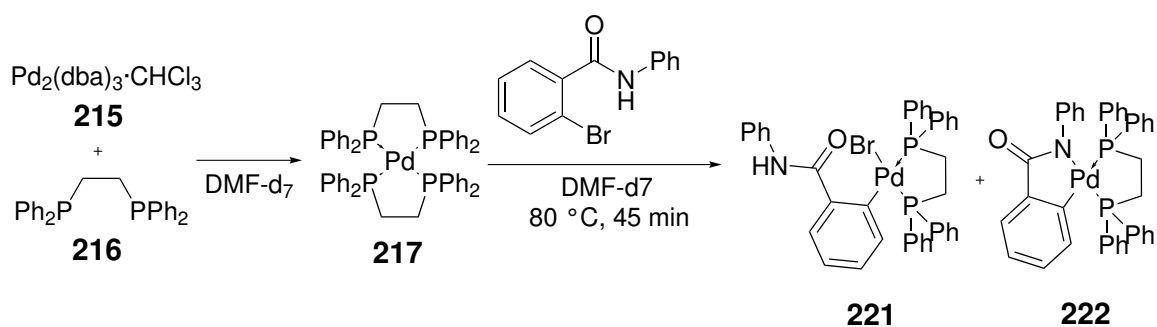
Scheme 67: ^{31}P NMR analysis of the reaction of 2-bromo-*N*-phenylbenzamide.

Spectrum 1 shows the catalyst system and is close to what was observed before. A peak was seen at 29.43 ppm, corresponding to the Pd(dppe)$_2$ complex **217**. Two doublets with a coupling constant of 6 Hz were observed at 35.10 and 36.56 ppm, corresponding to the two phosphorus atoms in the Pd(dppe)(dba) complex **219**. A small fourth peak was seen at 57.42 ppm which was an unknown phosphorus species.

After addition of the substrate, the same peaks were observed immediately after addition of the substrate. A spectrum was recorded after 45 minutes heating at 80 $^\circ$C. Two sets of doublets appeared at 41.78 and 59.05 ppm with a coupling constant of 28 Hz. These are presumed to be the two phosphorus atoms in Pd(Ar)Br(dppe) **221**. ^{31}P NMR signals for oxidative addition products of this type tend to be found around 50 and 35 ppm.[130,131] A higher chemical shift would be expected due to the electron-withdrawing nature of the amide carbonyl. The previously reported catalyst peaks were observed along with a new singlet peak at 65.83 ppm. The peak observed previously at 57.35 ppm had either shifted to 56.77 ppm and increased to 10% of total phosphorus or had disappeared and a new species formed.

After 16 hours heating, the original complex peaks at 29.44, 35.10 and 36.56 ppm had disappeared, leaving only the two doublets at 41.77 and 59.05 ppm, and two singlets at 56.55 and 65.83 ppm. The doublet peaks were small, only 4% of the total phosphorus observed. It was concluded from this final ^{31}P NMR spectrum that the singlet peaks at 56.55 and 65.83 ppm, which grew significantly over the course of the reaction were degradation products. The NMR tube contained black precipitate (Pd black) and so the peaks likely correspond to free phosphorus species in solution.
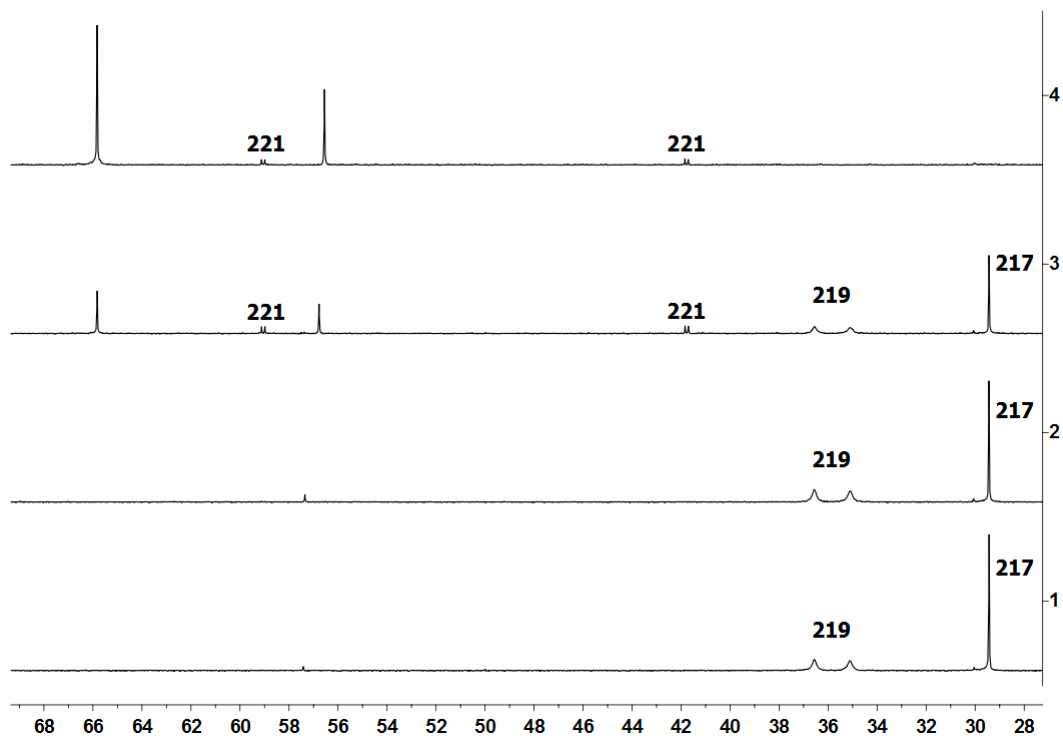
Figure 67: ^{31}P NMR (203 MHz, DMF-d$_7$) spectra of the reaction of 2-bromo-*N*-phenylbenzamide taken by solution state NMR: (1) Pd$_2$dba$_3 \cdot$ CHCl$_3$ and dppe taken at rt, t = 0 mins; (2) taken after addition of substrate at rt, t = 5 mins; (3) taken after 45 minutes heating at 80 °C; (4) taken after 16 hours heating at 80 °C.

This reaction was repeated with a sample taken for MS analysis after 45 minutes heating at 80 °C. The ^{31}P NMR spectrum taken before sampling was identical to that of spectrum 3, above. The mass spectrum showed many Pd species, three of which have been identified. Complex **217** is the palladium species seen in the NMR studies formed when the Pd pre-catalyst reacts with dppe. Complex **222** is formed when the substrate oxidatively adds to the active catalyst, followed by replacement of the bromine with the nitrogen of the amide and elimination of HBr. It is possible that complex **222** is formed *via* loss of bromine in the mass spectrometer from complex **221** and it is actually complex **221** in solution.
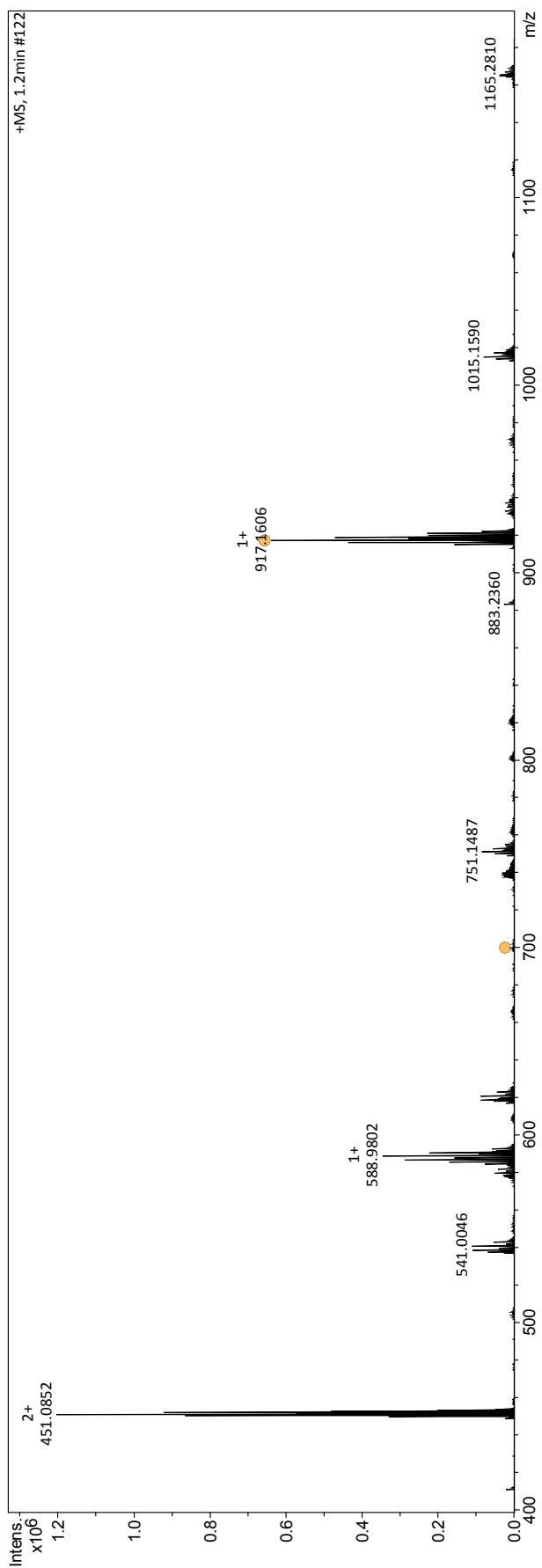
Figure 68: ESI-Mass spectrum of the reaction of 2-bromo-*N*-phenyl-benzamide
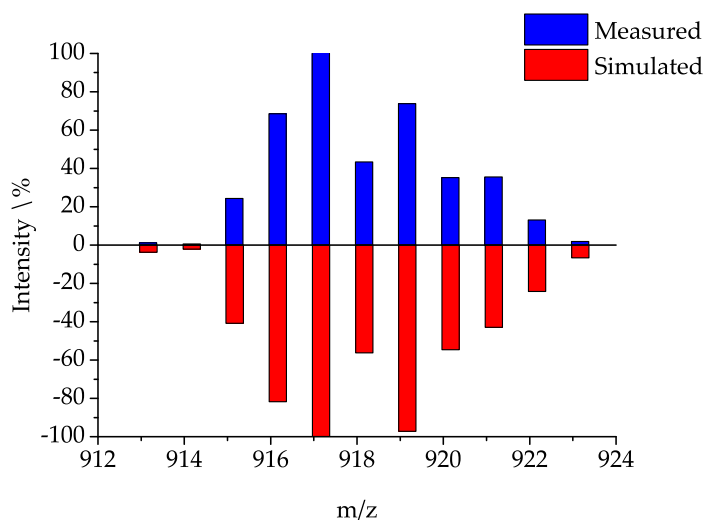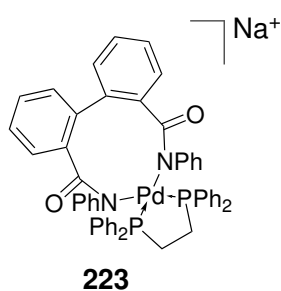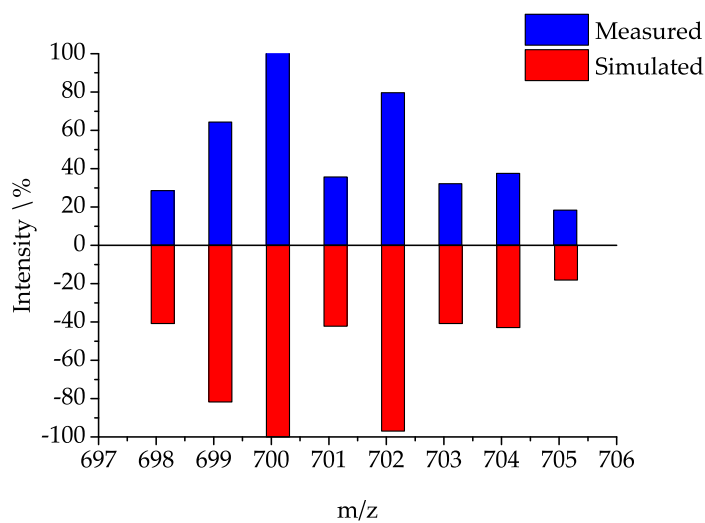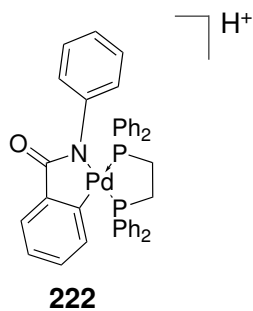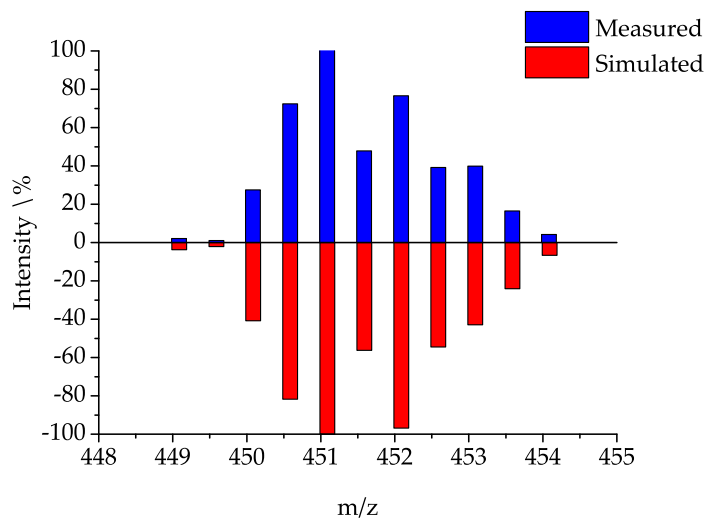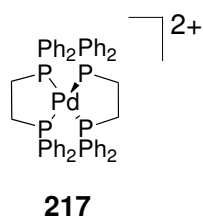
Figure 69: Measured and theoretical isotope patterns and proposed structures for species **217**, **222** and **223**, observed in the reaction mixture of $Pd_2dba_3 \cdot CHCl_3$, dppe and amide **163** in DMF-d^7 by ESI-MS after 45 minutes heating at 80 °C (Scheme 67).[132]

Complex **223** is the proposed structure for the peak seen at 917 m/z. It would be formed through homocoupling of the starting material with the nitrogen atoms bonded to the Pd. The theoretical isotope distribution has been calculated for each of the complexes seen and these are compared with the observed patterns in Figure 69. Each observed pattern closely matches the theoretical which supports the proposed Pd species. It is worth noting that the reaction was exposed to air prior to analysis by mass spectrometry although this was not thought to affect the complexes detected.

The logical next step would be to monitor the reaction containing base by NMR spectroscopy to observe species formed later in the cycle. Addition of base to the NMR-scale reaction above would not be possible as potassium carbonate is only sparingly soluble in DMF. This would cause broadening of the peaks, making the data unreliable. To overcome this problem, the reaction was performed on small scale (3 mg substrate) with 5 mol% catalyst in a solid state NMR rotor containing 50 μL DMF-d$_7$ (Scheme 68). The increase in catalyst loading was to allow turnover of the reaction while maintaining a high enough concentration of Pd species to be observed by NMR spectroscopy.
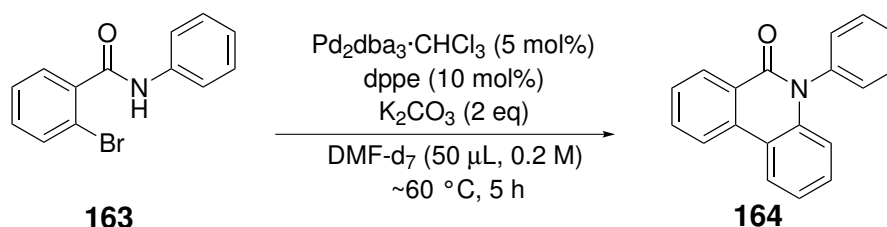
Scheme 68: Reaction conducted in a rotor for monitoring by solid state NMR analysis.

Spectra were recorded every 30 minutes, with the first spectrum at room temperature and the rest with the NMR spectrometer set to 70 °C. It was anticipated that these conditions would allow slow formation of intermediates in the reaction which could be observed by NMR spectroscopy.

Between the first two spectra (Figure 70), the peak at 29.15 ppm disappeared and the two doublet peaks of Pd(dppe)$_2$ **217** at 34.80 and 36.42 ppm were observed growing in. The peak at 56.78 ppm disappeared and a new peak was seen at 66.36 ppm. As the reaction was heated, possible reaction intermediates were observed. Four sets of doublets were clearly seen at 59.18 and 38.06 (set 1, J = 27.5 and 29.0 Hz); 56.95 and 40.57 (set 2, J = 26.0 and

171

25.5 Hz); 36.42 and 34.80 (set 3, J = 11.0 Hz); 26.27 and 22.08 (set 4, J = 53.5 and 55.0 Hz).

Set 3 belongs to the Pd(dppe)$_2$ complex **217** which was formed over approximately 30 minutes and then was consumed over a period of two hours. Set 2 appeared after 30 minutes heating and was present in the reaction mixture for 4 hours after heating began. Set 1 was clearly visible from an hour after heating began and remained in the reaction mixture until monitoring was stopped at 6.5 hours (spectrum 15). Small peaks can be seen in the ^{31}P NMR spectrum even after 20 hours heating. Sets 1 and 2 are difficult to distinguish as they are both present in the reaction near the beginning and have similar coupling constants. One of these sets belongs to the oxidative addition product, complex **221**. Set 4 belongs to a phosphorus species which appears slowly over approximately two hours and remains in the reaction mixture until the end of monitoring at 6.5 hours. These peaks are no longer present after 20 hours heating.

Three small singlets are seen between 29.0 and 30.5 ppm. These peaks grow throughout the reaction along with a peak at 30.11 ppm which grows significantly throughout the reaction and is the main species after 20 hours heating. This is believed to be the oxidised phosphine ligand, 1,2-bis(diphenylphosphoryl)ethane.[127]

^{1}H NMR analysis of the reaction showed only starting material and product formation. As the aromatic region of the NMR is complex, it is difficult to observe species forming or being consumed during the reaction.

The analysis of the catalyst system by ^{31}P NMR spectroscopy allowed the identification of the species present before the substrate is added to the reaction, and from these, the active catalyst could be proposed. From the analysis of the reaction by ^{31}P NMR spectroscopy, there were at least nine phosphorus species, four of which were unsymmetrical Pd species, as shown by the sets of doublets observed. Three of the phosphorus species seen were identified by mass spectrometry and these could be placed in a catalytic cycle for the formation of 5-phenylphenanthridin-6(5*H*)-one. This mass spectrometry analysis also suggested the presence of many other Pd species in the reaction.
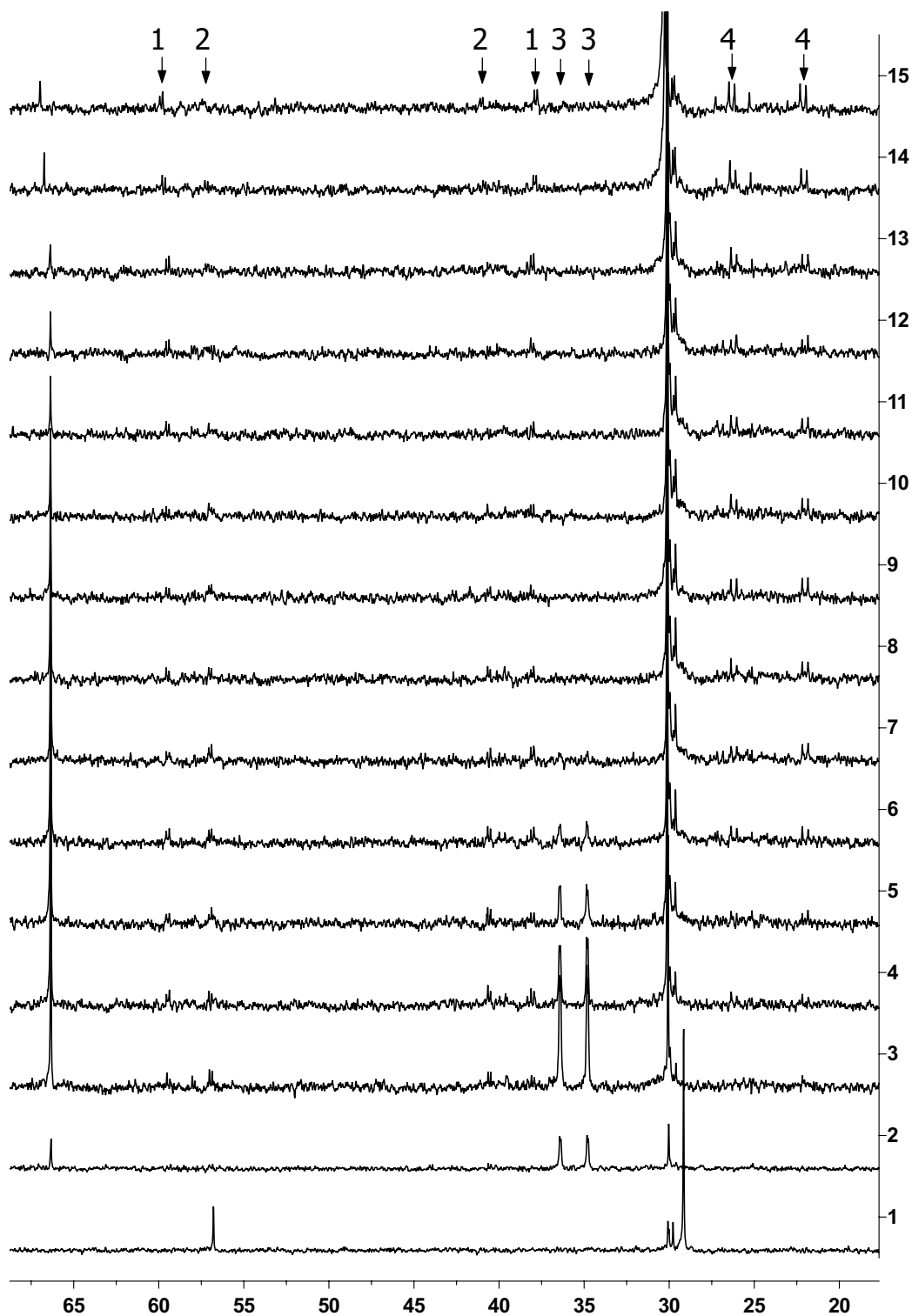
Figure 70: ^{31}P NMR (162 MHz, DMF-d$_7$) spectra of the reaction of 2-bromo-*N*-phenylbenzamide **163** taken by solid-state-MAS NMR spectroscopy. Spectrum 1 was recorded at 20 °C and the temperature increased to 70 °C before spectra were recorded every 30 minutes.

5.5.5 Kinetic analysis

Kinetic analysis of reactions is used to give information on the rate-determining states in the reaction. To begin with, a reaction was conducted using $Pd_3(OAc)_6$ as the catalyst precursor with samples taken over the course of the reaction. The samples were filtered through Celite, diluted in ethyl acetate, washed with 2M HCl and brine, and analysed by GC.

The reaction was conducted by mixing K_2CO_3 (1.5 mmol) in DMF (6 mL) followed by the addition of biphenyl (0.75 mmol) as an internal standard and substrate **163** (0.75 mmol). The catalyst system, $Pd_3(OAc)_6$ (37.5 μmol) and dppe (37.5 μmol) in DMF (1.5 mL), was added last and the overall substrate concentration was 0.08 M. In the first experiment (shown in red on the graph in Figure 71), the catalyst solution was added at room temperature before the reaction was exposed to heat and a kink in the curve was noticed. This suggested an induction period was present and that heat caused a change to a more active catalyst, which when formed, allowed the substrate to be rapidly consumed.

To investigate the change in rate after 10 minutes, the reaction was repeated with the catalyst system pre-heated before addition to the pre-heated reaction mixture. As is seen in Figure 71 the curve obtained looks simpler, smoother and steeper. During this investigation, a colour change was observed upon activation of the catalyst. When mixing $Pd_3(OAc)_6$, dppe and K_2CO_3 in DMF, a yellow solution was obtained. As this was heated to 80 °C, a colour change through green to red was observed. The solution remained red until the substrate was added at which point it turned back to yellow. It is assumed that the red solution is the most active catalyst and pre-forming this may allow a faster reaction rate.
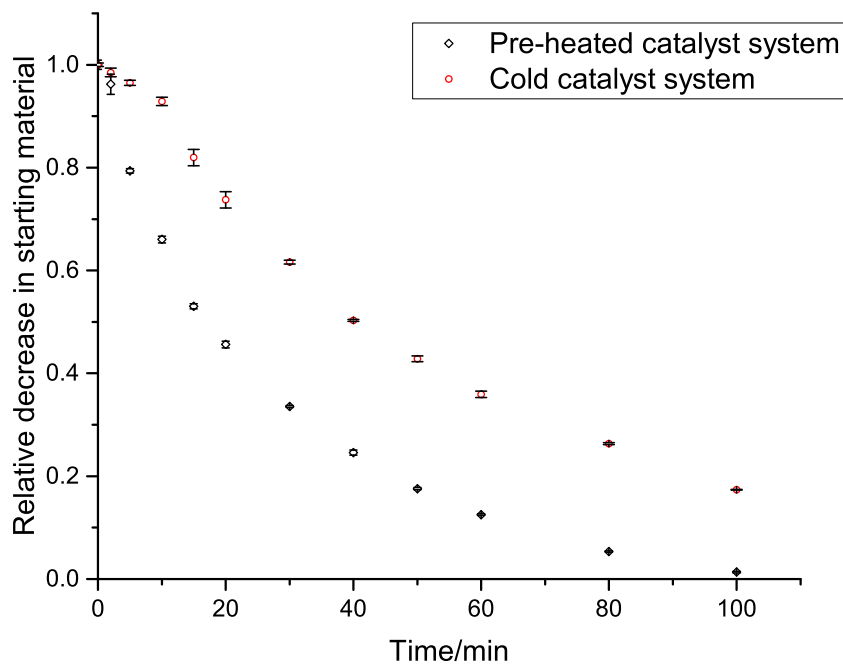
Figure 71: Decrease in 2-bromo-*N*-phenylbenzamide **163** measured by GC analysis. Two reactions were conducted at 80 °C over 2 h; with a catalyst system added at rt, and with a catalyst system pre-heated at 80 °C for 2 minutes. Curves normalised to allow direct comparison. Laboratory work performed by A. Pagett.

To further investigate the difference between the cold and pre-heated catalyst systems, plots of ln[**163**] and 1/[**163**] against time were prepared to provided some kinetic data. For the reaction with the cold catalyst system, the data in the second order graph curved and a linear line could not be fitted. A linear fit to the first order graph over the first seven points after the induction period was applied. Beyond this point the data did not fit the linear line as well. This suggested that the reaction was first order with respect to the starting material and therefore the rate determining step of the reaction involved only one molecule of starting material.
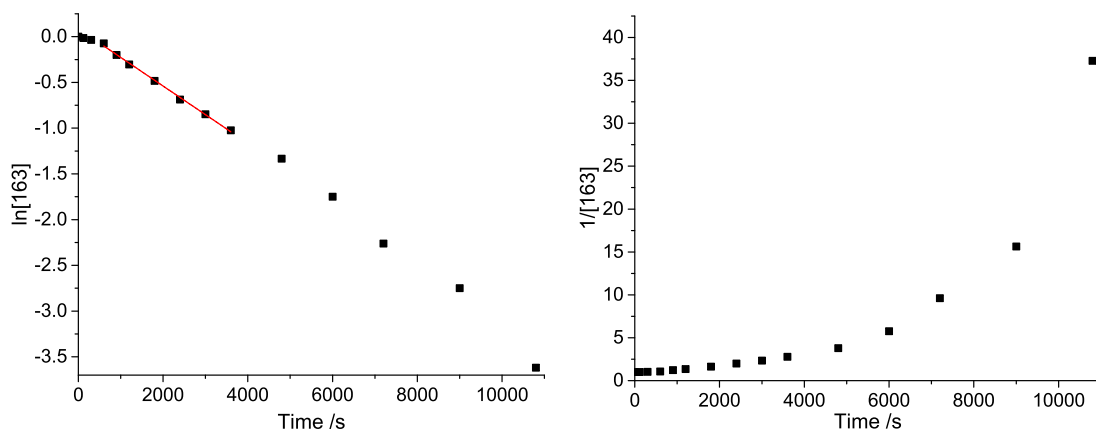
Figure 72: ln[**163**] vs. time and 1/[**163**] vs. time for the reaction where the substrate was added to a cold catalyst system. A linear fit to the first seven data points after the induction period was applied of the 1st order graph with a gradient of -3.13×10^{-4} and R^2 value of 0.997.

The reaction with the pre-heated catalyst system was not as simple. At first, the data were thought to be neither first or second order kinetics. The data in the first order graph are reasonably linear but have a slightly sigmoidal shape and if a linear fit is applied, the data curves on either side of the line. Closer examination of the second order graph revealed that the data are linear over the first seven data points at which point it begins to curve, suggesting that the reaction is second order but there is a change in mechanism after 30 minutes. This change could be induced by the formation of a product which then takes part in the reaction or from a change in the active catalyst such as the formation of Pd nanoparticles and the change to a heterogeneous mechanism. A linear fit to the first seven points was applied and data were extracted from this for rate comparison with the cold catalyst system.
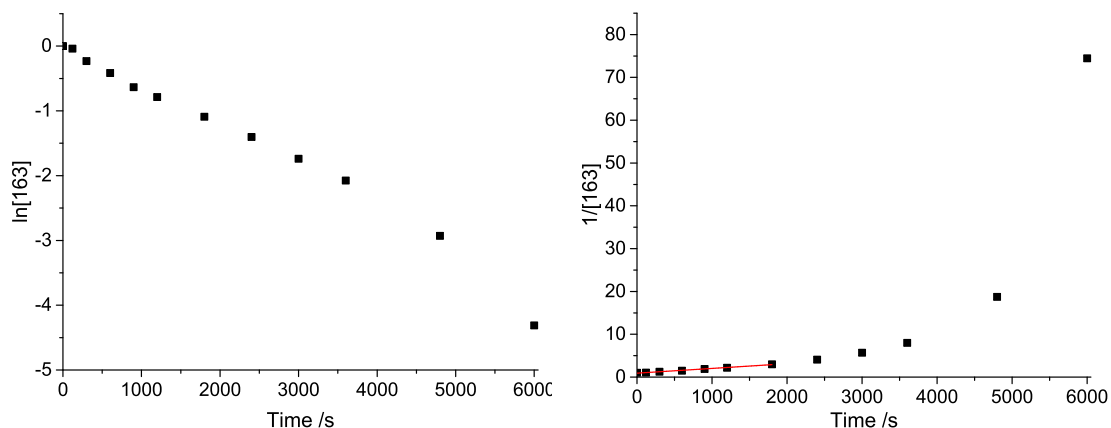
Figure 73: ln[**163**] vs. time and 1/[**163**] vs. time for the reaction where the substrate was added to a pre-heated catalyst system. A linear fit to the first seven data points was applied of the 2nd order graph with a gradient of 11.0×10^{-4} and R^2 value of 0.992.

Table 36 shows the calculated k_{obs} values along with the half lives. For the reaction where the substrate was added to a pre-heated catalyst system (Figure 73), the k value is much higher, 3.5 times that of the cold reaction (Figure 72), and the half life much lower. It is clear that pre-heating the catalyst system is critical in the formation of a highly active catalyst.

Table 36: Calculated k_{obs} values and half lives for 5-phenylphenanthridin-6(5*H*)-one **164** synthesis with both a cold and pre-heated catalyst system.

	Cold system	Pre-heated system
k_{obs} / $\times 10^{-4}$ s^{-1}	3.13 ± 0.07	11.0 ± 0.40
$t_{1/2}$ / s	2215 ± 50	630.1 ± 24

Evaluating the overall yields of experiments done with or without the pre-activation of the catalyst, there does not appear to be any correlation so it is assumed, at this point, that the rate of reaction makes no difference to the overall distribution of products. Further work into this could be valuable from a mechanistic point of view. This analysis showed that the reaction kinetics are complex and the mechanism far from simple. The other mechanistic data collected, particularly the number of side-products obtained and the number of Pd species seen by mass spectrometry, also lead us to expect that the mechanism is complicated.

Future work could include the examination of the reaction at different temperatures and with increased sampling to allow better monitoring of the substrate concentration. Further investigation of the catalyst system and the change in consumption of starting material when the catalyst system is added at room temperature would be necessary before a conclusion can be drawn as to the cause and it would be interesting to investigate whether the reaction profiles are similar with a $Pd_2dba_3 \cdot CHCl_3$ pre-catalyst. Monitoring formation of the reaction products would also be of interest as there are products which may be formed from each other and observing product formation might allow these to be identified.

5.5.6 Mechanism for the formation of 5-phenylphenanthridin-6(5*H*)-one 164

Based on all of the information gathered by experiment, two mechanisms for the formation of 5-phenylphenanthridin-6(5*H*)-one **164** have been proposed (Figure 74). In the middle of the cycles is the active Pd^0dppe complex **220**. Amide **163** oxidatively adds to complex **220** to give complex **221**. At this point the pathway splits. Path A involves a second oxidative addition of compound **163** which results in Pd^{IV} complex **224**. Reductive elimination from this complex results in complex **225** in which the organic fragment is co-ordinated to the Pd *via* one of the nitrogen atoms. Loss of HBr and formation of a bond between one of the nitrogen atoms and Pd gives complex **226** and further loss of HBr gives complex **223** which has been detected by MS. Complex **223** would then undergo a decarbamoylation reaction to release phenyl isocyanate **165** and produce complex **229** from which reductive elimination would give the expected phenanthridinone product **164** and regenerate the Pd^0 complex **220**. As shown on Figure 74, the phenyl isocyanate released could break down to give CO_2 and aniline which could then react with phenyl isocyanate to produce urea **207**.

Following path B from complex **221**, deprotonation and the loss of HBr results in formation of complex **222** which was detected by MS analysis of a stoichiometric reaction. This Pd^{II} complex then undergoes oxidative addition of a second molecule of amide **163** to give the Pd^{IV} complex **227** which can undergo reductive elimination to give complex **226** which is also a proposed intermediate in path A. Deco-ordication of the amide gives complex **228**

which can be transformed into complex **229** through the loss of HBr and phenyl isocyanate **165**.
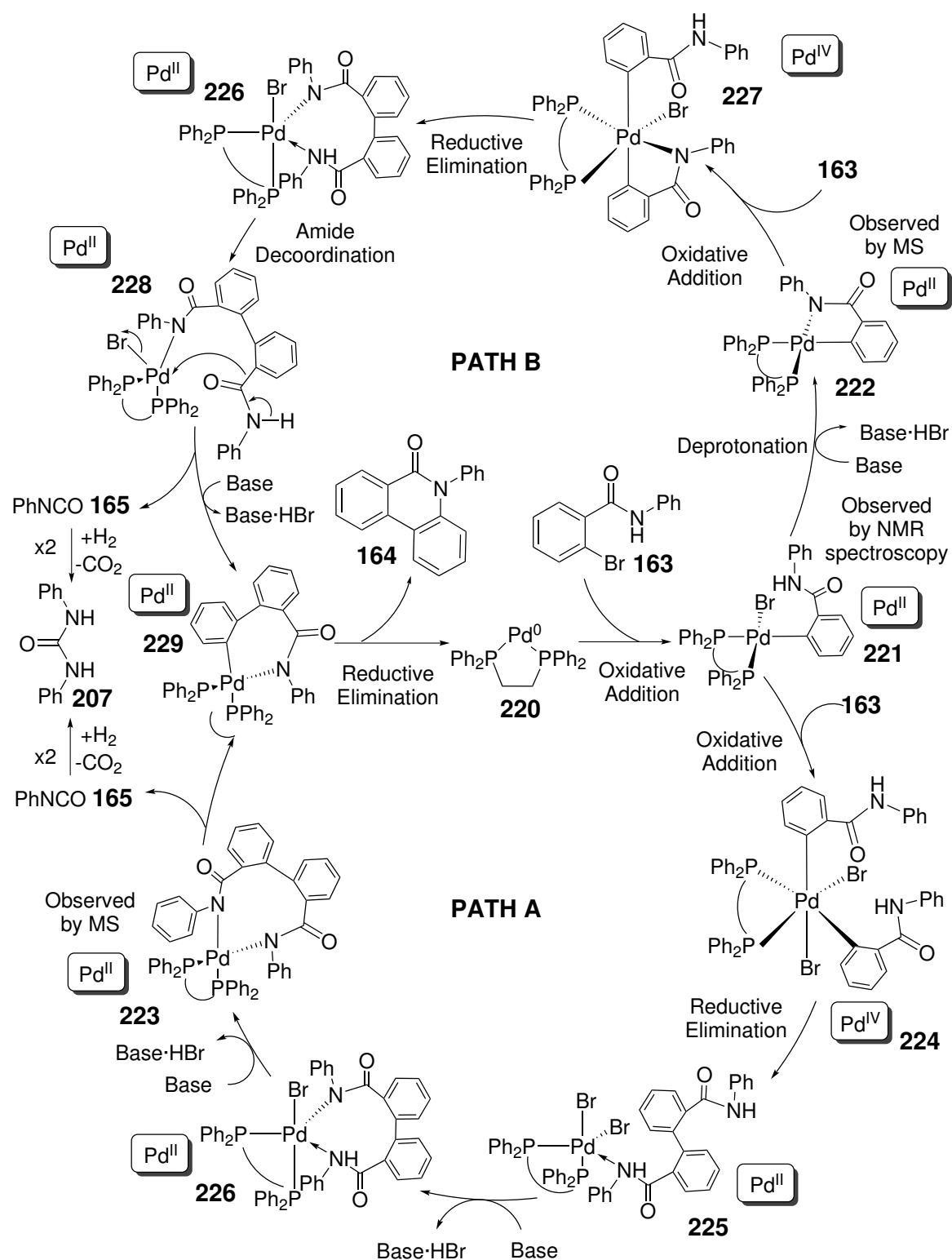
Figure 74: Proposed mechanism of the Pd-catalysed 5-phenylphenanthridin-6(5*H*)-one **164** synthesis.

It is difficult to promote one of these pathways over the other. Complex **226** is common to both pathways and so from complex **226** to complex **229** both pathways could proceed *via* either complex **223** or complex **228**. Experimental evidence suggests the mechanism proceeds *via* complex **223** which was detected as a sodium cation by MS. Protonated complex **222** was also detected by MS but, as discussed earlier, the compound detected could have been complex **221** after the loss of bromide. If this is the case, there is no evidence to support either pathway over the other. Porée *et al.* propose that the mechanism goes *via* complex **227** as that is the lowest energy pathway according to their computational calculations but they do not propose either **223** or **228** as intermediates.[89]

As described earlier, 8*H*-indolo[3,2,1-*de*]phenanthridin-8-one **196** can be formed by an oxidative C–H functionalisation reaction of the product. Simple oxidative C–H functionalisation reactions use a Pd[II] catalyst and may involve an additive which assists in the C–H activation of the starting material, which results in a pseudohalide on the palladium[IV] intermediate **230**. In this case, there is bromide available in the reaction mixture from the first step of the reaction which may allow this step to take place. A further C-H functionalisation occurs with the loss of HX to give complex **231** which can reductively eliminate to release compound **196**.
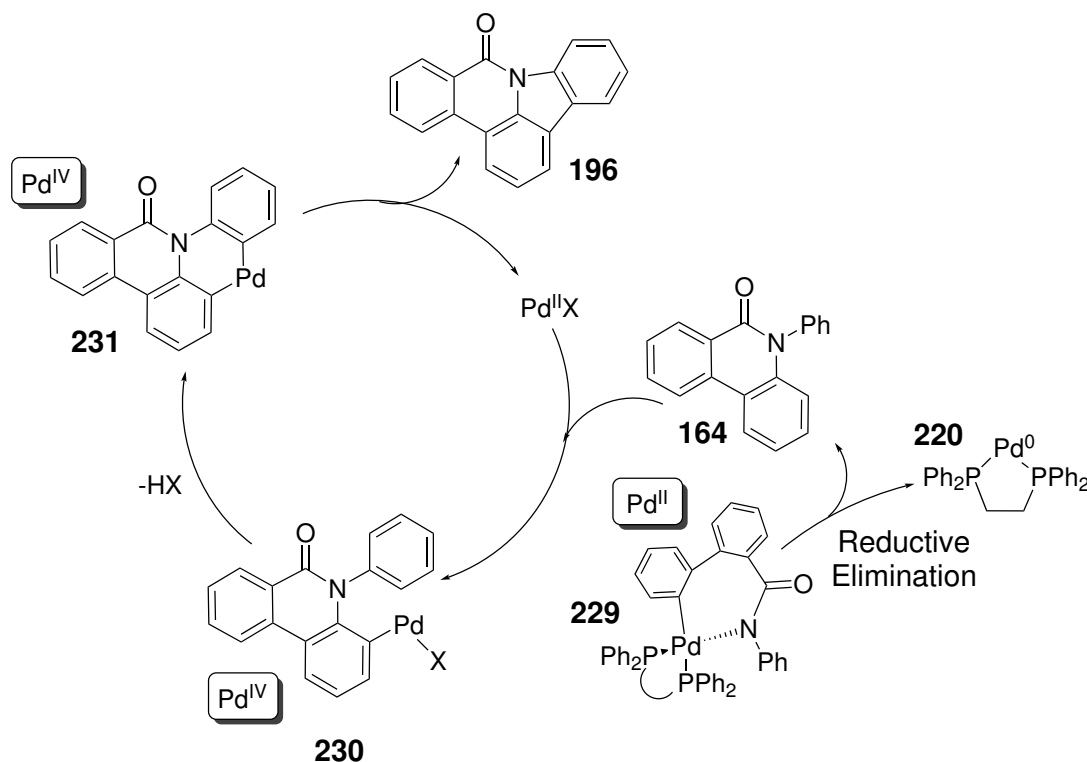
Figure 75: Proposed mechanism of the Pd-catalysed formation of 8*H*-indolo[3,2,1-*de*]phenanthridin-8-one **196** (ligands around the Pd^{II} and Pd^{IV} centres are not specified.

Figure 76 shows the route to forming the homocoupled product **201** using the beginning of the route for the major product. From path A, compound **201** could easily be released from the cycle by deco-ordination of the amide from complex **225**. This may lend support to path A as the mechanism for the formation of compound **164**. In this method, the Pd^{II} complex **232** needs to be reduced back to Pd^0 which would be possible with the high temperature of the reaction.

From path B, the bromide in complex **226** would need to be replaced by a hydride, most likely coming from DMF, before reductive elimination to give compound **201** and releasing Pd^0 complex **220** back into the cycle.
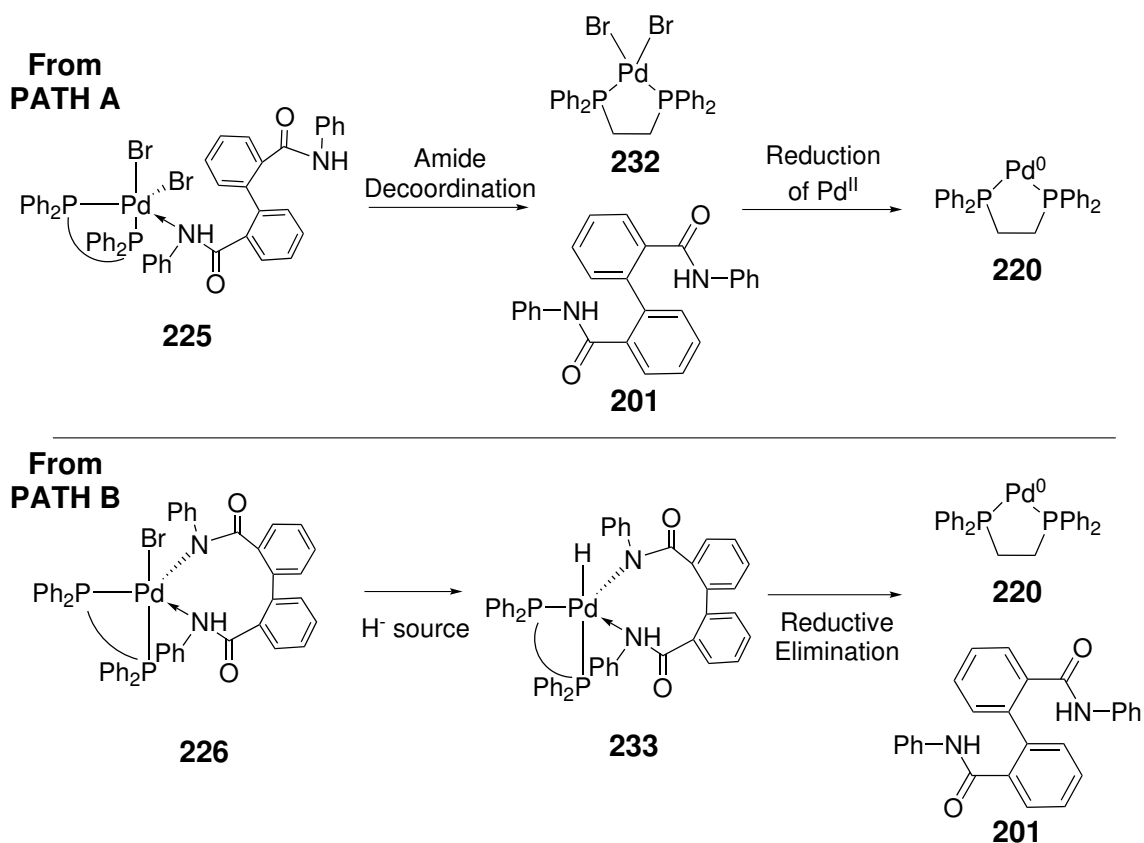
Figure 76: Proposed mechanism of the Pd-catalysed homo-coupling of 2-bromo-*N*-phenylbenzamide **163** involving either Pd^{II} (Path A), or hydridic source (Path B).

In order to form compound **208**, a direct arylation *via* a C–H functionalisation is required. This can be proposed to happen through the oxidative addition of the starting material **163** to the Pd^0 complex **220** as with the major product pathway. This would be followed by the C–H activation of the product **164** to give complex **223**. The organic fragments could then be reductively eliminated from the palladium centre to produce compound **208** and regenerate the Pd^0 catalyst.
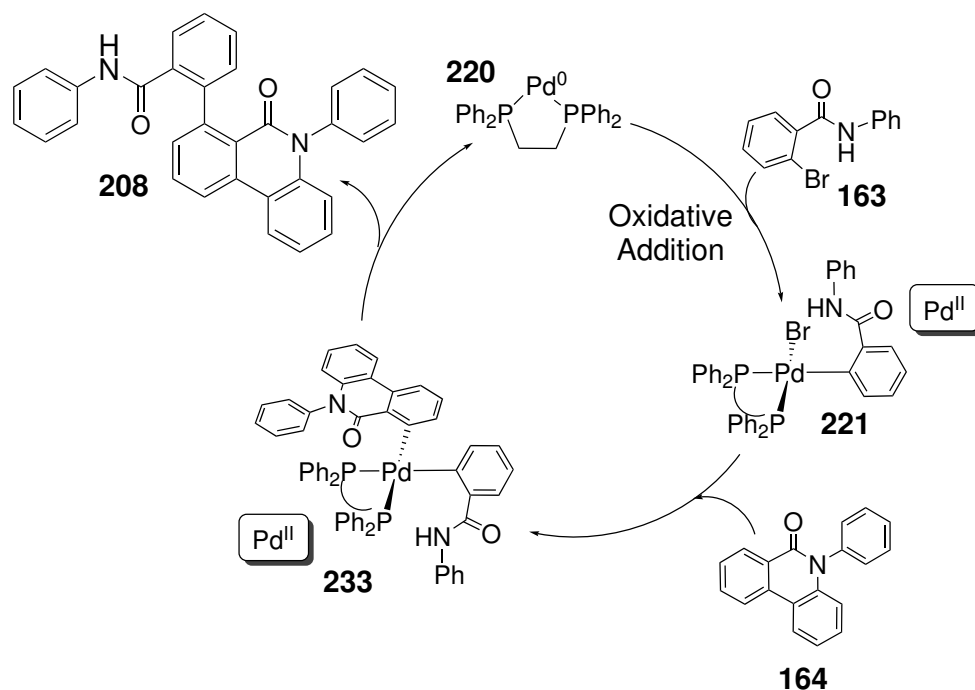
Figure 77: Proposed mechanism of the palladium-catalysed synthesis of 2′-(6-oxophenanthridin-5(6*H*)-yl)-*N*-phenyl[1,1′-biphenyl]-2-carboxamide **208**.

Two structures, **210** and **211**, were proposed for the mass of 413 m/z. The formation of both compounds could both be envisaged from the major catalytic cycle. Compound **210** could be produced from path A. Deco-ordination of the amide would be required along with a C–H functionalisation on one of the phenyl rings, meta to the carbonyl. This would give complex **234** from which a reductive elimination would give compound **210**.

Compound **211** could be formed from a C–N bond formation leading from path B. Complex **227** could undergo reductive elimination to give complex **235**. Loss of HBr would give palladacycle **236** which could then undergo reductive elimination to give compound **221**.
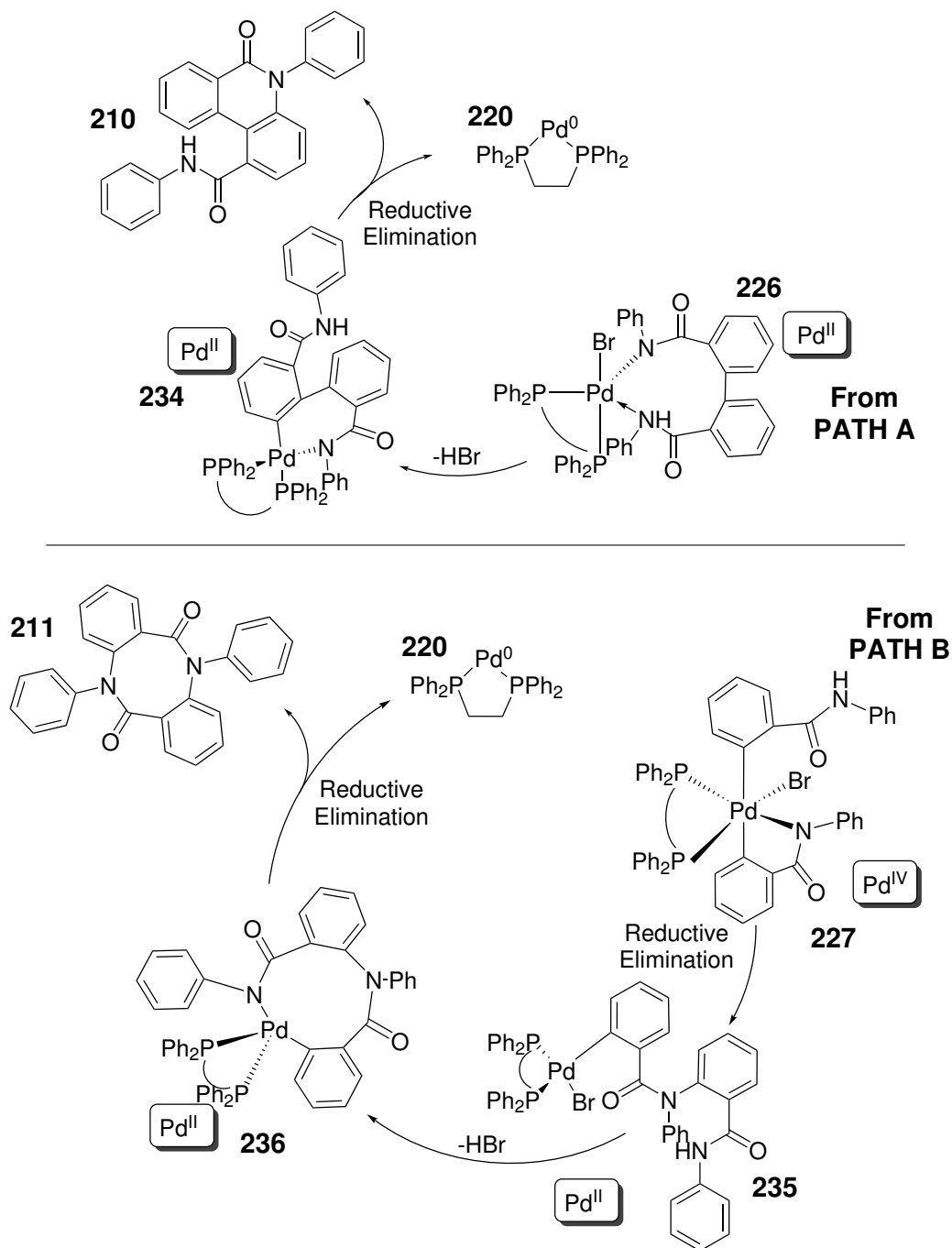
Figure 78: Proposed mechanisms of the palladium-catalysed synthesis of compounds **45** and **46**.

As the analytical data suggests that the mass of 413 m/z belongs to the sodium adduct compound **210**, this would mean that path A is the likely mechanism for the formation of compound **164**. The homocoupled product **201** also lends support to path A, as this compound can be easily released from the cycle. More experimental data, particularly of Pd intermediates, is needed to confirm this hypothesis.

5.6 Conclusions

The principal aim of this study was to investigate the unusual direct C–H bond functionalisation reaction of 2-bromo-N-phenylbenzamide to give 5-phenylphenanthridin-6($5H$)-one. This reaction used two equivalents of starting material to produce one equivalent of product. The reaction was successful in both the presence and absence of air when $Pd_3(OAc)_6$ was used but worked only in the presence of air when $Pd_2dba_3 \cdot CHCl_3$ was the Pd precursor. A variety of bidentate phosphine ligands were tested, all of which were successful in the reaction, with the best ligand identified as dppp.

Mechanistic studies were carried out on the reaction. No evidence was found for a benzyne intermediate and the use of amide **189** with a methyl substituent provided evidence of a double C–Br coupling mechanism. This was corroborated by literature data[69,87,89,110] which also supported the proposed side products which were obtained from the crude reaction mixture. One of these products was thought to be a urea by-product. This was supported by the introduction of phenyl isocyanate into the reaction to trap any aniline formed from the breakdown of the isocyanate by-product which is left after formation of the phenanthridinone **164**. Both symmetrical and mixed ureas were detected by MS analysis.

Further analytical studies of the reaction were carried out using NMR and MS analysis. ^{31}P NMR analysis of a stoichiometric reaction involving the catalyst system and substrate showed five phosphorus species forming over a 45 minute period. Addition of base to a substoichiometric reaction and monitoring over 6.5 hours showed the five species detected previously and four new species. Altogether there were four sets of doublets suggesting four main Pd-based intermediates containing dppe ligands with different phosphorus chemical environments in the reaction. MS analysis showed only organic products, however, MS analysis of a stoichiometric reaction without base showed several identifiable Pd species which could be placed into the context of a potential catalytic cycle.

Based on the data obtained, two catalytic cycles have been proposed for the formation of 5-phenylphenanthridin-6($5H$)-one **164** from 2-bromo-N-phenylbenzamide **163**. Further MS analysis including MS-MS analysis of the Pd species may help to support one of these mechanisms.

Chapter 6

Conclusions and Future Work

6.1 Silica-catalysed amide bond formation reactions

Optimisation of the silica-catalysed reaction conditions highlighted the importance of measuring the background reaction in these types of catalysed processes. Increasing the temperature above 110 °C and conducting the reaction with no solvent was found to significantly increase the conversion of background reaction. A variety of commercial silica materials were tested as catalysts, with the aim of making the catalyst even cheaper and more readily available. Some of these gave moderate yields of amide but did not match the activity of K60 silica. Porosimetry results suggested that an effective silica catalyst should have a large surface area with a narrow distribution of small pores.
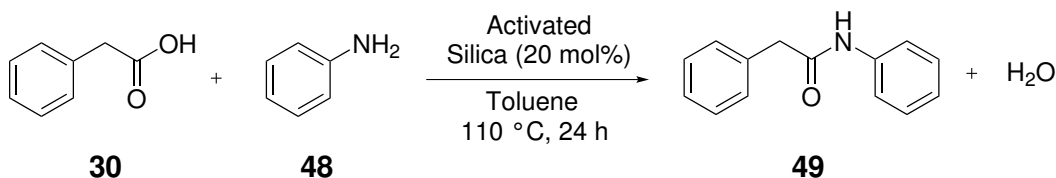
Scheme 69: Reaction used to probe reaction conditions of K60 silica catalyst.

Analysis of the activated silica catalyst by ^{29}Si NMR spectroscopic analysis showed a small difference in the proportion of the Q2, Q3 and Q4 environments which confirms that the catalyst is changing upon activation and it also suggests that the catalyst does slightly deactivate over time. Monitoring the reaction using DRIFT spectroscopy and ammonia gas as the amine was unsuccessful. Further work is needed to synthesise the silica catalyst loaded with an appropriate carboxylic acid before this study can be resumed.

An activated alumina balls catalyst was tested in two reactions, one which synthesised 2,*N*-diphenylacetamide **49** and the other, *N*-4-chlorophenylheptanamide **47**. The results suggested that catalyst was not as effective as reported, with the background reaction of the

latter high and the catalysed reaction of the former lower than expected. Analysis of the catalyst showed a significant amount of trace metals which could be responsible for catalytic activity.
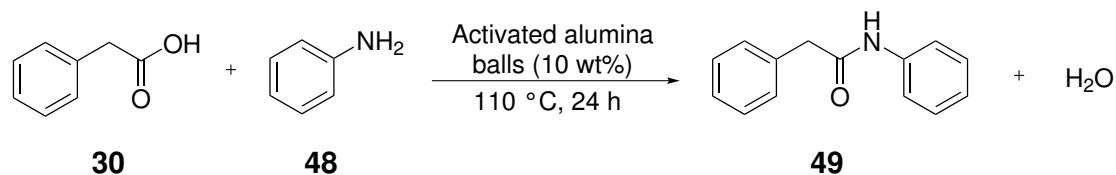
Scheme 70: Reaction used to examine the activated alumina balls catalyst.

Work to expand the substrate scope of the activated silica catalysts showed that they have limitations in amidation reactions. Small conversions were seen when *N*-boc proline **84** and isonicotinic acid **79** were reacted with aniline **48**. The K60 silica catalyst was found to be more effective in these reaction when activated at 300 °C rather than 700 °C. The results suggested that bulky or particularly polar acids are not suited to this type of catalysis. The mechanisms proposed for the reaction support the theory that the acids need to be quite electrophilic to react with the silanols in the silica and form the chemically bound intermediate.

Phthalic acid **98** was screened against a variety of primary and secondary amines and gave a variety of cyclic products depending on the amine used. Further work is required to scale these reactions up to measure the conversion and isolate the products. The importance of measuring the background reaction was highlighted with the reaction between mandelic acid **146** and aniline **48** where the background reaction mimicked the catalysed.
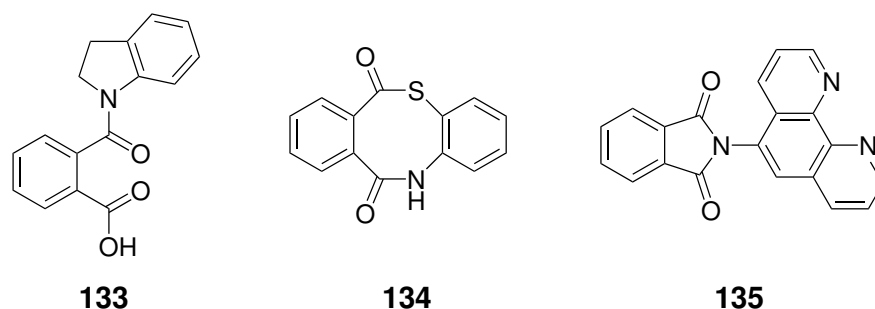
Figure 79: Cyclic compounds synthesised from phthalic acid and amines using the K60 silica catalyst.

An anti-TB drug, isoniazid **76** was synthesised using the K60 silica catalyst activated at 300 °C in good yields. Green metrics analysis was used to highlight the problems in this reaction compared to the current state of the art in the literature. Further work on a new solvent for the reaction would improve the green metrics and development of a system to activate the catalyst without rapid deactivation occurring upon cooling would be beneficial. This reaction could become commercially viable after some process development work to transfer it into a flow system.
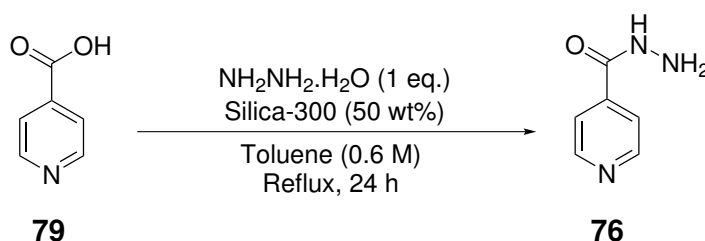
Scheme 71: Reaction developed to synthesise anti-TB drug, isoniazid **76**.

6.2 Pd-catalysed oxidative C–H functionalisation of amides

Two new Pd catalysts, developed within the Fairlamb group, were successfully tested in the oxidative C–H bond functionalisation reaction of *N*-phenylbenzamide **66** to synthesise phenanthridin-6(5*H*)-one **148**. The single crystal structure of Pd(tfs)$_2$(MeCN)$_2$ **160** was obtained and showed the tetrafluorosuccinimide ligands in a *cis*-configuration. Having shown promise in the intramolecular reaction of *N*-phenylbenzamide **66**, this catalyst could now be tested in a variety of other oxidative C–H bond functionalisation reactions.
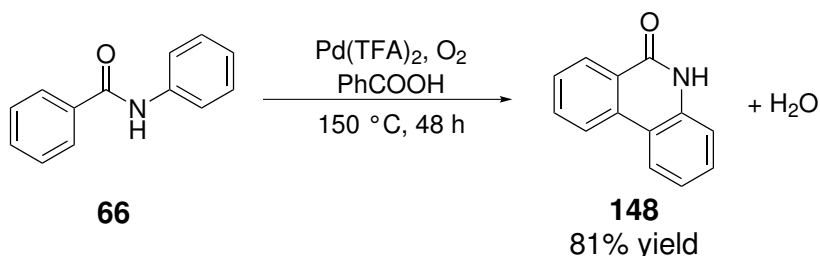
Scheme 72: Reaction used to test new palladium catalysts in oxidative C–H functionalisation reactions

Efforts were made to develop a one-pot synthesis of phenanthridin-6(5*H*)-one **148** with the aim of conducting the reaction from acid and amine to phenanthridinone with only one solid-supported, recoverable catalyst. The range of reaction conditions and reaction vessels tested resulted, generally, in full conversion to the amide intermediate but very little conversion to phenanthridinone **148**. The cause was thought to be the sublimation of the benzoic acid used as solvent and the water formed in the first step of the reaction. Finding a suitable method for removal of the water from the reaction and an alternative solvent may overcome this problem and the focus of this research could then be directed towards the development and testing of solid-supported catalysts.
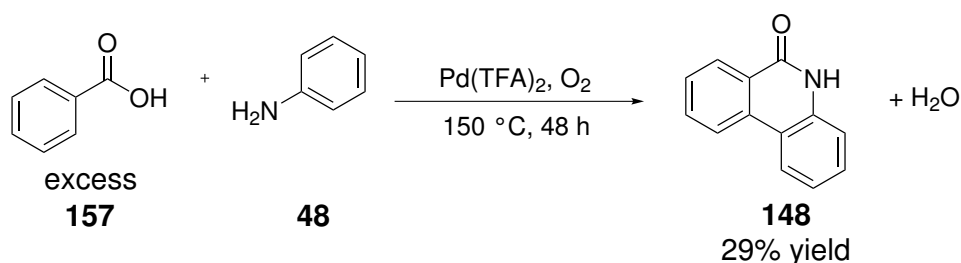
Scheme 73: The best result obtained for the one-pot reaction between benzoic acid and aniline to form phenanthridin-6(5*H*)-one **148**

6.3 Mechanistic investigation of the synthesis of 5-phenyl-phenanthridin-6(5*H*)-one 164

The reaction of 2-bromo-*N*-phenylbenzamide **163** has been investigated. The main product of this reaction was 5-phenylphenanthridin-6(5*H*)-one **164** which was synthesised from 2 equivalents of the starting material. Firstly, a ligand and catalyst screen was carried out. Dppp was proposed to be the best ligand due to its favourable bite angle with Pd. Two catalyst systems were used in the reaction. The first, $Pd_3(OAc)_6$, gave good yield in both the presence and absence of air. The second, $Pd_2(dba)_3 \cdot CHCl_3$, gave good yields in the presence of air, but no conversion of starting material in the absence of air.
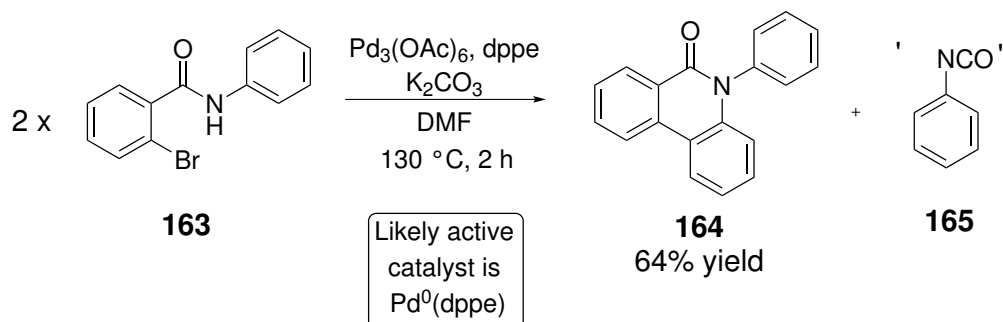
Scheme 74: The reaction of 2-bromo-*N*-phenylbenzamide **163** to produce 5-phenylphenanthridin-6(5*H*)-one **164.**

The main interest in this reaction was from a mechanistic perspective. A double C–Br coupling mechanism was deduced from the use of a methylated substrate which was supported by literature data. Eight side products were proposed in the reaction (Figure 80), two of which, **196** and **201**, were characterised by single crystal XRD. Diphenyl urea **207** was detected by MS in the reaction, which was thought to originate from aniline and phenyl isocyanate, both of which could be released as by-products from the main reaction.

196
MNa+ 291

202
MNa+ 236

204
MNa+ 296

66
MNa+ 220

201
MNa+ 415

210
MNa+ 413

208
MNa+ 489

207
MNa+ 235
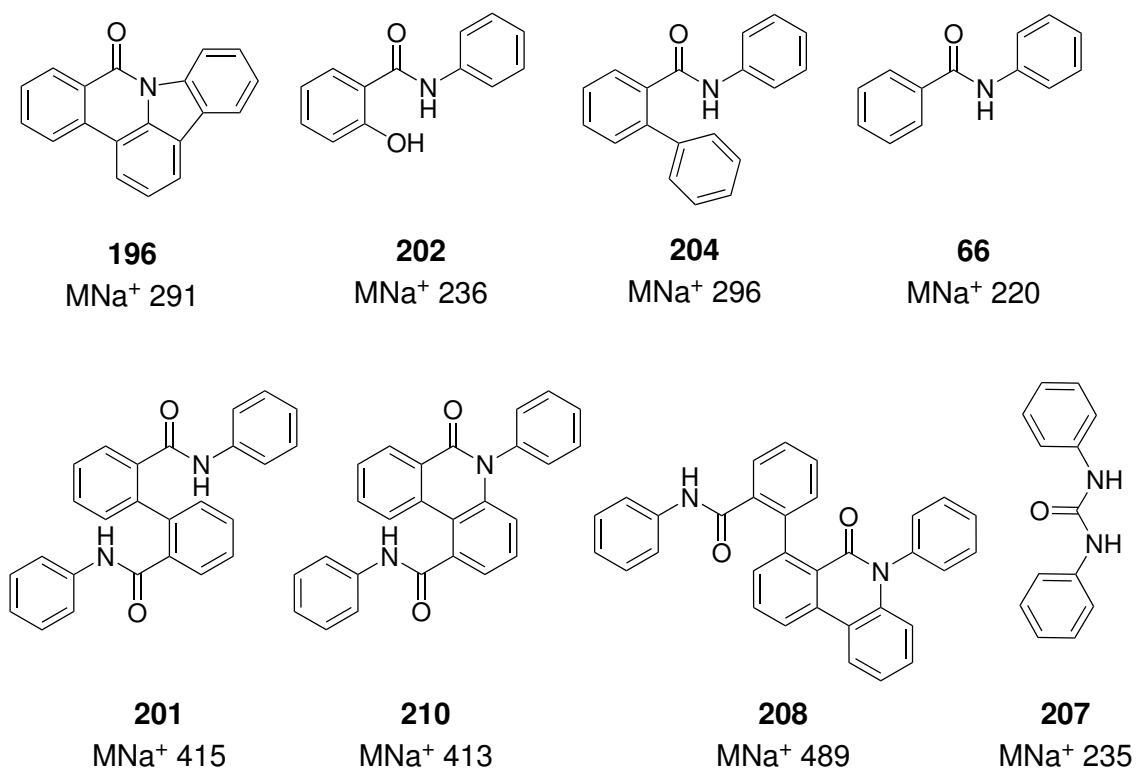
Figure 80: Eight side products identified by MS

The reaction was studied by MS and NMR analysis. Five phosphorus species were seen by NMR spectroscopy analysis, three of which were identified by MS analysis. The species could be placed in the catalytic cycle. Four more phosphorus species were seen when the reaction was studied by solid state NMR with the addition of base. This indicated that the reaction mechanism was complex. The phosphorus species identified by MS, along with the known side products and the data that could be obtained from them allowed the proposition of a catalytic cycle for the formation of the major product. From this it was possible to put forward mechanisms for the synthesis of the reaction side products.

The reaction is complex and, as such, gives the scope for further research. More data is required to support the mechanism, including further identification of phosphorus species. Analysis of the reaction by mass spectrometry showed many more Pd species which at present could not be identified. Further analysis of these by MS-MS may overcome this.

The eight products detected in the reaction provide a new avenue for research. The good yields of 5-phenylphenanthridin-6(5*H*)-one **164** clearly show that the reaction conditions used are selective for this product. An interesting alternative would be to screen reaction conditions for selectivity for one of the other products seen. To do this a method for efficiently analysing the reactions would be necessary. Work to this effect is already under way in the Fairlamb group by a new PhD student, George Clark.

6.4   Solid-supported palladium acetate catalyst

The use of solid-supported catalysts is encouraged in green chemistry as it allows the easy recovery, and possible re-use, of the catalyst. The future of this project would be to introduce solid supported catalysts into the C–H functionalisation reaction of 2-bromo-*N*-phenylbenzamide. To this end a silica-supported palladium acetate catalyst has been developed in collaboration with Dr Chris Parlett at Aston University. The silica support was developed at Aston following the procedures described by Clark *et al.* for their silica-supported cobalt catalyst (shown in Scheme 75).[133]
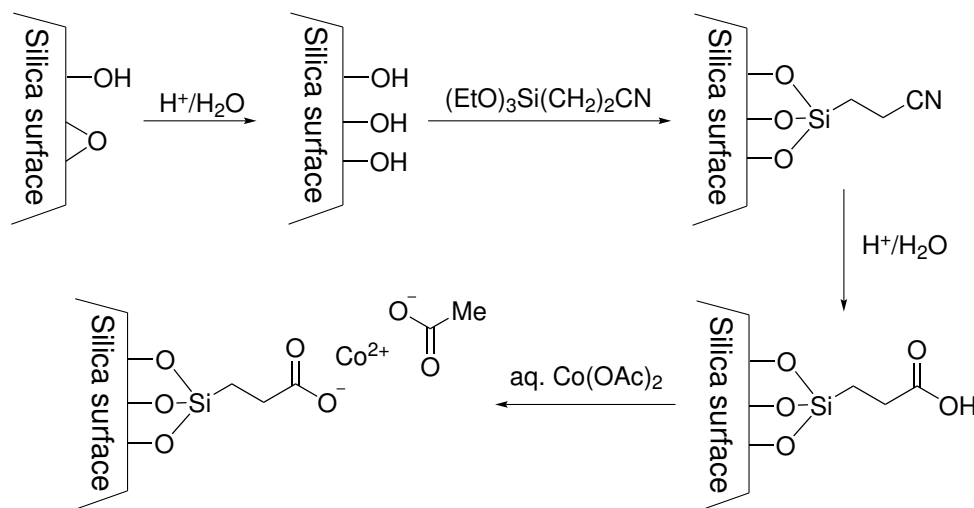
Scheme 75: Scheme showing the synthesis of a silica-supported cobalt acetate catalyst.[133]

6.4.1 Synthesis of silica-supported palladium acetate catalyst

Two methods were tested to load $Pd_3(OAc)_6$ onto the silica support. Firstly, the $Pd_3(OAc)_6$ and silica support were ground together in a pestle and mortar for 20 minutes in total. It was anticipated that the heat produced from the mortar and pestle would facilitate the reaction between the Pd and the acid group on the silica. This was unsuccessful and washing of the catalyst with cold DCM resulted in the removal of the $Pd_3(OAc)_6$ from the system.

The second method was to add the silica support (450 mg) to a 0.05 M solution of $Pd_3(OAc)_6$ in MeCN. This mixture was gently heated at 50 $^\circ$C for 4 hours with stirring. The catalyst was then separated from the reaction mixture by filtration and washed with cold diethyl ether resulting in a yellow powder. This reaction resulted in an increase of 27.7 mg which along with the colour change suggested the reaction had been successful.
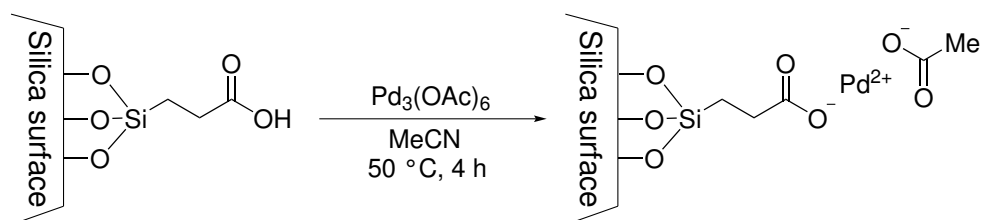
Scheme 76: Synthesis of a silica-supported palladium acetate catalyst

6.4.2   Characterisation of silica-supported palladium acetate catalyst

To determine if the reaction had successfully loading Pd onto the silica support, the catalyst was characterised by DRIFT and NMR spectroscopy. Figure 81 shows an overlay of the DRIFT spectra obtained. The green line of $Pd_3(OAc)_6$ shows two clear bands at 1604 and 1431 cm^{-1}, corresponding to C=O and C–H stretches, which were not present in the silica support. In the sample of catalyst prepared by the method above, peaks were seen at 1530 and 1428 cm^{-1}. The peak seen at 1530 cm^{-1} was relatively broad which could mean that there are two overlapping C=O peaks. These peaks suggest that the $Pd_3(OAc)_6$ has been loaded on to the silica support as anticipated.
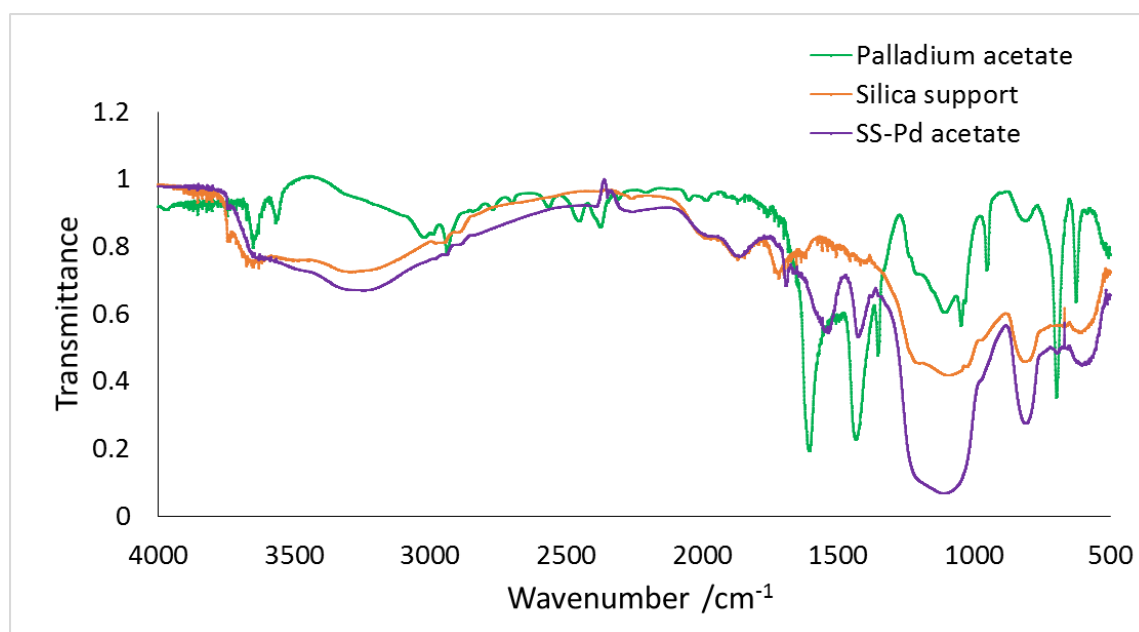
Figure 81: IR spectra of silica support, $Pd_3(OAc)_6$, and silica-supported palladium acetate.

The catalyst sample was analysed by solid state NMR spectroscopy and compared with the solid support. Figure 82 shows four spectra; the bottom two are standard spectra of the support and the catalyst, while the top two are spectra of the support and the catalyst measured using dipolar dephasing which removes signals from carbons that are directly bonded to hydrogen.

Five carbon signals are seen in the silica support, one of which is directly bonded to hydrogen. This does not match the expected data, which would be 3 signals, two of which are directly bonded to hydrogen. As both carbons with hydrogens are CH_2 groups, it is possible

that they could both be represented by the peak at 10.9 ppm. There are still extra peaks to consider, however, which suggests that the synthesis of the support was not clean. It is possible that the hydrolysis did not go to completion which would explain the small peak at 125 ppm as the C–N.

The catalyst spectrum also showed five peaks, two of which were directly bonded to hydrogen. Three carbons bonded to hydrogen would be expected; the methyl group and the two CH_2 group. As with the support, it is possible that the two CH_2 groups could be overlapping peaks. There are two peaks in the C=O region, at 153 and 184 ppm, accounting for both of the carbonyls expected in the catalyst.
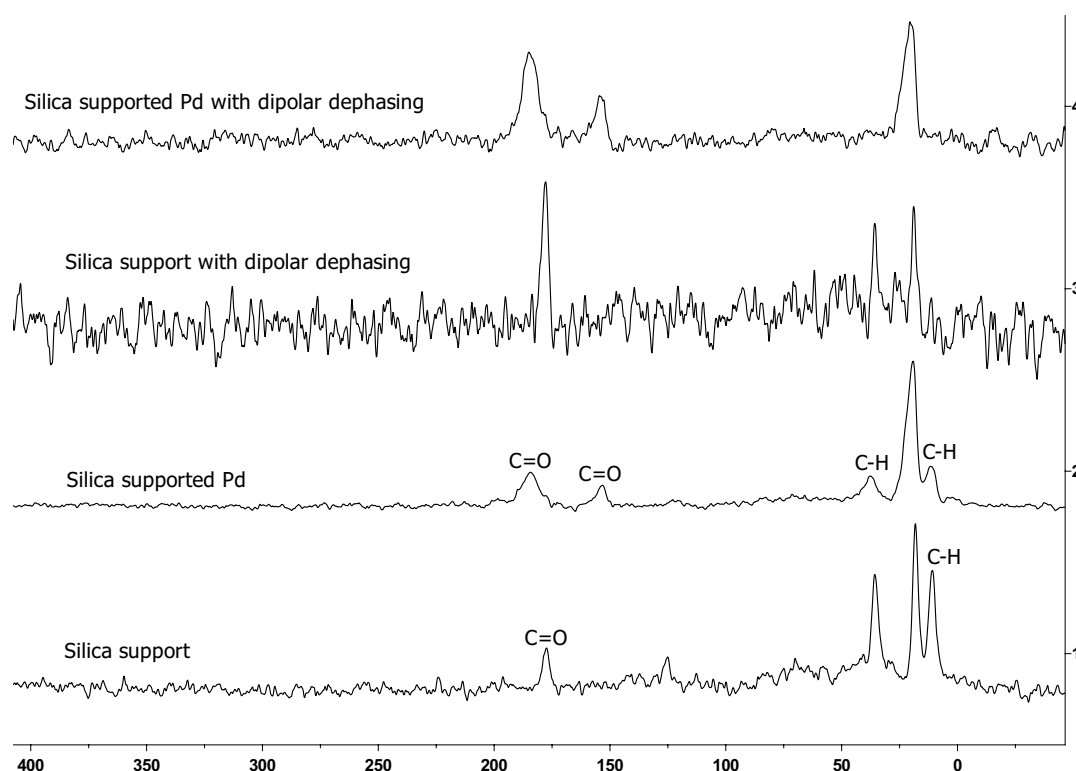
Figure 82: ^{13}C MAS-NMR (100 MHz) spectra of the silica support and silica-supported palladium acetate. The top two spectra include dipolar dephasing where the carbons directly bonded to hydrogen are removed from the spectrum.

These results clearly show that the silica has been modified and indicate that the desired reaction has taken place. It is clear that the silica surface is not simple, and further investigation may reveal the origin of the other peaks seen by ^{13}C MAS-NMR. This catalyst could now be tested in the C–H functionalisation reaction of 2-bromo-*N*-phenylbenzamide **163**. It

would also require some testing to determine if the catalyst undergoes Pd leaching and to what extend it is stable towards various solvents and temperatures.

Chapter 7

Experimental

7.1   General Experimental

Reagents and Solvents

Reagents were purchased from Sigma-Aldrich, Alfa Aesar, Fisher Scientific, Acros Organics, VWR or Fluorochem and used as received unless otherwise stated. The alumina balls used as a catalyst were obtained from Sorbead India. Petroleum ether refers to the fraction of petroleum that is collected at $40 - 60\ ^{\circ}$C. Dry DMF and DMAc were purchased from Acros Organics; DMF was degassed by bubbling nitrogen gas through the solvent with sonication, DMAc was stored over 3 Å molecular sieves and degassed without sonication before use. Aniline was distilled before used and stored under nitrogen.

Water removal from reactions was performed using Dean Stark apparatus between the flask and the condenser or adding 4 Å molecular sieves. Catalysts were activated using a Barnstead Thermolyne 6000 Furnace.

Chromatography

TLC analysis was carried out using Merck 5554 aluminium backed silica plates, and visualised using UV light (254 nm). All column chromatography was performed using silica gel K60 and a solvent system as stated in the text.

NMR Spectroscopy

^{1}H, ^{19}F, ^{31}P and ^{13}C NMR spectra were recorded on a Jeol ECS400 (400 and 100 MHz respectively). Chemical shifts are reported in parts per million and were referenced to residual undeuterated solvent. Coupling constants have been quoted to the nearest 0.1 Hz. ^{1}H

NMR chemical shifts are given to 2 decimal places; ^{13}C NMR chemical shifts are given to 1 decimal place. Spectra were typically recorded at 298 K. ^{13}C spectra were obtained with ^{1}H decoupling. ^{1}H NOE spectra were recorded on a Bruker AV500 (500 MHz) with 32 scans and a 5 second relaxation delay. Spectra were processed using MestreNova.

Solid-state ^{29}Si NMR spectra were obtained at the EPSRC UK National Solid-state NMR Service at Durham. Spectra were recorded at 79.44 MHz using a Varian VNMRS spectrometer and a 6 mm (rotor o.d.) magic-angle spinning probe. They were obtained using direct excitation with a 30.0 s recycle delay, 40 ms contact time, at ambient probe temperature ($\sim$298 K) and at a sample spin-rate of 6.8 kHz. Between 400 and 2000 repetitions were accumulated. Spectral referencing was with respect to an external sample of neat tetramethylsilane.

All other solid state NMR experiments were acquired using a 400 MHz Bruker Avance III HD spectrometer equipped with a Bruker 4mm H(F)/X/Y triple-resonance probe and 9.4T Ascend® superconducting magnet. The ^{13}C$\{^{1}$H$\}$ CPMAS experiment employed a 2 ms linearly-ramped contact pulse, a ^{1}H flipback pulse, spinning rate of 10000 $\pm$2 Hz, 20 second recycle delay, spinal-64 heteronuclear decoupling (at νrf=85 kHz) and is the sum of 160 co-added transients. Chemical shifts are reported with respect to TMS, and were referenced using adamantane (29.5 ppm) as an external secondary reference. The ^{13}C$\{^{19}$F$\}$ CPMAS experiment employed a 2 ms linearly-ramped contact pulse, a ^{19}F flipback pulse, spinning rate of 10000 $\pm$ 2 Hz, 20 second recycle delay, spinal-64 heteronuclear decoupling (at νrf=87 kHz) and is the sum of 160 co-added transients. Chemical shifts are reported with respect to TMS, and were referenced using adamantane (29.5 ppm) as an external secondary reference. ^{19}F Bloch-decay spectra were acquired at spinning rates of 10 and 12.5 $\pm$ 0.002 kHz employing a 30 degree tip-angle pulse (νrf=87 kHz), a 10 s recycle delay and are the sum of 32 co-added transients. Chemical shifts are reported with respect to CFCl$_3$, and were referenced using C$_6$F$_6$ (-165 ppm) as an external secondary reference. ^{1}H Bloch-decay spectra were acquired at a spinning rates of 10 $\pm$ 0.002 kHz employing a 90 degree tip-angle pulse (νrf=87 kHz), a 20 s recycle delay and is the sum of 32 co-added transients. Chemical shifts are reported with respect to TMS, and were referenced using the methyl signal of methanol (3.31 ppm) as an external secondary reference.

Infrared Spectroscopy

IR spectroscopy was performed using a Bruker Vertex 70, a Bruker Alpha or a Perkin Elmer Spectrum Two instrument with an ATR attachment. DRIFTS analysis was performed using a Bruker Equinox 55 with an environmental chamber. The environmental chamber was filled with nitrogen unless otherwise stated and the background measured using finely ground KBr. Samples were prepared by grinding approximately 10 mg sample with 100 mg dry KBr until it resembled a fine powder. This was placed in the sample holder within the environmental chamber and the IR spectrum measured.

Mass Spectrometry

Electrospray ionization (ESI) mass spectrometry was performed using a Bruker daltronics micrOTOF spectrometer, with less than 5 ppm error for all HRMS. Inductively coupled plasma (ICP) analysis was carried out on a Varian ICP with axial OES. The samples were digested in reverse aqua-regia using a CEM mars Xpress microwave. GC-MS was performed using a Perkin Elmer Clarus 500 with a ZB-5HT Column (30 m x 0.25 mm, 0.25 mm film thickness) with temperature ramp from 60 to 360 $^\circ$C at 8 $^\circ$C min^{-1}. The GC had a transfer line to a Perkin Elmer Clarus 560 S EI$^+$-MS.

Elemental Analysis

Elemental analysis was carried out using an Exeter Analytical CE-440 Elemental Analyser, with the percentages reported as an average of two runs where possible.

X-ray Crystallography

Diffraction data were collected at 110 K on an Agilent SuperNova diffractometer with Mo Kα radiation (λ = 0.71073 Å). Data collection, unit cell determination and frame integration were carried out with CrysalisPro. Absorption corrections were applied using face indexing and the ABSPACK absorption correction software within CrysalisPro. Structures were solved and refined using Olex2[134] implementing SHELX algorithms and the Super-

flip[135–137] structure solution program. Structures were solved by charge flipping, Patterson or direct methods and refined with the ShelXL[138] package using full-matrix least squares minimisation. All non-hydrogen atoms were refined anisotropically. Tables of crystallographic data are given in Appendix A.

Optical Rotation

Optical rotations were recorded at 20 °C (using the sodium D line; 589 nm), and $[\alpha]D$ values are given in units of 10^{-1} deg cm^3 g^{-1}. Concentrations are given in g 100 mL^{-1}.

Melting points

Melting points were recorded using a Stuart digital SMP3 machine. All melting points were rounded to the nearest whole number.

Gas Chromatography

Analysis of reaction samples was performed using either an Agilent 6890 GC equipped with a 7683B Series Injector equipped with a ZB-5HT Column (30 m x 0.25 mm, 0.25 mm film thickness) with carrier gas flow rate of 2 mL min^{-1} and a temperature ramp from 50 to 290 °C at 20 °C min^{-1}. The injection volume was 1 μL with a split ratio of 10; or a Varian CP-3800 GC equipped with a CP-8400 Autosampler. Separation was achieved using a DB-1 column (30 m x 0.32 mm, 0.25 mm film thickness) with carrier gas flow rate of 3 mL min^{-1} and a temperature ramp from 50 to 250 °C at 20 °C min^{-1}. The injection volume was 1 μL with a split ratio of 50.

Supercritical fluid chromatography

Supercritical fluid chromatography was carried out using a Thar SuperPure Discovery Series system with a Water 2995 photodiode array detector (ultraviolet/visible light spectrophotometer) and a Water 2424 Evaporative Light Scattering detector. The column used was a Phenomenex Luna 5 μm HILIC 200 Å, 250 x 4.6 mm and samples were run at 100 bar,

40 °C in 30% MeOH in CO_2 (99.8% purity from BOC). An injection loop of 100 μL was used and the sample injection volume was 20 μL.

Microwave Reactions

Microwave reactions were carried out using a CEM Discover S-class instrument (maximum limits set for Power = 300 W and Pressure = 250 psi).

Thermal Gravimetric Analysis

Thermal gravimetric analysis was performed using a Netzsch 409 STA.

Porosimetry

Porosimetry measurements were carried out using a Micromeritics ASAP 2020 Surface Area and Porosity Analyser with a degas temperature of 350 °C and an analysis temperature of 77 K.

Error Analysis

Where possible measurements were recorded in triplicate and an average of the measurements used. Errors were calculated using the maximum measurement and any appropriate calibration (see Appendices B and C).

7.2   Synthetic Procedures and Compound Data

Compounds are listed in numerical order, except from compounds numbered **196**, **202**, **207**, **208**, **201** and **210**, located after compound **164**, as these were isolated from a single reaction.

_N_-4-Chlorophenylheptanamide 47
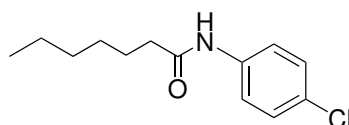
Heptanoic acid (1.30 g, 10 mmol), 4-chloroaniline (1.28 g, 10 mmol) and activated alumina balls (0.26 g, 10 wt%) were stirred at 140 °C for 24 hours. The reaction mixture was dissolved in ethyl acetate, filtered to remove the alumina balls and concentrated to give the crude product (a blue solid) with a conversion of 70% by ^{1}H NMR. The crude product was recrystallised from DCM and hexane to give the title compound as a pale blue solid (1.45 g, 61%); mp 92-94 °C (lit. 93.5 °C[139]); δH (400 MHz, CDCl$_3$) 0.88 (3H, t, _Jz_=6.5 Hz, CH$_3$), 1.31 (6H, m, CH$_2$), 1.70 (2H, app. quin, _J_=7.5 Hz CH$_2$), 2.34 (2H, t _J_=7.5 Hz, CH$_2$), 7.24 (2H, d, _J_=8.7 Hz), 7.46 (2H, d, _J_=8.7 Hz), 7.71 (1H, s); δC (100 MHz, CDCl$_3$) 14.1, 22.6, 25.7, 29.1, 31.7, 37.8, 121.3, 129.0, 129.2, 136.7, 172.0; IR (ATR, cm^{-1}) ν_{max} 1494, 1526 (CO-NH), 1596, 1668 (_CO_-NH), 2856, 2935, 3316 (CO-_NH_ stretch); m/z HRMS (ESI+) C$_{13}$H$_{19}$ClNO ([M+H]$^+$) requires 240.1150; found 240.1152 (-1.8 ppm), C$_{13}$H$_{18}$ClNNaO ([M+Na]$^+$) requires 262.0969; found 262.0976 (-2.3 ppm).

Labbook reference number: LAL1-77, Literature data[139]

Table 7: following the procedure above with various catalysts:

Variables	Conversion by GC /%	Labbook Number
Catalyst = none	73	LAL1-74
Catalyst = Silica-700	76	LAL1-73
Catalyst = Alumina balls, time = 3 h	31	LAL1-72
Catalyst = Alumina balls	76	LAL1-77

Following general procedure 1, heptanoic acid (1.30 g, 10 mmol), 4-chloroaniline (1.28 g, 10 mmol) and catalyst (where appropriate) (0.26 g, 10 wt%) were stirred at 110 °C for 24 hours. Samples were removed from the reaction mixture at 0.5, 1, 2, 4 and 24 hours and analysed by GC. The crude product was analysed by NMR to obtain a conversion.

Graph 10: following the procedure above with various catalysts:

Variables	Conversion by GC /%	Labbook Number
Catalyst = none	51	LAL1-88
Catalyst = Silica-700	55	LAL1-82
Catalyst = Alumina balls	42	LAL1-84

2,N-Diphenylacetamide 49
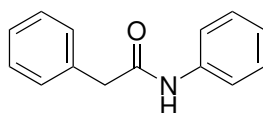
General procedure 1: Phenylacetic acid (1.63 g, 12 mMol), silica (0.55 g, 20 wt%), tetradecane as internal standard (200 μL) and toluene (20 cm^3) were heated to 110 °C with stirring. Aniline (1.11g, 12 mMol) was added and the mixture refluxed for 24 hours. After 24 hours a sample was analysed by GC and the mixture cooled, filtered and solvent removed *in vacuo*. The crude product was recrystallised in ethyl acetate and hexane to give a white solid (2.16 g, 85%); mp 118-119 °C (Lit.118-119 °C[140]); δH (400 MHz, CDCl$_3$) 3.71 (2H, s, CH$_2$), 7.09 (1H, t, J=7.5 Hz, ArH), 7.27 (2H, t, J=8.0 Hz, ArH), 7.30-7.36 (3H, m, ArH), 7.36-7.42 (2H, m, ArH), 7.44 (2H, d, J=8.0 Hz, ArH), 7.48 (1H, s, NH); δC (100 MHz, CDCl$_3$) 44.8 (CH$_2$), 120.0 (ArC), 124.5 (ArC), 127.7 (ArC), 129.0 (ArC), 129.2 (ArC), 129.6 (ArC), 134.6 (ArC), 137.8 (ArC), 169.4 (C=O); IR (ATR, cm^{-1}) ν_{max} 1454, 1496, 1544, 1618, 1656 (C=O stretch), 3061 (C-H stretch) and 3255 (N-H stretch); m/z HRMS (ESI+) C$_{14}$H$_{14}$NO ([M+H]$^+$) requires 212.1070; found 212.1061 (+4.1 ppm), C$_{14}$H$_{13}$NNaO ([M+Na]$^+$) requires 234.0889; found 234.0895 (-2.1 ppm).

Labbook reference number: LAL1-10, Literature data[140]

Table 2: following general procedure 1 with a change in temperature:

Variable	Yield /%	Labbook Number
Temperature = 20 °C	4	LAL1-16
Temperature = 40 °C	6	LAL1-16
Temperature = 60 °C	7	LAL1-16
Temperature = 80 °C	16	LAL1-16
Temperature = 100 °C	48	LAL1-16
Temperature = 110 °C	67	LAL1-16

Table 3: following general procedure 1 with a change in concentration:

Variable	Yield /%	Labbook Number
Concentration = 0.4 mol l^{-1}	15	LAL1-21e
Concentration = 0.6 mol l^{-1}	42	LAL1-21d
Concentration = 0.9 mol l^{-1}	36	LAL1-21c
Concentration = 1.2 mol l^{-1}	46	LAL1-21b
Concentration = 2.4 mol l^{-1}	60	LAL1-21a
Concentration = 4.0 mol l^{-1}	66	LAL1-65
Concentration = 12.0 mol l^{-1}	73	LAL1-67
Concentration = 24.0 mol l^{-1}	74	LAL1-68
Neat	50	LAL1-20

Graph 9: following general procedure 1 with no solvent and a change in temperature. Conversion measured by GC after 8 hours:

Variable	Conversion /%	Labbook Number
Temperature = 110 °C	15	LAL1-20
Temperature = 120 °C	56	LAL1-22a
Temperature = 130 °C	74	LAL1-22b
Temperature = 140 °C	90	LAL1-22c
Temperature = 150 °C	100	LAL1-22d

Table 4: following general procedure 1 with no solvent, a reaction time of 4 hours and a change in temperature:

Variable	Yield /%	Labbook Number
Temperature = 120 °C	57	LAL1-23a
Temperature = 130 °C	62	LAL1-23b
Temperature = 140 °C	73	LAL1-23c
Temperature = 150 °C	77	LAL1-23d

Following general procedure 1 with no solvent, a temperature of 140 °C and a change in time:

Variable	Yield /%	Labbook Number
Time = 6h	74	LAL1-24a
Time = 8h	77	LAL1-24b

Background reaction following the general procedure with no catalyst or solvent at 140 °C, conversion = 86% (GC), *Labbook reference number*: LAL2-117

Following general procedure 1 with microwave heating:

Variables	Conversion by GC /%	Labbook Number
Scale = 3 mmol, Time = 30 min	5	LAL1-39
Scale = 3 mmol, Time = 30 min, Graphite (75 mg) added, Temperature = 150 °C	18	LAL1-51
Scale = 3 mmol, Time = 30 min, No solvent	15	LAL1-40
Scale = 3 mmol, Time = 30 min, No solvent or catalyst	7	LAL1-41

Table 5: following general procedure 1 with different silicas:

Variables	Conversion by GC /%	Labbook Number
Catalyst = Gasil	54	LAL1-39
Catalyst = Cabosil	42	LAL1-51
Catalyst = Hi-sil	33	LAL1-40
Catalyst = Aerosil	26	LAL1-41

Table 6: following general procedure 1 with alumina catalysts:

Variables	Conversion by GC /%	Labbook Number
Catalyst = Calcined alumina balls	16	LAL1-99
Catalyst = Neutral alumina	9	LAL1-54
Catalyst = Acidic alumina	5	LAL1-55
Catalyst = Basic alumina	7	LAL1-56

Following general procedure 1 with alumina catalysts and no solvent at 140 $^\circ$C:

Variables	Conversion by GC /%	Labbook Number
Catalyst = Activated alumina balls	55	LAL1-100
Catalyst = Alumina balls	67	LAL1-31
Catalyst = Crushed alumina balls	46	LAL1-33

N-Phenylbenzamide 66
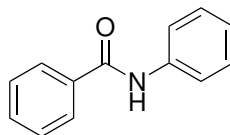
Benzoyl chloride (0.84 g, 6 mmol) was added dropwise to a stirred solution of aniline (0.56 g, 6 mmol) and Et$_3$N (0.84 mL, 0.61 g, 6 mmol) at 0 $^\circ$C and the reaction stirred at room temperature for 4 hours. Water (2 mL) was added and the product was extracted with DCM

(20 mL) and washed with water (20 mL) and brine (20 mL). The organic layer was dried over $MgSO_4$ and the solvent removed *in vacuo*. The crude product was recrystallised from acetone and petroleum ether to give the title compound as a white solid (0.512 g, 43%); mp 164-165 °C (lit. 162-164 °C[141]); δH (400 MHz, CDCl$_3$) 7.16 (1H, tt, *J*=7.4, 1.2 Hz), 7.38 (2H, app. t, *J*=8.4 Hz), 7.47-7.52 (2H, m), 7.53-7.58 (1H, m), 7.65 (2H, dd, *J*=8.5, 1.2 Hz), 7.82 (1H, br. s), 7.86-7.89 (2H, m); δC (100 MHz, CDCl$_3$) 120.3, 124.7, 127.1, 128.9, 129.2, 131.9, 135.1, 138.0, 165.9; IR (thin film, cm^{-1}) ν_{max} 507, 640, 688, 790, 1435, 1487, 1524, 1597, 1653, 3051, 3341; m/z HRMS (ESI+) $C_{13}H_{12}NO$ ([M+H]$^+$) requires 198.0913; found 198.0914 (+0.2 ppm), $C_{13}H_{11}NNaO$ ([M+Na]$^+$) requires 220.0733; found 220.0731 (+0.5 ppm).

Labbook reference number: LAL2-136, Literature data[141]

The synthesis above was repeated with a change in isolation for metrics calculations. The reaction mixture was extracted with ethyl acetate instead of DCM and the recrystallisation was performed using ethyl acetate and petroleum ether to give the title compound as a white solid (1.17 g, 99%). Analytical data matched that reported above.

Labbook reference number: LAL3-265

Benzoic acid (0.18 g, 1.5 mmol), aniline (0.14 g, 1.5 mmol) and silica-700 (0.16 g, 50 wt%) were stirred in xylene (2.5 mL) at 130 °C for 24 hours. Ethyl acetate (10 mL) was added and the reaction mixture filtered. The solvent was removed *in vacuo* and the crude product recrystallised from ethyl acetate and hexane to give the title compound as a white solid (0.20 g, 69%). Analytical data matched that reported above.

Labbook reference number: LAL2-146

Isoniazid 76
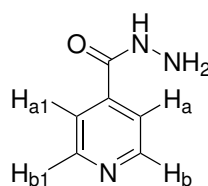
General Procedure 2: Isonicotinic acid (0.37 g, 3 mmol), hydrazine (0.145 cm^3, 3 mmol) and silica-700 (0.10 g, 20 wt%) were stirred in toluene (5 mL) at reflux for 24 hours. The solvent was removed to give the crude product which was then dissolved in ethyl acetate, filtered and concentrated *in vacuo* to the give the title compound as a yellow solid (74.6 mg, 18%, 78% purity); mp 154-158 °C (lit. 153-154 °C[142,143]); δH (400 MHz, SO(CD$_3$)$_2$) 7.72 (2H, AA′XX′ system[a], J_{AX}= 5.6 Hz, $J_{AX'}$= 0.5 Hz, $J_{XX'}$= 1.8 Hz, $J_{AA'}$= 1.8 Hz), 8.70 (2H, AA′XX′ system, J_{AX}= 6.0 Hz, $J_{AX'}$= 0.1 Hz, $J_{XX'}$= 2.4 Hz, $J_{AA'}$= 2.4 Hz), 10.10 (1H, s); δC (100 MHz, SO(CD$_3$)$_2$) 121.1 (C3 and C5), 140.3 (C4), 150.3 (C2 and C6), 164.0 (C=O); IR (ATR, cm^{-1}) ν_{max} 1494, 1529 (CO-NH), 1603, 1636 (CO-NH), 3053, 3196; m/z HRMS (ESI+) C$_6$H$_8$N$_3$O ([M+H]$^+$) requires 138.0662; found 138.0658 (+2.9 ppm), C$_6$H$_8$N$_3$NaO ([M+Na]$^+$) requires 160.0481; found 160.0481 (+0.3 ppm).

[a] The protons in this compound are split in an AA'XX' pattern. This is because the A protons are magnetically equivalent and have the same chemical shift but each A proton couples differently to the X and X' protons. This results in four coupling constants.

Labbook reference number: LAL1-86, Literature data[142,143]

For all the following isoniazid experiments, products were not isolated and conversion was determined by SFC analysis.

Initial experiments: following general procedure 2:

Variables	Conversion /%	Labbook Number
As above	17	LAL2-122
Catalyst = none	23	LAL1-101
Catalyst = none, 4 Å Molecular sieves added	5	LAL2-129
Dean-Stark apparatus fitted to flask, 30 mmol scale	-	LAL1-87

Table 12: following general procedure 2:

Variables	Conversion /%	Labbook Number
Catalyst Loading = 50 wt%	33	LAL1-103
Catalyst Loading = 100 wt%	38	LAL2-111

Table 13: following general procedure 2:

Variables	Conversion /%	Labbook Number
Solvent = CPME	41	LAL1-105
Solvent = Me-THF	0	LAL1-106
Solvent = tBuOAc	24	LAL2-109
Solvent = Water	0	LAL2-116
Solvent = DMSO	0	LAL2-118
Solvent = None	17	LAL2-112

Following general procedure 2:

Variables	Conversion /%	Labbook Number
1.5 eq $N_2H_2 \cdot H_2O$	25	LAL2-119
1 eq $N_2H_2 \cdot HCl$	0	LAL2-114
1 eq $N_2H_2 \cdot HCl$, no catalyst	0	LAL2-115

Table 14: following general procedure 2:

Variables	Conversion /%	Labbook Number
Catalyst = none	23	LAL1-101
Catalyst = Silica-300	43	LAL2-140
Catalyst = Silica-rt	10	LAL2-133
Catalyst = 25 wt% Silica-300, 25 wt% Silica-700	10	LAL2-134

Following general procedure 2 using Silica-300 as catalyst and xylene as solvent. Conversions were not determined as more than 2 species were present by SFC analysis:

Variables	Labbook Number
Temperature = 120 °C	LAL2-141
Temperature = 130 °C	LAL2-142

Table 15: following general procedure 2:

Variables	Conversion /%	Labbook Number
Catalyst Loading = 10 wt%	46	LAL3-260
Catalyst Loading = 20 wt%	39	LAL3-259
Catalyst Loading = 50 wt%	44	LAL3-257
Catalyst Loading = 50 wt%, Atmosphere = N_2	58	LAL3-261
Catalyst Loading = 100 wt%	53	LAL3-258

Table 16: following general procedure 2 using freshly activated silica-300 (50 wt%) in toluene at 110 °C:

Variables	Conversion /%	Labbook Number
Repeat 1	77	LAL2-165
Repeat 2	80	LAL2-166
Repeat 3	75	LAL2-167

A large scale reaction was carried out following general procedure 2 at 15 mmol scale with 50 wt% silica-300 in toluene at 110 °C using an open reflux setup; conversion = 9%; Labbook Reference number = LAL2-164.

(*S*)-t-Butyl-2-(phenylcarbamoyl)pyrrolidine-1-carboxylate 86
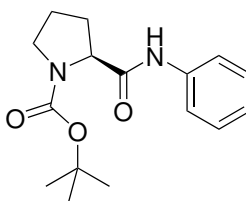
N-boc (*S*)-proline (0.65 g, 3 mmol), aniline (0.27 mL, 3 mmol), tetradecane as internal standard (50 μL) and silica (0.19 g, 20 wt%) were stirred in toluene (5 mL) at reflux for 48 h. The crude product was obtained by filtration and evaporation. This was purified by flash chromatography using a solvent gradient of 12:88 to 100:0 ethyl acetate:hexane (v/v) then recrys-

tallised from ethyl acetate and hexane to give (*S*)-t-butyl-2-(phenylcarbamoyl)pyrrolidine-1-carboxylate as a white solid (0.12 g, 14%); $[\alpha]_D^{20}$ −142.03 (*c* 1.0, CHCl$_3$); mp: 186-188 °C (Lit. 187-188 °C[144]); δH (400 MHz, SO(CD$_3$)$_2$) 1.27 (9H, s, CH$_3$), 1.71-1.96 (2H, m, CH$_2$), 2.07-2.25 (1H, m, CH$_2$), 3.27-3.46 (2H, m, CH$_2$), 4.18 (1H, dd, *J*= 8.2, 4.6 Hz, CH), 7.03 (1H, t, *J*=7.3 Hz, ArH), 7.30 (2H, app. t, *J*=7.8 Hz, ArH), 7.43-7.59 (2H, d, *J*=7.5 Hz, ArH), 9.97 (1H, s, NH); Selected data for minor rotamer of boc group: 1.37 (9H, s, CH$_3$), 4.25 (1H, dd, *J*= 8.3, 3.3 Hz, CH); δC (100MHz, CDCl$_3$) 24.7 (CH$_2$-b), 27.2 (CH$_2$-c), 28.5 (CH$_3$), 47.3 (CH$_2$-a), 60.6 (CH), 81.0 (C(CH$_3$)$_3$), 119.7 (ArC), 123.9 (ArC), 129.0 (ArC), 156.8, 169.9 (N-C(=O)-C), 194.5 (N-C(=O)-O); IR (ATR, cm^{-1}) ν_{max} 1545, 1602, 1669 (Ar C=C bending), 1694 (C=O stretch), 2972 (C-H stretch), 3288 (N-H stretch); m/z HRMS (ESI+) C$_{16}$H$_{23}$N$_2$O$_3$ ([M+H]$^+$) requires 291.1703; found 291.1698 (+1.9 ppm), C$_{16}$H$_{22}$N$_2$NaO$_3$ ([M+Na]$^+$) requires 313.1523; found 313.1519 (+1.6 ppm).

Labbook reference number: LAL1-6/LAL1-13, Literature data[144]

The reaction was conducted as above with no catalyst; conversion calculated by GC = 23%; Labbook reference number: LAL1-15

(*S*)-t-Butyl-2-(benzylcarbamoyl)pyrrolidine-1-carboxylate 87
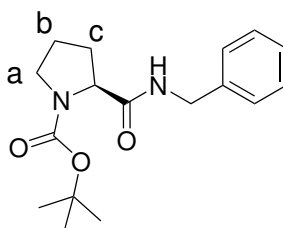
N-boc (*S*)-proline (0.65 g, 3 mmol), benzylamine (0.33 mL, 3 mmol), tetradecane as internal standard (50 µL) and silica (0.19 g, 20 wt%) were stirred in toluene (5 mL) at reflux for 24 h. The crude product was obtained by filtration and evaporation. This was purified by recrystallisation from ethyl acetate and hexane to give (*S*)-t-butyl-2-(benzylcarbamoyl)pyrrolidine-1-carboxylate as a white solid (0.71 g, 78%); mp 126-127 °C (lit.130-131 °C[145]); $[\alpha]_D^{20}$ −90.36 (*c* 1.0, CHCl$_3$); δH (400 MHz, SO(CD$_3$)$_2$) 1.28 (9H, s, CH$_3$), 1.70-1.89 (2H, m, CH$_2$-b), 2.02-2.18 (2H, m, CH$_2$-c), 3.23-3.45 (2H, m, CH$_2$-a), 4.04-4.25 (2H, m, CH$_2$Ph),

4.29-4.39 (1H, m, CH), 7.17-7.34 (5H, m, ArH), 8.30-8.43 (1H, m, NH); Selected data for minor rotamer of boc group: 1.41 (9H, s, CH$_3$); δC (100MHz, CDCl$_3$) 23.8 (CH$_2$-b), 28.3 (CH$_3$), 31.1 (CH$_2$-c), 43.4 (CH$_2$Ph), 47.2 (CH$_2$-a), 60.1 (CH), 80.6 (C(CH$_3$)$_3$), 127.4 (ArC), 127.7 (ArC), 127.8 (ArC), 128.7 (ArC), 138.3 (ArC), 155.9 (ArC), 172.4 (C=O); Selected data for minor rotamer: 24.7 (CH$_2$-b), 61.4 (CH), 154.8 (ArC), 172.0 (C=O); IR (ATR, cm^{-1}) v_{max} 1393, 1528, 1653, 1682 (C=O stretch), 2874, 2979 (C-H stretch), 3311 (N-H stretch); m/z HRMS (ESI+) C$_{17}$H$_{24}$N$_2$NaO$_3$ ([M+Na]$^+$) requires 327.1679; found 327.1671 (+2.5 ppm).

Labbook reference number: LAL1-7, Literature data[145]

The reaction was conducted as above with no catalyst; conversion calculated by GC = 78%; Labbook reference number: LAL1-9

N-Phenyladamantane-1-carboxamide 89
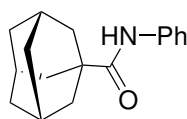
Adamantane carboxylic acid (2.16 g, 12 mmol), aniline (1.09 mL, 12 mmol), tetradecane as internal standard (200 μL) and silica (0.66 g, 20 wt%) were stirred in toluene (20 mL) at reflux for 24 h. The mixture was filtered and the solvent removed *in vacuo* to give the crude product which was analysed by NMR. No conversion of starting material was observed by ^{1}H NMR or GC.

Labbook reference number: LAL1-5

This reaction was also conducted with benzylamine (1.31 mL, 12 mmol) as the amine. No conversion of starting material was observed by ^{1}H NMR or GC.

Labbook reference number: LAL1-4

High throughput screen of substrates

Toluene (0.83 mL) was measured by syringe by the Chemspeed® robot into 49 vials. 0.5 mmol of each acid and amine were measured into the vials arranged in a grid measuring 7x7. Liquid reagents were dispensed first by syringe followed by solid reagents which were weighed using the Chemspeed® robot. Silica-700 catalyst (70 mg) was added to each vial before the vials were capped, stirred by mechanical shaking and heated to 120 °C for 24 hours. The solvent from each vial was then removed *in vacuo* before a small sample was taken for analysis.

Each reaction was labelled with a code to denote the acid and amine used.

Code	Acid	Code	Amine
170	Coumalic acid	A	Phenanthrolin-5-amine
171	Phthalic acid	B	Piperidine
172	Isonicotinic acid	C	Azepane
173	Nicotinic acid	D	Tetrahydroquinoline
174	Picolinic acid	E	Indoline
175	3-quinoline carboxylic acid	F	Thiazolidine
176	2-chloropyridine-3-carboxylic acid	G	2-aminothiophenol

The mass of the expected product from each reaction and the masses detected by MS

Reaction Number	Expected MH⁺	MH⁺ seen in MS
LAL2-170A	317	196, 212, 224, 246, 250, 272, 282, 304, 391, 413, 463
LAL2-170B	207	87, 207, 233, 289, 327, 341, 371
LAL2-170C	221	100, 141, 211, 235, 261, 288, 317, 353, 390
LAL2-170D	255	184, 212, 238, 266, 288, 315, 341, 369
LAL2-170E	241	170, 198, 224, 274, 287, 313
LAL2-170F	211	194, 208, 224, 234
LAL2-170G	247	228, 256, 282, 283, 284, 285, 310
LAL2-171A	343	196, 212, 326, 348, 413,
LAL2-171B	233	87, 319, 347
LAL2-171C	247	100, 347, 375,
LAL2-171D	281	100, 134, 184, 261, 263, 282, 287, 310, 347, 381, 409
LAL2-171E	267	120, 268, 290, 306, 353, 367,
LAL2-171F	237	104, 207, 238, 270, 283, 309, 341
LAL2-171G	273	256, 347, 355, 375
LAL2-172A	300	196, 391, 413
LAL2-172B	190	86, 171, 207, 234, 256, 299, 319, 333
LAL2-172C	204	100, 191, 211, 235, 262, 288, 304, 347, 419
LAL2-172D	238	134, 146, 170, 245, 261, 277, 291
LAL2-172E	224	120, 251
LAL2-172F	194	207, 227, 247, 316, 328, 242, 367
LAL2-172G	230	236, 249, 271, 323, 339, 394, 413
LAL2-173B	190	86, 207, 299, 319
LAL2-173C	204	100, 191, 235, 288, 304
LAL2-173D	238	134, 146, 245, 261, 277
LAL2-173E	224	120, 225, 251, 338
LAL2-173F	194	90, 102, 124, 132, 207, 244, 278, 298, 316, 342, 367
LAL2-173G	230	149, 271

Reaction Number	Expected MH$^+$	MH$^+$ seen in MS
LAL2-174A	300	195, 391, 413
LAL2-174B	190	86, 183, 207, 269, 276, 299
LAL2-174C	204	100, 191, 235, 261, 288, 297, 304, 313, 419
LAL2-174D	238	134, 152, 184, 261
LAL2-174E	224	152, 170, 225, 310, 324
LAL2-174F	194	90, 124, 195, 258, 284, 306, 385
LAL2-174G	230	124, 156, 213, 235, 249, 258, 320
LAL2-175A	350	196, 413
LAL2-175B	240	86, 171, 207, 246, 299, 319
LAL2-175C	254	100, 221, 235, 288
LAL2-175D	288	130, 261
LAL2-175E	274	120, 247
LAL2-175F	244	90, 174, 219, 231, 303, 342
LAL2-175G	280	130, 174, 196, 236, 261
LAL2-176A	334.5	196, 218, 413
LAL2-176B	224.5	86, 207, 235, 292
LAL2-176C	238.5	100, 177, 221, 306, 320
LAL2-176D	272.5	134, 255, 261, 354
LAL2-176F	228.5	104, 168, 207, 271
LAL2-176G	264.5	247, 275, 368, 396, 424

Aniline screen

General procedure 4: Carboxylic acid (1 mmol), aniline (92 μL, 1 mmol) and catalyst (30 mg) were stirred in cymene (2 mL) for 24 hours. The mixture was filtered and the solvent removed *in vacuo* to give the crude product which was analysed by ^{1}H NMR spectroscopy to obtain a conversion.

A = isonicotinic acid (123 mg) B = coumalic acid (140 mg) C = thiophene carboxylic acid (128 mg) D = *N*-boc-L-proline (215 mg) E = 3-quinoline carboxylic acid (173 mg) F =

2-chloropyridine-3-carboxylic acid (158 mg)

Table 21: following general procedure 4:

Variables	Conversion /%	Labbook Number
Acid = A, Catalyst = silica-700	7	LAL3-233
Acid = A, Catalyst = silica-300	10	LAL3-234
Acid = A, Catalyst = none	0	LAL3-235
Acid = B, Catalyst = silica-700	0	LAL3-236
Acid = B, Catalyst = silica-300	0	LAL3-237
Acid = B, Catalyst = none	0	LAL3-238
Acid = C, Catalyst = silica-700	0	LAL3-239
Acid = C, Catalyst = silica-300	0	LAL3-240
Acid = C, Catalyst = none	0	LAL3-241
Acid = D, Catalyst = silica-700	10	LAL3-242
Acid = D, Catalyst = silica-300	20	LAL3-243
Acid = D, Catalyst = none	4	LAL3-244
Acid = E, Catalyst = silica-700	0	LAL3-245
Acid = E, Catalyst = silica-300	0	LAL3-246
Acid = E, Catalyst = none	0	LAL3-247
Acid = F, Catalyst = silica-700	0	LAL3-248
Acid = F, Catalyst = silica-300	0	LAL3-249
Acid = F, Catalyst = none	0	LAL3-250

(*R*)-2-Hydroxydiphenylacetamide 147
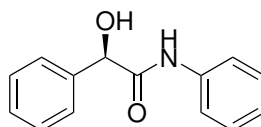
General procedure 3: (*R*)-2-Hydroxyphenylacetic acid (114 mg, 0.75 mmol) and aniline (70 mg, 0.75 mmol) were stirred in toluene at 80 °C for 24 hours. The solvent was removed and analysis by ^{1}H NMR showed approximately 50% conversion based on the aniline peaks. The

crude mixture was dissolved in ethyl acetate and washed with 1M HCl, sat. $NaHCO_3$ and water before drying over $MgSO_4$ and evaporating the solvent *in vacuo* to give the title compound as a white solid (90 mg, 53%); mp 143-145 °C (lit. 145-147 °C[146]); $[\alpha]_D^{20}$ −70.60 (*c* 1.0, $CHCl_3$); δH (400 MHz, $CDCl_3$) 4.16 (1H, br. s), 5.03 (1H, s), 7.11 (1H, t, *J*=7.3 Hz), 7.29 (2H, t, *J*=7.8 Hz), 7.31-7.37 (3H, m), 7.38-7.43 (2H, m), 7.47 (2H, d, *J*=8.1 Hz), 8.45 (1H, s); δC (100 MHz, $CDCl_3$) 74.8, 119.9, 124.9, 127.0, 129.0, 129.1, 129.2, 137.2, 139.0, 170.1; IR (ATR, cm^{-1}) ν_{max} 556, 690, 721, 751, 1057, 1245, 1443, 1531, 1660, 1665, 3060, 3289; m/z HRMS (ESI+) $C_{14}H_{14}NO_2$ ([M+H]$^+$) requires 228.1019; found 228.1023 (-2.0 ppm), $C_{14}H_{13}NNaO_2$ ([M+Na]$^+$) requires 250.0838; found 250.0845 (-2.3 ppm).

Labbook reference number: LAL3-274, Literature data[146]

The catalysed reaction was conducted as above with the addition of activated silica-700 (37 mg, 20 wt%) which was removed by filtration after the reaction. Analytical data matched that reported above; $[\alpha]_D^{20}$ −74.50 (*c* 1.0, $CHCl_3$).

Labbook reference number: LAL3-273

Table 23: following general procedure 3:

Variables	Yield /%	Labbook Number
Temperature = 20 °C	0	LAL3-275
Temperature = 40 °C	0	LAL3-276
Temperature = 60 °C	9	LAL3-277
Temperature = 70 °C	32	LAL3-278
Temperature = 120 °C	73	LAL3-272
Temperature = 20 °C, silica-700 (37 mg, 20 wt%) added	0	LAL3-279
Temperature = 40 °C, silica-700 (37 mg, 20 wt%) added	0	LAL3-280
Temperature = 60 °C, silica-700 (37 mg, 20 wt%) added	9	LAL3-281
Temperature = 70 °C, silica-700 (37 mg, 20 wt%) added	26	LAL3-282
Temperature = 120 °C, silica-700 (37 mg, 20 wt%) added	61	LAL3-271

Phenanthridin-6-(5*H*)-one 148
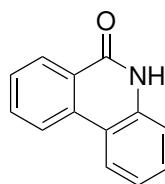
General procedure 5: *N*-phenylbenzamide (19.7 mg, 0.1 mmol), Pd(OCOCF$_3$)$_2$ (2.3 mg, 0.007 mmol) and benzoic acid (1 g) were placed in a 10 mL microwave vial and flushed with O$_2$. The reaction was stirred at 150 °C under O$_2$ (1 atm). After 48 hours the reaction was dissolved in EtOAc (15 mL) and washed with Na$_2$CO$_3$ (2 x 10 mL). The aqueous layer was extracted with ethyl acetate (10 mL) and the combined organic portions washed with water and brine before being dried over MgSO$_4$ and concentrated in vacuo. The crude product was purified by column chromatography with ethyl acetate/petroleum ether 40-60 (3:7) as eluent to give the title compound as a pale yellow solid (15.7 mg, 0.08 mmol, 81%); mp 274-277 °C (lit. 291-293 °C[69]); δH (400 MHz, CDCl$_3$) 7.27 (1H, ddd, *J*=7.9, 7.2, 1.3 Hz), 7.36 (1H, dd, *J*=8.1, 1.3 Hz), 7.49 (1H, ddd, *J*=8.2, 7.1, 1.3 Hz), 7.65 (1H, app. td, J=7.4, 0.9 Hz), 7.86 (1H, ddd, *J*=8.0, 7.1, 1.5 Hz), 8.32 (1H, dd, *J*=7.9, 1.5 Hz), 8.39 (1H, d, *J*=8.2 Hz), 8.51 (1H, d, *J*=8.1 Hz), 11.69 (1H, s); δC (100 MHz, SO(CD$_3$)$_2$) 116.1, 117.6, 122.3, 122.6, 123.3, 125.7, 127.5, 127.9, 129.6, 132.8, 134.3, 136.6, 160.8; IR (thin film, cm^{-1}) ν_{max} 725, 748, 1022, 1086, 1152, 1260, 1360, 1422, 1469, 1510, 1556, 1605, 1633, 1652, 2889, 2962, 3039, 3101, 3158; m/z HRMS (ESI+) C$_{13}$H$_{10}$NO ([M+H]$^+$) requires 196.0757; found 196.0754 (+1.4 ppm), C$_{13}$H$_9$NNaO ([M+Na]$^+$) requires 218.0576; found 218.0580 (-1.9 ppm).

Labbook reference number: LAL2-145, Literature data[69]

Table 25: following general procedure 5 with a change in Pd catalyst. Conversions calculated by ^{1}H NMR using peaks at 8.55 and 7.12:

Variables	Conversion /%	Labbook Number
Pd$_2$(tfs)$_2$(MeCN)$_2$ (3.7 mg, 7 mol%)	42	LAL2-187
Pd$_2$(tfs)$_2$(MeCN)$_2$ (3.7 mg, 7 mol%)	52[a]	LAL3-219
[Pd(8-methylquinoline)(OAc)]$_2$ (4.3 mg, 7 mol%)	29	LAL2-197

[a] Yield of isolated product

Table 29: following general procedure 5. Conversions calculated by ^{1}H NMR using peaks at 8.55 and 7.12:

Variables	Conversion /%	Labbook Number
As above	47	LAL3-218
Reaction conducted in metal high pressure reactor	0	LAL4-325/326

Phenanthridin-6(5*H*)-one 148 synthesis from aniline and benzoic acid

General Procedure 6: Benzoic acid (1 g), Pd(OCOCF$_3$)$_2$ (4.6 mg, 0.014 mmol) and aniline (20 μL, 0.21 mmol) were placed in a 10 mL microwave vial which was then flushed with O$_2$. The reaction was stirred at 150 °C in a metal heating block under a positive pressure of O$_2$ from a balloon. After 48 hours the reaction was dissolved in EtOAc (15 mL) and washed with Na$_2$CO$_3$ (2 x 10 mL). The aqueous layer was extracted with ethyl acetate (10 mL) and the combined organic portions washed with water and brine before being dried over MgSO$_4$ and concentrated *in vacuo*. The crude product was purified by column chromatography with ethyl acetate/petroleum ether 40-60 (3:7) as eluent to give the product as a pale yellow solid (12.0 mg, 0.06 mmol, 29%); Analytical data matched that reported above.

Labbook reference number: LAL2-180

For the following reactions, conversions were calculated by integration of well resolved peaks in the ^{1}H NMR spectrum of the crude reaction mixture.

Table 26: following general procedure 6:

Variables	Conversion /%	Labbook Number
As above	30:70:0	LAL2-189
As above	30:60:10	LAL2-147
Using freshly distilled aniline	4:87:9	LAL3-199
Temperature = 130 °C	0:84:16	LAL3-200
Vessel was capped using a Subaseal with an O_2 balloon	5:95:0	LAL2-193
Vessel was sealed using a Subaseal	0:100:0	LAL2-192
Vessel was heated in a graphite bath	5:95:0	LAL3-205
Vessel = rbf	decomp	LAL2-190
Vessel = sealed Schlenk tube	0:100:0	LAL2-191
Vessel = Schlenk with O_2 balloon, 4 Å molecular sieves added	13:87:0	LAL2-196

Table 27: following general procedure 6:

Variables	Conversion /%	Labbook Number
Solvent = benzoic anhydride (1 g)	15:85:0	LAL2-204
Solvent = benzoic acid (0.5 g) and propylene carbonate (0.5 g)	0:1:0	LAL2-201
Solvent = benzoic acid (0.5 g) and benzoic anhydride (0.5 g)	0:1:0	LAL2-202
Solvent = benzoic acid (0.5 g) and methyl benzoate (0.5 g)	0:1:0	LAL2-203

Table 28: following general procedure 6 under microwave heating. The vessels were placed under an oxygen atmosphere and sealed before heating:

Variables	Conversion /%	Labbook Number
Time = 1 h	0:20:80	LAL2-206
Time = 2 h,	0:90:10	LAL2-207
Time = 2 h, O_2 replenished at 1 h, Vessel = 30 mL vial	0:17:83	LAL2-210
Time = 4 h, O_2 replenished at 2 and 3 h	10:80:10	LAL2-211
Time = 6 h, O_2 replenished at 3, 4 and 5 h	5:85:10	LAL2-214

Tetrafluorosuccinimide 159
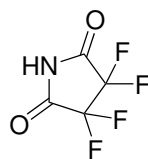
Following the procedure described by Reeds,[72] tetrafluorosuccinamide (1.00 g, 5.31 mmol, 1 eq) was placed in a dry Schlenk tube under an atmosphere of N_2 and concentrated sulphuric acid (0.29 mL, 5.44 mmol, 1.03 eq) was added *via* syringe. The mixture was stirred under a static vacuum (0.7 mmHg, 10 mins), and placed back under N_2 before a cold finger (-196 °C) was added. This was placed under a static vacuum (0.7 mmHg) and heated to 120 °C over 1 hour. The product was collected on the cold finger and resublimed at 0.7 mmHg, 60 °C to give the title compound as a white crystalline powder (0.4593 g, 2.68 mmol 51%); δH (400 MHz, $(CD_3)_2CO$) 3.75 (1H, br s); δF (376 MHz, $(CD_3)_2CO$) -128.0 (s); δC (100 MHz, $(CD_3)_2CO$) 109.4 (t, J=29.8 Hz), 160.6 (t, J=29.3 Hz); IR (ATR, cm^{-1}) ν_{max} 1168, 1291, 1424, 1680, 1756, 3227; m/z HRMS (ESI-) $C_4F_4NO_2$ ([M-H]$^-$) requires 169.9871; found 169.9873 (-1.4 ppm).

Labbook reference number: LAL2-154 and LAL2-183, Literature data[72]

Pd(tfs)$_2$(MeCN)$_2$ 160
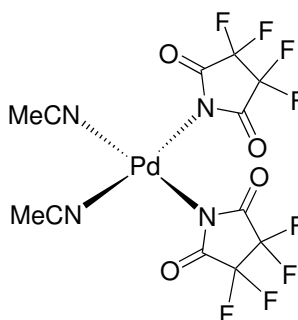
Tetrafluorosuccinimide (274 mg, 1.6 mmol, 2 eq) and Pd$_3$(OAc)$_6$ (180 mg, 0.8 mmol, 1 eq) were placed under a N_2 atmosphere in a Schlenk tube. MeCN (7 mL, dry) was added and the vessel sealed and stirred for 16 hours at room temperature to give a green-yellow solution.

This solution was filtered through a sinter and diethyl ether and petroleum ether 40-60 were added until a homogenous solution formed. The solution was placed in the freezer and a precipitate allowed to form. The precipitate was separated by filtration and washed with cold acetonitrile, petroleum ether 40-60 and diethyl ether and dried *in vacuo* to give the title compound as a yellow powder (283 mg, 0.53 mmol, 67%); mp >200 celsius decomp. δH (400 MHz, Solid) 2.94 (s); δF (376 MHz, Solid) -123.7; δC (100 MHz, Solid) 3.4, 4.3, 5.2, 106.3, 124.6, 169.7, 243.8; IR (ATR, cm^{-1}) ν_{max} 622, 750, 1013, 1061, 1191, 1302, 1703, 2314, 2343; Anal. calcd. for $C_{12}H_6F_8N_4O_4Pd$ C 27.27, H 1.14, N 10.60; found C 27.28, H 1.15, N 10.18.

An X-ray diffraction crystal structure of this compound was obtained. See Appendix A.

Labbook reference number: LAL2-158 and LAL2-184, Literature data[72]

2-Bromo-*N*-phenylbenzamide 163
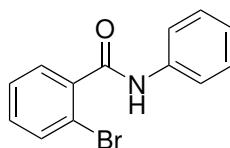
Oxalyl chloride (0.76 mL, 6 mmol) was added to a solution of 2-bromobenzoic acid (1.2 g, 6 mmol) and *N,N*-dimethylformamide (1 drop, ca. 10 μL) in CH_2Cl_2 (5 mL) at 0 $^\circ$C. The solution was stirred for 30 minutes at rt and concentrated *in vacuo* to provide the 2-bromobenzoyl chloride intermediate. The 2-bromobenzoyl chloride (6 mmol) was added dropwise to a stirred solution of aniline (0.54 mL, 6 mmol) and Et$_3$N (0.84 mL, 0.61 g, 6 mmol) at 0 $^\circ$C and the reaction stirred at room temperature for 2 hours. Water (2 mL) was added and the product was extracted with DCM (20 mL) and washed with water (20 mL) and brine (20 mL). The organic layer was dried over MgSO$_4$ and the solvent removed *in vacuo*. The crude product was recrystallised from DCM and hexane to give the title compound as a white solid (1.18 g, 71%); mp 119-120 $^\circ$C (Lit. 122-123 $^\circ$C[147]); δH (400 MHz, CDCl$_3$) 7.18 (1H, t, *J*=7.4 Hz), 7.34 (1H, app. td, *J*=7.7, 1.7 Hz), 7.39-7.42 (2H, m), 7.43 (1H, app. td, *J*=7.5, 1.2 Hz), 7.61-7.69 (5H, m); δC (100 MHz, CDCl$_3$) 119.4, 120.2, 125.0, 127.9, 129.3, 129.9, 131.8, 133.6, 137.6, 137.9, 165.7; IR (ATR, cm^{-1}) ν_{max} 505, 587,

692, 759, 893, 1025, 1328, 1442, 1488, 1546, 1598, 1640, 3136, 3239; m/z HRMS (ESI+) $C_{13}H_{11}BrNO$ ([M+H]$^+$) requires 276.0019; found 276.0013 (+1.4 ppm), $C_{13}H_{10}BrNNaO$ ([M+Na]$^+$) requires 297.9838; found 297.9830 (+2.4 ppm).

Labbook reference number: LAL4-333, Literature data[147]

2-bromobenzoic acid (0.30 g, 1.5 mmol), aniline (0.14 g, 1.5 mmol) and silica-700 (0.22 g, 50 wt%) were stirred in xylene (2.5 mL) at 140 °C for 24 hours. Ethyl acetate (10 mL) was added and the reaction mixture filtered. The solvent was removed *in vacuo* and the crude product recrystallised from diethyl ether and hexane to give the title compound as a white solid (0.24 g, 59%). Analytical data matched that reported above.

Labbook reference number: RC1-23 *(Reaction was conducted by R. Campbell)*

5-Phenylphenanthridin-6(5*H*)-one 164
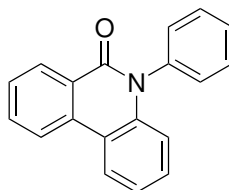
General Procedure 7: Pd$_3$(OAc)$_6$ (5.6 mg, 0.025 mmol, 5 mol%), dppp (10.4 mg, 0.025 mmol, 5 mol%) and K$_2$CO$_3$ (138 mg, 1 mmol, 2 eq) were placed in a schlenk tube under nitrogen. DMA (1.5 mL) was added and the mixture was stirred at 130 °C for 2 minutes. 2-bromo-*N*-phenylbenzamide (138 mg, 0.5 mmol) in DMA (1 mL) was added *via* cannula. Gas was seen to be released from the solution at this point. The reaction mixture was stirred at 130 °C for 2 hours after which it was cooled and diluted with ethyl acetate (10 mL). The reaction mixture was filtered through Celite and washed with 1M HCl (10 mL) and brine (10 mL) before the organic layer was dried over MgSO$_4$, filtered and the solvent removed *in vacuo*. The crude product was purified by column chromatography (10-20% ethyl acetate in petroleum ether) to give the title compound as a white solid (32.9 mg, 49%); R_f 0.33 (EtOAc/petrol, 3:7, *v/v*); mp 228-230 °C (lit. 227-229 °C[148]); δH (400 MHz, CDCl$_3$) 6.67-6.74 (1H, m), 7.26-7.32 (2H, m), 7.33-7.37 (2H, m), 7.55 (1H, tt, *J*=8.3, 1.3 Hz), 7.60-7.66 (3H, m), 7.82 (1H, ddd, *J*=8.1, 7.3, 1.5 Hz), 8.29-8.33 (1H, m), 8.35 (1H, d, *J*=8.3 Hz) and

8.58 (1H, dd, J=8.0, 1.3 Hz); δC (100 MHz, CDCl$_3$) 117.1, 119.1, 121.9, 122.8, 123.1, 126.0, 128.3, 128.9, 129.1, 129.2, 129.2, 130.3, 132.9, 134.1, 138.4, 139.3 and 161.8; IR (ATR, cm^{-1}) ν_{max} 512, 644, 686, 745, 801, 1040, 1290, 1320, 1430, 1485, 1603, 1651, 3059; m/z HRMS (ESI+) C$_{19}$H$_{14}$NO ([M+H]$^+$) requires 272.1070; found 272.1074 (-1.0 ppm), C$_{19}$H$_{13}$NNaO ([M+Na]$^+$) requires 294.0889; found 294.0894 (-1.4 ppm).

An X-ray diffraction crystal structure of this compound was obtained. See Appendix A.

Labbook reference number: LAL4-330, Literature data[148]

Table 30: following general procedure 7 on a 0.25 mmol scale using DMF as solvent (*Reactions conducted by A. Pagett and R. Campbell*):

Variables	Yield /%	Labbook Number
Ligand = dppm, Time = 6 hours	52	AP11
Ligand = dppe, Time = 0.5 hours	64	AP4
Ligand = dppb, Time = 6 hours	71	AP7
Ligand = dppf, Time = 6 hours	58	AP10
Precatalyst = Pd$_2$dbaphos$_2$, no added ligand, Time = 5 hours	0	RC1-30

Table 31: following general procedure 7 on a 0.25 mmol scale using dppe as a ligand and DMF as solvent at 80 °C (*Reactions AP23 and AP24 conducted by A. Pagett*):

Variables	Yield /%	Labbook Number
Catalyst: Pd$_3$(OAc)$_6$, air free	54	LAL3-288
Catalyst: Pd$_3$(OAc)$_6$, 5 mL air added after reaction started	58	LAL3-284
Catalyst: Pd$_2$dba$_3 \cdot$ CHCl$_3$, air free	0	AP23
Catalyst: Pd$_2$dba$_3 \cdot$ CHCl$_3$, Ligand = dppp, Temperature = 130 °C, Solvent = DMAc bubbled with air for 5 min	73	LAL4-332
Catalyst: PdCl$_2$, air free	41	AP24

The reaction was conducted following general procedure 7 with changes of solvent at 80 °C:

Variables	Yield /%	Labbook Number
Solvent = ethylene carbonate	56	AP27
Solvent = cyrene	0	LAL4-292

Large scale reaction performed for isolation of side products

$Pd_3(OAc)_6$ (14 mg, 0.063 mmol, 5 mol%), dppe (25 mg, 0.063 mmol, 5 mol%) and K_2CO_3 (345 mg, 2.5 mmol, 2 eq) were placed in a schlenk tube under nitrogen. DMF (15 mL) was added and the mixture was stirred at 80 °C for 2 minutes. 2-bromo-*N*-phenylbenzamide (345 mg, 1.25 mmol) was added directly to the reaction mixture. The reaction mixture was stirred at 80 °C for 2 hours after which it was cooled and diluted with ethyl acetate (40 mL). The reaction mixture was filtered through Celite and washed with 1M HCl (20 mL) and brine (20 mL) before the organic layer was dried over $MgSO_4$, filtered and the solvent removed *in vacuo*. The crude product was purified by column chromatography (10-20% ethyl acetate in petroleum ether) to give the title compound as a white solid (17.0 mg, 28%); Analytical data obtained for the major product, 5-phenylphenanthridin-6(5*H*)-one, matched that detailed above.

Labbook reference number: LAL4-297

Seven fractions were obtained from the column of the 1.25 mmol reaction. Fraction 3 was the major component mentioned above.

Fraction 1: 8*H*-Indolo[3,2,1-*de*]phenanthridin-8-one 196
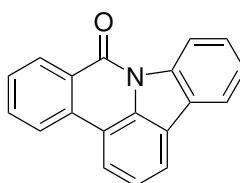
Data for this compound: 3.7 mg, 2.2%; R_f 0.58 (EtOAc/petrol, 3:7, *v/v*); δH (400 MHz, CDCl$_3$) 7.52 (1H, app. td, *J* = 7.5, 0.9 Hz), 7.60-7.66 (2H, m), 7.69 (1H, ddd, *J* = 8.0,

7.1, 1.1 Hz), 7.86 (1H, ddd, J = 8.0, 7.3, 1.4 Hz), 8.09-8.14 (2H, m), 8.23 (1H, d, J = 7.8 Hz), 8.37 (1H, d, J = 8.0 Hz), 8.72 (1H, dd, J = 8.0, 1.1 Hz), 8.87 (1H, d, J = 8.1 Hz); δC (100 MHz, CDCl$_3$) 117.4, 117.5, 120.5, 121.0, 121.2, 122.7, 124.3, 124.7, 125.0, 126.6, 127.9, 128.3, 128.5, 129.5, 133.2, 134.0, 138.7, 160.3; IR (thin film, cm^{-1}) ν_{max} 479, 674, 688, 733, 760, 1272, 1305, 1339, 1351, 1421, 1444, 1516, 1597, 1664, 2853, 2923, 3303; m/z HRMS (ESI+) C$_{19}$H$_{12}$NO ([M+H]$^+$) requires 270.0913; found 270.0925 (-4.8 ppm), C$_{19}$H$_{11}$NNaO ([M+Na]$^+$) requires 292.0733; found 292.0743 (-3.1 ppm).

An X-ray diffraction crystal structure of this compound was obtained. See Appendix A.

Labbook reference number: LAL4-297f1, Literature data[108]

Fraction 2: 2-Hydroxy-*N*-phenylbenzamide 202
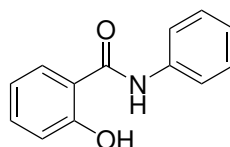
Selected data: 5.0 mg, 2.9%; R_f 0.45 (EtOAc/petrol, 3:7, *v/v*); δH (400 MHz, CDCl$_3$) 6.89-6.98 (1H, m) 7.04 (1H, d, J = 8.3 Hz), 7.18-7.24 (1H, m), 7.40 (2H, app. t, J = 7.7 Hz), 7.43-7.51 (1H, m), 7.53 (1H, d, J = 8.3 Hz), 7.58 (2H, d, J = 8.3 Hz), 7.95 (1H, br. s), 11.99 (1H, s); δC (100 MHz, CDCl$_3$) 114.6, 119.0, 119.1, 121.3, 125.5, 128.9, 129.2, 134.8, 136.7, 162.0, 171.3; IR (thin film, cm^{-1}) ν_{max} 691, 752, 1443, 1500, 1537, 1598, 1644, 2850, 2921, 3296, 3059; m/z HRMS (ESI+) C$_{19}$H$_{15}$NNaO ([M+Na]$^+$) requires 296.1046; found 296.1044 (-0.6 ppm).

Labbook reference number: LAL4-297f2, Literature data[114]

Fraction 4: *N,N′*-Diphenylurea 207
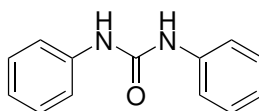
Selected data: 6.8 mg, 2.6%; R_f 0.27 (EtOAc/petrol, 3:7, *v/v*); δH (400 MHz, CDCl$_3$) 6.95-7.04 (2H, m), 7.24-7.31 (4H, m), 7.44 (4H, d, *J* = 7.6 Hz), 8.37 (2H, s); IR (thin film, cm^{-1}) ν_{max} 694, 752, 1231, 1321, 1349, 1444, 1498, 1546, 1598, 1641, 1712, 2853, 2925, 2958, 3062, 3136, 3287; m/z HRMS (ESI+) C$_{13}$H$_{12}$N$_2$NaO ([M+Na]$^+$) requires 235.0842; found 235.0840 (-0.8 ppm).

Labbook reference number: LAL4-297f4, Literature data[121]

Fraction 5: 2$'$-(6-Oxophenanthridin-5(6*H*)-yl)-*N*-phenyl[1,1$'$-biphenyl]-2-carboxamide 208
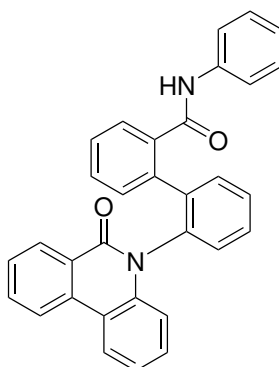
Selected data: 23.1 mg, 11.9 % based on 3 eq. starting amide; R_f 0.17 (EtOAc/petrol, 3:7, *v/v*); δH (400 MHz, CDCl$_3$) 6.62-6.68 (1H, m), 6.95 (1H, app. td, *J* = 1.1, 7.3 Hz), 7.10 (1H, d, *J* = 7.9 Hz), 7.13-7.19 (2H, m), 7.22-7.28 (3H, m), 7.30-7.39 (6H, m), 7.48-7.54 (1H, m), 7.54-7.60 (2H, m), 7.74 (1H, app. t, *J* = 7.3 Hz), 8.31-8.35 (1H, m), 8.37(1H, d, *J* = 8.2 Hz), 8.93 (1H, s), 9.13 (1H, s); δC (100 MHz, CDCl$_3$) 117.2, 119.3, 119.5, 122.2, 123.2, 123.3, 123.7, 123.8, 127.2, 127.5, 128.8, 128.8, 129.2, 129.3, 129.5, 129.6, 130.4, 130.5, 132.1, 132.3, 135.6, 135.7, 138.2, 138.5, 139.1, 141.3, 143.3, 162.7, 168.5; IR (thin film, cm^{-1}) ν_{max} 513, 694, 753, 908, 1256, 1321, 1443, 1491, 1543, 1600, 1638, 2854, 2927, 2962, 3062, 3131, 3190, 3254; m/z HRMS (ESI+) C$_{32}$H$_{23}$N$_2$O$_2$ ([M+H]$^+$) requires 467.1754; found 467.1756 (-0.3 ppm), C$_{32}$H$_{22}$N$_2$NaO$_2$ ([M+Na]$^+$) requires 489.1573; found 489.1570 (+0.5 ppm).

Labbook reference number: LAL4-297f5, Novel compound

Fraction 6: *N2,N2′*-Diphenyl[1,1′-biphenyl]-2,2′-dicarboxamide 201
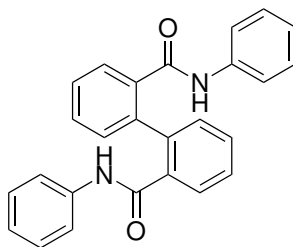
Selected data: 31.2 mg, 12.7%; R_f 0.16 (EtOAc/petrol, 3:7, *v/v*); δH (400 MHz, CDCl$_3$) 7.05 (2H, t, *J* = 7.6 Hz), 7.09-7.15 (2H, m) 7.23 (4H, app. t, *J* = 7.5 Hz), 7.27-7.40 (4H, m), 7.42 (4H, d, *J* = 8.5 Hz), 7.61-7.67 (2H, m), 9.22 (2H, s); δC (100 MHz, CDCl$_3$) 120.1, 124.5, 127.4, 128.1, 129.0, 129.8, 130.2, 136.2, 138.1, 139.2, 168.5; IR (thin film, cm^{-1}) ν_{max} 692, 754, 895, 1256, 1329, 1442, 1499, 1545, 1600, 1646, 2977, 3039, 3061, 3131, 3192, 3245, 3269; m/z HRMS (ESI+) C$_{26}$H$_{21}$N$_2$O$_2$ ([M+H]$^+$) requires 393.1598; found 393.1594 (+1.1 ppm), C$_{26}$H$_{20}$N$_2$NaO$_2$ ([M+Na]$^+$) requires 415.1417; found 415.1409 (+2.4 ppm).

An X-ray diffraction crystal structure of this compound was obtained. See Appendix A.

*Labbook reference number*: LAL4-297f6, Literature data[110]

Fraction 7: 6-Oxo-*N*,5-diphenyl-5,6-dihydrophenanthridine-1-carboxamide 210
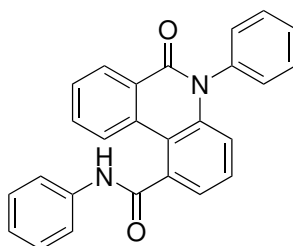
Selected data: 1.6 mg, 0.7%; R_f 0.09 (EtOAc/petrol, 3:7, *v/v*); δH (400 MHz, CDCl$_3$) 6.53 (1H, d, *J* = 8.0 Hz), 6.61 (1H, d, *J* = 8.5 Hz), 6.84 (1H, t, *J* = 7.6 Hz), 6.91 (1H, t, *J* = 6.9 Hz), 6.96-7.05 (1H, m), 7.08 (1H, d, *J* = 7.8 Hz), 7.13 (1H, app. t, *J* = 7.5 Hz), 7.15-7.25 (2H, m, 8.0 Hz), 7.35-7.45 (3H, m), 7.64 (2H, app. t, *J* = 8.6 Hz), 7.68 (1H, d, *J* = 7.7 Hz), 7.78 (1H, app. t, *J* = 7.5 Hz), 8.38 (1H, d, *J* = 8.4 Hz), 9.27 (1H, s); δC (100 MHz, CDCl$_3$) 116.4, 118.6, 120.1, 120.2, 123.4, 123.8, 123.9, 125.3, 126.0, 127.1, 127.1, 128.0, 128.2,

128.4, 128.6, 128.9, 129.1, 129.3, 129.5, 130.1, 130.3, 130.4, 130.5, 131.1, 132.2, 133.6, 134.3, 135.5, 136.9, 137.3, 137.4, 137.8, 137.8, 138.6, 139.5, 142.3, 144.6, 161.6, 169.2; IR (thin film, cm^{-1}) ν_{max} 693, 752, 908, 1258, 1322, 1442, 1498, 1545, 1599, 1641, 2934, 2964, 3062, 3135, 3251; m/z HRMS (ESI+) $C_{26}H_{18}N_2NaO_2$ ([M+Na]$^+$) requires 413.1260; found 413.1237 (-5.7 ppm).

Labbook reference number: LAL4-297f8, Novel compound

2-Bromo-*N*-(pentadeuterophenyl)benzamide 163-d$_5$
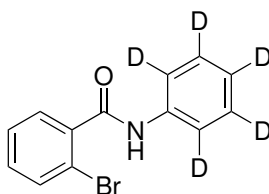
Oxalyl chloride (0.38 mL, 3 mmol) was added to a solution of 2-bromobenzoic acid (0.6 g, 3 mmol) and *N,N*-dimethylformamide (1 drop, ca. 10 μL) in CH_2Cl_2 (5 mL) at 0 °C. The solution was stirred for 30 minutes at rt and concentrated *in vacuo* to provide the 2-bromobenzoyl chloride intermediate. The 2-bromobenzoyl chloride (3 mmol) was added dropwise to a stirred solution of d$_5$-aniline (0.29 mL, 3 mmol) and Et$_3$N (0.42 mL, 3 mmol) at 0 °C and the reaction stirred at room temperature for 2 hours. Water (2 mL) was added and the product was extracted with DCM (20 mL) and washed with water (20 mL) and brine (20 mL). The organic layer was dried over MgSO$_4$ and the solvent removed *in vacuo*. The crude product was recrystallised from DCM and hexane to give the title compound as a white solid (0.6 g, 72%); mp 118-120 °C; δH (400 MHz, CDCl$_3$); 7.32 (1H, app. td, *J*=7.8, 1.8 Hz), 7.40 (1H, app. td, *J*=7.5, 1.2 Hz), 7.61-7.65 (2H, m), 7.73 (1H, s); δC (100 MHz, CDCl$_3$) 119.4, 127.9, 129.9, 131.8, 133.7, 137.9, 165.6; IR (ATR, cm^{-1}) ν_{max} 447, 555, 690, 889, 1025, 1261, 1315, 1332, 1385, 1467, 1590, 1639, 3088, 3160, 3260; m/z HRMS (ESI+) $C_{13}H_6BrD_5NO$ ([M+H]$^+$) requires 281.1332; found 281.0320 (+4.1 ppm), $C_{13}H_5BrD_5NNaO$ ([M+Na]$^+$) requires 303.0152; found 303.0140 (+4.1 ppm).

Labbook reference number: RC1-33 *(Reaction was conducted by R. Campbell)*, Novel compound

5-(Pentadeuterophenyl)phenanthridin-6(5H)-one 164-d$_5$
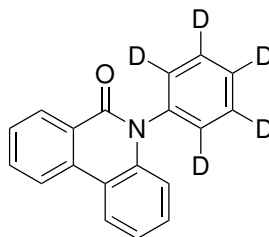
Pd$_3$(OAc)$_6$ (7 mg, 0.031 mmol, 5 mol%), dppe (12.5 mg, 0.031 mmol, 5 mol%) and K$_2$CO$_3$ (173 mg, 1.25 mmol, 2 eq) were placed in a schlenk tube under nitrogen. DMF (7.5 mL) was added and the mixture was stirred at 130 °C for 2 minutes. 2-bromo-N-d$_5$-phenylbenzamide (173 mg, 0.63 mmol) was added directly to the reaction mixture. The reaction mixture was stirred at 130 °C for 2 hours after which it was cooled and diluted with ethyl acetate (20 mL). The reaction mixture was filtered through Celite and washed with 1M HCl (20 mL) and brine (20 mL) before the organic layer was dried over MgSO$_4$, filtered and the solvent removed *in vacuo*. The crude product was purified by column chromatography (10-22.5% ethyl acetate in petroleum ether) to give the title compound as a white solid (52.0 mg, 61%); R_f 0.33 (EtOAc/petrol, 3:7, *v/v*); δH (400 MHz, CDCl$_3$) 6.68-6.73 (1H, m) 7.30 (2H, AA′XX′ system, J_{AX}= 7.6 Hz, $J_{AX'}$= 5.2 Hz, $J_{XX'}$= 2.4 Hz, $J_{AA'}$= 11.1 Hz), 7.62 (1H, ddd, J=8.0, 7.4, 1.0 Hz), 7.82 (1H, ddd, J=8.1, 7.2, 1.4 Hz), 8.28-8.33 (1H, m), 8.35 (1H, d, J=8.3 Hz), 8.58 (1H, dd, J=8.0, 1.4 Hz) δC (100 MHz, CDCl$_3$) 117.1, 119.1, 121.9, 122.8, 123.1, 126.0, 128.2, 129.1, 129.2, 132.9, 134.1, 138.3, 139.3, 161.8; IR (thin film, cm^{-1}) ν_{max} 549, 724, 747, 1267, 1316, 1331, 1391, 1435, 1486, 1588, 1608, 1655, 3072; m/z HRMS (ESI+) C$_{19}$H$_9$D$_5$NO ([M+H]$^+$) requires 277.1384; found 277.1377 (+2.4 ppm), C$_{19}$H$_8$D$_5$NNaO ([M+Na]$^+$) requires 299.1203; found 299.1196 (+2.2 ppm).

Labbook reference number: LAL4-315, Novel compound

Six fractions were obtained from the column of the 0.63 mmol reaction. Fraction 3 was the major component mentioned above.

Fraction 1: 4,5,6,7-Tetradeutero-8*H*-indolo[3,2,1-*de*]phenanthridin-8-one 196-d₄
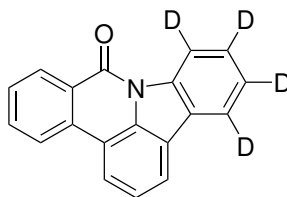
Data for this compound: 1.8 mg, 2%; R_f 0.46 (EtOAc/petrol, 3:7, *v/v*); δH (400 MHz, CDCl₃) 7.63 (1H, app. t, *J*= 7.8 Hz), 7.69 (1H, ddd, *J*=8.1, 7.0, 1.2 Hz), 7.86 (1H, app. td, *J*=7.6, 1.4 Hz), 8.13 (1H, d, *J*=7.6 Hz), 8.23 (1H, d, *J*=7.8 Hz), 8.37 (1H, d, *J*=7.8 Hz), 8.72 (1H, dd, *J*=8.1, 1.4 Hz); IR (thin film, cm^{-1}) ν_{max} 769, 1265, 1305, 1384, 1461, 1667, 1739, 2854, 2923, 2958; m/z HRMS (ESI+) $C_{19}H_7D_4NNaO$ ([M+Na]$^+$) requires 296.0984; found 296.0990 (-1.4 ppm).

Labbook reference number: LAL4-315f2, Novel compound

Fraction 2: *N*-(Pentadeuterophenyl)-[1,1′-biphenyl]-2-carboxamide 204-d₅
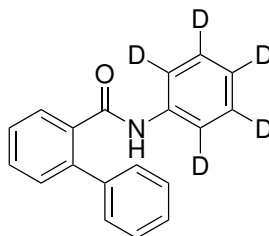
Selected data: 4.5 mg, 2.6% based on 1 eq. starting amide; R_f 0.41 (EtOAc/petrol, 3:7, *v/v*); δH (400 MHz, CDCl₃) 7.39-7.45 (3H, m), 7.45-7.51 (3H, m), 7.53-7.58 (1H, m), 7.86-7.92 (2H, m); IR (thin film, cm^{-1}) ν_{max} 446, 553, 700, 746, 1075, 1308, 1333, 1388, 1513, 1567, 1584, 1651, 1736, 2851, 2924, 3297; m/z HRMS (ESI+) $C_{19}H_{11}D_5NO$ ([M+H]$^+$) requires 279.1540; found 279.1535 (+1.8 ppm), $C_{19}H_{10}D_5NNaO$ ([M+Na]$^+$) requires 301.1360; found 301.1354 (+1.8 ppm).

Labbook reference number: LAL4-315f3, Novel compound

Fraction 4: *N*,*N*′-Bis(pentadeuterophenyl)urea 207-d$_{10}$
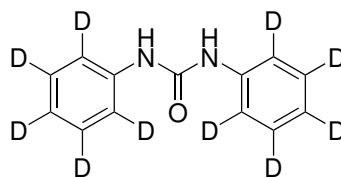
Selected data: 6.3 mg, 4.5%; R_f 0.25 (EtOAc/petrol, 3:7, *v/v*); IR (thin film, cm^{-1}) ν_{max} 461, 550, 622, 725, 749, 1315, 1390, 1435, 1589, 1608, 1657, 2926, 3074, 3279; m/z HRMS (ESI+) C$_{13}$H$_2$D$_{10}$N$_2$NaO ([M+Na]$^+$) requires 245.1475; found 245.1477 (+0.8 ppm).

Labbook reference number: LAL4-315f5, Novel compound

Fraction 5: 2′,3′,4′,5′-Tetradeutero-*N*-(pentadeuterophenyl)-6′-(6-oxophenanthridin-5 (6*H*)-yl)[1,1′-biphenyl]-2-carboxamide 208-d$_{10}$
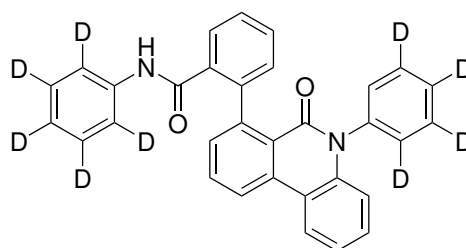
Selected data: 7.5 mg, 7.6 %; R_f 0.19 (EtOAc/petrol, 3:7, *v/v*); δH (400 MHz, CDCl$_3$) 6.62-6.67 (1H, m), 7.03-7.08 (1H, m), 7.18-7.22 (1H, m), 7.33 (2H, dd, *J* = 3.3, 6.2 Hz), 7.35-7.37 (1H, m), 7.37-7.39 (1H, m), 7.75 (1H, dd, *J* = 7.5, 8.2 Hz), 8.32-8.35 (1H, m), 8.37 (1H, dd, *J* = 1.0, 8.5 Hz), 8.92 (2H, m); δC (100 MHz, CDCl$_3$) 117.2, 119.3, 122.2, 123.2, 123.3, 123.7, 127.2, 127.5, 128.8, 129.5, 129.6, 132.1, 132.3, 135.6, 135.8, 136.3, 139.1, 139.2, 141.3, 143.4, 162.8, 168.5; IR (thin film, cm^{-1}) ν_{max} 447, 552, 755, 821, 1191, 1269, 1312, 1389, 1516, 1567, 1593, 1637, 2926, 2967, 3080, 3279; m/z HRMS (ESI+) C$_{32}$H$_{13}$D$_{10}$N$_2$O$_2$ ([M+H]$^+$) requires 477.2387; found 477.2396 (+1.9 ppm), C$_{32}$H$_{12}$D$_{10}$N$_2$NaO$_2$ ([M+Na]$^+$) requires 499.2207; found 499.2215 (+1.6 ppm).

Labbook reference number: LAL4-315f6, Novel compound

Fraction 6: $N^2,N^{2'}$-Bis-(pentradeuterophenyl)[1,1′-biphenyl]-2,2′-dicarboxamide 201-d$_{10}$
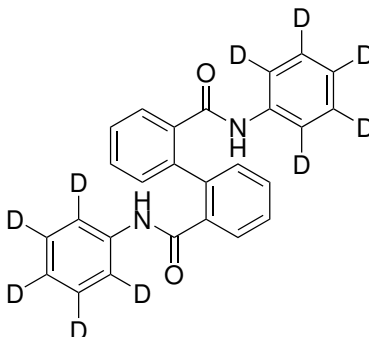
Selected data: 15.8 mg, 12.6%; R_f 0.14 (EtOAc/petrol, 3:7, *v/v*); δH (400 MHz, CDCl$_3$) 7.09-7.15 (2H, m) 7.27-7.40 (4H, m), 7.61-7.67 (2H, m), 9.14 (2H, s); δC (100 MHz, CDCl$_3$) 127.4, 128.2, 129.8, 130.3, 136.2, 138.0, 139.2, 168.5; IR (thin film, cm^{-1}) ν_{max} 446, 553, 757, 1275, 1314, 1335, 1389, 1518, 1566, 1590, 1647, 3080, 3267; m/z HRMS (ESI+) C$_{26}$H$_{11}$D$_{10}$N$_2$NaO$_2$ ([M+H]$^+$) requires 403.2225; found 403.2225 (+0.5 ppm), C$_{26}$H$_{10}$D$_{10}$N$_2$NaO$_2$ ([M+Na]$^+$) requires 425.2045; found 425.2041 (+1.2 ppm).

Labbook reference number: LAL4-315f7, Novel compound

2-Bromo-4-methyl-*N*-phenylbenzamide 189
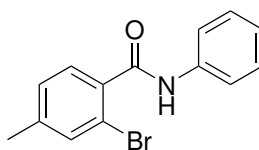
Oxalyl chloride (78 μL, 0.92 mmol) was added to a solution of 2-bromo-4-methylbenzoic acid (200 mg, 0.92 mmol) and *N,N*-dimethylformamide (1 drop, ca. 10 μL) in CH$_2$Cl$_2$ (5 mL) at 0 °C. The solution was stirred for 2 hours at rt and concentrated *in vacuo* to provide the 2-bromo-4-methylbenzoyl chloride intermediate. The 2-bromo-4-methylbenzoyl chloride (0.92 mmol) was added dropwise to a stirred solution of aniline (84 μL, 0.92 mmol) and Et$_3$N (128 μL, 93.2 mg, 0.92 mmol) at 0 °C and the reaction stirred at room temperature for 2 hours. Water (2 mL) was added and the product was extracted with DCM (10 mL) and

washed with water (10 mL) and brine (10 mL). The organic layer was dried over MgSO$_4$ and the solvent removed *in vacuo*. The crude product was recrystallised from DCM and hexane to give the title compound as a white solid (203 mg, 76%); mp 145-146 °C; δH (400 MHz, CDCl$_3$) 2.36 (3H, s), 7.12-7.20 (2H, m), 7.36 (2H, app. t, *J*=7.8 Hz), 7.44 (1H, s) 7.50-7.54 (1H, m), 7.63 (2H, d, *J*=7.9 Hz), 7.86 (1H, br s); δC (100 MHz, CDCl$_3$) 21.1, 119.2, 120.1, 124.8, 128.6, 129.2, 129.9, 134.0, 134.8, 137.8, 142.5, 165.7; IR (ATR, cm^{-1}) ν_{max} 420, 512, 586, 693, 755, 827, 926, 1039, 1143, 1259, 1281, 1327, 1442, 1490, 1541, 1596, 1645, 3238; m/z HRMS (ESI+) C$_{14}$H$_{13}$BrNO ([M+H]$^+$) requires 290.0175; found 290.0165 (+2.6 ppm), C$_{14}$H$_{12}$BrNNaO ([M+Na]$^+$) requires 311.9994; found 311.9977 (+4.9 ppm); Anal. calcd. for C$_{14}$H$_{12}$BrNO C 57.95, H 4.17, N 4.83; found C 57.38, H 4.14, N 4.74.

Labbook reference number: LAL4-336, Novel compound

2,9-Dimethyl-5-phenylphenanthridin-6(5*H*)-one 190
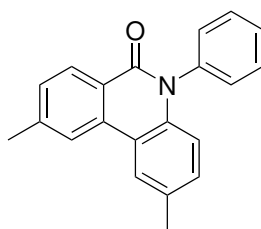
Pd$_3$(OAc)$_6$ (14 mg, 0.063 mmol, 5 mol%), dppe (25 mg, 0.063 mmol, 5 mol%) and K$_2$CO$_3$ (345 mg, 2.5 mmol, 2 eq) were placed in a schlenk tube under nitrogen. DMF (15 mL) was added and the mixture was stirred at 80 °C for 2 minutes. 2-bromo-4-methyl-*N*-phenyl benzamide (363 mg, 1.25 mmol) was added directly to the reaction mixture. The reaction mixture was stirred at 80 °C for 2 hours after which it was cooled and diluted with ethyl acetate (40 mL). The reaction mixture was filtered through Celite and washed with 2M HCl (20 mL) and brine (20 mL) before the organic layer was dried over MgSO$_4$, filtered and the solvent removed *in vacuo*. The crude product was purified by column chromatography (10-30% ethyl acetate in petroleum ether) to give the title compound as a white solid (79.9 mg, 43%); R_f 0.47 (EtOAc/petrol, 1:4, *v/v*); mp 170-171 °C; δH (500 MHz, CDCl$_3$) 2.46 (3H, s), 2.60 (3H, s), 6.58 (1H, d, *J*=8.5 Hz), 7.10 (1H, ddd, *J*= 8.6, 1.9, 0.6 Hz), 7.32 (2H, AA$'$XX$'$ system, J_{AX}= 7.8 Hz, $J_{AX'}$= 0.6 Hz, $J_{XX'}$= 0 Hz, $J_{AA'}$= 4.5 Hz), 7.42 (1H, ddd, *J*=8.1, 1.6,

0.6 Hz), 7.52 (1H, ddt, J=8.3, 6.8, 1.3 Hz), 7.58-7.62 (2H, m), 8.09 (1H, d, J=1.3 Hz), 8.12 (1H, d, J=0.6 Hz), 8.44 (1H, d, J=8.2 Hz); δC (100 MHz, CDCl$_3$) 21.1, 22.3, 117.0, 118.9, 121.9, 123.1, 123.8, 128.7, 129.1, 129.2, 130.1, 130.2, 132.0, 134.0, 137.4, 137.4, 138.6, 143.3, 161.7; IR (thin film, cm^{-1}) ν_{max} 694, 732, 1308, 1339, 1453, 1492, 1508, 1582, 1616, 1651, 2241, 2920, 3061; m/z HRMS (ESI+) C$_{21}$H$_{18}$NO ([M+H]$^+$) requires 300.1383; found 300.1379 (+0.7 ppm), C$_{21}$H$_{17}$NNaO ([M+Na]$^+$) requires 322.1202; found 322.1198 (+0.9 ppm); Anal. calcd. for C$_{21}$H$_{17}$NO C 84.25, H 5.72, N 4.68; found C 84.13, H 5.80, N 4.69.

An X-ray diffraction crystal structure of this compound was obtained. See Appendix A.

Labbook reference number: LAL4-349, Novel compound

Novel compound **197**, 2,12-dimethyl-9*H*-indolo[3,2,1-*de*]phenanthridin-9-one, was also isolated

from this reaction in 2.3 mg, 1.2% yield:
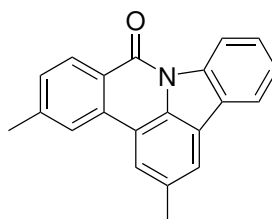
Analytical data: R_f 0.67 (EtOAc/petrol, 1:4, *v/v*); δH (400 MHz, CDCl$_3$) 2.61 (3H, s), 2.68 (3H, s), 7.48 (2H, app. t, J=7.6 Hz), 7.60 (1H, app. t, J=7.8 Hz), 7.91 (1H, s), 8.01 (1H, s), 8.05 (1H, d, J=7.7 Hz), 8.12 (1H, s), 8.57 (1H, d, J=8.1 Hz), 8.82 (1H, d, J=8.1 Hz); IR (thin film, cm^{-1}) ν_{max} 754, 782, 1133, 1351, 1617, 1678, 2854, 2924, 2961; m/z HRMS (ESI+) C$_{21}$H$_{15}$NNaO ([M+Na]$^+$) requires 320.1046; found 230.1032 (+3.8 ppm).

Addition of dienone for trapping of possible benzyne intermediate

Following general procedure 7, 1,2,3,4-tetraphenylcyclopentadienone (96.1 mg, 0.25 mmol) was added to the reaction containing 2-bromo-*N*-phenylbenzamide (138 mg, 0.5 mmol), Pd$_3$(OAc)$_6$ (5.6 mg, 0.025 mmol), dppp (10.4 mg, 0.025 mmol) and K$_2$CO$_3$ (138 mg, 1 mmol). The reaction was heated for 3 hours at 130 °C and the crude reaction mixture was analysed by NMR and MS. NMR analysis showed peaks corresponding to the dienone at

δH 6.90-6.94 (4H, m), 7.14-7.19 (4H, m) and 7.21-7.23 (12H, m). MS analysis showed peaks at 272 m/z (MH$^+$ for product) and 384 m/z (MH$^+$ for dienone) but no peak at 423 m/z for the naphthyl compound.

Labbook reference number: LAL4-356, Literature data[149,150]

Addition of phenylisocyanate for trapping of aniline by-product

Following general procedure 7, phenylisocyanate (29.8 mg, 0.25 mmol) was added to the reaction containing 2-bromo-*N*-phenylbenzamide (138 mg, 0.5 mmol), Pd$_3$(OAc)$_6$ (5.6 mg, 0.025 mmol), dppp (10.4 mg, 0.025 mmol) and K$_2$CO$_3$ (138 mg, 1 mmol). The reaction was heated for 2 hours at 130 $^\circ$C and the crude reaction mixture was analysed by NMR and MS. m/z HRMS (ESI+) C$_{13}$H$_{12}$N$_2$NaO ([M+Na]$^+$) requires 235.0842; found 235.0837 (+3.8 ppm).

Labbook reference number: LAL4-368

Following general procedure 7, phenylisocyanate (29.8 mg, 0.25 mmol) was added to the reaction containing Pd$_3$(OAc)$_6$ (5.6 mg, 0.025 mmol), dppp (10.4 mg, 0.025 mmol), 2-bromo-*N*-(pentadeuterophenyl)benzamide (140 mg, 0.5 mmol) and K$_2$CO$_3$ (138 mg, 1 mmol). The reaction was heated for 2 hours at 130 $^\circ$C and the crude reaction mixture was analysed by NMR and MS. m/z HRMS (ESI+) C$_{13}$H$_7$D$_5$N$_2$NaO ([M+Na]$^+$) requires 240.1156; found 240.1157 (-0.7 ppm), C$_{13}$H$_2$D$_{10}$N$_2$NaO ([M+Na]$^+$) requires 245.1471; found 245.1421 (-22.0 ppm).

Labbook reference number: LAL4-379

Monitoring of the synthesis of 5-phenylphenanthridin-6(5*H*)-one by mass spectrometry

Following general procedure 7, Pd$_3$(OAc)$_6$ (5.6 mg, 0.025 mmol, 5 mol%), dppp (10.4 mg, 0.025 mmol, 5 mol%) and K$_2$CO$_3$ (138 mg, 1 mmol, 2 eq) were placed in a schlenk tube under nitrogen. DMA (2.5 mL) was added and the mixture was stirred at 100 $^\circ$C for 2 minutes. 2-bromo-*N*-phenylbenzamide (138 mg, 0.5 mmol) was added and the reaction

mixture was stirred at 100 °C for 30 minutes. 0.1 mL aliquots were removed from the solution at 2, 5, 10 and 15 minutes after the substrate was added. The solvent was removed from these samples *in vacuo* and the sample dissolved in ethyl acetate (1 mL), filtered and analysed by ESI-MS. m/z HRMS (ESI+) $C_{13}H_{11}BrNO$ ([M+H]$^+$) requires 276.0019; found 276.0036 (+6.2 ppm), $C_{13}H_{10}BrNNaO$ ([M+Na]$^+$) requires 297.9838; found 297.9828 (-3.4 ppm), $C_{26}H_{20}Br^{81}Br_2N_2NaO_2$ ([M+Na]$^+$) requires 574.9769; found 574.9760 (-1.6 ppm), $C_{19}H_{13}NNaO$ ([M+Na]$^+$) requires 294.0889; found 294.0889 (0.0 ppm), $C_{32}H_{22}N_2NaO_2$ ([M+Na]$^+$) requires 489.1573; found 489.1551 (-4.5 ppm), $C_{26}H_{20}N_2NaO_2$ ([M+Na]$^+$) requires 415.1417; found 415.1418 (+0.2 ppm).

Labbook reference number: LAL4-321

Catalyst system analysis by solution state ^{31}P NMR spectroscopy

Dry, degassed DMF (1 mL) was added to $Pd_3(OAc)_6$ (10 mg, 0.04 mmol) and dppe (18 mg, 0.04 mmol) under nitrogen and stirred for 30 minutes. A 0.5 mL aliquot was removed from the solution and placed in a dry Youngs NMR tube under nitrogen. 0.2 mL dry acetone-d_6 was added and the mixture analysed by ^{31}P NMR; δP (162 MHz, $(CD_3)_2CO$) 30.0 (s), 30.1 (s), 59.1 (s).

Labbook reference number: RC1-18 *(Reaction was conducted by R. Campbell)*

Dry, degassed DMF (1 mL) was added to $Pd_2dba_3 \cdot CHCl_3$ (10 mg, 0.01 mmol) and dppe (8.7 mg, 0.02 mmol) under nitrogen and stirred for 30 minutes. A 0.5 mL aliquot was removed from the solution and placed in a dry Youngs NMR tube under nitrogen. 0.2 mL dry acetone-d_6 was added and the mixture analysed by ^{31}P NMR; δP (162 MHz, $(CD_3)_2CO$) 30.0 (s), 35.5 (br. s), 37.0 (br. s), 56.7 (s), 65.9 (s).

Labbook reference number: RC1-14 *(Reaction was conducted by R. Campbell)*

Dry, degassed DMF (1 mL) was added to $Pd_3(OAc)_6$ (10 mg, 0.04 mmol), dppe (18 mg, 0.04 mmol) and dibenzylideneacetone (10 mg, 0.04 mmol) under nitrogen and stirred for 30 minutes. A 0.5 mL aliquot was removed from the solution and placed in a dry Youngs NMR tube under nitrogen. 0.2 mL dry acetone-d_6 was added and the mixture analysed by ^{31}P NMR; δP (162 MHz, $(CD_3)_2CO$) 29.5 (s), 29.6 (s), 29.8 (s), 29.9 (s), 30.1 (s), 35.6 (br.

s), 37.1 (br. s), 59.1 (s).

Labbook reference number: RC1-20 *(Reaction was conducted by R. Campbell)*

Monitoring of the synthesis of 5-phenylphenanthridin-6(5*H*)-one by solution state ^{31}P NMR spectroscopic analysis

Degassed DMF-d$_7$ (0.5 mL) was added to Pd$_2$dba$_3 \cdot$ CHCl$_3$ (5.0 mg, 5.5 μmol) and dppe (4.3 mg, 0.011 mmol) under nitrogen in a Youngs NMR tube. The sample was analysed by ^{31}P NMR. 2-bromo-*N*-phenylbenzamide (3.0 mg, 0.011 mmol) was then added to the catalyst system under nitrogen and a ^{31}P NMR spectrum recorded. The reaction was then heated for 45 minutes and a ^{31}P NMR spectrum recorded before further heating for 16 hours and analysis by ^{31}P NMR.

Spectrum 1: δP (203 MHz, (CD$_3$)$_2$NCOD) 29.4 (s), 35.1 (d, *J* = 6.0 Hz), 36.6 (d, *J* = 6.1 Hz), 57.4 (s).

Spectrum 2: δP (203 MHz, (CD$_3$)$_2$NCOD) 29.4 (s), 35.1 (br. s), 36.6 (br. s), 57.4 (s).

Spectrum 3: δP (203 MHz, (CD$_3$)$_2$NCOD) 29.4 (s), 35.1 (br. s), 36.6 (br. s), 41.8 (d, *J* = 28 Hz), 56.8 (s), 59.1 (d, *J* = 28 Hz), 65.83 (s).

Spectrum 4: δP (203 MHz, (CD$_3$)$_2$NCOD) 41.8 (d, *J* = 28 Hz), 56.6 (s), 59.1 (d, *J* = 28 Hz), 65.83 (s).

Labbook reference number: LAL4-391

The reaction was repeated with a ^{31}P NMR spectrum taken after 45 minutes heating. The reaction was then opened to air and one drop of the solution was removed, diluted in MeCN and analysed by ESI-MS. Ten peaks showing Pd isotope patterns were detected, three of which have been identified; m/z HRMS (ESI+) C$_{39}$H$_{34}$NOP$_2$Pd ([M+H]$^+$) requires 700.1159; found 700.1130 (+4.6 ppm), C$_{52}$H$_{42}$N$_2$NaO$_2$P$_2$Pd ([M+Na]$^+$) requires 917.1667; found 917.1606 (+6.3 ppm), C$_{52}$H$_{48}$P$_4$Pd ([M]$^{2+}$) requires 451.0865; found 451.0852 (-2.9 ppm)

Labbook reference number: LAL4-393

Monitoring of the synthesis of 5-phenylphenanthridin-6(5H)-one by solid state ^{31}P NMR spectroscopic analysis

DMF-d$_7$ (50 μL) was added to Pd$_2$dba$_3 \cdot$ CHCl$_3$ (0.5 mg, 0.55 μmol), dppe (0.43 mg, 1.1 μmol), K$_2$CO$_3$ (3 mg, 0.011 mmol) and 2-bromo-N-phenylbenzamide (3.0 mg, 0.011 mmol) under air in a solid state NMR rotor. The sample was analysed by ^{1}H and ^{31}P MAS NMR with 3000 Hz spin rate every 30 minutes over a 6.5 hour time period during which it was heated to 55 °C. The rotor was then heated in a sand bath at 70 °C overnight and ^{1}H (400 MHz) and ^{31}P NMR (162 MHz) spectra recorded.

Labbook reference number: LAL4-392

Monitoring of the reaction by GC

K$_2$CO$_3$ (207 mg, 1.5 mmol) was added to dry, degassed DMF (6 mL) at 80 °C under nitrogen, followed by biphenyl as internal standard (117 mg, 0.75 mmol) and 2-bromo-N-phenylbenzamide (207 mg, 0.75 mmol) in DMF (1 mL). After the addition of each material, the solution was allowed to equilibrate for 5 minutes. A solution of Pd$_3$(OAc)$_6$ (8.4 mg, 0.0375 mmol) and dppe (15 mg, 0.0375 mmol) in DMF (1.5 mL) was added to the reaction and the flask rinsed with DMF (0.5 mL). The reaction was stirred at 80 °C for 180 minutes. 0.1 mL aliquots were removed from the reaction mixture at 0, 2, 5, 10, 15, 20, 30, 40, 50, 60, 80, 100, 120, 150 and 180 minutes. The aliquots were filtered through Celite with ethyl acetate (1 mL) and washed with 2M HCl (1 mL) and brine (1 mL) before being analysed by GC.

Labbook reference number: AP16-1

The reaction was repeated but with the pre-heating of the catalyst system (a solution of Pd$_3$(OAc)$_6$ (8.4 mg, 0.0375 mmol) and dppe (15 mg, 0.0375 mmol) in DMF (1.5 mL)) at 80 °C for 2 minutes. The catalyst solution turned from yellow to red.

Labbook reference number: AP16-2

Preparation of silica-supported palladium acetate catalyst

To a 0.05 M solution of $Pd_3(OAc)_6$ in MeCN was added the silica support (450 mg). The mixture was heated at 50 °C for 4 hours with stirring. The catalyst was then separated from the reaction mixture by filtration and washed with cold diethyl ether until the filtrate ran clear. The resulting solid was a yellow powder (480 mg, 6% increase by weight); δC (100 MHz, Solid) 11.5, 19.5, 37.8, 153.4, 184.3; IR (DRIFT, cm^{-1}) ν_{max} 593, 699, 802, 1109, 1428, 1530, 1692, 1869, 1972, 2255, 2385, 3267, 3622.

Labbook reference number: LAL3-289

7.3 Analytical Procedures, Preparation and Data for Heterogeneous Catalysts

Preparation of silica and alumina catalysts

Materials were heated in a furnace to 700 °C at 10 °C min^{-1} then held for 4 hours. The 4 samples were then cooled in air and transferred to vials. The silica S-300 was heated to 300 °C using the same method.

Solid-state NMR spectroscopic analysis

K60 silica; δSi (79.44 MHz, solid) -101.23, -110.96.

Activated K60 silica; δSi (79.44 MHz, solid) -109.78.

Used activated K60 silica; δSi (79.44 MHz, solid) -109.54.

Thermal Gravimetric Analysis of Silica

50 mg of used activated silica was placed in a TGA cup and the balance set to zero. The sample was slowly heated to 300 °C and any change in mass was recorded. 1.13 mg water was lost from a 50 mg samples of K60 silica.

TG /%

Mass Change: -2.26 %

Temperature /°C
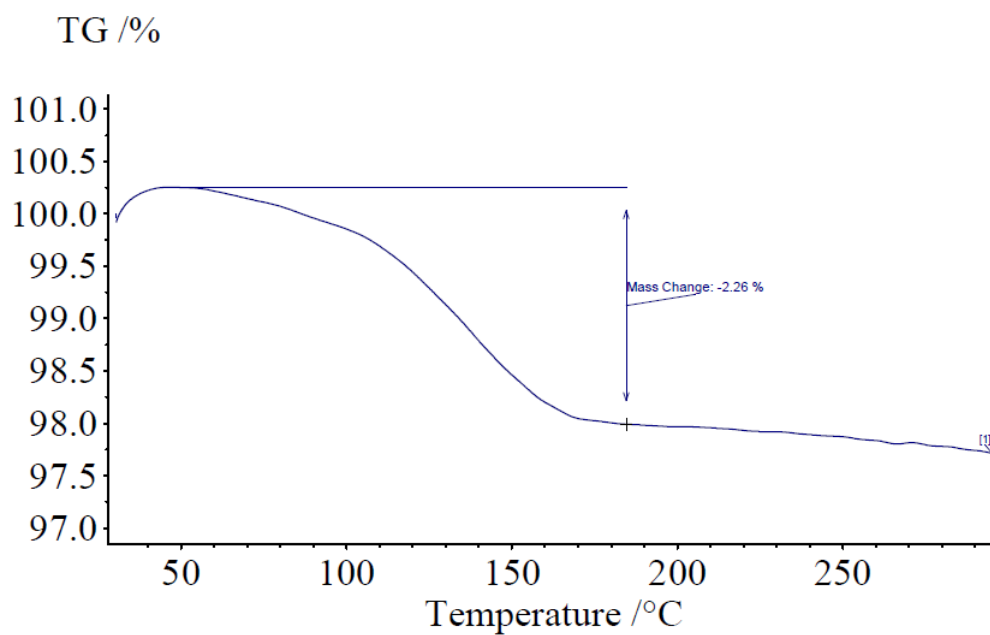
Figure 83: Thermal gravimetric analysis of activated silica after use showing the mass of water absorbed on the surface during the reaction

Inductively-coupled plasma analysis of alumina balls

Alumina Balls were crushed and analysed by ICP-MS. It was assumed that they contained no organic matter and so the amount of each metal was calculated as a percentage of the total metal. This does not take into account the oxygen bound within the sample.

The % of metals in a sample of alumina balls

Metal	ppm	%	Metal	ppm	%
Ag	<0.01		Mo	1.41	0.000
Al	278428	97.772	Na	4199.75	1.475
As	5.67	0.002	Ni	0.28	0.000
Au	<0.01		P	95.18	0.033
B	<0.01		Pb	<0.01	
Ba	2.58	0.001	Pd	0.02	0.000
Be	0.16	0.000	Pt	<0.01	
Bi	1.09	0.000	Rb	6.64	0.002
Ca	407.2	0.143	S	563	0.198
Cd	<0.01		Sb	<0.01	
Zr	2.5	0.001	Sc	0.09	0.000
Co	0.62	0.000	Se	<0.01	
Cr	1.1	0.000	Si	325.85	0.114
Cu	13.92	0.005	Sn	1.46	0.001
Fe	309.41	0.109	Sr	4.97	0.002
Hg	<0.01		Zn	47.75	0.017
K	170.44	0.060	Te	<0.01	
La	1.33	0.000	Ti	17.58	0.006
Li	<0.01		Tl	5.83	0.002
Mg	141.85	0.050	V	1.29	0.000
Mn	7.87	0.003	W	8.35	0.003

Porosimetry

Porosimetry analysis of K60 Silica

Approximately 50 mg was accurately weighed into a clean, dry porosimetry tube to which was then added a filler rod. The mass of the glassware and sample were recorded and the sample was degassed. The tube was evacuated with a vacuum setpoint of 10 mmHg at a temperature of 350 °C (with a ramp rate of 10 °Cmin^{-1}) for 480 minutes. The mass was remeasured for use in the analysis. The analysis gas used was nitrogen and the analysis temperature was 77 K. Measurements were taken every 120 minutes with an equilibration time of 10 s at P/P$_0$ = 1.000 and 600 s at P/P$_0$ = ≤0.995. The following conditions were used for analysis:

Surface area	5 point
t-plot micropore	5 point
BJH adsorption	20 point
BJH desorption	20 point

Parameters calculated included BET surface area; t-Plot micropore volume;, BJH adsoption and desorption cumulative volume of pores between 8.500 Å and 1500 Å; BJH adsorption and desorption average pore radius, and the average particle size.

DRIFTS of silica and alumina samples tested as catalysts

Spectra were measured at rt, 50 °C 100 °C and 150 °C. Spectra changed very little between temperatures so 150 °C is reported below.

K60 silica

v_{max} 565, 807, 1084 (R$_3$SiOSiR$_3$), 1634, 1866, 2357 (R$_3$SiH), 3745 (Free Si-OH).

Hi-sil

v_{max} 558, 809, 1111 (R$_3$SiOSiR$_3$), 1635, 1867, 3746 (Free Si-OH)

Gasil

ν_{max} 562, 806, 1095 ($R_3SiOSiR_3$), 1630, 1874, 3745 (Free Si-OH)

Cabosil

ν_{max} 561, 813, 1100 ($R_3SiOSiR_3$), 1630, 1856, 3743 (Free Si-OH)

Aerosil

ν_{max} 549, 808, 1107 ($R_3SiOSiR_3$), 3747 (Free Si-OH)

Crushed Alumina Balls

ν_{max} 610, 1060, 1571, 3455

Neutral Alumina

ν_{max} 1538, 3500

Silica loaded with acid samples for reaction with ammonia gas

K60 silica activated at 700 $^{\circ}$C (0.5 g) was stirred with acetic acid (2 cm^3) in toluene (15 cm^3) at reflux for 3 hours. The solvent was removed *in vacuo* and the sample analysed by DRIFTS. Treatment with ammonia was carried out as follows. Ammonia gas in nitrogen was prepared by bubbling at a rate of 1 in 10 into the environmental chamber of the DRIFTS. This mixture was flowed over the sample for 2 minutes followed by 1 minute of flushing with nitrogen before a spectrum was taken. Spectra were taken at room temperature under nitrogen unless otherwise indicated. Treatment with nitrogen was carried out as follows. Nitrogen gas was flushed through the environmental chamber and spectra were recorded at 0 minutes (before any nitrogen was added), 5, 10 and 15 minutes.

K60 silica activated at 700 $^{\circ}$C (1.5 g) was stirred with phenylacetic acid (3 g) in toluene (20 cm^3) at reflux for 3 hours. The silica was filtered off, washed with ethyl acetate 50 cm^3) and dried in air before the sample was analysed by DRIFTS. Treatment with nitrogen was carried out as follows. Nitrogen gas was flushed through the environmental chamber and spectra were recorded at room temperature (rt), 50 $^{\circ}$C 75 $^{\circ}$C and 100 $^{\circ}$C.

Appendix A

XRD Data
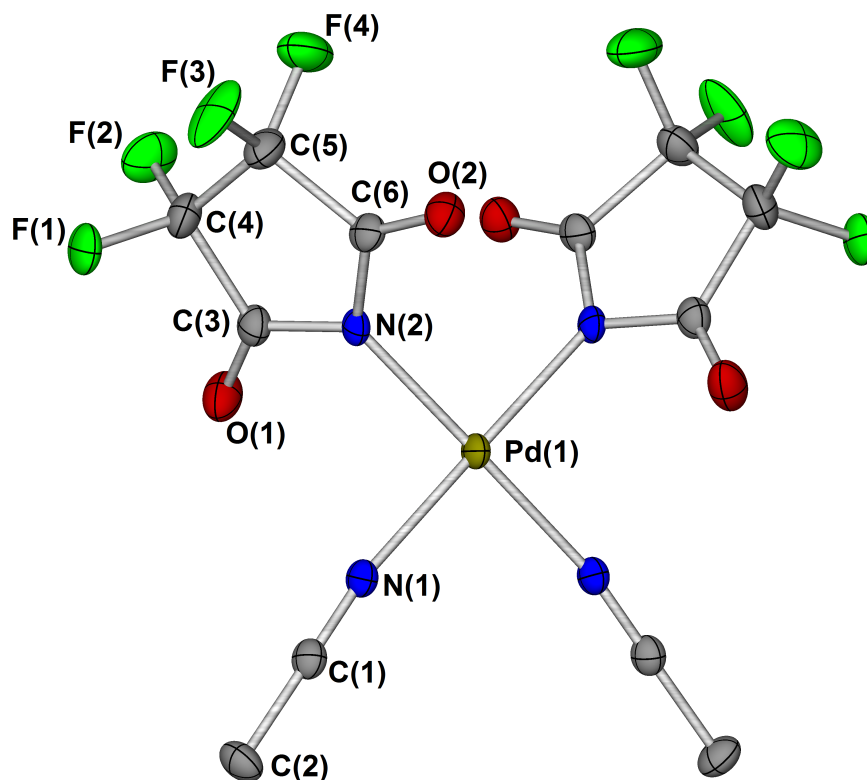
Figure 84: Single crystal X-ray diffraction structure of Pd(tfs)$_2$(MeCN)$_2$ **160**. Hydrogen atoms removed for clarity. Thermal ellipsoids shown with probability of 50%. The fluorines exhibited disorder and each was modelled with refined occupancies of 0.78:0.22(4). Selected bond lengths (Å): Pd(1)–N(1): 1.9826(14), Pd(1)–N(2): 1.9929(15). Selected bond angles (°): N(1)–Pd(1)–N(1): 88.23(8), N(1)–Pd(1)–N(2): 92.03(6), N(2)–Pd(1)–N(2): 87.93(8).

Table 37: Crystal data and structure refinement for ijsf1428 (compound **160**).

|	
Identification code	ijsf1428
Empirical formula	$C_{12}H_6F_8N_4O_4Pd$
Formula weight	528.61
Temperature/K	110
Crystal system	monoclinic
Space group	$C2/_c$
a/Å	14.6616(4)
b/Å	13.1340(4)
c/Å	8.8209(3)
$\alpha/°$	90
$\beta/°$	96.566(3)
$\gamma/°$	90
Volume/Å^3	1687.46(8)
Z	4
ρ_{calc}mg/mm^3	2.081
m/mm^{-1}	1.214
F(000)	1024.0
Crystal size/mm^3	0.1692 x 0.1347 x 0.0344
Radiation	MoKα (λ = 0.71073)
2Θ range for data collection	6 to 63.898°
Index ranges	-21 ≤ h ≤ 21, -15 ≤ k ≤ 18, -9 ≤ l ≤ 13
Reflections collected	4980
Independent reflections	2634 [R_{int} = 0.0380, R_{sigma} = 0.0528]
Data/restraints/parameters	2634/4/146
Goodness-of-fit on F^2	1.053
Final R indexes [I>=2σ (I)]	R_1 = 0.0369, wR_2 = 0.0869
Final R indexes [all data]	R_1 = 0.0431, wR_2 = 0.0934
Largest diff. peak/hole / e Å^{-3}	0.99/-1.15
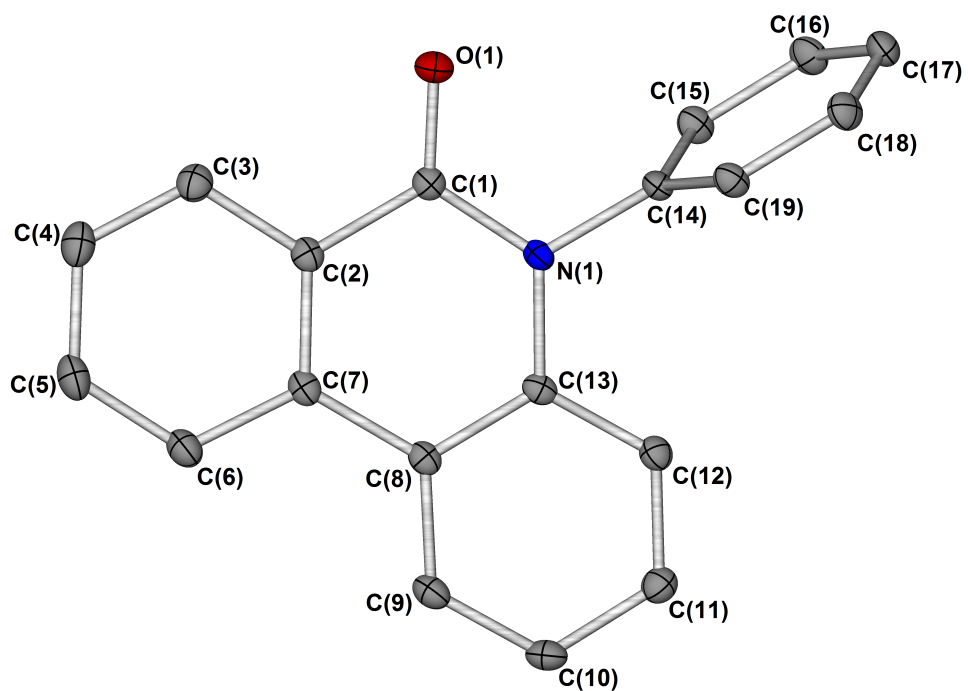
Figure 85: Single crystal X-ray diffraction structure of 5-phenylphenanthridin-6(5*H*)-one **164**. Hydrogen atoms removed for clarity. Thermal ellipsoids shown with probability of 50%.

Table 38: Crystal data and structure refinement for ijsf1415 (compound **164**).

Identification code	ijsf1415
Empirical formula	$C_{19}H_{13}NO$
Formula weight	271.30
Temperature/K	110.05(10)
Crystal system	monoclinic
Space group	$P2_{1/c}$
a/Å	5.4029(3)
b/Å	23.0685(11)
c/Å	10.6735(6)
$\alpha/°$	90
$\beta/°$	102.643(5)
$\gamma/°$	90
Volume/Å^3	1298.05(12)
Z	4
ρ_{calc}mg/mm^3	1.388
m/mm^{-1}	0.086
F(000)	568.0
Crystal size/mm^3	0.2809 x 0.2072 x 0.1389
Radiation	MoKα (λ = 0.7107)
2Θ range for data collection	6.58 to 60°
Index ranges	$-4 \leq h \leq 7$, $-14 \leq k \leq 32$, $-15 \leq l \leq 11$
Reflections collected	6611
Independent reflections	3781 [R_{int} = 0.0212, R_{sigma} = 0.0356]
Data/restraints/parameters	3781/0/190
Goodness-of-fit on F^2	1.057
Final R indexes [I>=2σ (I)]	R_1 = 0.0479, wR_2 = 0.1222
Final R indexes [all data]	R_1 = 0.0594, wR_2 = 0.1322
Largest diff. peak/hole / e Å^{-3}	0.34/-0.27
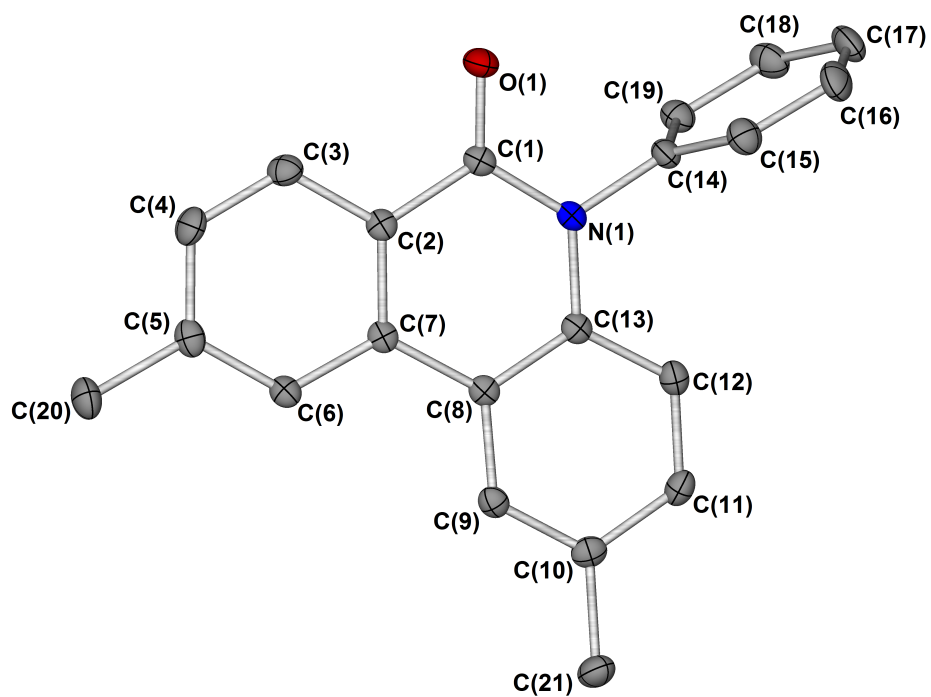
Figure 86: Single crystal X-ray diffraction structure of 2,9-dimethyl-5-phenylphenanthridin-6(5H)-one **190**. Hydrogen atoms removed for clarity. Thermal ellipsoids shown with probability of 50%.

**Table 39:** Crystal data and structure refinement for ijsf1521 (compound **190**).

Identification code	ijsf1521
Empirical formula	$C_{22}H_{18}Cl_3NO$
Formula weight	418.72
Temperature/K	109.9(2)
Crystal system	monoclinic
Space group	$P2_{1/c}$
a/Å	12.15159(18)
b/Å	11.14359(18)
c/Å	14.5618(2)
$\alpha/°$	90
$\beta/°$	92.0114(14)
$\gamma/°$	90
Volume/Å^3	1970.64(5)
Z	4
ρ_{calc}mg/mm^3	1.411
μ/mm^{-1}	4.300
F(000)	864.0
Crystal size/mm^3	0.192 x 0.139 x 0.12
Radiation	CuKα (λ = 1.54184)
2Θ range for data collection	9.998 to 134.156°
Index ranges	$-14 \leq h \leq 11$, $-11 \leq k \leq 13$, $-10 \leq l \leq 17$
Reflections collected	7076
Independent reflections	3519 [R_{int} = 0.0189, R_{sigma} = 0.0240]
Data/restraints/parameters	3519/0/246
Goodness-of-fit on F^2	1.060
Final R indexes [I>=2σ (I)]	R_1 = 0.0359, wR_2 = 0.0884
Final R indexes [all data]	R_1 = 0.0393, wR_2 = 0.0911
Largest diff. peak/hole / e Å^{-3}	0.51/-0.69
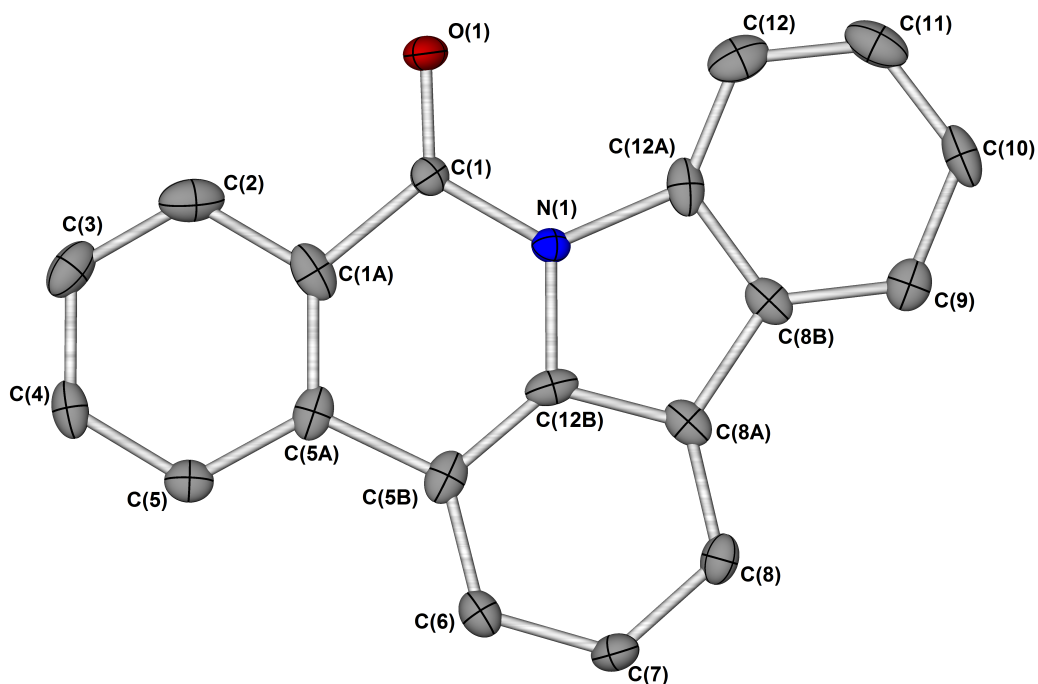
Figure 87: Single crystal X-ray diffraction structure of the phenanthridinone-based side product, 8*H*-indolo[3,2,1-*de*]phenanthridin-8-one **196**. Hydrogen atoms removed for clarity. Thermal ellipsoids shown with probability of 50%. The molecule can adopt two different orientations and this has been modelled by placing the amide in two positions with the refine occupancy 0.708: 0.292(3).

Table 40: Crystal data and structure refinement for ijsf1507 (compound **196**).

Identification code	ijsf1507
Empirical formula	$C_{19}H_{11}NO$
Formula weight	269.29
Temperature/K	110.05(10)
Crystal system	orthorhombic
Space group	$P2_12_12_1$
a/Å	6.12041(14)
b/Å	13.4413(3)
c/Å	15.2868(4)
$\alpha/°$	90
$\beta/°$	90
$\gamma/°$	90
Volume/Å^3	1257.59(5)
Z	4
ρ_{calc}mg/mm^3	1.422
μ/mm^{-1}	0.697
F(000)	560.0
Crystal size/mm^3	0.2138 x 0.1642 x 0.1202
Radiation	CuKα (λ = 1.54184)
2Θ range for data collection	8.76 to 142.408°
Index ranges	$-6 \leq h \leq 7, -16 \leq k \leq 14, -18 \leq l \leq 18$
Reflections collected	8225
Independent reflections	2407 [R_{int} = 0.0302, R_{sigma} = 0.0249]
Data/restraints/parameters	2407/3/206
Goodness-of-fit on F^2	1.123
Final R indexes [I>=2σ (I)]	R_1 = 0.0342, wR_2 = 0.0845
Final R indexes [all data]	R_1 = 0.0349, wR_2 = 0.0851
Largest diff. peak/hole / e Å^{-3}	0.12/-0.24
Flack parameter	-0.45(17)
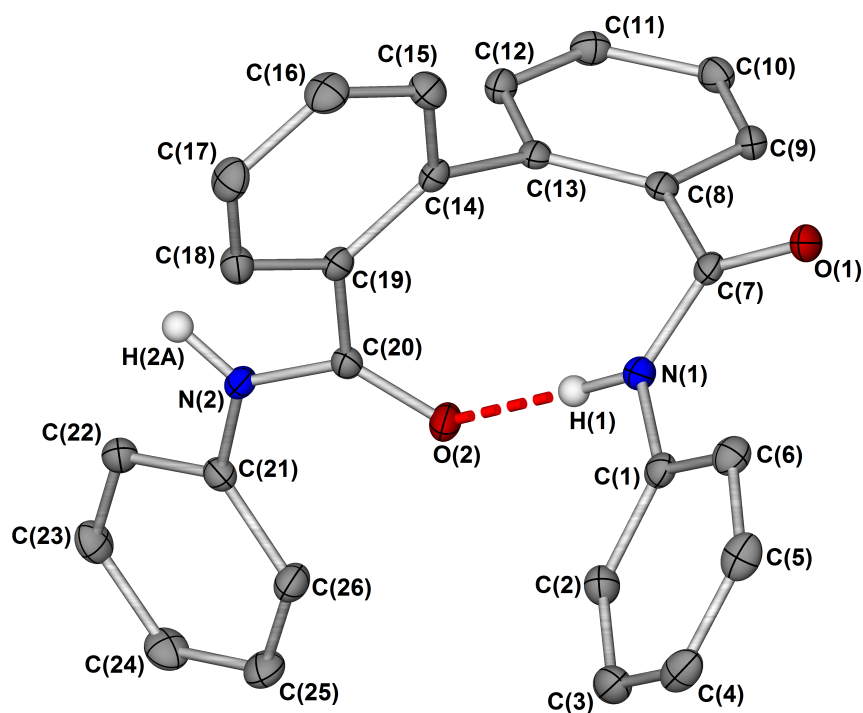
Figure 88: Single crystal X-ray diffraction structure of homocoupled starting material, *N*2,*N*2'-diphenyl[1,1'-biphenyl]-2,2'-dicarboxamide **201**. Hydrogen atoms removed for clarity. Thermal ellipsoids shown with probability of 50%.

Table 41: Crystal data and structure refinement for ijsf1607 (compound **201**).

Identification code	ijsf1607
Empirical formula	$C_{26}H_{20}N_2O_2$
Formula weight	392.44
Temperature/K	110.0(3)
Crystal system	tetragonal
Space group	$P4_32_12$
a/Å	10.71833(9)
b/Å	10.71833(9)
c/Å	35.3505(6)
$\alpha/°$	90
$\beta/°$	90
$\gamma/°$	90
Volume/Å^3	4061.16(10)
Z	8
ρ_{calc}mg/mm^3	1.284
μ/mm^{-1}	0.651
F(000)	1648.0
Crystal size/mm^3	0.288 x 0.274 x 0.091
Radiation	CuKα (λ = 1.54184)
2Θ range for data collection	8.62 to 142.29°
Index ranges	$-12 \leq h \leq 11, -12 \leq k \leq 12, -43 \leq l \leq 35$
Reflections collected	15290
Independent reflections	3845 [R_{int} = 0.0220, R_{sigma} = 0.0205]
Data/restraints/parameters	3845/0/279
Goodness-of-fit on F^2	1.048
Final R indexes [I>=2σ (I)]	R_1 = 0.0276, wR_2 = 0.0675
Final R indexes [all data]	R_1 = 0.0295, wR_2 = 0.0686
Largest diff. peak/hole / e Å^{-3}	0.13/-0.17
Flack parameter	-0.04(8)

Appendix B

SFC Calibration

Calculation of Conversion from Peak Areas

Where possible, an average of the peak areas of 3 injections was used.

To calculate the substrate concentration in SFC sample:

$$[substrate] = \frac{av.\ peak\ area(substrate)}{RF} \qquad \text{Eq. (5)}$$

To calculate the product concentration in SFC sample:

$$[product] = \frac{av.\ peak\ area(product)}{RF} \qquad \text{Eq. (6)}$$

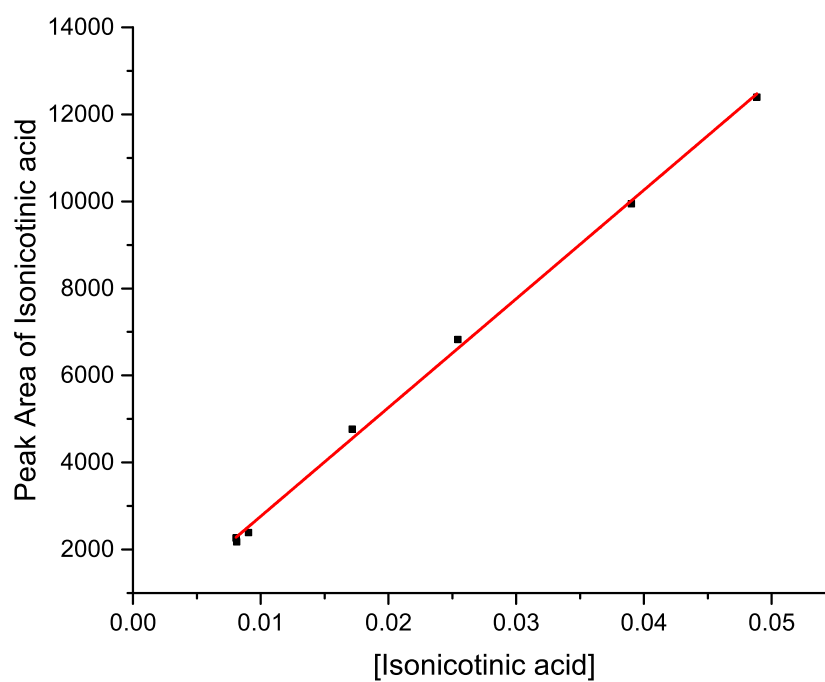To convert substrate concentration into conversion:

$$Conversion\ (\%) = \frac{[substrate]}{[substrate]\ +\ [product]} \times 100 \qquad \text{Eq. (7)}$$

Calibration of Isonicotinic Acid and Isoniazid

Five solutions were prepared with varying concentrations of both isonicotinic acid and isoniazid as shown in the table below. Peak areas were measured and plotted as a function of concentration. Two graphs were obtained based on the two compounds measured.

Table 42: Concentrations of calibration solutions for the SFC analysis of isoniazid synthesis

SM:Prod	Concentration of SM (mmol ml^{-1})	Concentration of Product (mmol ml^{-1})
6:1	0.049	0.008
3:1	0.025	0.008
1:1	0.008	0.008
1:3	0.008	0.022
1:6	0.009	0.044

Figure 89: Calibration curve for isonicotinic acid in the isoniazid analysis by SFC

Equation	y = a + b*x
Weight	No Weighting
Residual Sum of Squares	132000
Pearson's r	0.9993
Adj. R-Square	0.9984

	Value	Standard Error
Intercept	263.0	109.3
Slope	250000	4063
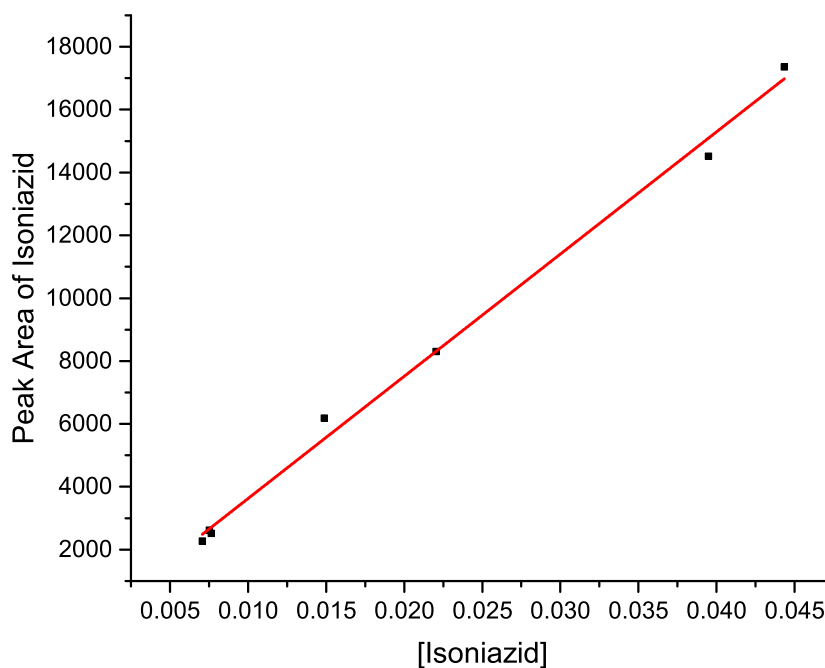
Figure 90: Calibration curve for isoniazid in the isoniazid analysis by SFC

Equation	y = a + b*x
Weight	No Weighting
Residual Sum of Squares	986600
Pearson's r	0.9978
Adj. R-Square	0.9947

	Value	Standard Error
Intercept	-263.1	289.8
Slope	388900	11560

Appendix C

GC Calibrations

Calculation of Conversion from Peak Areas

To calculate the substrate concentration:

$$[substrate] = \frac{av.\ ratio\ (peak\ area(substrate)/peak\ area(IS))}{RRF} \times [IS] \qquad \text{Eq. (8)}$$

To convert substrate concentration into conversion:

$$Conversion\ (\%) = \frac{[substrate]}{[initial\ substrate]} \times 100 \qquad \text{Eq. (9)}$$

Calculation of Error

This is based on the standard deviation of peak areas for three injections, as well as the standard error of the slope from the calibration curve:

$$Error\ of\ value = \frac{std.\ deviation}{RRF\ \times\ (1 - std.\ error)} \qquad \text{Eq. (10)}$$
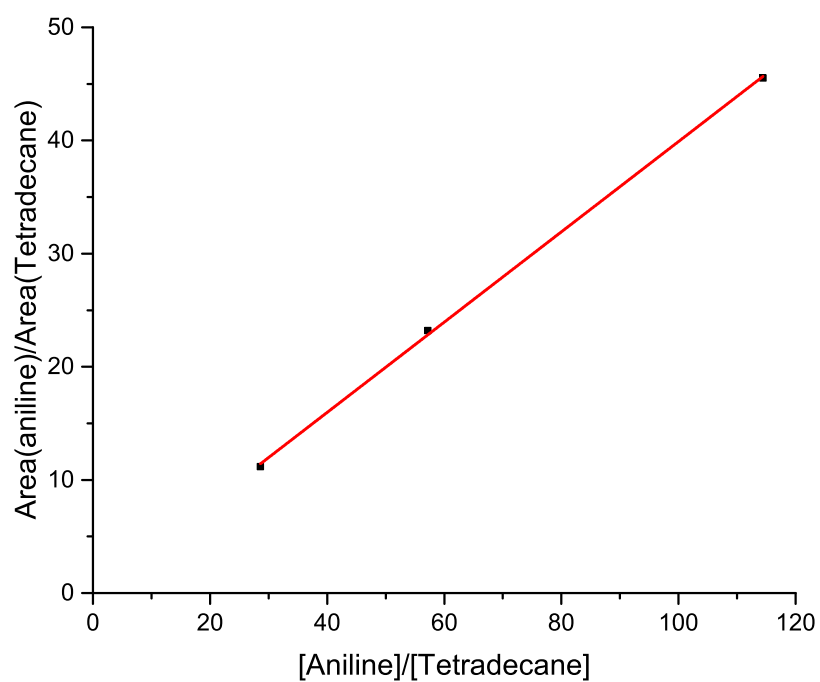
Figure 91: Calibration plot to determine relative response factor for aniline **48**

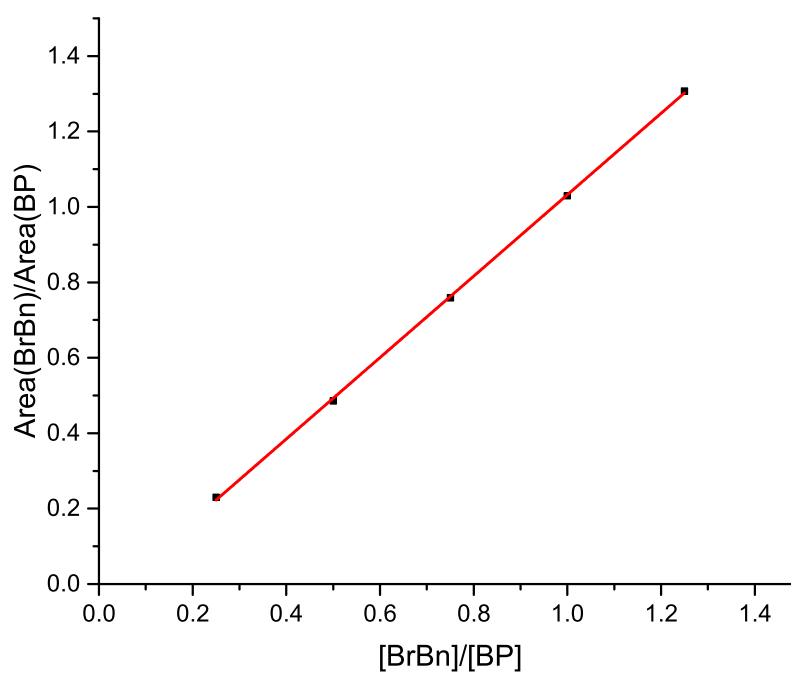| Equation	y = a + b*x
Weight	No Weighting
Residual Sum of Squares	0.2257
Pearson's r	0.9998
Adj. R-Square	0.9993

	Value	Standard Error
Intercept	0.00602	0.5818
Slope	0.3990	0.00769
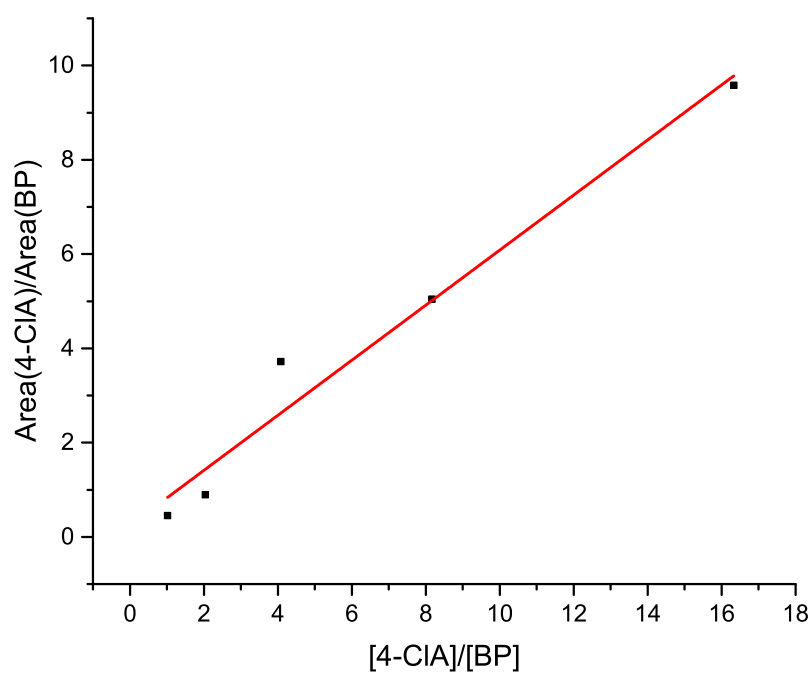
Figure 92: Calibration plot to determine relative response factor for 4-chloroaniline **46**

Equation	y = a + b*x
Weight	No Weighting
Residual Sum of Squares	1.6715
Pearson's r	0.9846
Adj. R-Square	0.9591

	Value	Standard Error
Intercept	0.2431	0.5053
Slope	0.5841	0.05996

Figure 93: Calibration plot to determine relative response factor for 2-bromo-*N*-phenylbenzamide **66**

Equation	y = a + b*x
Weight	No Weighting
Residual Sum of Squares	0.0001524
Pearson's r	0.9999
Adj. R-Square	0.9997

	Value	Standard Error
Intercept	-0.04711	0.00747
Slope	1.079	0.00901

Appendix D

NMR Spectra
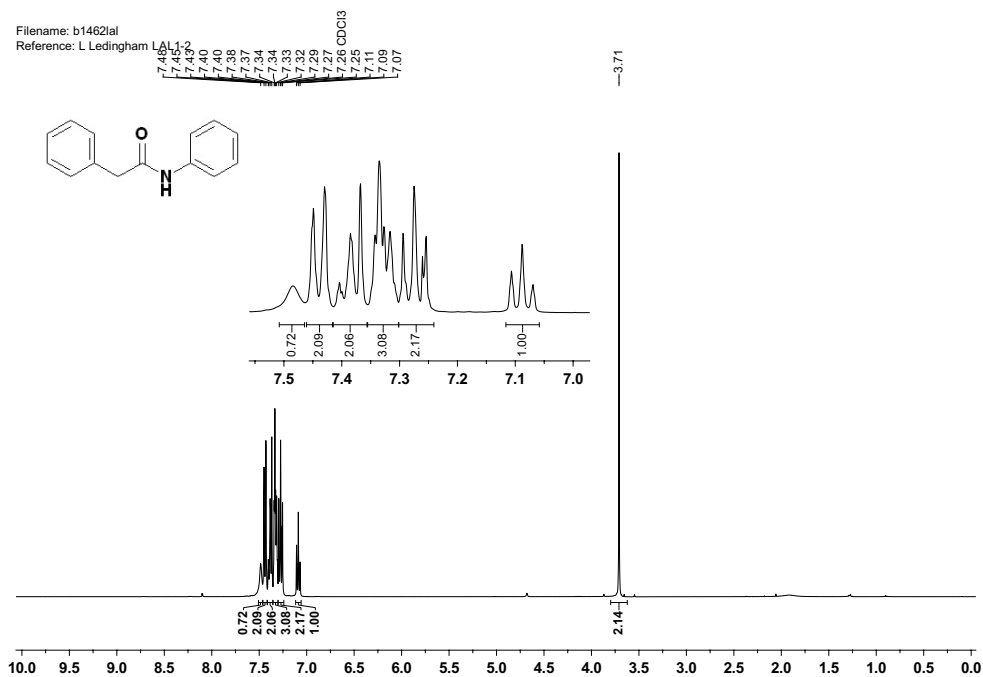
^{1}H NMR (400 MHz, CDCl$_3$) spectrum of 2N-diphenylacetamide **49**
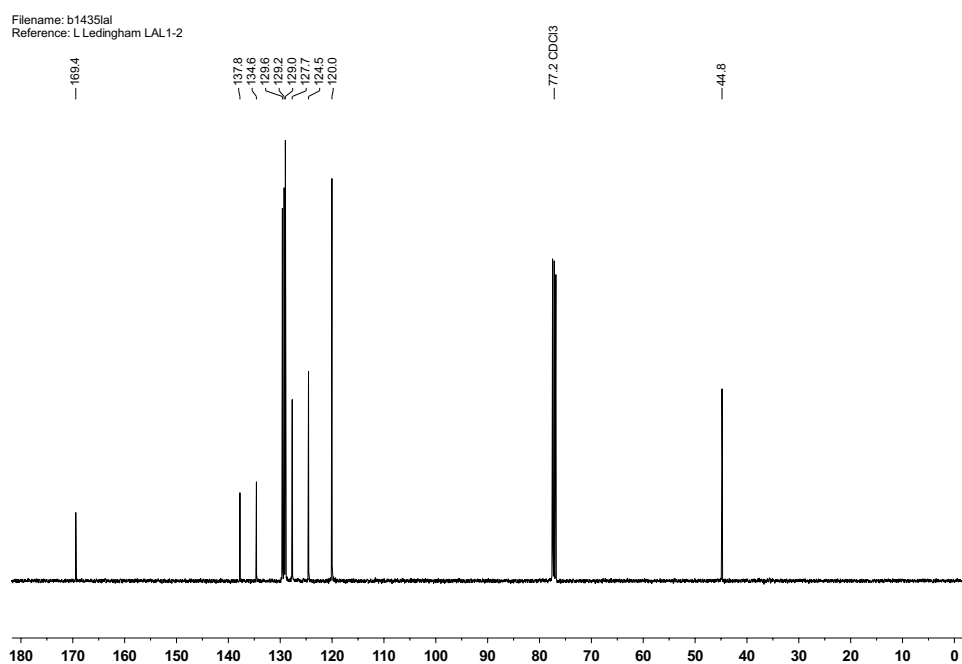
^{13}C NMR (100 MHz, CDCl$_3$) spectrum of 2N-diphenylacetamide **49**
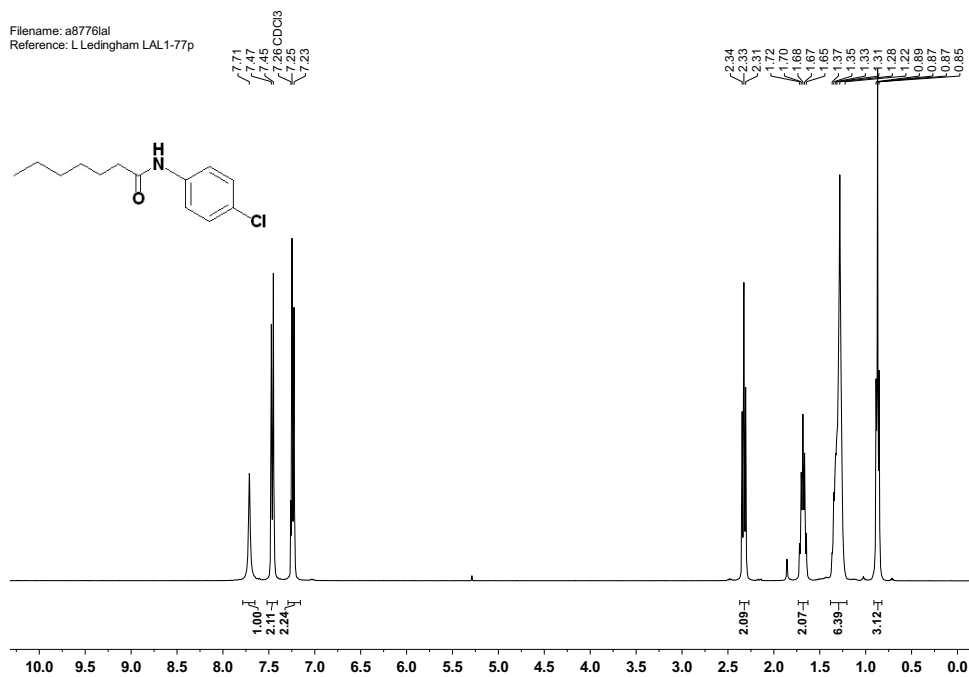
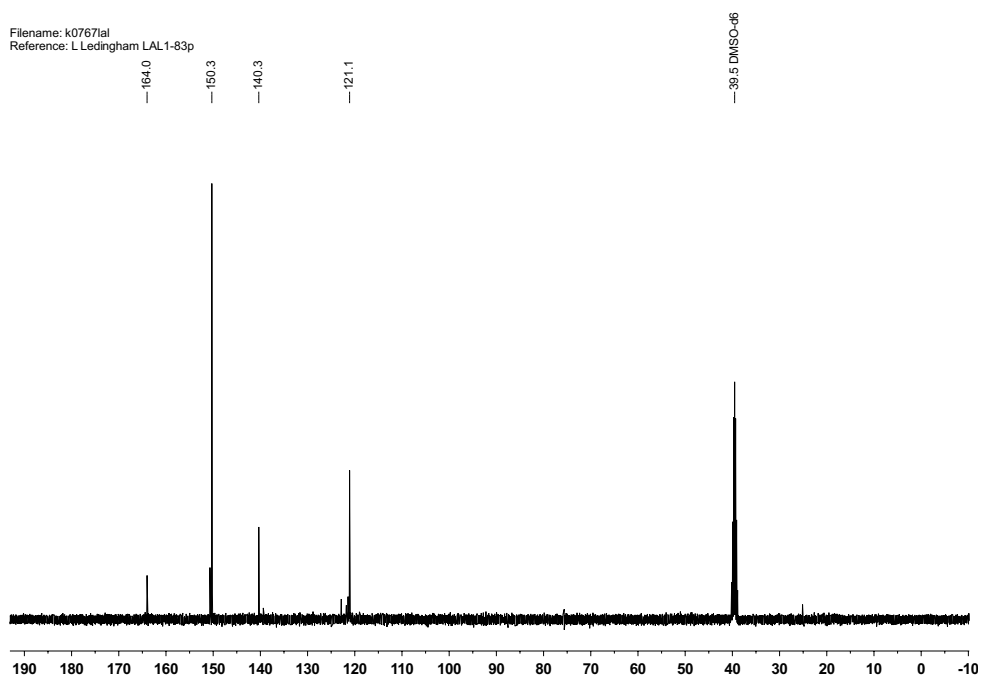^{1}H NMR (400 MHz, CDCl$_3$) spectrum of *N*-(4-chlorophenyl)heptanamide **47**
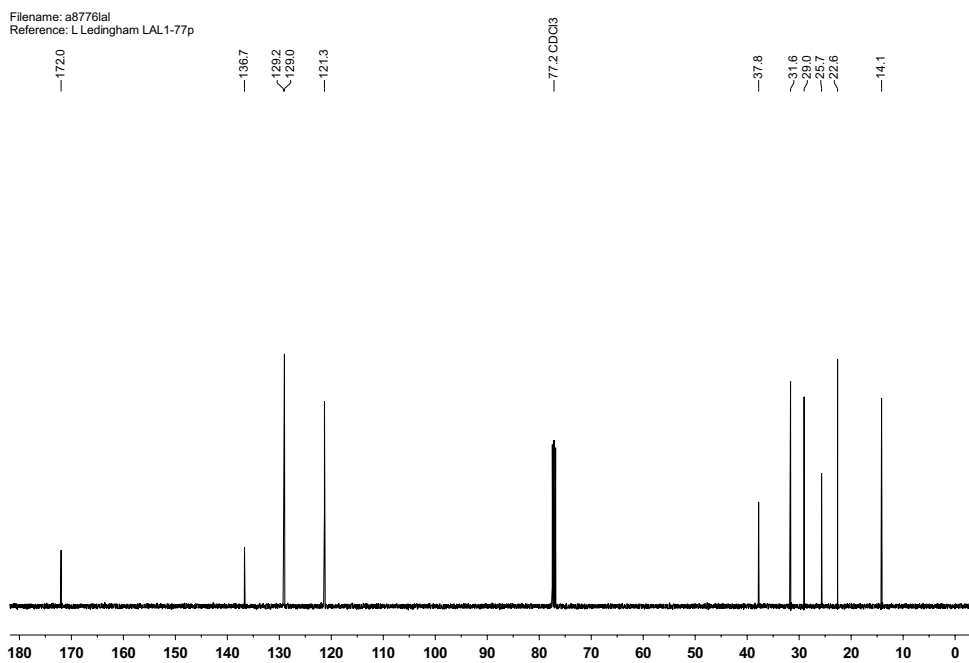
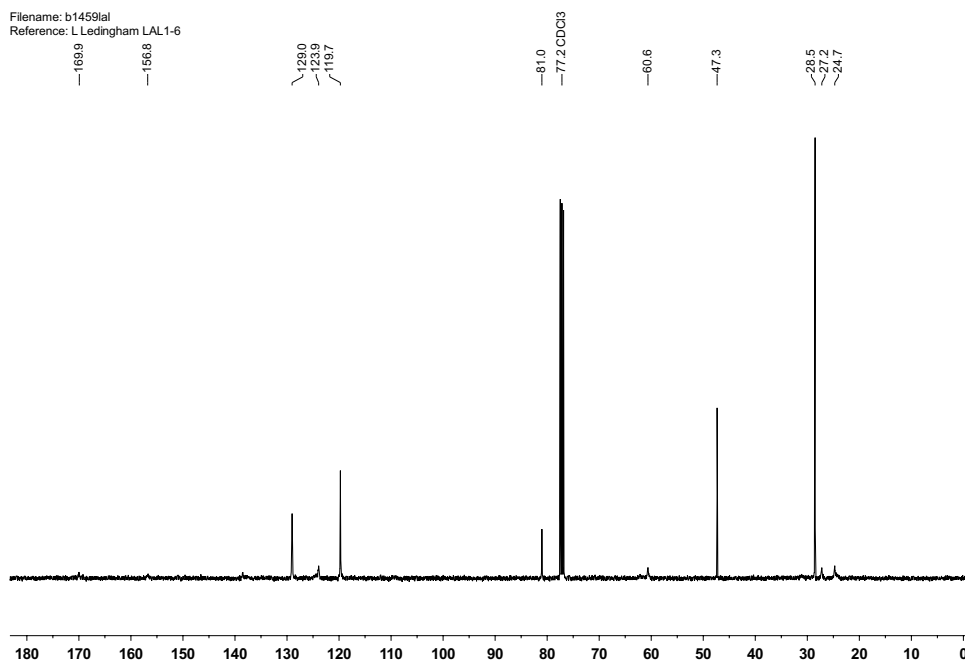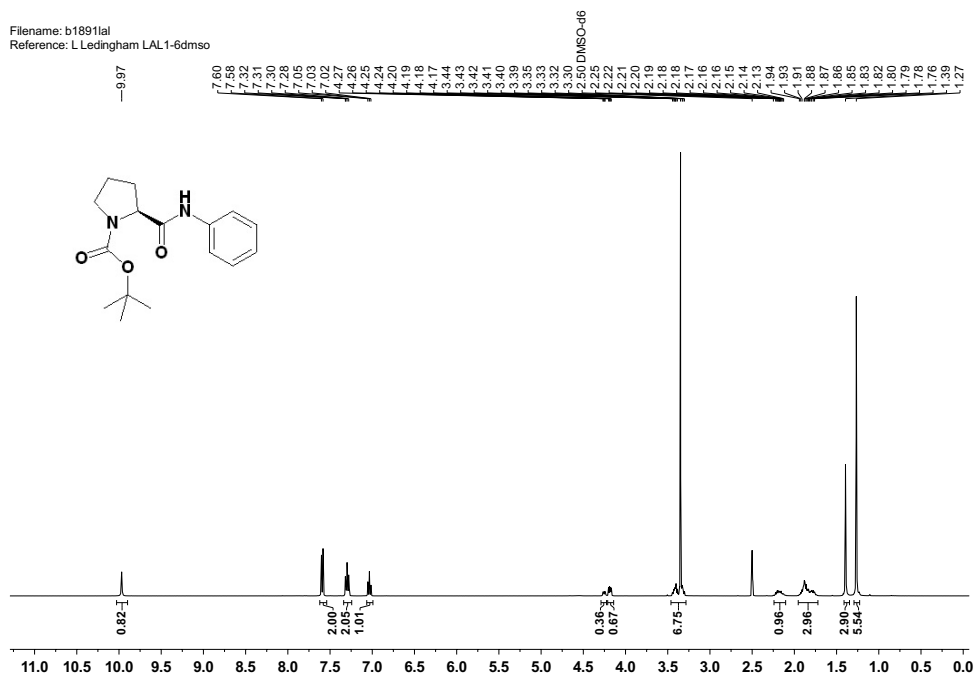^{13}C NMR (100 MHz, CDCl$_3$) spectrum of *N*-(4-chlorophenyl)heptanamide **47**
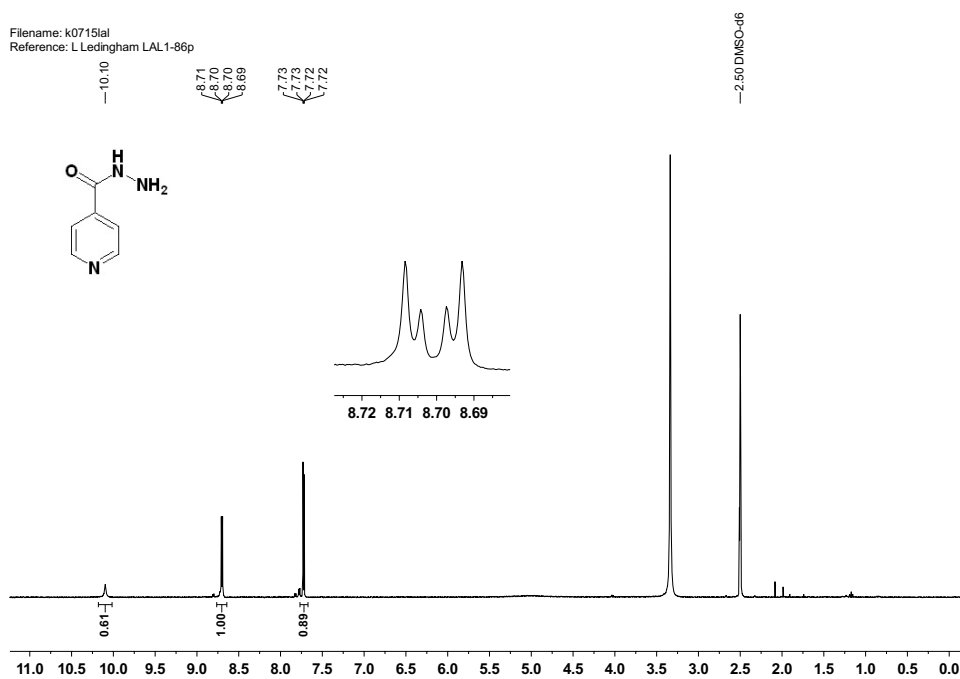
^{1}H NMR (400 MHz, SO(CD$_3$)$_2$) spectrum of isoniazid **76**

^{13}C NMR (100 MHz, SO(CD$_3$)$_2$) spectrum of isoniazid **76**
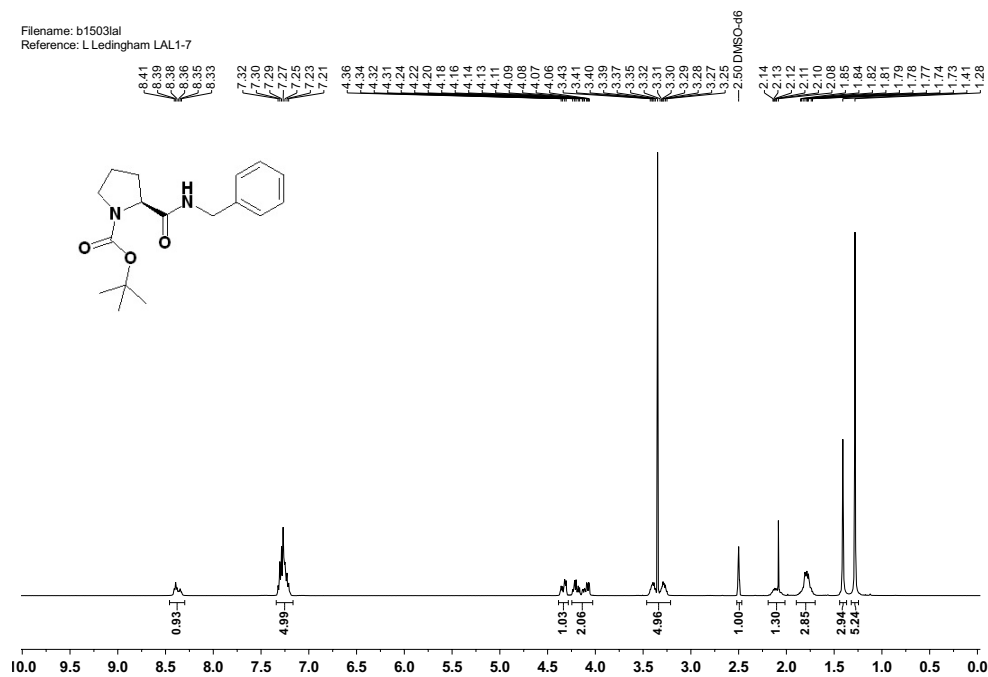
^{1}H NMR (400 MHz, SO(CD$_3$)$_2$) spectrum of (*S*)-t-butyl-2-(phenylcarbamoyl)pyrrolidine-1-carboxylate **86**

^{13}C NMR (100 MHz, CDCl$_3$) spectrum of (*S*)-t-butyl-2-(phenylcarbamoyl)pyrrolidine-1-carboxylate **86**

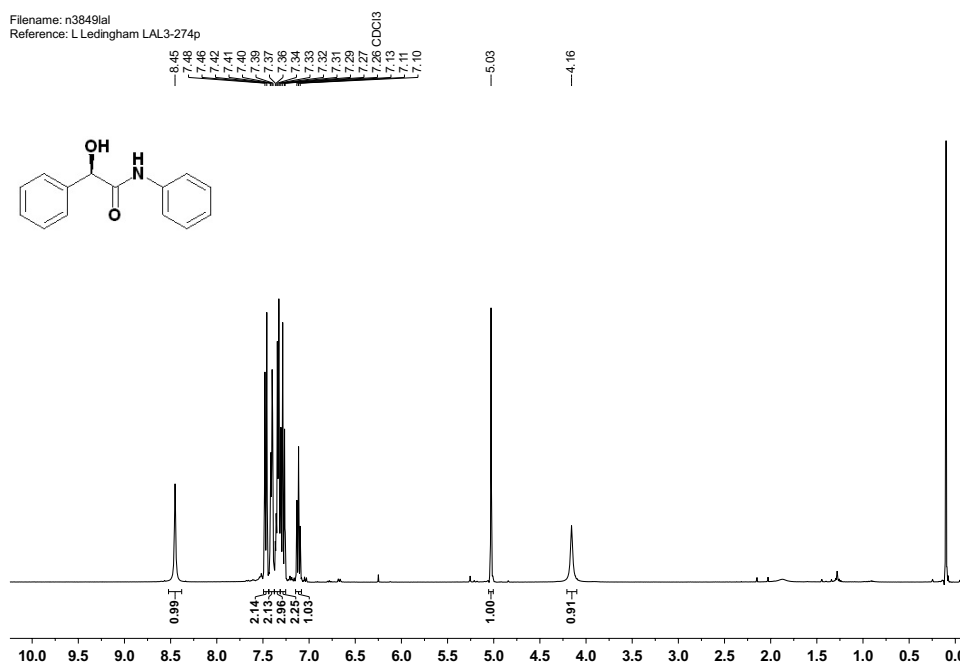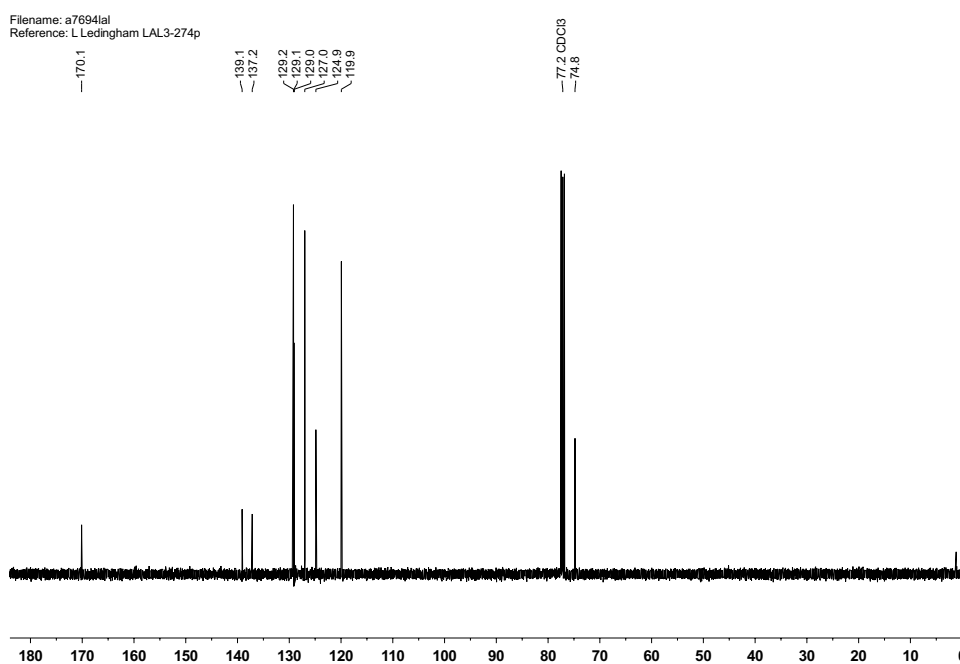^{1}H NMR (400 MHz, SO(CD$_3$)$_2$) spectrum of (*S*)-t-butyl-2-(benzylcarbamoyl)pyrrolidine-1-carboxylate **87**
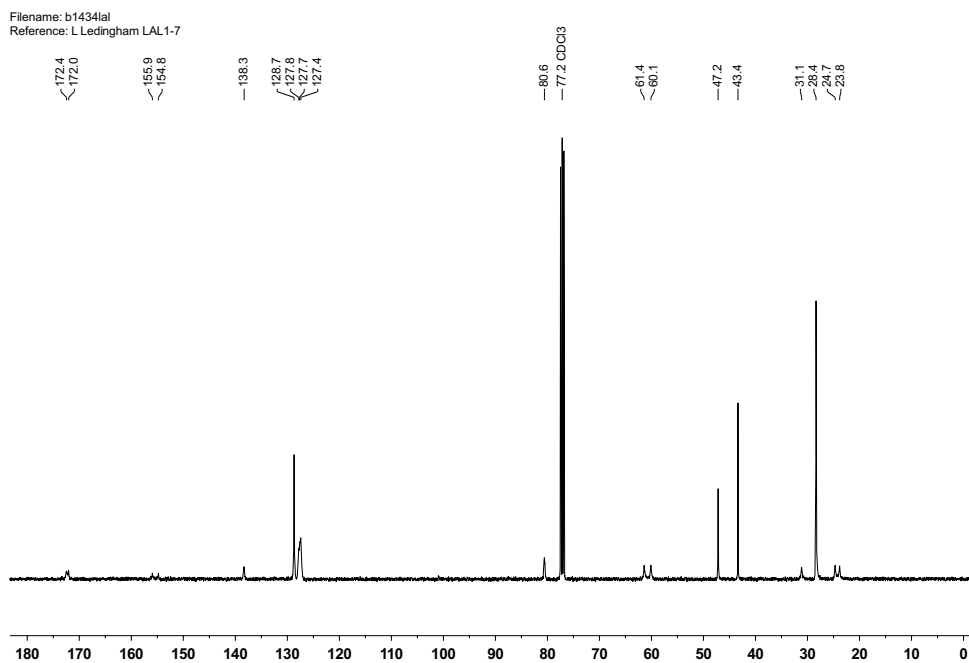
^{13}C NMR (100 MHz, CDCl$_3$) spectrum of (*S*)-t-butyl-2-(benzylcarbamoyl)pyrrolidine-1-carboxylate **87**

^{1}H NMR (400 MHz, CDCl$_3$) spectrum of (*R*)-2-hydroxydiphenylacetamide **147**

^{13}C NMR (100 MHz, CDCl$_3$) spectrum of (*R*)-2-hydroxydiphenylacetamide **147**

—3.75

—2.05 (CD3)2CO

1.00

0.0 9.5 9.0 8.5 8.0 7.5 7.0 6.5 6.0 5.5 5.0 4.5 4.0 3.5 3.0 2.5 2.0 1.5 1.0 0.5 0.0
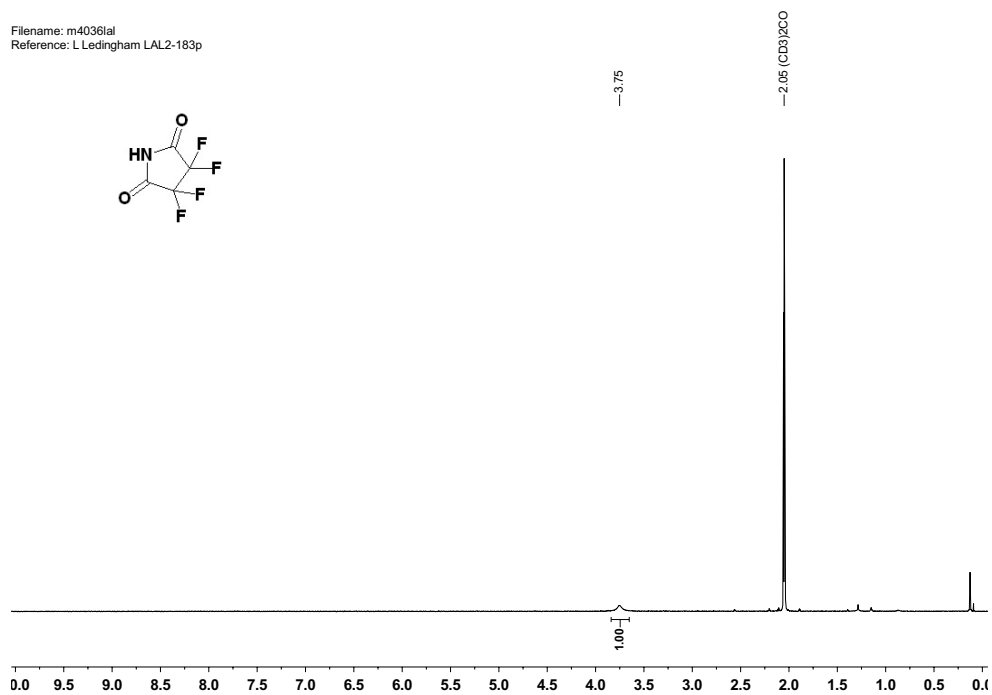
^{1}H NMR (400 MHz, (CD$_3$)$_2$CO) spectrum of tetrafluorosuccinimide **159**

—128.0

-127.90 -127.95 -128.00 -128.05 -128.10 -128.15

90 80 70 60 50 40 30 20 10 0 -10 -30 -50 -70 -90 -110 -130 -150 -170 -190

^{19}F NMR (376 MHz, (CD$_3$)$_2$CO) spectrum of tetrafluorosuccinimide **159**

Filename: m0496lal
Reference: L Ledingham LAL2-154c

160.9
160.6
160.3

109.7
109.4
109.1

29.8 (CD3)2CO

160.88
160.59
160.30

109.68
109.38
109.08

161.0   160.0   159.0   111.0   110.0   109.0   108.0

180 170 160 150 140 130 120 110 100 90 80 70 60 50 40 30 20 10 0
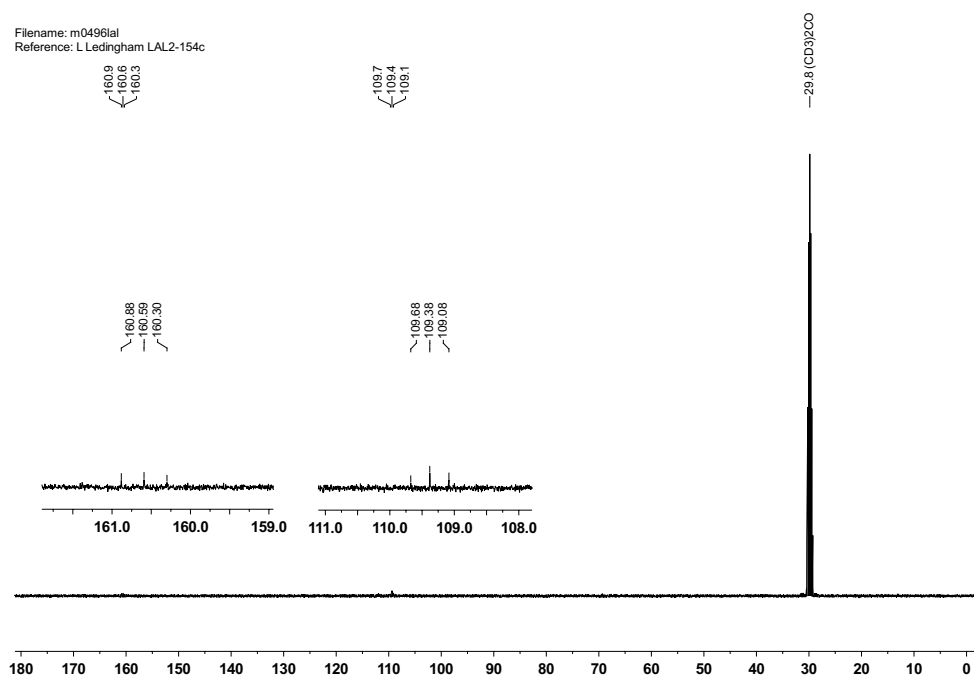
^{13}C NMR (100 MHz, (CD$_3$)$_2$CO) spectrum of tetrafluorosuccinimide **159**

Reference: Sample: PdTFS (111 mg)
1H MAS
srate = 12000 Hz

—2.94

140 130 120 110 100 90 80 70 60 50 40 30 20 10 0 -10 -20 -30 -40 -50 -60 -70 -80 -90 -100 -110 -120 -130 -140
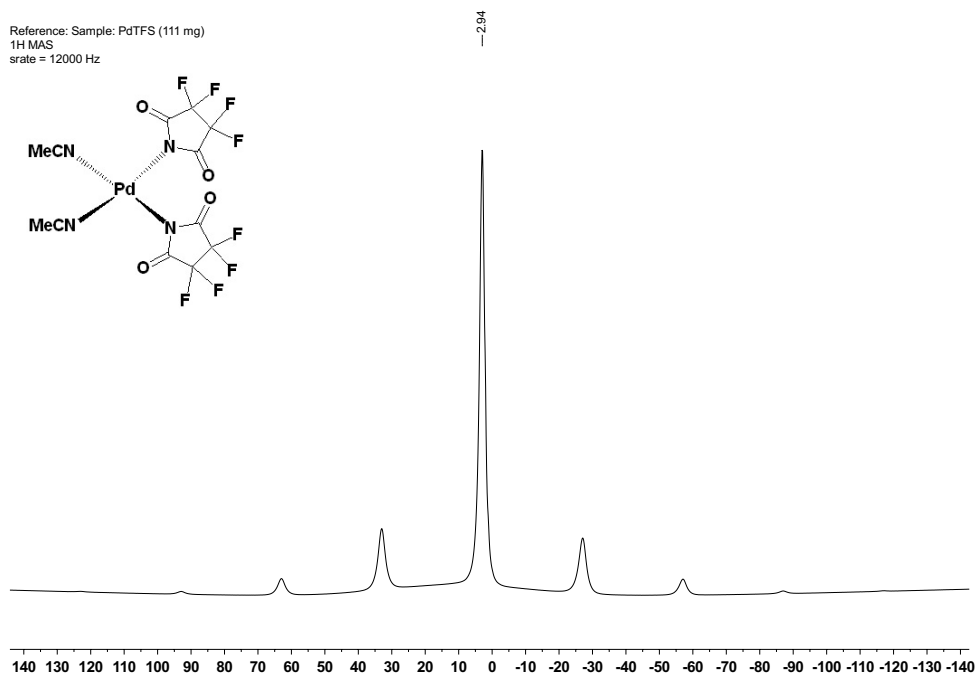
^{1}H NMR (400 MHz, solid) spectrum of Pd(tfs)$_2$(MeCN)$_2$ **160**

Reference: Sample: PdTFS (111 mg)
19F MAS
srate = 12500 Hz

—-123.74

80 60 40 20 0 -20 -40 -60 -80 -100 -120 -140 -160 -180 -200 -220 -240 -260 -280 -300 -320
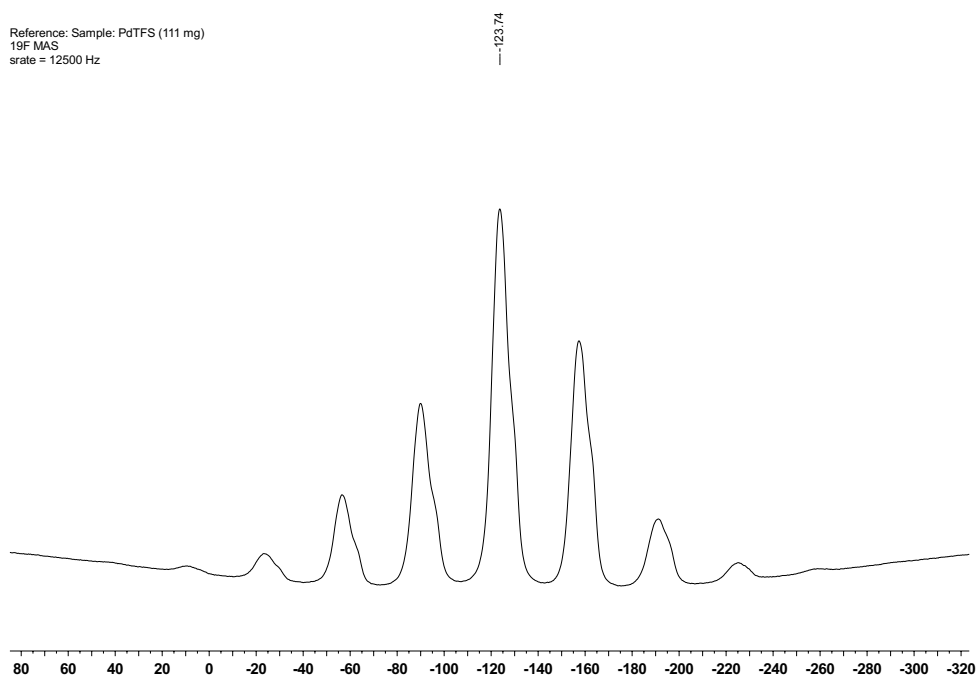
^{19}F NMR (376 MHz, solid) spectrum of Pd(tfs)$_2$(MeCN)$_2$ **160**

Filename: LLedingham_PdTFS
Reference: Sample: PdTFS (111 mg)
13C{1H} CPMAS
srate = 12000 Hz

243.8

169.7

124.6

5.2
4.3
3.4

300 290 280 270 260 250 240 230 220 210 200 190 180 170 160 150 140 130 120 110 100 90 80 70 60 50 40 30 20 10 0 -10 -20

$^{13}C\{^1H\}$ NMR (100 MHz, solid) spectrum of Pd(tfs)$_2$(MeCN)$_2$ **160**

Filename: LLedingham_PdTFS
Reference: Sample: PdTFS (111 mg)
13C{19F} CPMAS
srate = 10000 Hz

169.6
168.4

106.3
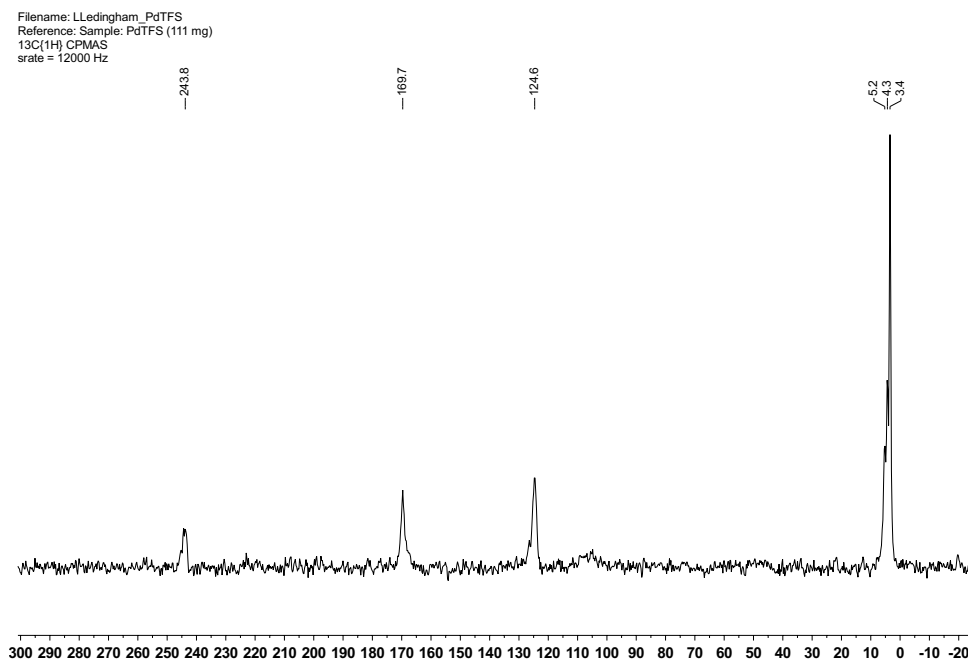
290 280 270 260 250 240 230 220 210 200 190 180 170 160 150 140 130 120 110 100 90 80 70 60 50 40 30 20 10 0 -10
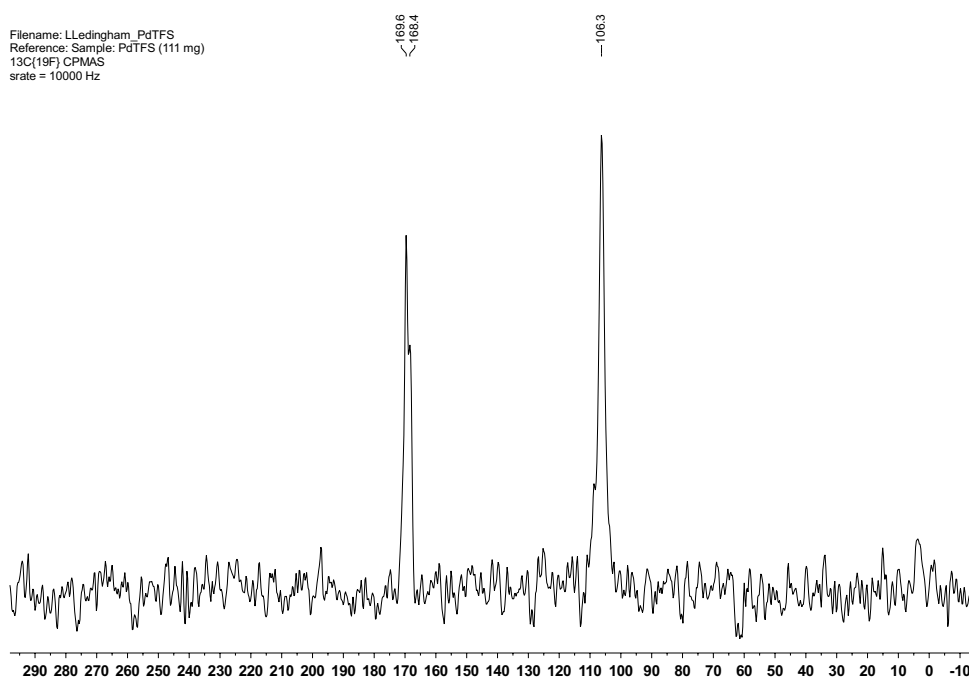
$^{13}C\{^{19}F\}$ NMR (100 MHz, solid) spectrum of Pd(tfs)$_2$(MeCN)$_2$ **160**
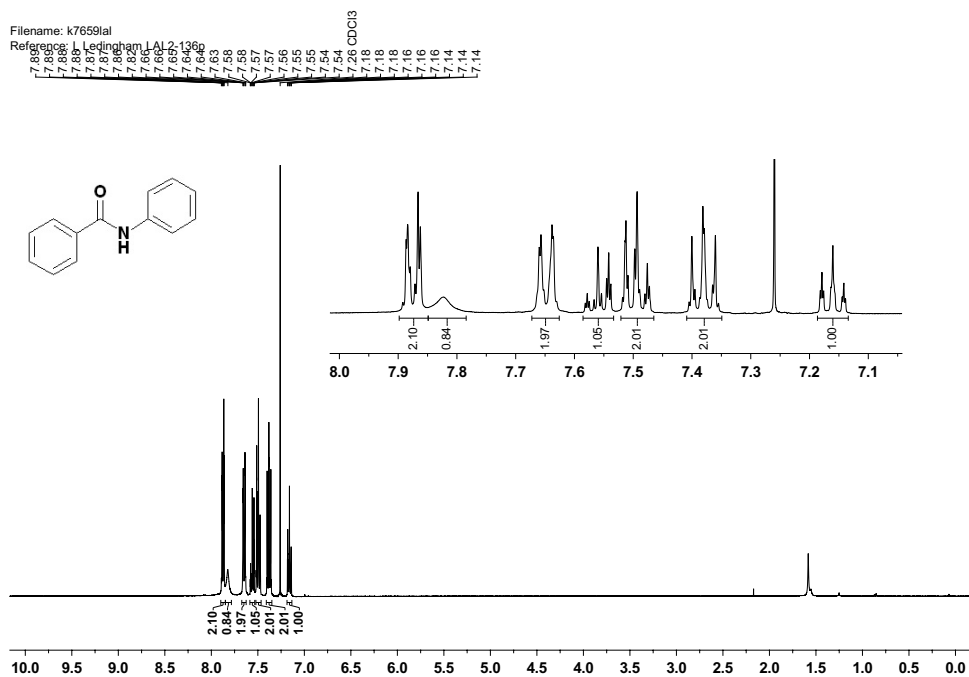
^{1}H NMR (400 MHz, CDCl$_3$) spectrum of *N*-phenylbenzamide **66**
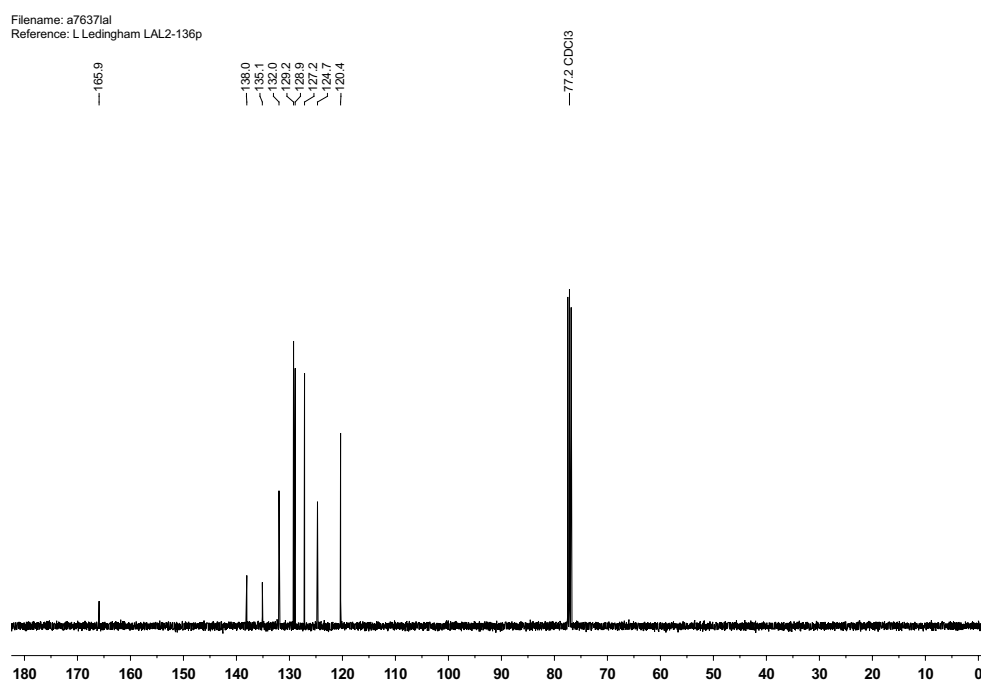
^{13}C NMR (100 MHz, CDCl$_3$) spectrum of *N*-phenylbenzamide **66**
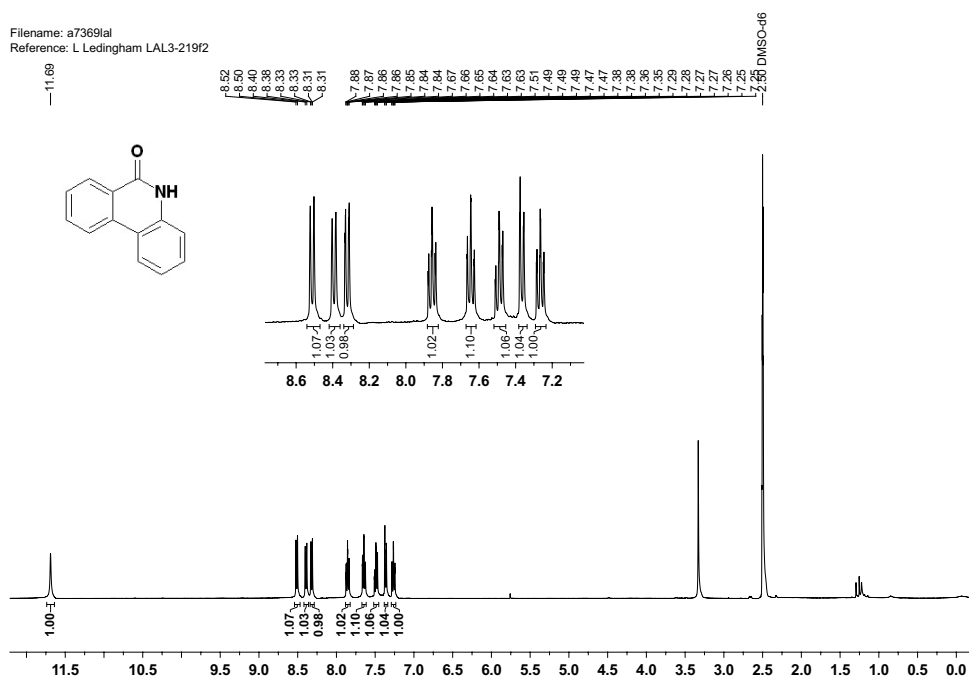
^{1}H NMR (400 MHz, CDCl$_3$) spectrum of phenanthridin-6-(5*H*)-one **148**
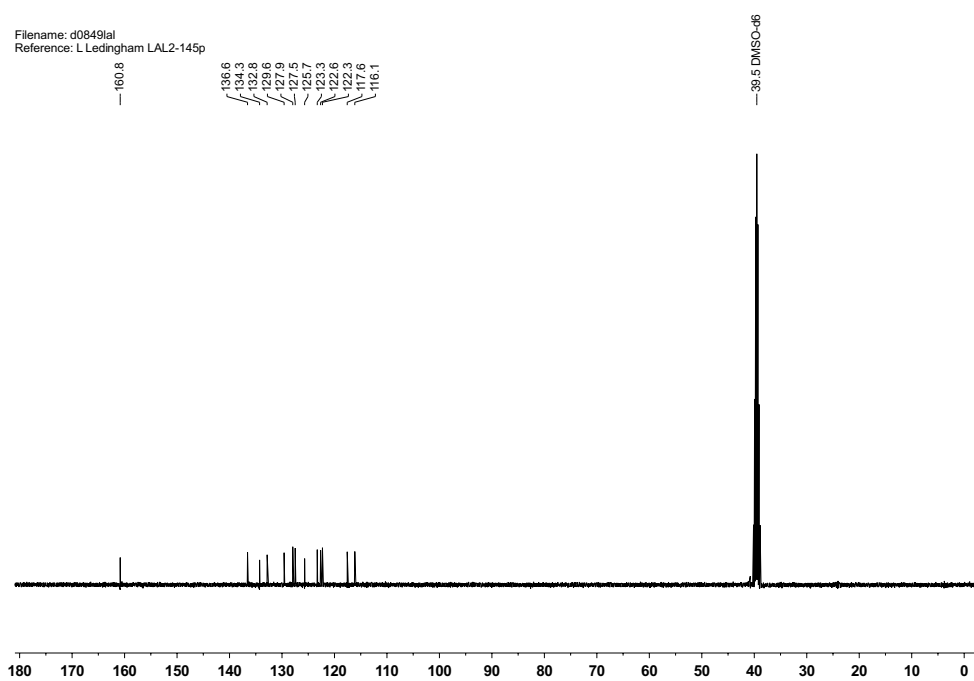
^{13}C NMR (100 MHz, SO(CD$_3$)$_2$) spectrum of phenanthridin-6-(5*H*)-one **148**
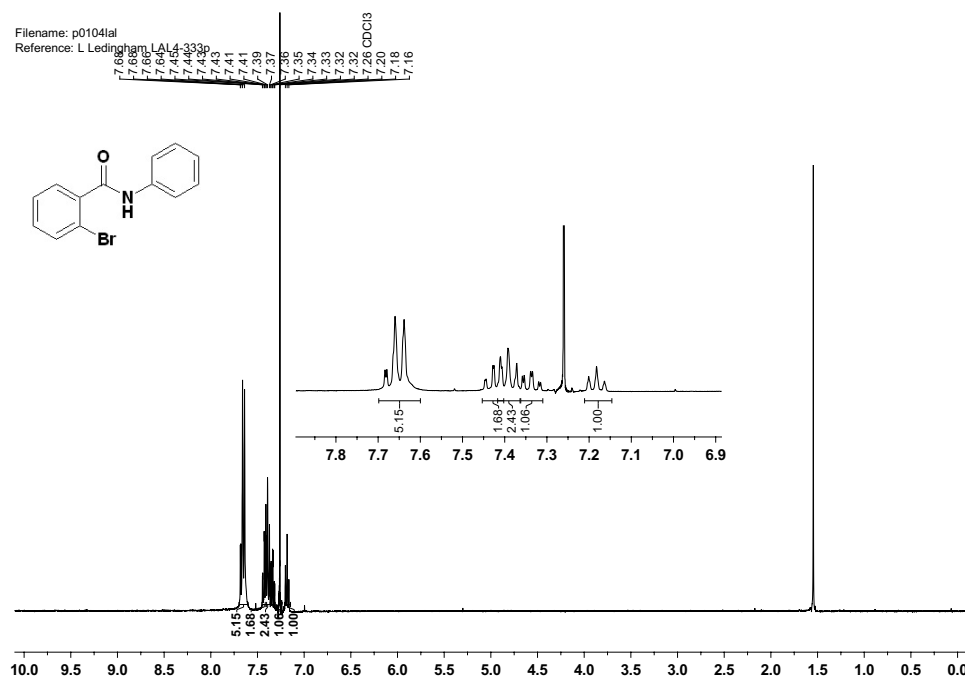
^{1}H NMR (400 MHz, CDCl$_3$) spectrum of 2-bromo-*N*-phenylbenzamide **163**
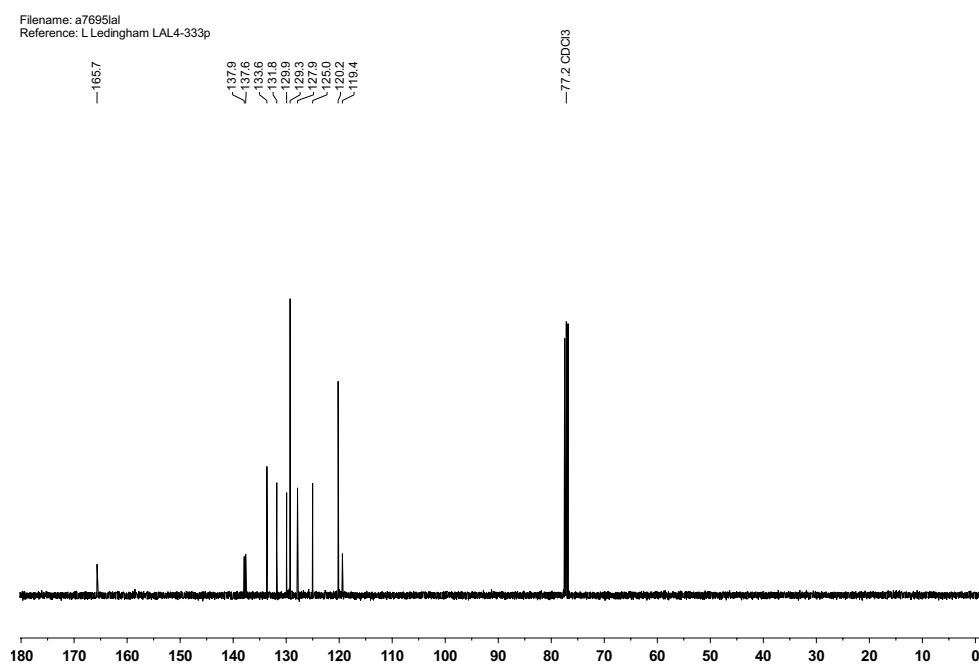
^{13}C NMR (100 MHz, CDCl$_3$) spectrum of 2-bromo-*N*-phenylbenzamide **163**
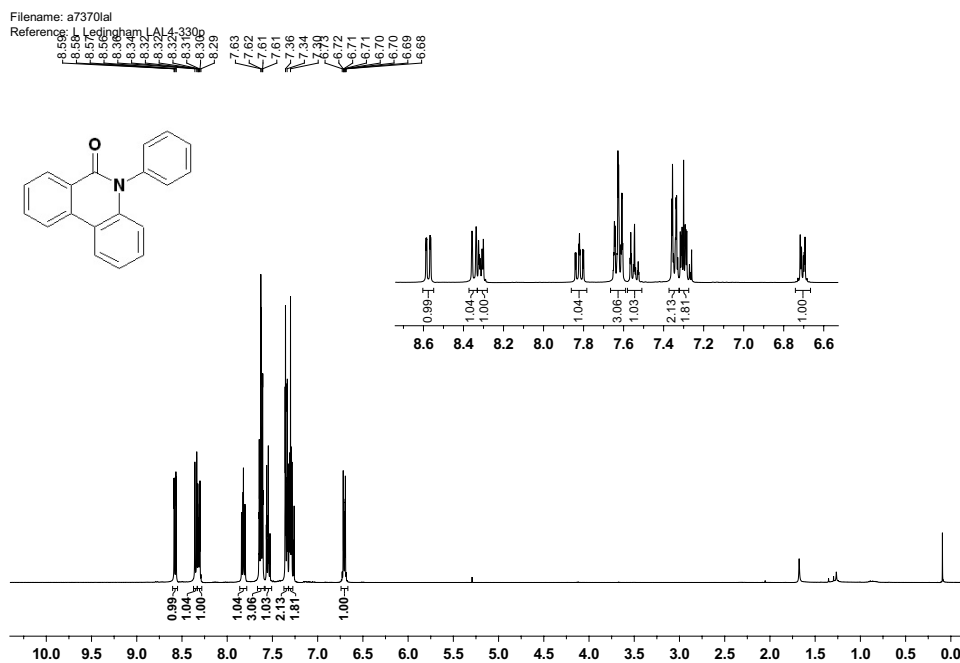
Filename: a7370lal
Reference: L Ledingham LAL4-330p

8.59, 8.58, 8.57, 8.56, 8.38, 8.36, 8.34, 8.32, 8.32, 8.30, 8.29
7.63, 7.62, 7.61, 7.61
7.36, 7.34, 7.30, 7.29
6.72, 6.71, 6.71, 6.70, 6.70, 6.69, 6.68

0.99, 1.04, 1.00, 1.04, 3.06, 1.03, 2.13, 1.81, 1.00

8.6 8.4 8.2 8.0 7.8 7.6 7.4 7.2 7.0 6.8 6.6

0.99, 1.04, 1.00, 1.04, 3.06, 1.03, 2.13, 1.81, 1.00

10.0 9.5 9.0 8.5 8.0 7.5 7.0 6.5 6.0 5.5 5.0 4.5 4.0 3.5 3.0 2.5 2.0 1.5 1.0 0.5 0.0

[^1]H NMR (400 MHz, CDCl$_3$) spectrum of 5-phenylphenanthridin-6(5*H*)-one **164**

Filename: n7004lal
Reference: L Ledingham LAL4-297f3

161.8
139.3, 138.4, 134.1, 133.0, 130.3, 129.2, 129.1, 129.1, 128.9, 128.3, 128.0, 126.0, 123.1, 122.8, 121.9, 119.1, 117.1
77.2 CDCl3

180 170 160 150 140 130 120 110 100 90 80 70 60 50 40 30 20 10 0
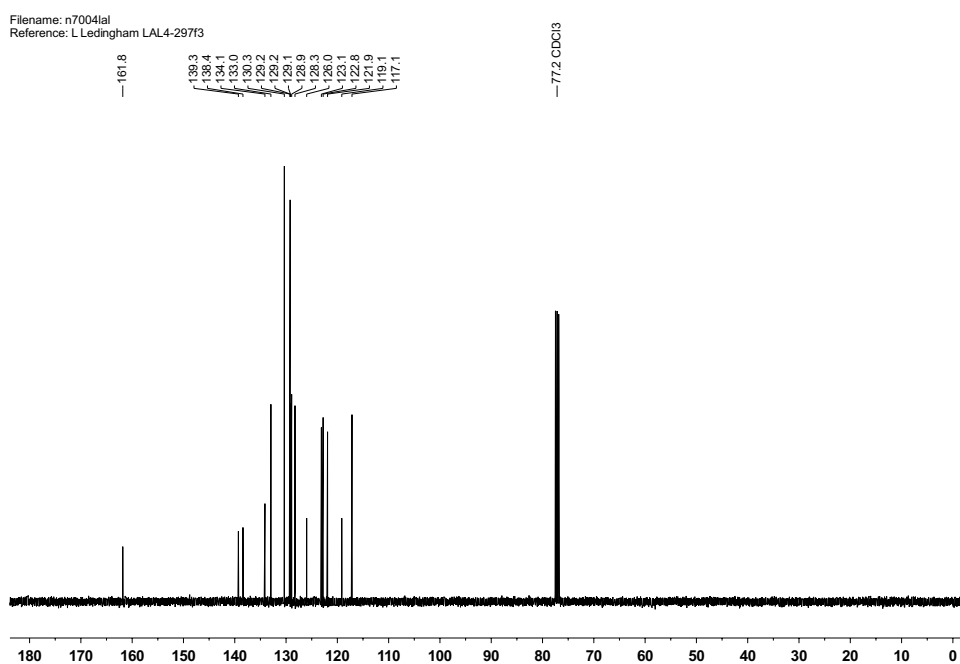
[^13]C NMR (100 MHz, CDCl$_3$) spectrum of 5-phenylphenanthridin-6(5*H*)-one **164**

^{1}H NMR (400 MHz, CDCl$_3$) spectrum of 8*H*-indolo[3,2,1-*de*]phenanthridin-8-one **196**

^{13}C NMR (100 MHz, CDCl$_3$) spectrum of 8*H*-indolo[3,2,1-*de*]phenanthridin-8-one **196**

^{1}H NMR (400 MHz, CDCl$_3$) spectrum of 2-hydroxy-*N*-phenylbenzamide **202**
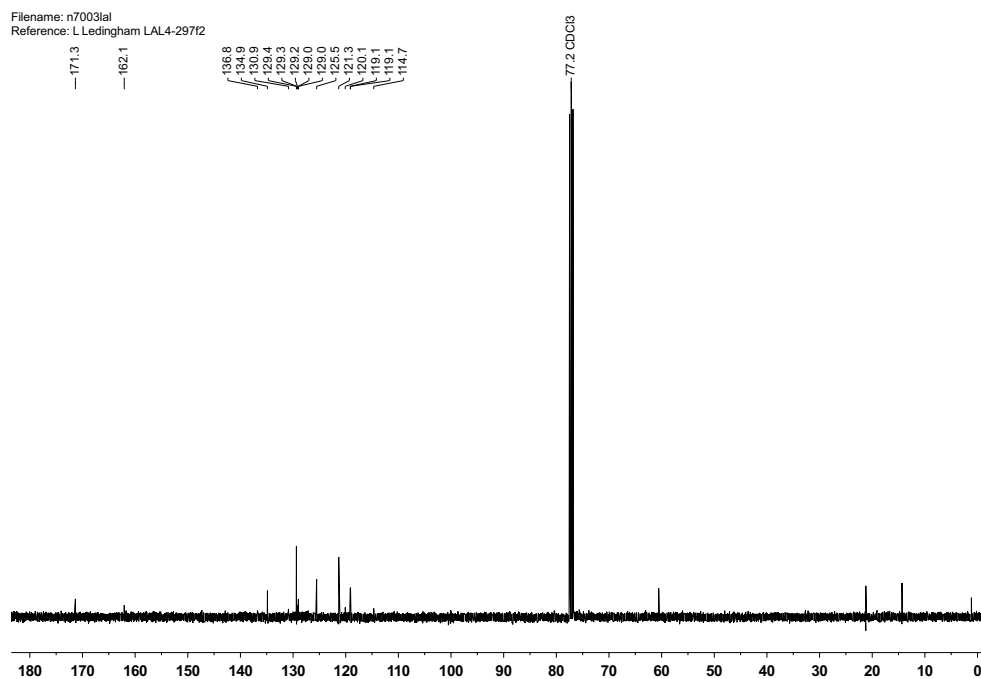
^{13}C NMR (100 MHz, CDCl$_3$) spectrum of 2-hydroxy-*N*-phenylbenzamide **202**
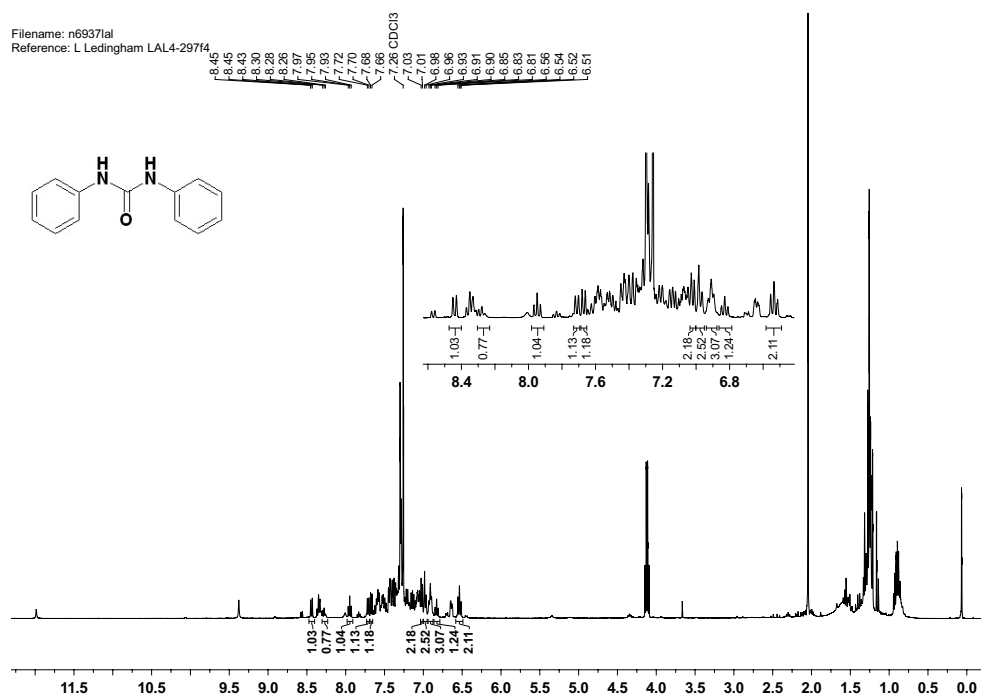
^{1}H NMR (400 MHz, CDCl$_3$) spectrum of *N*,*N'*-diphenylurea **207**
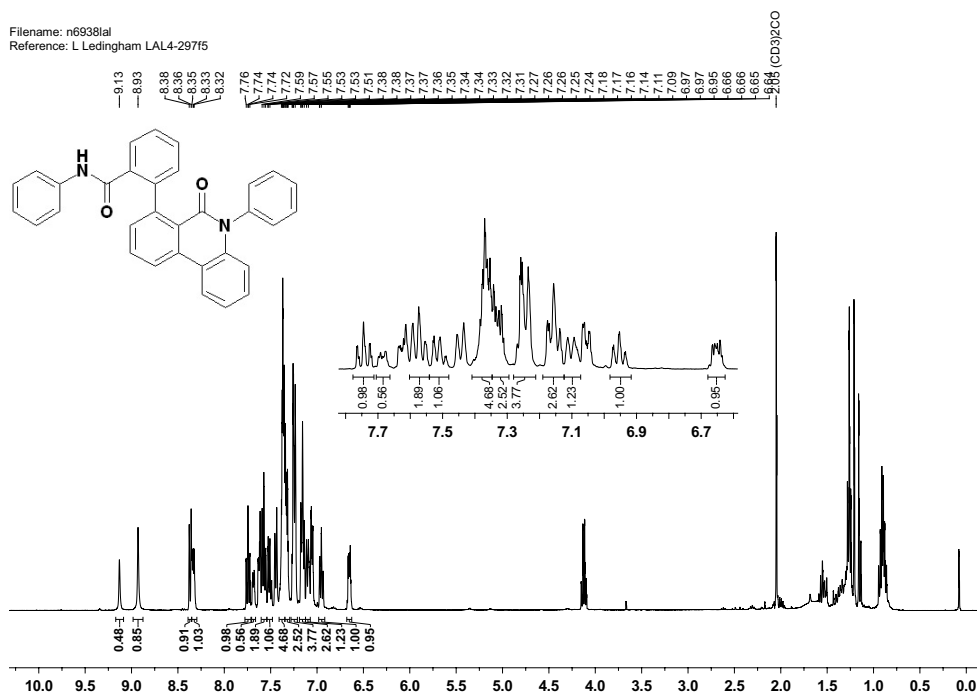
^{1}H NMR (400 MHz, CDCl$_3$) spectrum of 2′-(6-oxophenanthridin-5(6*H*)-yl)-*N*-phenyl[1,1′-biphenyl]-2-carboxamide **208**
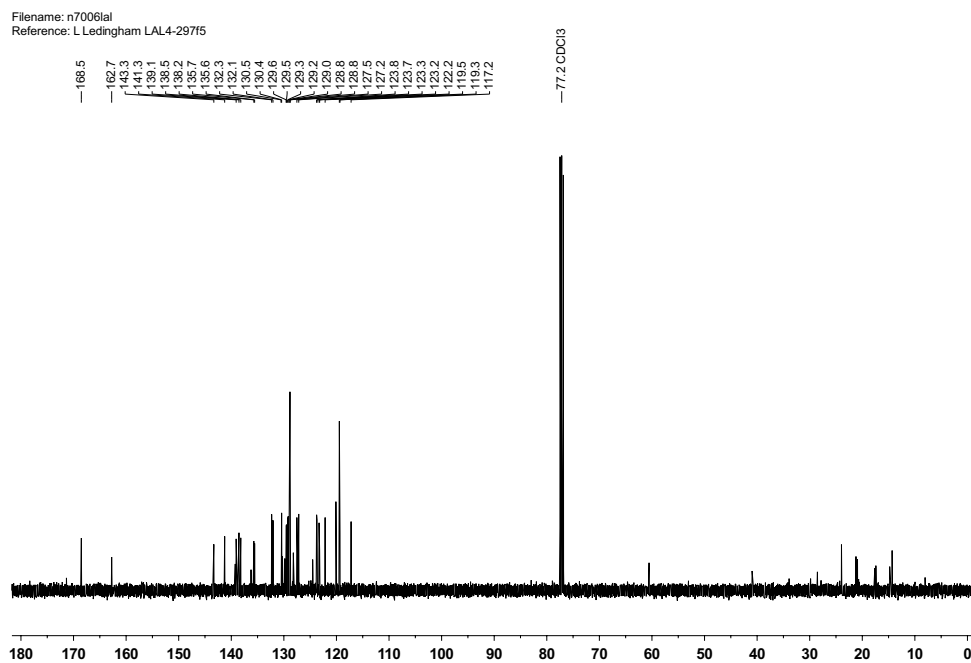
^{13}C NMR (100 MHz, CDCl$_3$) spectrum of 2′-(6-oxophenanthridin-5(6*H*)-yl)-*N*-phenyl[1,1′-biphenyl]-2-carboxamide **208**
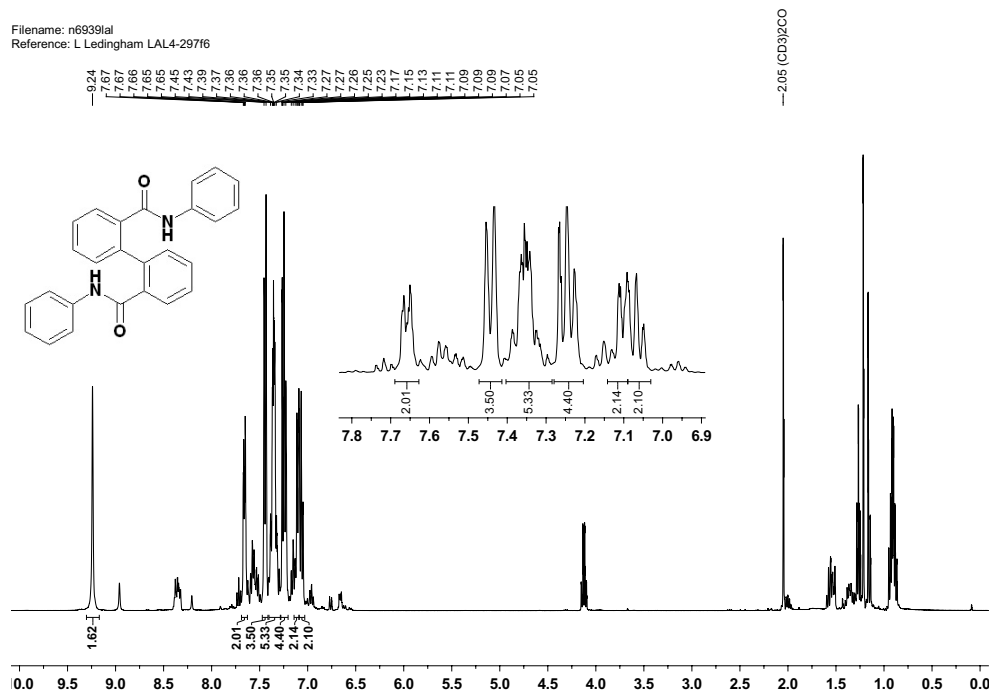
^{1}H NMR (400 MHz, CDCl$_3$) spectrum of *N2,N2′*-diphenyl[1,1′-biphenyl]-2,2′-dicarboxamide **201**
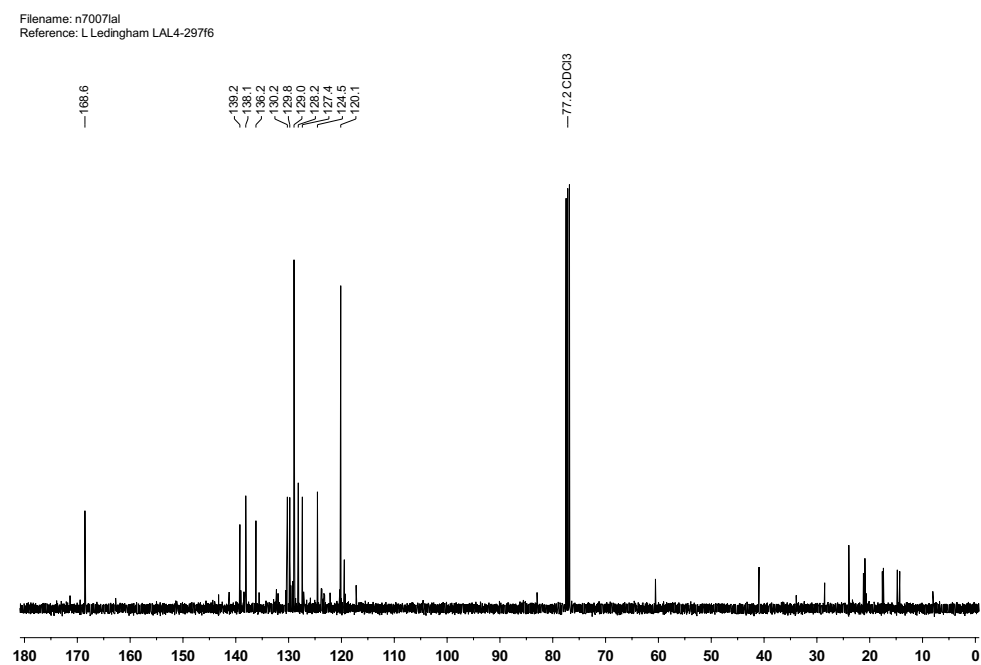
^{13}C NMR (100 MHz, CDCl$_3$) spectrum of *N2,N2′*-diphenyl[1,1′-biphenyl]-2,2′-dicarboxamide **201**
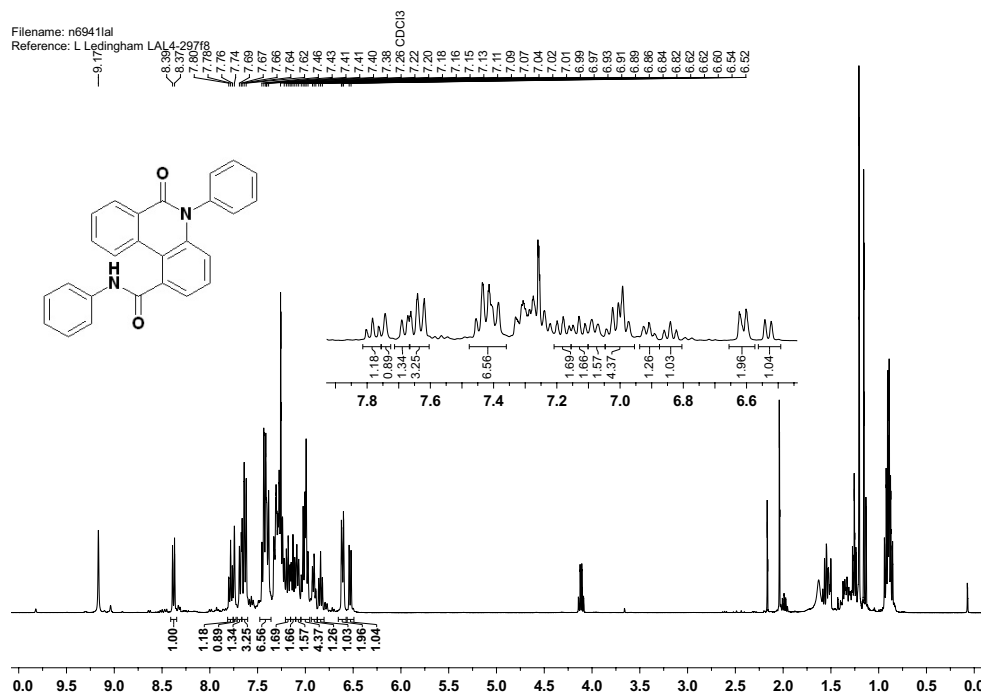
^{1}H NMR (400 MHz, CDCl$_3$) spectrum of 6-oxo-*N*,5-diphenyl-5,6-dihydrophenanthridine-1-carboxamide **210**
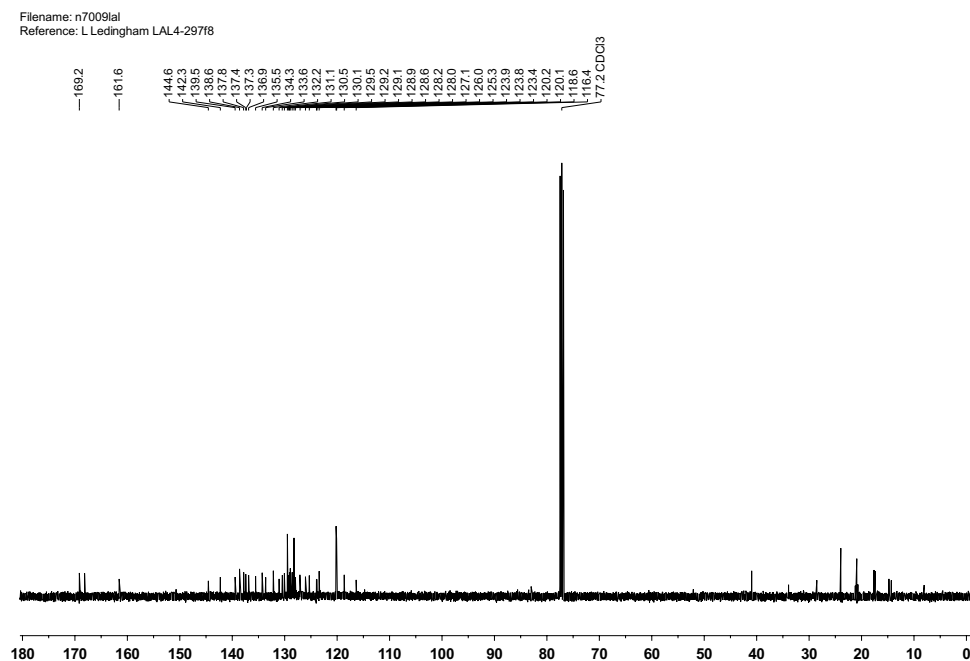
^{13}C NMR (100 MHz, CDCl$_3$) spectrum of 6-oxo-*N*,5-diphenyl-5,6-dihydrophenanthridine-1-carboxamide **210**
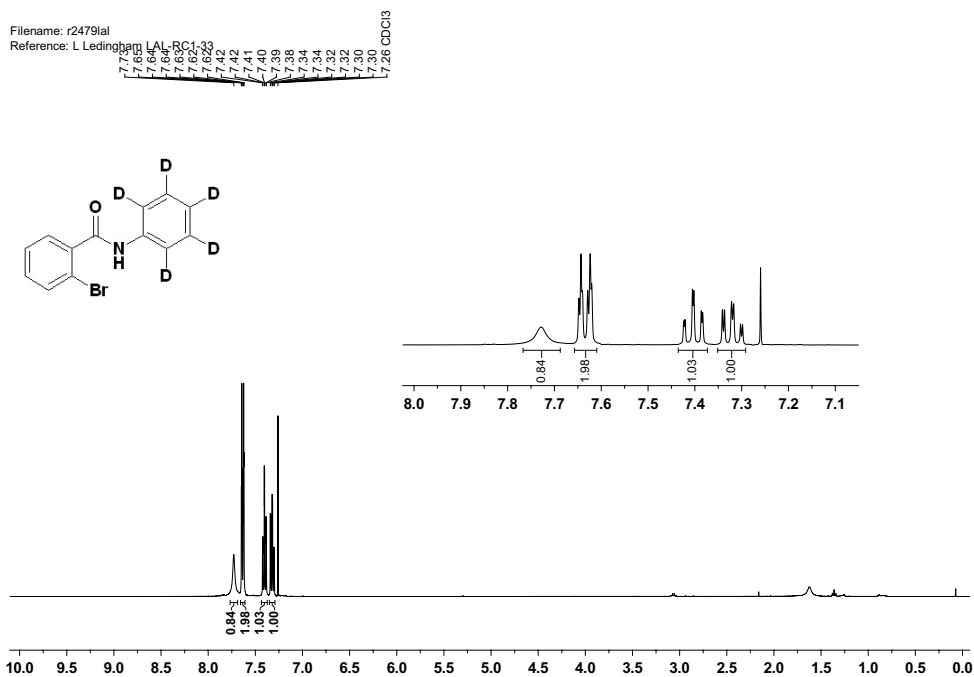
^{1}H NMR (400 MHz, CDCl$_3$) spectrum of 2-bromo-*N*-(pentadeuterophenyl)benzamide **163-d$_5$**
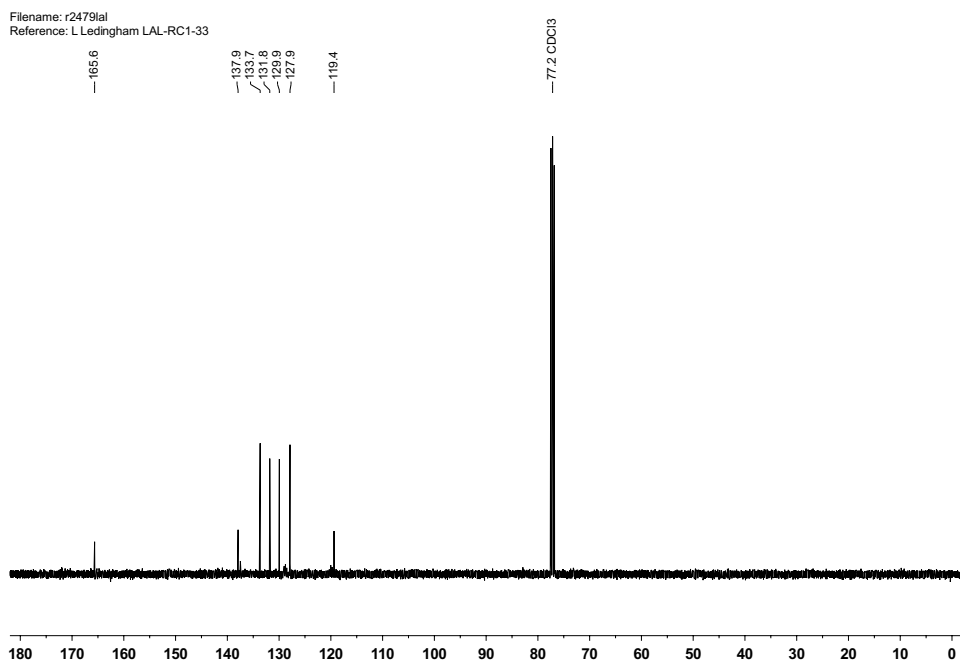
^{13}C NMR (100 MHz, CDCl$_3$) spectrum of 2-bromo-*N*-(pentadeuterophenyl)benzamide **163-d$_5$**
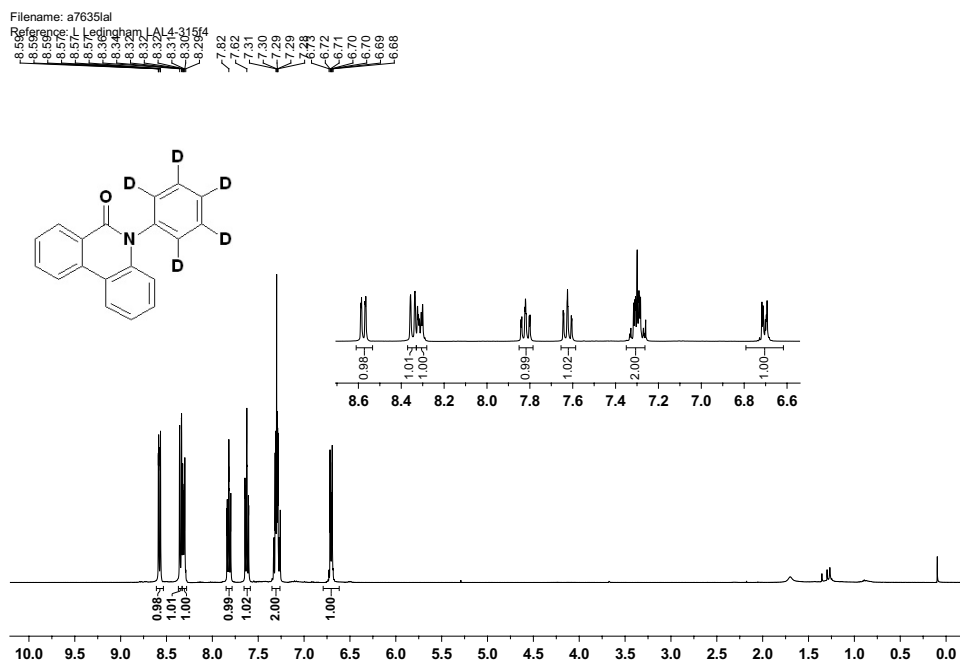
Filename: a7635lal
Reference: L Ledingham LAL4-315f4

8.59, 8.59, 8.58, 8.57, 8.57, 8.57, 8.36, 8.34, 8.32, 8.32, 8.31, 8.30, 8.29

7.82, 7.62, 7.31, 7.30, 7.29, 7.29, 7.28

6.73, 6.72, 6.71, 6.70, 6.70, 6.69, 6.68

^{1}H NMR (400 MHz, CDCl$_3$) spectrum of 5-(pentadeuterophenyl)phenanthridin-6(5*H*)-one

164-d$_5$

Filename: a7462lal
Reference: L Ledingham LAL4-315f4

161.8

139.3, 138.3, 134.1, 132.9, 129.2, 129.1, 128.2, 126.0, 123.1, 122.8, 121.9, 119.1, 117.1

77.2 CDCl3

^{13}C NMR (100 MHz, CDCl$_3$) spectrum of 5-(pentadeuterophenyl)phenanthridin-6(5*H*)-one

164-d$_5$

283
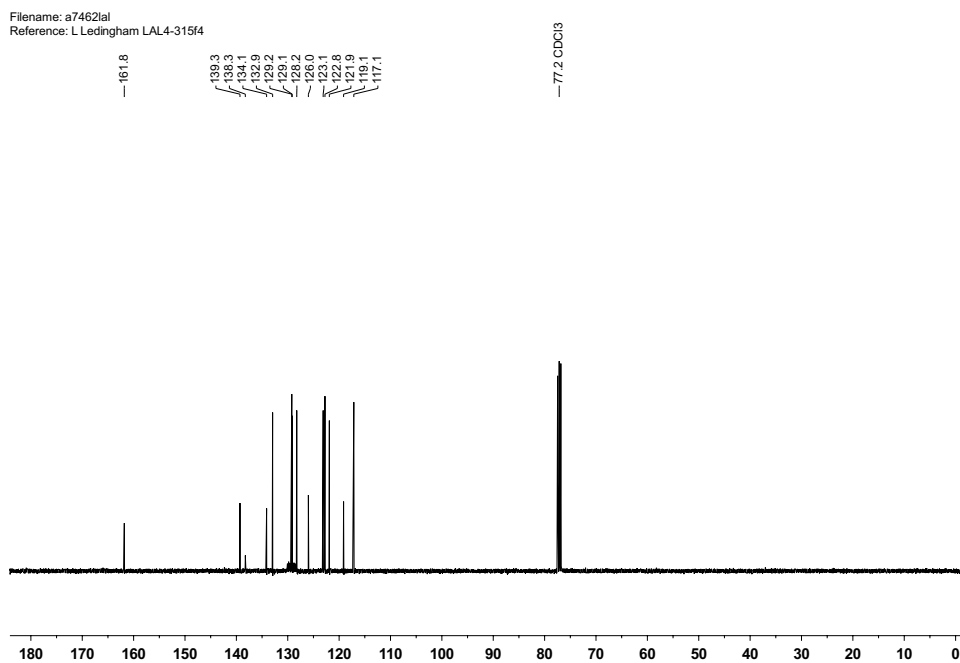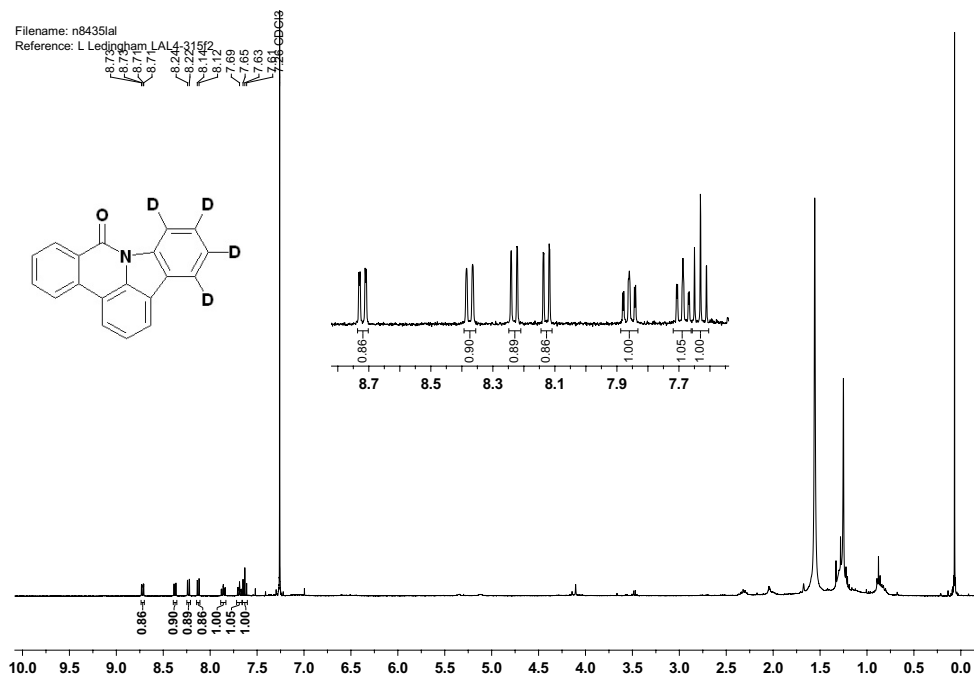
^{1}H NMR (400 MHz, CDCl$_3$) spectrum of 4,5,6,7-tetradeutero-8*H*-indolo[3,2,1-*de*]phenanthridin-8-one **196-d$_4$**
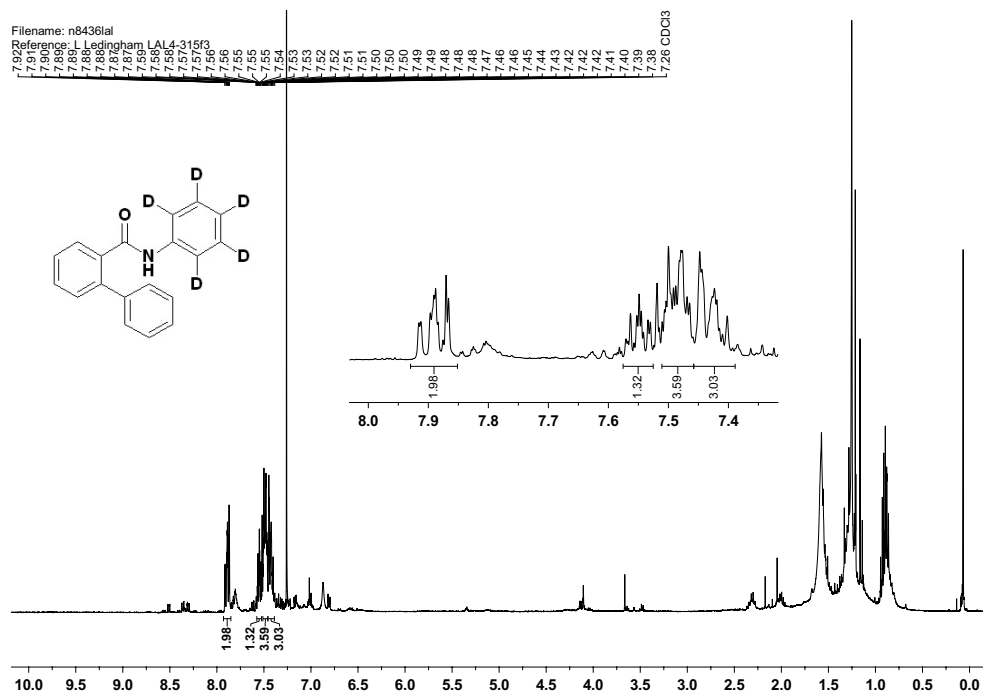
^{1}H NMR (400 MHz, CDCl$_3$) spectrum of *N*-(pentadeuterophenyl)-[1,1′-biphenyl]-2-carboxamide **204-d$_5$**
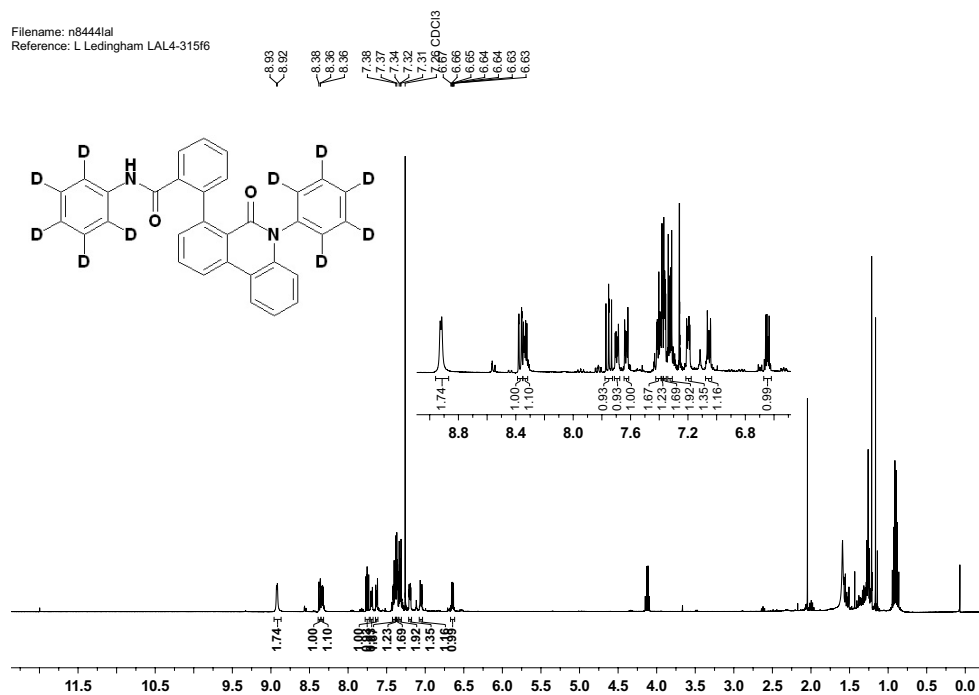
^{1}H NMR (400 MHz, CDCl$_3$) spectrum of 2′,3′,4′,5′-tetradeutero-*N*-(pentadeuterophenyl)-6′-(6-oxophenanthridin-5(6*H*)-yl)[1,1′-biphenyl]-2-carboxamide **208-d$_{10}$**
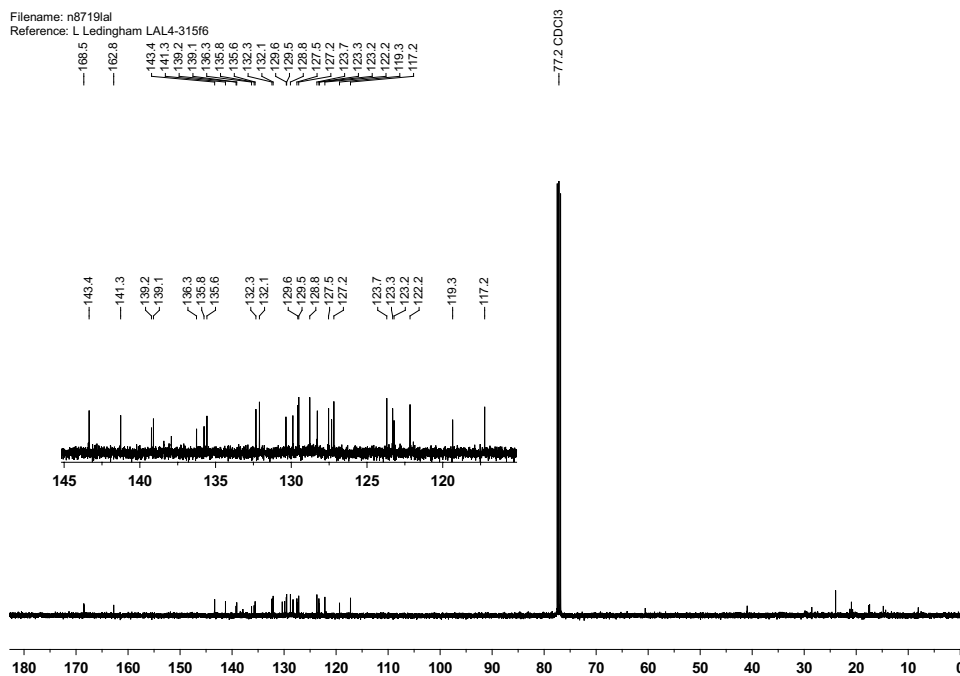
^{13}C NMR (100 MHz, CDCl$_3$) spectrum of 2′,3′,4′,5′-tetradeutero-*N*-(pentadeuterophenyl)-6′-(6-oxophenanthridin-5(6*H*)-yl)[1,1′-biphenyl]-2-carboxamide **208-d$_{10}$**
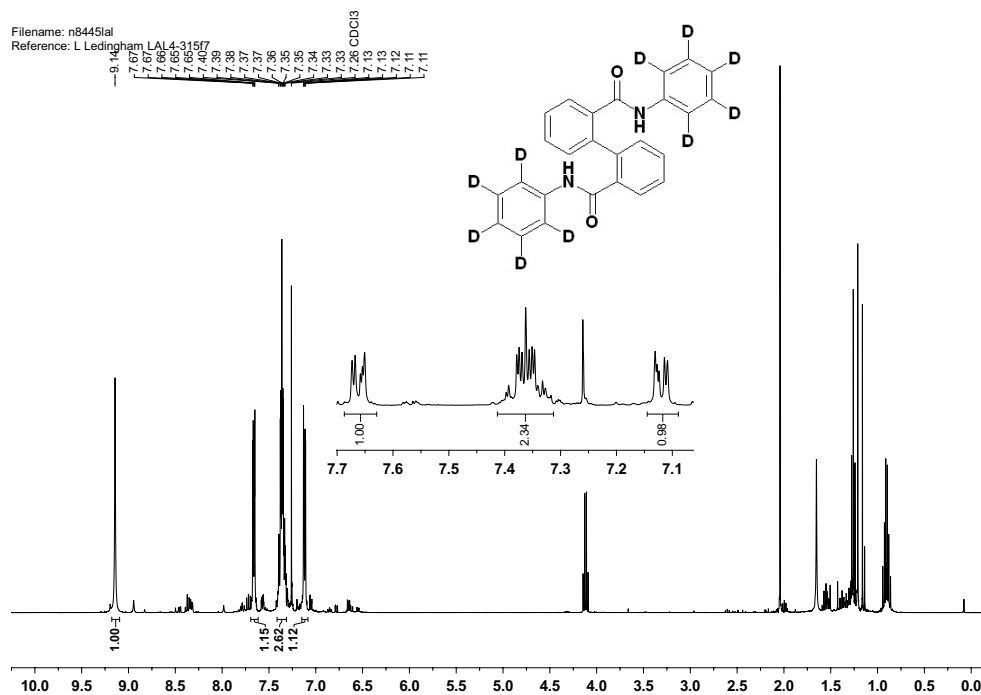
^{1}H NMR (400 MHz, CDCl$_3$) spectrum of $N2,N2'$-bis-(pentradeuterophenyl)[1,1'-biphenyl]-2,2'-dicarboxamide **201-d$_{10}$**. Trace ethyl acetate observable.
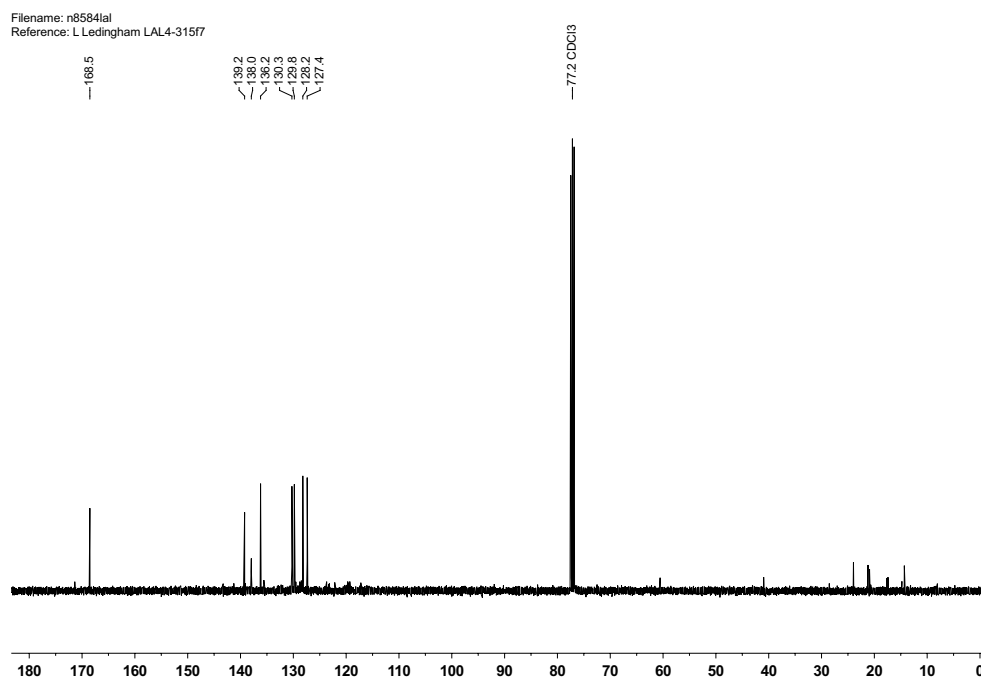
^{13}C NMR (100 MHz, CDCl$_3$) spectrum of $N2,N2'$-bis-(pentradeuterophenyl)[1,1'-biphenyl]-2,2'-dicarboxamide **201-d$_{10}$**

286
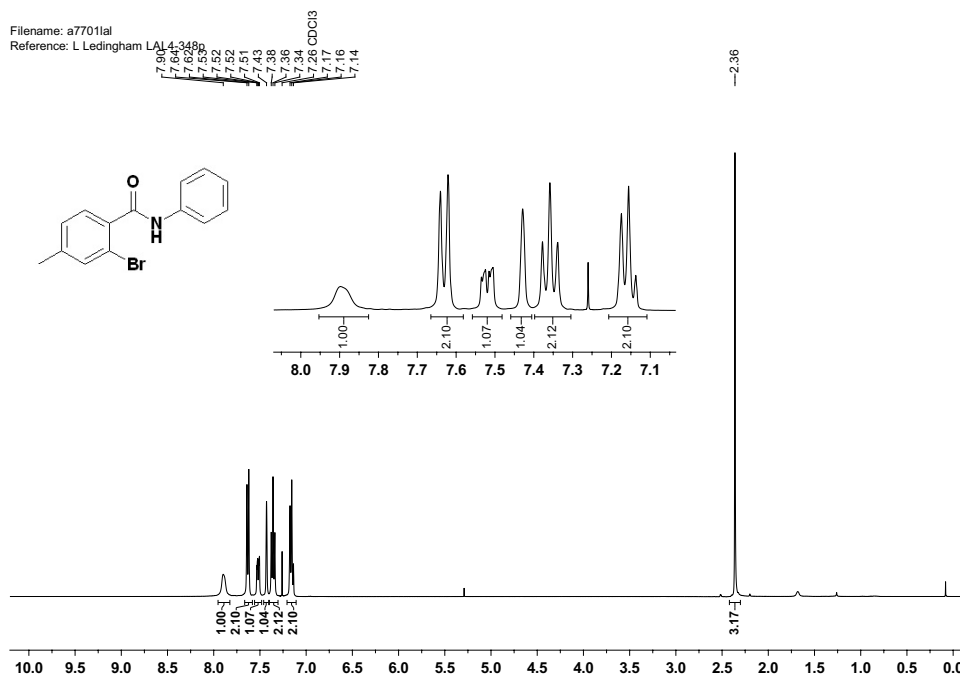
^{1}H NMR (400 MHz, CDCl$_3$) spectrum of 2-bromo-4-methyl-*N*-phenylbenzamide **189**
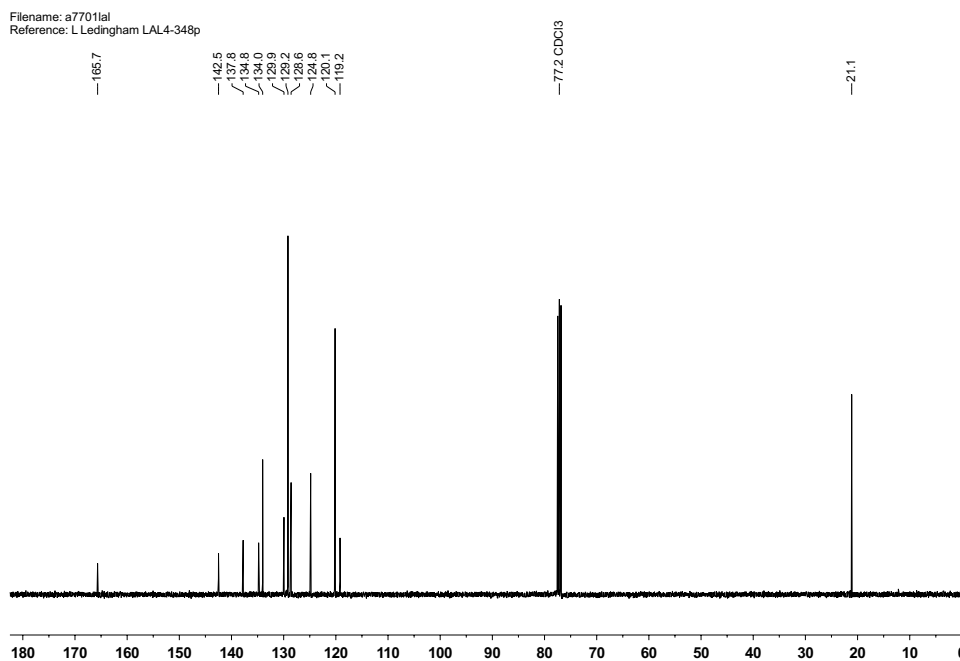
^{13}C NMR (100 MHz, CDCl$_3$) spectrum of 2-bromo-4-methyl-*N*-phenylbenzamide **189**
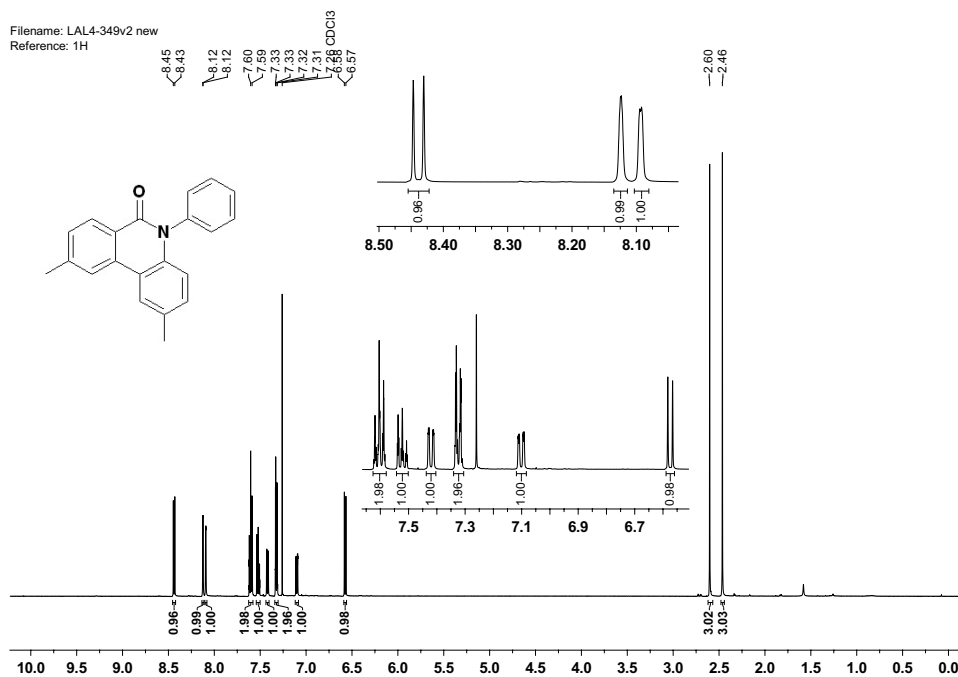
^{1}H NMR (500 MHz, CDCl$_3$) spectrum of 2,9-dimethyl-5-phenylphenanthridin-6(5H)-one

190
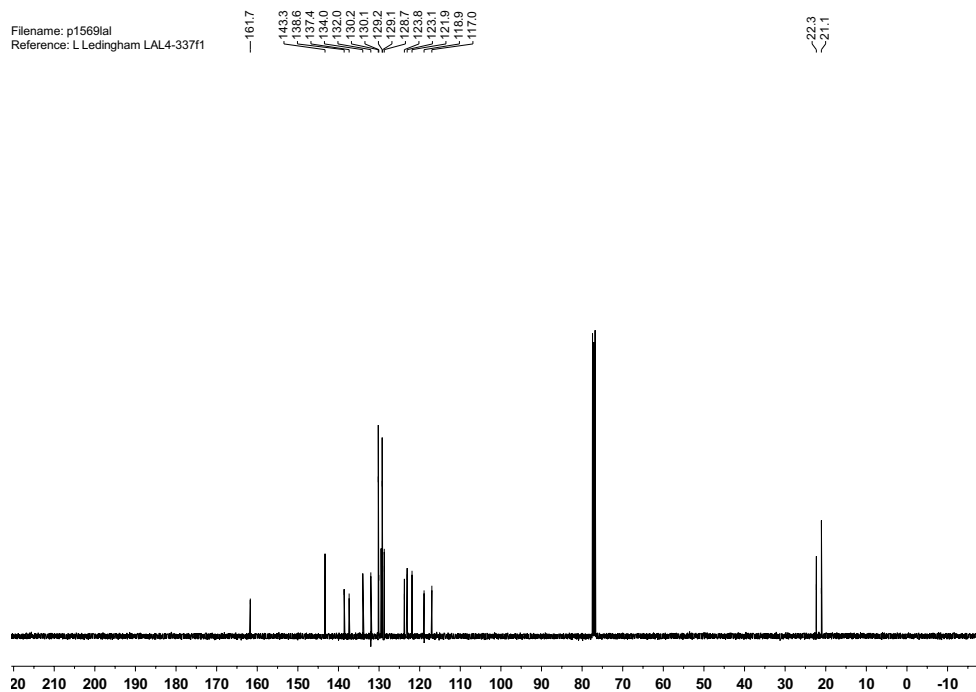
^{13}C NMR (100 MHz, CDCl$_3$) spectrum of 2,9-dimethyl-5-phenylphenanthridin-6(5H)-one

190
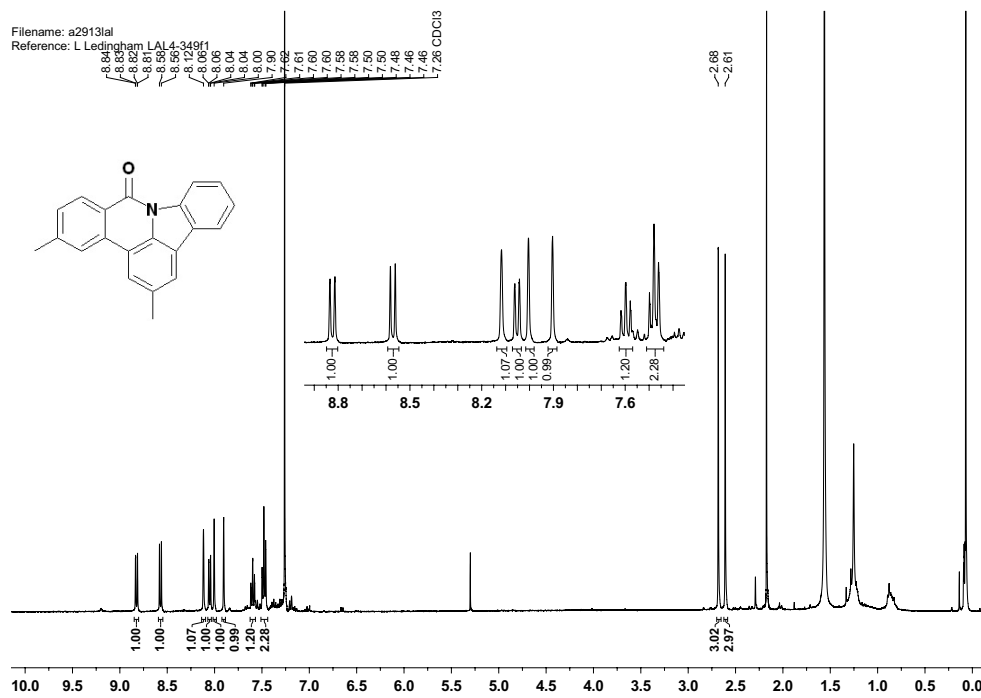
^{1}H NMR (400 MHz, CDCl$_3$) spectrum of 2,12-dimethyl-9H-indolo[3,2,1-*de*]phenanthridin-9-one **197**

Abbreviations

Ac	acetyl
ADPR	Adenosine diphosphate ribose
AE	atom economy
app.	apparent
approx.	approximately
aq.	aqueous
ATR	attenuated total reflection
BET	Brunauer–Emmett–Teller
BJH	Barrett, Joyner and Halenda
Bn	benzyl
Boc	*tert*-butoxycarbonyl
Bu	butyl
c	concentration
CAL-B	*Candida Antarctica Lipase B*
COSY	homonuclear correlation spectroscopy
CPMAS	cross polarisation magic angle spinning
dba	dibenzylideneacetone
DCC	*N,N'*-Dicyclohexylcarbodiimide
DFT	density functional theory
DIC	*N,N'*-Diisopropylcarbodiimide
DMAc	dimethylacetamide
DMF	dimethylformamide
DMSO	dimethylsulfoxide
dppb	1,4-bis(diphenylphosphino)butane
dppe	1,2-bis(diphenylphosphino)ethane
dppf	1,1'-bis(diphenylphosphino)ferrocene
dppm	1,1-bis(diphenylphosphino)methane
dppp	1,3-bis(diphenylphosphino)propane

DRIFTS	diffuse reflectance infra-red fourier transform spectroscopy
EI	electron impact
eq.	equivalents
ESI	electrospray ionisation
Et	ethyl
FWHM	full width at half maximum
GC	gas chromatography
GSK	Glaxo-Smith-Kline
HMBC	heteronuclear multiple bond correlation spectroscopy
HMQC	heteronuclear multiple-quantum correlation spectroscopy
HPLC	high performance liquid chromatography
HRMS	high resolution mass spectrometry
Hz	hertz
ICP	inductively-coupled plasma
InhA	Inhibin alpha
IR	infra-red
K60	Kieselgel 60
L	ligand
LCMS	liquid chromatography mass spectrometry
MAS	magic angle spinning
Me	methyl
MI	mass intensity
mp	melting point
MS	mass spectrometry
M.S.	molecular sieves
MW	molecular weight
NAD	nicotinamide adenine dinucleotide
NMP	*N*-Methyl-2-pyrrolidone
NMR	nuclear magnetic resonance
NOE	nuclear Overhauser effect

NOESY   nuclear Overhauser effect spectroscopy

PARP   poly ADP ribose polymerase

Ph   phenyl

ppm   parts per million

Pr   propyl

R_f retention factor

RF   response factor

RRF   relative response factor

RME   reaction mass efficiency

rt   ambient temperature

SBA   Santa Barbara Amorphous

SEM   scanning electron microscopy

SFC   supercritical fluid chromatography

t-   *tertiary*

TB   tuberculosis

Tf   trifluoromethanesulfonate

TFA   trifluoroacetate, trifluoroacetic acid

TFP   trifuryl phosphine

TGA   thermal gravimetric analysis

TLC   thin layer chromatography

UV   ultra-violet

XRD   X-ray diffraction

References

[1] C. A. Busacca, D. R. Fandrick, J. J. Song and C. H. Senanayake, *Adv. Synth. Catal.*, 2011, **353**, 1825–1864.

[2] C. Barnard, *Platin. Met. Rev.*, 2008, **52**, 110–113.

[3] C. a. G. N. Montalbetti and V. Falque, *Tetrahedron*, 2005, **61**, 10827–10852.

[4] J. S. Carey, D. Laffan, C. Thomson and M. T. Williams, *Org. Biomol. Chem.*, 2006, **4**, 2337–2347.

[5] C. Schotten, *Berichte der Dtsch. Chem. Gesellschaft*, 1884, **17**, 2544–2547.

[6] E. Baumann, *Berichte der Dtsch. Chem. Gesellschaft*, 1886, **19**, 3218–3222.

[7] M. Bachman, S. E. Mann and T. D. Sheppard, *Org. Biomol. Chem.*, 2012, **10**, 162–170.

[8] P. C. I. Appl., *WO2012135641A2*, 2012.

[9] A. Bucio-Cano, A. Reyes-Arellano, J. Correa-Basurto, M. Bello, J. Torres-Jaramillo, H. Salgado-Zamora, E. Curiel-Quesada, J. Peralta-Cruz and A. Avila-Sorrosa, *Bioorg. Med. Chem.*, 2015, **23**, 7565–7577.

[10] E. Valeur and M. Bradley, *Chem. Soc. Rev.*, 2009, **38**, 606–631.

[11] J. R. Dunetz, Y. Xiang, A. Baldwin and J. Ringling, *Org. Lett.*, 2011, **13**, 5048–5051.

[12] S. van Pelt, R. L. M. Teeuwen, M. H. A. Janssen, R. A. Sheldon, P. J. Dunn, R. M. Howard, R. Kumar, I. Martinez and J. W. Wong, *Green Chem.*, 2011, **13**, 1791–1798.

[13] S. Lal and T. J. Snape, *J. Mol. Catal. B-Enzymatic*, 2012, **83**, 80–86.

[14] K. Ishihara, S. Ohara and H. Yamamoto, *J. Org. Chem.*, 1996, **61**, 4196–4197.

[15] T. Maki, K. Ishihara and H. Yamamoto, *Org. Lett.*, 2005, **7**, 5043–5046.

[16] T. Maki, K. Ishihara and H. Yamamoto, *Org. Lett.*, 2006, **8**, 1431–1434.

[17] N. Gernigon, R. M. Al-Zoubi and D. G. Hall, *J. Org. Chem.*, 2012, **77**, 8386–8400.

[18] N. Gernigon, H. Zheng and D. G. Hall, *Tetrahedron Lett.*, 2013, **54**, 4475–4478.

[19] R. M. Lanigan, P. Starkov and T. D. Sheppard, *J. Org. Chem.*, 2013, **78**, 4512–4523.

[20] T. Marcelli, *Angew. Chem. Int. Ed.*, 2010, **49**, 6840–6843.

[21] J. W. Comerford, J. H. Clark, D. J. Macquarrie and S. W. Breeden, *Chem. Commun.*, 2009, 2562–2564.

[22] R. A. Sheldon, *Chem. Ind.*, 1992, 903–906.

[23] R. A. Sheldon, *Green Chem.*, 2007, **9**, 1273–1283.

[24] H. Lundberg, F. Tinnis and H. Adolfsson, *Chem. Eur. J.*, 2012, **18**, 3822–3826.

[25] X.-F. Wu, M. Sharif, A. Pews-Davtyan, P. Langer, K. Ayub and M. Beller, *Eur. J. Org. Chem.*, 2013, 2783–2787.

[26] S. Ghosh, A. Bhaumik, J. Mondal, A. Mallik, S. Sengupta and C. Mukhopadhyay, *Green Chem.*, 2012, **14**, 3220–3229.

[27] C. C. C. Johansson Seechurn, M. O. Kitching, T. J. Colacot and V. Snieckus, *Angew. Chem. Int. Ed.*, 2012, **51**, 5062–5085.

[28] J. Tsuji, in *Palladium Reagents Catal.*, John Wiley & Sons, Ltd, 2005, pp. 1–26.

[29] J. Yamaguchi, A. D. Yamaguchi and K. Itami, *Angew. Chem. Int. Ed.*, 2012, **51**, 8960–9009.

[30] J. A. Labinger and J. E. Bercaw, *Nature*, 2002, **417**, 507–514.

[31] L. Zhao, C. Bruneau and H. Doucet, *Tetrahedron*, 2013, **69**, 7082–7089.

[32] Y. Feng and G. Chen, *Angew. Chem. Int. Ed.*, 2010, **49**, 958–961.

[33] O. Daugulis, H.-Q. Do and D. Shabashov, *Acc. Chem. Res.*, 2009, **42**, 1074–1086.

[34] D. R. Stuart and K. Fagnou, *Science*, 2007, **316**, 1172–1175.

[35] F. Jafarpour, H. Hazrati, N. Mohasselyazdi, M. Khoobi and A. Shafiee, *Chem. Commun.*, 2013, **49**, 10935–10937.

[36] R. Henderson K., J. Kindervater and J. B. Manley, *Lessons learned through measuring green chemistry performance: The pharmaceutical experience*, ACS GCI PR Technical Report June, ACS GCI PR, 2007.

[37] C. Jimenez-Gonzalez, C. S. Ponder, Q. B. Broxterman and J. B. Manley, *Org. Process Res. Dev.*, 2011, **15**, 912–917.

[38] J. Comerford, *Ph.D. thesis*, York, 2010.

[39] S. P. Boureau and W. T. Cooper, *Anal. Chem.*, 1989, **61**, 41–47.

[40] E. F. Vansant, P. Van Der Voort and K. C. Vrancken, *Characterisation and Chemical Modification of the Silica Surface, Studies in Surface Science and Catalysis*, Elsevier, Netherlands, 1995, vol. 93.

[41] Y. Li, L. Ma, F. Jia and Z. Li, *J. Org. Chem.*, 2013, **78**, 5638–5646.

[42] X. Bantreil, N. Kanfar, N. Gehin, E. Golliard, P. Ohlmann, J. Martinez and F. Lamaty, *Tetrahedron*, 2014, **70**, 5093–5099.

[43] T. Ohshima, Y. Hayashi, K. Agura, Y. Fujii, A. Yoshiyama and K. Mashima, *Chem. Commun.*, 2012, **48**, 5434–5436.

[44] D. T. Nguyen, D. C. Lenstra and J. Mecinovic, *RSC Adv.*, 2015, **5**, 77658–77661.

[45] M. Luhmer, J. B. D'Espinose, H. Hommel and A. P. Legrand, *Magn. Reson. Imaging*, 1996, **14**, 911–913.

[46] J. W. Comerford, T. J. Farmer, D. J. Macquarrie, S. W. Breeden and J. H. Clark, *Arkivoc*, 2012, 282–293.

[47] K. Arnold, B. Davies, R. L. Giles, C. Grosjean, G. E. Smith and A. Whiting, *Adv. Synth. Catal.*, 2006, **348**, 813–820.

[48] CIEC, *Green Chemistry*, http://www.essentialchemicalindustry.org/processes/green-chemistry.html(accessed:November2016).

[49] R. Rawat, A. Whitty and P. J. Tonge, *Proc. Natl. Acad. Sci.*, 2003, **100**, 13881–13886.

[50] K. Johnsson, D. S. King and P. G. Schultz, *J. Am. Chem. Soc.*, 1995, **117**, 5009–5010.

[51] A. Dessen, A. Quemard, J. S. Blanchard, W. R. Jacobs and J. C. Sacchettini, *Science*, 1995, **267**, 1638–1641.

[52] K. Mdluli, R. A. Slayden, Y. Zhu, S. Ramaswamy, X. Pan, D. Mead, D. D. Crane, J. M. Musser and C. E. Barry, *Science*, 1998, **280**, 1607–1610.

[53] H. Meyer and J. Mally, *Monatsh. Chem.*, 1912, **33**, 393–414.

[54] T. P. Sycheva, T. N. Pavlova and M. N. Shchukina, *Pharm. Chem. J. (English Transl. Khimiko-Farmatsevticheskii Zhurnal)*, 1972, **6**, 1973.

[55] *4-Pyridinecarbonitrile*, http://www.sigmaaldrich.com/catalog/product/aldrich/c95005?lang=en{&}region=GB(accessed:April2016).

[56] *Isonicotinic acid*, http://www.sigmaaldrich.com/catalog/product/aldrich/i17508?lang=en{&}region=GB(accessed:April2016).

[57] *4-cyanopyridine SDS*, https://www.fishersci.com/shop/products/4-cyanopyridine-98-acros-organics-5/p-95287(accessed:November2016).

[58] H. Charville, D. Jackson, G. Hodges and A. Whiting, *Chem. Commun.*, 2010, **46**, 1813–1823.

[59] D. Prat, A. Wells, J. Hayler, H. Sneddon, C. R. McElroy, S. Abou-Shehada and P. J. Dunn, *Green Chem.*, 2016, **18**, 288–296.

[60] Z. Lin, V. Nikolakis and M. Ierapetritou, *Ind. Eng. Chem. Res.*, 2015, **54**, 2366–2378.

[61] *Charact. Chem. Modif. Silica Surf.*, ed. P. V. D. V. E.F. Vansant and K. C. Vrancken, Elsevier, 1995, vol. 93, pp. 3–146.

[62] W. K. Lowen and E. C. Broge, *J. Phys. Chem.*, 1961, **65**, 16–19.

[63] M. Srinivasan and A. K. Dunker, *Int. J. Pept.*, 2012, **2012**, 1–14.

[64] *Reactions performed by Dr Lee Boulton and Janette McKnight as part of GSK's contribution to CHEM21 under the Innovative Medicines Initiative Joint Undertaking*

[65] N. C. Mamillapalli and G. Sekar, *Chem. – A Eur. J.*, 2015, **21**, 18584–18588.

[66] D. Weltin, V. Picard, K. Aupeix, M. Varin, D. Oth, J. Marchal, P. Dufour and P. Bischoff, *Int. J. Immunopharmacol.*, 1995, **17**, 265–271.

[67] K. Tanimoto, N. Nakagawa, K. Takeda, M. Kirihata and S. Tanimori, *Tetrahedron Lett.*, 2013, **54**, 3712–3714.

[68] D. Liang, Z. Hu, J. Peng, J. Huang and Q. Zhu, *Chem. Commun.*, 2013, **49**, 173–175.

[69] D. E. Ames and A. Opalko, *Tetrahedron*, 1984, **40**, 1919–1925.

[70] R. Bernini, S. Cacchi, G. Fabrizi and A. Sferrazza, *Synthesis*, 2008, **2008**, 729–738.

[71] N. Ishida, Y. Nakanishi, T. Moriya and M. Murakami, *Chem. Lett.*, 2011, **40**, 1047–1049.

[72] J. P. Reeds, *PhD Thesis*, University of York, 2010.

[73] H. Adams, N. A. Bailey, T. N. Briggs, J. A. McCleverty, H. M. Colquhoun and D. J. Williams, *J. Chem. Soc. Dalt. Trans.*, 1986, 813–819.

[74] C. M. Crawforth, S. Burling, I. J. S. Fairlamb, A. R. Kapdi, R. J. K. Taylor and A. C. Whitwood, *Tetrahedron*, 2005, **61**, 9736–9751.

[75] J. Ruiz, C. Vicente, N. Cutillas and J. Perez, *Dalt. Trans.*, 2005, 1999–2006.

[76] G. Sanchez, J. Garcia, M. Martinez, A. R. Kapdi, J. Perez, L. Garcia and J. Luis Serrano, *Dalt. Trans.*, 2011, **40**, 12676–12689.

[77] H. E. Gottlieb, V. Kotlyar and A. Nudelman, *J. Org. Chem.*, 1997, **62**, 7512–7515.

[78] T. Gebauer, F. Gerlinde and D. Kurt, *Zeitschrift für Naturforsch. B*, 1992, **47**, 1505.

[79] D. S. Suslov, M. V. Bykov, P. A. Abramov, M. V. Pahomova, I. A. Ushakov, V. K. Voronov and V. S. Tkach, *RSC Adv.*, 2015, **5**, 104467–104471.

[80] P. K. Owens, *MSc*, University of York, 2013.

[81] J. Ruiz, N. Cutillas, J. Torregrosa, G. Garcia, G. Lopez, P. A. Chaloner, P. B. Hitchcock and R. M. Harrison, *J. Chem. Soc. Dalt. Trans.*, 1994, 2353–2357.

[82] T. W. Lyons, K. L. Hull and M. S. Sanford, *J. Am. Chem. Soc.*, 2011, **133**, 4455–4464.

[83] C. L. Allen and J. M. J. Williams, *Chem. Soc. Rev.*, 2011, **40**, 3405–3415.

[84] C. L. Allen, A. R. Chhatwal and J. M. J. Williams, *Chem. Commun.*, 2012, **48**, 666–668.

[85] M. B. Gawande, S. N. Shelke, R. Zboril and R. S. Varma, *Acc. Chem. Res.*, 2014, **47**, 1338–1348.

[86] T. Furuta, Y. Kitamura, A. Hashimoto, S. Fujii, K. Tanaka and T. Kan, *Org. Lett.*, 2007, **9**, 183–186.

[87] R. Ferraccioli, D. Carenzi, E. Motti and M. Catellani, *J. Am. Chem. Soc.*, 2005, **128**, 722–723.

[88] H. Liu, W. Han, C. Li, Z. Ma, R. Li, X. Zheng, H. Fu and H. Chen, *Eur. J. Org. Chem.*, 2016, **2016**, 389–393.

[89] L. Donati, P. Leproux, E. Prost, S. Michel, F. Tillequin, V. Gandon and F.-H. Porée, *Chem. – A Eur. J.*, 2011, **17**, 12809–12819.

[90] S. Caddick and W. Kofie, *Tetrahedron Lett.*, 2002, **43**, 9347–9350.

[91] T. Furuta, J. Yamamoto, Y. Kitamura, A. Hashimoto, H. Masu, I. Azumaya, T. Kan and T. Kawabata, *J. Org. Chem.*, 2010, **75**, 7010–7013.

[92] W. A. Carole and T. J. Colacot, *Chem. – A Eur. J.*, 2016, **22**, 7686–7695.

[93] S. E. Bajwa, T. E. Storr, L. E. Hatcher, T. J. Williams, C. G. Baumann, A. C. Whitwood, D. R. Allan, S. J. Teat, P. R. Raithby and I. J. S. Fairlamb, *Chem. Sci.*, 2012, **3**, 1656–1661.

[94] A. R. Kapdi, A. C. Whitwood, D. C. Williamson, J. M. Lynam, M. J. Burns, T. J. Williams, A. J. Reay, J. Holmes and I. J. S. Fairlamb, *J. Am. Chem. Soc.*, 2013, **135**, 8388–8399.

[95] A. G. Jarvis, P. E. Sehnal, S. E. Bajwa, A. C. Whitwood, X. Zhang, M. S. Cheung, Z. Lin and I. J. S. Fairlamb, *Chem. – A Eur. J.*, 2013, **19**, 6034–6043.

[96] Z. Qin, M. C. Jennings and R. J. Puddephatt, *Inorg. Chem.*, 2001, **40**, 6220–6228.

[97] *N,   N-Dimethylformamide*,   http://www.sigmaaldrich.com/catalog/product/sial/ 227056?lang=en{&}region=GB(accessed:June2016).

[98] *N,N-Dimethylacetamide*,   http://www.sigmaaldrich.com/catalog/product/sigma/ d5511?lang=en{&}region=GB(accessed:June2016).

[99] B. Schäffner, F. Schäffner, S. P. Verevkin and A. Börner, *Chem. Rev.*, 2010, **110**, 4554–4581.

[100] J. Sherwood, M. De bruyn, A. Constantinou, L. Moity, C. R. McElroy, T. J. Farmer, T. Duncan, W. Raverty, A. J. Hunt and J. H. Clark, *Chem. Commun.*, 2014, **50**, 9650–9652.

[101] H. L. Parker, J. Sherwood, A. J. Hunt and J. H. Clark, *ACS Sustain. Chem. Eng.*, 2014, **2**, 1739–1742.

[102] K. L. Wilson, A. R. Kennedy, J. Murray, B. Greatrex, C. Jamieson and A. J. B. Watson, *Beilstein J. Org. Chem.*, 2016, **12**, 2005–2011.

[103] Z. Liang, J. Zhang, Z. Liu, K. Wang and Y. Zhang, *Tetrahedron*, 2013, **69**, 6519–6526.

[104] Y. Yang, H. Huang, L. Wu and Y. Liang, *Org. Biomol. Chem.*, 2014, **12**, 5351–5355.

[105] S. R. Landor, O. O. Sonola and A. R. Tatchell, *Bull. Chem. Soc. Jpn.*, 1984, **57**, 1658–1661.

[106] S. Ghosh, D. B. Datta, I. Datta and T. K. Das, *Tetrahedron*, 1989, **45**, 3775–3786.

[107] J. H. Markgraf, A. A. Dowst, L. A. Hensley, C. E. Jakobsche, C. J. Kaltner, P. J. Webb and P. W. Zimmerman, *Tetrahedron*, 2005, **61**, 9102–9110.

[108] A. P. Gehring, T. Tremmel and F. Bracher, *Synthesis*, 2014, **46**, 893–898.

[109] W. Cong, L. Zhao, X. Wu, J. Xu and H. Yao, *Tetrahedron*, 2014, **70**, 312–317.

[110] S. Goswami, A. K. Adak, R. Mukherjee, S. Jana, S. Dey and J. F. Gallagher, *Tetrahedron*, 2005, **61**, 4289–4295.

[111] J. F. Gallagher, P. T. M. Kenny and M. J. Sheehy, *Acta Crystallogr. Sect. C*, 1999, **55**, 1257–1260.

[112] J. F. Gallagher, P. T. M. Kenny and M. J. Sheehy, *Inorg. Chem. Commun.*, 1999, **2**, 200–202.

[113] A. Imramovský, K. Pauk, Z. Padělková and J. Hanusek, *Crystals*, 2012, **2**, 349.

[114] P. Nimnual, J. Tummatorn, C. Thongsornkleeb and S. Ruchirawat, *J. Org. Chem.*, 2015, **80**, 8657–8667.

[115] K. W. Anderson, T. Ikawa, R. E. Tundel and S. L. Buchwald, *J. Am. Chem. Soc.*, 2006, **128**, 10694–10695.

[116] A. Sergeev, T. Schulz, C. Torborg, A. Spannenberg, H. Neumann and M. Beller, *Angew. Chem. Int. Ed.*, 2009, **48**, 7595–7599.

[117] D. Baranano and J. F. Hartwig, *J. Am. Chem. Soc.*, 1995, **117**, 2937–2938.

[118] F. E. Goodson, T. I. Wallow and B. M. Novak, *J. Am. Chem. Soc.*, 1997, **119**, 12441–12453.

[119] V. V. Grushin, *Organometallics*, 2000, **19**, 1888–1900.

[120] A. M. Zawisza and J. Muzart, *Tetrahedron Lett.*, 2007, **48**, 6738–6742.

[121] N. V. Reddy, P. S. Kumar, P. S. Reddy, M. L. Kantam and K. R. Reddy, *New J. Chem.*, 2015, **39**, 805–809.

[122] J. Louie and J. F. Hartwig, *Tetrahedron Lett.*, 1995, **36**, 3609–3612.

[123] A. S. Guram, R. A. Rennels and S. L. Buchwald, *Angew. Chem. Int. Ed.*, 1995, **34**, 1348–1350.

[124] M. S. Driver and J. F. Hartwig, *J. Am. Chem. Soc.*, 1996, **118**, 7217–7218.

[125] L. Donati, S. Michel, F. Tillequin and F.-H. Porée, *Org. Lett.*, 2010, **12**, 156–158.

[126] C. Amatore, G. Broeker, A. Jutand and F. Khalil, *J. Am. Chem. Soc.*, 1997, **119**, 5176–5185.

[127] Y. Saga, D. Han, S.-i. Kawaguchi, A. Ogawa and L.-B. Han, *Tetrahedron Lett.*, 2015, **56**, 5303–5305.

[128] C. Bianchini, H. Man Lee, A. Meli, W. Oberhauser, M. Peruzzini and F. Vizza, *Organometallics*, 2002, **21**, 16–33.

[129] W. A. Herrmann, W. R. Thiel, C. Broißmer, K. Öfele, T. Priermeier and W. Scherer, *J. Organomet. Chem.*, 1993, **461**, 51–60.

[130] G. Mann, D. Baranano, J. F. Hartwig, A. L. Rheingold and I. A. Guzei, *J. Am. Chem. Soc.*, 1998, **120**, 9205–9219.

[131] M. Ludwig, S. Strömberg, M. Svensson and B. Åkermark, *Organometallics*, 1999, **18**, 970–975.

[132] L. Patiny and A. Borel, *J. Chem. Inf. Model.*, 2013, **53**, 1223–1228.

[133] A. J. Butterworth, J. H. Clark, P. H. Walton and S. J. Barlow, *Chem. Commun.*, 1996, 1859–1860.

[134] O. V. Dolomanov, L. J. Bourhis, R. J. Gildea, J. A. K. Howard and H. Puschmann, *J. Appl. Crystallogr.*, 2009, **42**, 339–341.

[135] L. Palatinus and A. van der Lee, *J. Appl. Crystallogr.*, 2008, **41**, 975–984.

[136] L. Palatinus and G. Chapuis, *J. Appl. Crystallogr.*, 2007, **40**, 786–790.

[137] L. Palatinus, S. J. Prathapa and S. van Smaalen, *J. Appl. Crystallogr.*, 2012, **45**, 575–580.

[138] G. M. Sheldrick, *Acta Crystallogr. Sect. A*, 2008, **64**, 112–122.

[139] H. Kameoka, *Nippon Kagaku Zasshi*, 1960, **81**, 950–953.

[140] P. S. Chaudhari, S. D. Salim, R. V. Sawant and K. G. Akamanchi, *Green Chem.*, 2010, **12**, 1707–1710.

[141] P. Nordeman, L. R. Odell and M. Larhed, *J. Org. Chem.*, 2012, **77**, 11393–11398.

[142] G. L. Backes, B. S. Jursic and D. M. Neumann, *Bioorg. Med. Chem.*, 2015, **23**, 3397–3407.

[143] J. Holt, T. Andreassen, J. M. Bakke and A. Fiksdahl, *J. Heterocycl. Chem.*, 2005, **42**, 259–264.

[144] T. Kanemitsu, A. Umehara, R. Haneji, K. Nagata and T. Itoh, *Tetrahedron*, 2012, **68**, 3893–3898.

[145] S. K. Davidsen, P. D. May and J. B. Summers, *J. Org. Chem.*, 1991, **56**, 5482–5485.

[146] Z. Min, S. Imm, S. Bähn, L. Neubert, H. Neumann and M. Beller, *Angew. Chem. Int. Ed.*, 2012, **51**, 3905–3909.

[147] Y. Wang, D. Zhu, L. Tang, S. Wang and Z. Wang, *Angew. Chem. Int. Ed.*, 2011, **50**, 8917–8921.

[148] S. A. Glover and A. Goosen, *J. Chem. Soc. Perkin Trans. 1*, 1974, 2353–2356.

[149] Q. Luo, C. Wang, W.-X. Zhang and Z. Xi, *Chem. Commun.*, 2008, 1593–1595.

[150] A. Bej, A. Chakraborty and A. Sarkar, *RSC Adv.*, 2013, **3**, 15812–15819.